



Swansea University  
Prifysgol Abertawe



## Swansea University E-Theses

---

# The cavitation properties of liquids: Temperature and stressing rate effects.

Chan, Hoi Houg

### How to cite:

---

Chan, Hoi Houg (2009) *The cavitation properties of liquids: Temperature and stressing rate effects..* thesis, Swansea University.

<http://cronfa.swan.ac.uk/Record/cronfa42968>

### Use policy:

---

This item is brought to you by Swansea University. Any person downloading material is agreeing to abide by the terms of the repository licence: copies of full text items may be used or reproduced in any format or medium, without prior permission for personal research or study, educational or non-commercial purposes only. The copyright for any work remains with the original author unless otherwise specified. The full-text must not be sold in any format or medium without the formal permission of the copyright holder. Permission for multiple reproductions should be obtained from the original author.

Authors are personally responsible for adhering to copyright and publisher restrictions when uploading content to the repository.

Please link to the metadata record in the Swansea University repository, Cronfa (link given in the citation reference above.)

<http://www.swansea.ac.uk/library/researchsupport/ris-support/>



# Swansea University Prifysgol Abertawe

## **The Cavitation Properties of Liquids: Temperature and Stressing Rate Effects**

By

**Chan Hoi Houg**

**M.Eng (Hons)**

A Thesis Submitted to the University of Wales  
in fulfillment of the requirements for the Degree of

**PHILOSIPHIAE DOCTOR**

Multidisciplinary Nanotechnology Centre (MNC)

Swansea University

July 2009

ProQuest Number: 10821358

All rights reserved

INFORMATION TO ALL USERS

The quality of this reproduction is dependent upon the quality of the copy submitted.

In the unlikely event that the author did not send a complete manuscript and there are missing pages, these will be noted. Also, if material had to be removed, a note will indicate the deletion.



ProQuest 10821358

Published by ProQuest LLC (2018). Copyright of the Dissertation is held by the Author.

All rights reserved.

This work is protected against unauthorized copying under Title 17, United States Code  
Microform Edition © ProQuest LLC.

ProQuest LLC.  
789 East Eisenhower Parkway  
P.O. Box 1346  
Ann Arbor, MI 48106 – 1346





## Summary

This Thesis contains an account of work in which both quasi-static and dynamic stressing techniques were used to subject samples of liquid to tension. For dynamic stressing, an improved form of the 'Bullet-Piston' (B-P) apparatus described by Couzens and Trevena (1969) was employed, whereas a version of the Berthelot tube (Berthelot, 1850) allied to high speed video photography was used for quasi-static stressing work. Work reported in Chapter 3 shows how, for the first time in the B-P apparatus, the rate of development of tension ( $\dot{\Omega}_r$ ) may be varied systematically in order to investigate its influence on the liquid's effective tensile strength,  $F_c$ . Results are reported in Chapter 4 for samples of degassed, deionised water. The experiments show an approximately four-fold increase of  $F_c$  at the highest stressing rate, this value being 224 bar ( $\dot{\Omega}_r = 1.79 \text{ bar}\mu\text{s}^{-1}$ ) compared to a value of 60 bar at a lower stress development rate ( $\dot{\Omega}_r = 0.432 \text{ bar}\mu\text{s}^{-1}$ ). The results substantiate the claim that  $\dot{\Omega}_r$  is an important consideration in understanding the cavitation properties of liquids. The work reported in Chapter 5 includes the effects of temperature ( $25 \text{ }^\circ\text{C} \leq T \leq 110 \text{ }^\circ\text{C}$ ), shear viscosity ( $0.001 \text{ Pas} \leq \mu \leq 0.203 \text{ Pas}$ ) and  $\dot{\Omega}_r$  ( $0.6 \text{ bar}\mu\text{s}^{-1} \leq \dot{\Omega}_r \leq 1.4 \text{ bar}\mu\text{s}^{-1}$ ) on  $F_c$  for commercial monograde and multigrade oils, the ambient environments in the car engine encountered under normal operating conditions. The results substantiate the claim that  $\dot{\Omega}_r$  is an important consideration in understanding the cavitation properties of liquids and may be an important consideration when evaluating a lubricant's cavitation performance. A significant aspect of this work is that, contrary to previously reported studies, results have been produced from a single technique, in experiments conducted within the same apparatus in which the rate of stressing is deliberately varied in a systematic manner. The results of such a study have not previously been reported.

The work described in Chapter 6 involved temperatures which extended into the supercooled regime. High speed photography recorded the initial formation and growth of a single, isolated, and apparently spherical cavitation bubble within a bulk sample of water. The cavitation event was seen to start with a single, approximately spherical cavity, growing not at (or from) the tube walls, but in the body of the liquid. The collapse phase clearly shows the formation of a liquid jet directed at the surface adjacent to the bubble. This feature of bubble dynamics has never previously been reported in Berthelot tube work. These results suggest that the Berthelot tube technique may have wider utility in cavitation research, having previously been confined to measurements of  $F_c$ . The work reported here shows that its use may be extended to studying potential cavitation damage mechanisms. Quasi-static stressing was extended into the supercooled regime for water to produce doubly-metastable (d-m) liquid. High-speed video was used to estimate the ice front's velocity of propagation following nucleation. The velocities recorded are higher than those previously reported for supercooled water at comparable temperatures – by an order of magnitude. The work reported in this Thesis is the first in which evidence is presented that the formation and growth of a cavitation bubble results in the nucleation of ice formation.

# Declaration

This work has not previously been accepted in substance for any degree and is not being concurrently submitted in candidature for any degree.

Signed.....(Candidate)

Date. 18/01/2010.....

## Statement 1

This thesis is the result of my own investigation, except where otherwise stated. Other sources are acknowledged, giving explicit references. A bibliography is appended.

Signed.....(Candidate)

Date. 18/01/2010.....

## Statement 2

I hereby consent for my thesis, if accepted, to be available for photocopying and for inter-library loan, and for the title and summary to be made available to outside organisations.

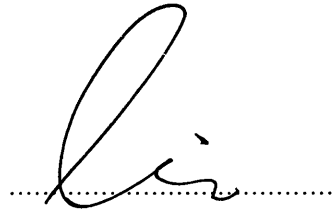
Signed.....(Candidate)

Date. 18/01/2010.....

# Certificate of Originality

This thesis is submitted to the Swansea University, under the supervision of Professor P.R. Williams in the Department of Multidisciplinary Nanotechnology Centre (MNC), University of Wales, Swansea, in candidature for the degree of Philosophiae Doctor. The material in this thesis is the original work of the author except where acknowledgement to other authors is expressly made.

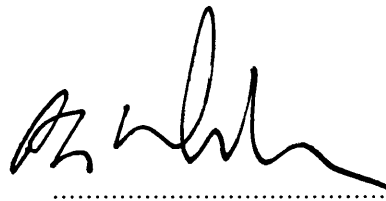
Signed,

A handwritten signature in black ink, appearing to be 'Choi', written over a horizontal dotted line.

Chan Hoi Houg

(Candidate)

Signed,

A handwritten signature in black ink, appearing to be 'P.R. Williams', written over a horizontal dotted line.

Professor P.R. Williams

(Supervisor)

Date: 18/01/2010.

# Acknowledgement

I would first like to express my deepest gratitude to my supervisor Professor P. R. Williams for his thoughtful guidance, support, enthusiasm, encouragement, and patience throughout the whole duration of my research work.

Beside that, I would like to thanks to all my laboratory colleagues, particularly, Dr. R. L. Williams, Dr. Matthew Barrow and Dr. A. Al-Hussany, and Dr. Dale Rogers for their guidance and assistance throughout my PhD research work. Without their guidance, this Thesis will not able to complete on time and successfully.

I would like to express my gratitude to so many friends especially Dr Samson Chang, Dr Brenda Lee, Dr Yong, Dr Michelle Tan, Dr Soo, Mr Sim, Miss Krystal Wong, Mrs May, Mr Chong in supporting and encouraging me through this PhD research course. I can never thank any of you enough for the laughter, care and love that you bring with your friendship. I am also grateful to Molly Chua who constantly provides support and unconditional love. I may not name all of you, but be assured that none is forgotten. Also not forgotten are bible study friends for the pleasant friendships along the way.

None of this would have been possible without the constant support of my family. Without a shadow of a doubt I would not have got this far without their limitless love and confidence in me. Their patience and encouragement during the time of disappointment, despair and frustration brings out a new surge of energy in me to carry on. I know how extremely blessed I am to have such a supportive family and friends, which things would be so much harder without them.

Most importantly, I want to thank God for His everlasting love and spiritual support throughout the challenging years during research. *'It is God who arms me with strength and makes my way perfect' (Psalm 18: 31-32)*

For my  
Family  
Especially  
My Mom

# CONTENTS

	<b>PAGE</b>
<b>Summary</b>	<b>I</b>
<b>Declaration</b>	<b>II</b>
<b>Certificate of Originality</b>	<b>III</b>
<b>Acknowledgments</b>	<b>IV</b>
<b>Dedication</b>	<b>V</b>
<b>Contents</b>	<b>VI</b>
<b>Nomenclature</b>	<b>XI</b>
<b>Chapter 1. Introduction and literature survey</b>	
1.1 Background of Cavitation	1-2
1.2 Historical Developments in the Field	2-3
1.3 Some process Involving Cavitation	3-6
1.4 Basic Theoretical Aspects of the Liquid State	6-8
1.4.1 Theoretical Estimates of Liquid Tensile Strength: Homogeneous Nucleation	8-10
1.4.2 Experimental Measurement of Tensile Strength: Heterogeneous Nucleation	10-12
1.4.3 Cavitation Bubble Dynamics	12-15
1.4.4 Cavitation Damage	15-16

1.5	Experimental Techniques for Measurement of Liquid Tensile Strength	
1.5.1	Static Stressing Technique	16
1.5.1.1	The Berthelot Tube Method	16-18
1.5.1.2	Quasi-Static Stressing: The Centrifugal Method	19-20
1.5.2	Dynamic Stressing Technique	20
1.5.2.1	Tube-Arrest Method	20-23
1.5.2.2	Shock Tube Method	24-25
1.5.2.3	Bullet-Piston Apparatus	25-26

## **Chapter 2. The development of B-P experiment**

2.1	Introduction	27-28
2.2	The Bullet-Piston Apparatus: Previous Related Work	28-29
2.3	Inadequate Transduction and a Neglect of the Effects of Wave Reflection in the Pulse-Reflection Work	30-31
2.3.1	Slow Respond Pressure Transducers	31-33
2.3.2	Data Sampling Consideration in B-P Work	33-35
2.3.3	Wave interference of pulse reflection in B-P work	36-40
2.4	Improved Bullet-Piston Apparatus	40-41

### **Chapter 3. Dynamic stressing liquids: Improved Bullet-Piston Apparatus**

3.1	Introduction	42
3.2	The Basic Description of 'Bullet-Piston' Apparatus	42-48
3.3	Cleaning Procedure	49
3.4	Signal Processing and its Analytic Work	
	3.4.1 Pressure Transducer (Section 1)	49-51
	3.4.2 Data Acquisition (Section 2)	52-54
	3.4.3 Dadisp Software (Section 3)	55-60
3.5	Determination of Cavitation Threshold, $F_c$ of Liquid Involving the Application of a Regulated Static Pressure (Section 4)	61-65

### **Chapter 4 The Effects of the Effective Dynamic Stressing Rates on the Measurements of the Tensile Strength of Deionised Water**

4.1	Abstract	66
4.2	Introduction	66-68
4.3	Experimental and Results	69-75
4.4	Discussion	76-78
4.5	Conclusion	79-80



**Chapter 5 The Cavitation Properties of Monograde and Multigrade Oils under  
Dynamic Stressing by Tension Pulses over a Wide Range of Temperature**

5.1	Abstract	81
5.2	Introduction	82-86
5.3	Experimental Techniques	86-87
5.4	The Dependence of $F_c$ on Temperature	88-92
5.5	The Dependence of $F_c$ on Shear Viscosity, $\mu$	93-101
5.6	The Dependence of $F_c$ on Stressing Rate, $\dot{\Omega}_f$	102-112
5.7	The Influence of the Polymer Concentration on the $F_c$	113-115
5.8	Conclusion	116-121

**Chapter 6 Studies of Doubly Metastable (d-m) Liquids under Quasi-Static Isotropic  
Tension in Berthelot Tube.**

6.1	Introduction	122-125
6.2	Previous Related Work	126-130
6.3	The Modified Berthelot Tubes	131-133
6.4	Determination of the Sealing Temperature, $T_0$ , in Order to Bring $D_2O$ (Heavy Water) Liquid Samples Into the Doubly Metastable Region in the Modified Berthelot Tube	134-139
6.5	The Records Obtained from High-Speed Imaging System	140
6.5.1	Initial Test Results	141-148

6.5.2	Experiments Involving d-m Heavy Water	148-152
6.5.3	Results of Experiments Involving Ice Formation In the d-m Regime	153-159
6.6	Conclusion	160-161
<b>Chapter 7 Conclusion and Recommendation for Future Work</b>		<b>162-165</b>
<b>References</b>		<b>166-177</b>

# Nomenclature

$F_c$	liquid tensile strength	bar
$V_c$	velocity at threshold	$\text{m s}^{-1}$
$v$	velocity of the liquid jet	$\text{m s}^{-1}$
$\rho$	density	$\text{kg m}^{-3}$
$\mu$	shear viscosity	Pas
$\sigma$	surface tension	$\text{N m}^{-1}$
$\tau_0$	instant time delay	ms
$\tau_i$	time delay	ms
$t_0$	initial time	s
$c$	speed of sound in water liquid	$\text{m s}^{-1}$
$c_v$	speed of sound in water vapour	$\text{m s}^{-1}$
$T$	temperature	$^{\circ}\text{C}$
$T_f$	heating temperature	$^{\circ}\text{C}$
$T_o$	sealing temperature	$^{\circ}\text{C}$
$T_c$	critical temperature	$^{\circ}\text{C}$
$T_b$	breaking temperature	$^{\circ}\text{C}$
$\omega$	angular velocity	$\text{rad s}^{-1}$
$\omega_c$	critical angular velocity	$\text{rad s}^{-1}$
$V$	volume	$\text{m}^3$
$\Delta V$	change of volume	$\text{m}^3$
$P$	pressure	$\text{N m}^{-2}$
$F$	tension	$\text{N m}^{-2}$
$D$	gap between stun gun and piston	cm
$P_s$	static pressure	$\text{N m}^{-2}$
$\dot{\Omega}_f$	rate of change of tension	$\text{bar}\mu\text{s}^{-1}$
$P_{\infty}$	pressure in undisturbed water	$\text{N m}^{-2}$
$p_o$	ambient pressure in the cavity	$\text{N m}^{-2}$
$p_v$	pressure in the cavity	$\text{N m}^{-2}$

Symbols not listed above are defined in the text.

# List of Tables

- Table 3.1: The table of individual parts of the stun gun
- Table 4.1: Tensile strength of water obtained by different stressing (quasi-static to dynamic) techniques at room temperature
- Table 4.2:  $F_c$  as a function of stressing rate for deionised water at 25 °C
- Table 5.1: Tensile strength and viscosity data for 10W monograde oil at various temperature under dynamic stressing with width gap  $D = 3.9$  cm
- Table 5.2: Tensile strength and viscosity data for 40 Diesel monograde oil at various temperature under dynamic stressing with width gap  $D = 3.9$  cm
- Table 5.3: Tensile strength and viscosity data for 10W-40 Diesel multigrade oil at various temperature under dynamic stressing with width gap  $D = 3.9$  cm
- Table 5.4: Tensile strength and viscosity data for 15W-40 Diesel multigrade oil at various temperature under dynamic stressing with width gap  $D = 3.9$  cm
- Table 5.5: Tensile strength data for 10W; API CC at various temperature and rate of dynamic stressing
- Table 5.6: Tensile strength data for 40 Diesel; API CC at various temperature and rate of dynamic stressing
- Table 5.7: Tensile strength data for 10W-40 Diesel; API CF at various temperature and rate of dynamic stressing
- Table 5.8: Tensile strength data for 15W-40 Diesel; API CF at various temperature and rate of dynamic stressing
- Table 6.1: Differences in physical properties between heavy water and ordinary water
- Table 6.2: Results obtained from experiments involving a range of sealing temperatures

# List of Figures

- Figure 1.1: Pressure distribution in convergent-divergent lubricating film
- Figure 1.2: Diagram of pressure against specific volume (Brennen, 1995)
- Figure 1.3: The van der Waals equation (Trevena, 1987)
- Figure 1.4: Results of a numerical integration of equation (1.5) illustrating the response of a cavity nucleus (initially at rest) to a pressure-tension cycle generated in the experiments. The resulting change in cavity radius involves several oscillatory cycles, of gradually diminishing amplitude and period (Williams and Williams, 2002)
- Figure 1.5: Berthelot tube experiment
- Figure 1.6: General Shape of (pressure, temperature) curve for water in a steel Berthelot tube (Chapman *et al*, 1975)
- Figure 1.7: Breaking tension as a function of temperature for water (Briggs, 1950)
- Figure 1.8: Improved Tube-Arrest tube Apparatus (Williams *et al*, 1996)
- Figure 1.9: Explanatory sketch of cyclic pressure record (after Overton and Trevena, 1981)
- Figure 1.10: Sketch showing main features of water shock tube (Richards *et al*, 1980)
- 
- Figure 2.1: Schematic diagram of the early form of bullet-piston apparatus (Trevena, 1987).
- Figure 2.2: (F, P) graph used to estimate the maximum tensile strength,  $F_c$ , of a liquid by Couzen and Trevena (1974).
- Figure 2.3: Results of experiments on degassed, deionised water. The pressure-tension cycles were recorded using the Kistler-type 603B at different sampling rates of 1 MHz, 10 kHz and 5 kHz.
- Figure 2.4: (a) Reflection of pressure pulse at the free surface of liquid column (as a fixed wall) (at the left) (b) Reflection of tension pulse at the base of liquid column (as a free end) (at the right).

Figure 2.5: Details of first pressure-tension cycle recorded in experiments on water by three dynamic pressure transducers in different locations along the B-P apparatus.

---

Figure 3.1: Overall descriptions of B-P experiment

Figure 3.2: The Bullet-Piston Apparatus (with heating jacket removed)

Figure 3.3: The magnum model 7000 cattle stun gun

Figure 3.4: Schematic of heating /cooling system

Figure 3.5: The Kistler 603B pressure transducer

Figure 3.6: GageScope data acquisition system: A typical pressure record obtained from a 603B transducer in an experiment on degassed, deionised water. The output voltages of the pressure transducer (Kistler 603B) were sampled at sampling rate at 1 MHz and 1,000,000 sampling points then fed into the GageScope C1610, 12 bit analogue to digital converter with 2 MB memory buffer

Figure 3.7: The signal processing software, Dadisp 4.0

Figure 3.8: Results of experiments on degassed, deionised water. The expanded, raw pressure-tension cycle was recorded using the Kistler 603B at a sampling rate of 1MHz with 1,000, 000 sample points.

Figure 3.9: Before removal of frequency spectrum

Figure 3.10: After removal of frequency Spectrum

Figure 3.11: Results of experiments on degassed, deionised water. The filtered pressure-tension cycle was obtained

Figure 3.12: Expanded pressure record obtained from a 603B transducer showing the time intervals  $\tau_i$  and  $\tau_0$

Figure 3.13: The time interval,  $\tau_i$  as a function of applied static pressure,  $P_s$  (in p.s.i.) for degassed, deionised water at 20 °C. Also shown is the value of the time interval,  $\tau_0$  used to estimate  $F_c$  (Williams and Williams, 2002)

Figure 3.14: Details of first pressure-tension cycle produced by the bullet striking to the bottom piston and the first pressure-tension pulse arising from the cavitation bubble collapse recorded in experiments on water by three dynamic transducers in different locations along the B-P apparatus

---

Figure 4.1: Pressure record showing the initial and reflected pulses produced by the piston (1-2) and the subsequent pressure-tension cycles (3-4), (5-6), (7-8) and etc generated by cavitation activity in experiments on water

Figure 4.2: The time interval,  $\tau_i$ , as a function of applied static pressure (in p.s.i) with four different stressing rates subjected to deionised water at 25 °C

Figure 4.3: ‘Primary’ pressure-tension cycles for degassed, deionised water at 25 °C for four different gap widths D ( $F_c = 224$  bar, D = 3.7 cm;  $F_c = 168$  bar, D = 3.9 cm ;  $F_c = 110$  bar, D = 4 cm ;  $F_c = 60$  bar, D = 4.2 cm)

Figure 4.4: Determination of  $\dot{\Omega}_r$  using a mean gradient approach from ‘primary’ tension pulse (#2 in figure 4.1) for D = 3.7 cm

Figure 4.5:  $F_c$  as a function of stressing rate on the water at 25 °C

---

Figure 5.1: Positive and negative pressure experienced by continuous, incompressible lubricating fluid flow through a journal bearing (from Dowson and Taylor, 1979)

Figure 5.2: ‘Primary’ pressure-tension cycles for SAE 10W-40 Diesel oil at two temperatures, 25 °C and 110 °C

Figure 5.3:  $F_c$  as a function of temperature for monograde (10W, 40 Diesel) and multigrade (10W-40 Diesel, 15W-40 Diesel)

Figure 5.4: Shear viscosity as a function of temperature for monograde (10W, 40 Diesel) and multigrade (10W-40 Diesel, 15W-40 Diesel) oils. These shear viscosities of the four types of engine oils were measured by ARES controlled-strain Rheometer (Rheometric Sci., USA)

Figure 5.5:  $F_c$  as a function of viscosity for various engine oils for constant gap, 3.9 cm widths D.

- Figure 5.6:  $F_c$  as a function of viscosity for 15W-40 Diesel multigrade oil for four gap widths D
- Figure 5.7:  $F_c$  as a function of viscosity for 40 Diesel monograde oil for four gap widths D
- Figure 5.8:  $F_c$  as a function of shear viscosity,  $\mu$  for four engine oils (10W, 40 Diesel, 10W-40 Diesel and 15W-40 Diesel) over the temperatures ( $25\text{ }^\circ\text{C} \leq T \leq 110\text{ }^\circ\text{C}$ ) for constant gap, 3.9 cm widths D
- Figure 5.9: The average speed of pulse produced by a bullet striking to the piston travels up the liquid column within the tube then return to the lower transducer's location over a wide range of temperature.
- Figure 5.10: Expanded series of 'prime' pressure-tension records obtained from different temperatures of experiments ( $25\text{ }^\circ\text{C} \leq T \leq 110\text{ }^\circ\text{C}$ ) with the constant gap, D = 3.9 cm
- Figure 5.11: Expanded series of 'prime' pressure-tension cycle at  $25\text{ }^\circ\text{C}$  records for 10W-40 Diesel oil for four gap widths D ( $F_c = 203\text{ bar}$ , D = 3.7 cm;  $F_c = 188\text{ bar}$ , D = 3.9 cm;  $F_c = 183\text{ bar}$ , D = 4.1 cm;  $F_c = 175\text{ bar}$ , D = 4.2 cm)
- Figure 5.12: The time delay,  $\tau_i$  as a function of applied static pressure  $P_s$  (in p.s.i) for SAE 10W-40 Diesel oil at  $25\text{ }^\circ\text{C}$  with two different gap widths D ( $F_c = 203\text{ bar}$ , D = 3.7 cm;  $F_c = 175\text{ bar}$ , D = 4.2 cm)
- Figure 5.13: Expanded series of 'prime' pressure-tension cycle at  $110\text{ }^\circ\text{C}$  records for 10W-40 Diesel oil for four gap widths D ( $F_c = 171\text{ bar}$ , D = 3.7 cm;  $F_c = 165\text{ bar}$ , D = 3.9 cm;  $F_c = 153\text{ bar}$ , D = 4.1 cm;  $F_c = 152\text{ bar}$ , D = 4.2 cm)
- Figure 5.14: The time delay,  $\tau_i$  as a function of applied static pressure  $P_s$  (in p.s.i) for SAE 10W-40 Diesel oil at  $110\text{ }^\circ\text{C}$  with two different gap widths D ( $F_c = 171\text{ bar}$ , D = 3.7 cm;  $F_c = 152\text{ bar}$ , D = 4.2 cm)
- Figure 5.15:  $F_c$  as a function of  $\dot{\Omega}_r$  for 10W oils over the temperature range  $25\text{ }^\circ\text{C} \leq T \leq 110\text{ }^\circ\text{C}$
- Figure 5.16:  $F_c$  as a function of  $\dot{\Omega}_r$  for 40 Diesel oils over the temperature range  $25\text{ }^\circ\text{C} \leq T \leq 110\text{ }^\circ\text{C}$
- Figure 5.17:  $F_c$  as a function of  $\dot{\Omega}_r$  for 10W-40 Diesel oils over the temperature range  $25\text{ }^\circ\text{C} \leq T \leq 110\text{ }^\circ\text{C}$
- Figure 5.18:  $F_c$  as a function of  $\dot{\Omega}_r$  for 15W-40 Diesel oils over the temperature range  $25\text{ }^\circ\text{C} \leq T \leq 110\text{ }^\circ\text{C}$



Figure 5.19:  $F_c$  as a function of  $\dot{\Omega}_r$ , for 10W and 40 Diesel monograde oils and 10W-40 Diesel and 15W-40 Diesel multigrade oils over the temperature range  $25\text{ }^\circ\text{C} \leq T \leq 110\text{ }^\circ\text{C}$

Figure 5.20: The effect of polymer concentration, PAA on tensile strength of water under dynamic stressing with a constant gap,  $D = 4.1\text{ cm}$  at  $25\text{ }^\circ\text{C}$

-----  
Figure 6.1: Phase diagram for water

Figure 6.2: Head of tension manometer modified, by bending, to allow supercooled of water under tension (after Hayward (1971))

Figure 6.3: The Berthelot-Bourdon tube and its (P, T) curve for water under tension (from Henderson and Speedy, 1980)

Figure 6.4: Images from a high speed video sequence showing nucleation and propagation of ice from d-m water in a 10 cm long NMR sample tube adapted to function as a 'Berthelot tube' (Rogers, 2004). (i) A cavitation bubble grows from the tube wall (*bottom right*) following tensile failure of the liquid at *ca.*  $-40\text{ bar}$ . As a result of the induced hydrodynamic pressure changes around the bubble it becomes encapsulated by a 'shell' of ice. (ii) The ice shell, formed in a wave of negative pressure, provides a new nucleating surface for subsequent bubble growth and the ice 'front' propagates through the supercooled water ( $-18\text{ }^\circ\text{C}$ ) by further bubble growth-freezing cycles. (iii) The process continues, at speeds commensurate with cavitation bubble growth but far more quickly than allowed by the free crystal growth rate. The tube is filled with an ice-air mixture in  $< 1\text{ second}$

Figure 6.5: Hillig's experimental results for the ice front velocity,  $v$ , as a function of the degree of supercooling for ice formation in a glass tube (line 1 is for imperfect crystal formation and line 2 is for perfect crystal formation) (from the chemical physics of ice, 1970)

Figure 6.6: Density against temperature curve for water under pressure and tension in the Berthelot tube experiments

Figure 6.7: Photograph of various lengths of the blue capped modified Berthelot tubes

Figure 6.8: Photograph of yellow capped modified Berthelot tubes

Figure 6.9: Five (pressure, temperature) curves for water under tension in the Berthelot tube experiments (Jones *et al*, 1981)

- Figure 6.10: High-speed images (captured at 24,000 fps) of the initial formation, growth and collapse of a single cavitation bubble in degassed heavy water ( $D_2O$ ) in an improved Berthelot tube (inner diameter 7 mm)
- Figure 6.11: High-speed images (captured at 24,000 fps) of the initial formation, growth and collapse of a single cavitation bubble in degassed heavy water ( $D_2O$ ) in an improved Berthelot tube (inner diameter 7 mm)
- Figure 6.12: High-speed images (captured at 24,000 fps) of the initial formation, growth and collapse of a single cavitation bubble in undegassed heavy water ( $D_2O$ ) in an improved Berthelot tube (inner diameter 7 mm)
- Figure 6.13: High-speed images were captured at 24,000 f.p.s shown that the initial formation of single, spherical cavity, apparently growing not from the PTFE walls, but in the body of a liquid. After the bubble collapse begins a liquid jet forms, the jet being directed towards the end of the tube
- Figure 6.14: The calculated average diameter of oscillating bubble as a function of elapsed time
- Figure 6.15: Twelve frames captured during ice formation in degassed heavy water contained in an improved Berthelot tube
- Figure 6.16: Twelve frames captured during ice formation after cavitation event took place contained in an improved Berthelot tube. In frame 8-9, three phases which are liquid, solid and vapour states coexists together in the deionised, degassed and boiled water at  $-19.5\text{ }^\circ\text{C}$  and unknown pressure
- Figure 6.17: Superheated ice produced from doubly metastable water in the improved Berthelot tube at  $-8.0\text{ }^\circ\text{C}$ . The high-speed video system was operating at 500 frames per second (f.p.s). The velocity of the ice front was  $2.78\text{ cms}^{-1}$
- Figure 6.18: Superheated ice produced from doubly metastable water in the improved Berthelot tube at  $-10\text{ }^\circ\text{C}$ . The high-speed video system was operating at 500 frames per second (f.p.s). The velocity of the ice front was  $5.62\text{ cms}^{-1}$
- Figure 6.19: Superheated ice produced from doubly metastable water in the improved Berthelot tube at  $-12\text{ }^\circ\text{C}$ . The high-speed video system was operating at 500 frames per second (f.p.s). The velocity of the ice front was  $7.03\text{ cms}^{-1}$
- Figure 6.20: Experimental results for the ice front velocity,  $v$ , as a function of the degree of supercooling for the ice formation in the modified Berthelot tube

Figure 6.21: Superheated ices produced from doubly metastable orange squash in the improved Berthelot tube at  $-12\text{ }^{\circ}\text{C}$ . The high-speed video system was operating at 500 frames per second (f.p.s). The velocity of the ice formation is  $2.78\text{ cms}^{-1}$

Figure 6.22: Superheated ices produced from doubly metastable orange squash in the improved Berthelot tube at  $-12\text{ }^{\circ}\text{C}$ . The high-speed video system was operating at 500 frames per second (f.p.s). The velocity of the ice formation is  $3.29\text{ cms}^{-1}$

# *Chapter 1*

## *Introduction and literature survey*

- 1.1 Background of Cavitation*
- 1.2 Historical Developments in the field*
- 1.3 Some Process Involving Cavitation*
- 1.4 Basic Theoretical Aspects of the Liquid State*
- 1.5 Experimental Techniques for Measurement of Liquid  
Tensile Strength*

## 1.1 Background of Cavitation

It has long been known that, under suitable conditions, liquids are capable of sustaining considerable tension or 'negative pressure' (Trevena, 1987). While under tension, the liquid is in a metastable state and, if tension exceeds its critical point, it changes irreversibly to the two phase systems which are liquid and vapour phase plus dissolved gas (Temperley and Chamber, 1946). Numerous experimental studies have shown that a liquid can stay under tension outside the stability region in its phase for periods of seconds, even hours (Trevena, 1987). In practice, any liquid can be prepared in a metastable state with respect to its vapour into two ways: the first involves superheating it above its boiling temperature; and the second involves stretching it (i.e. subjecting it to tension) below its saturated vapour pressure. For example, liquid water can be superheated up to 280°C at atmospheric pressure (Apfel, 1972) and it is also able to 'stretch' or withstand negative pressure up to -1400 bar, a remarkably large value (Zheng *et al*, 1991). Above this 'critical' value the liquid undergoes cavitation, a term which refers to the formation, growth and subsequent collapse of bubbles (or 'cavities') which may contain the vapour of the liquid or permanent gas or a mixture of both, within the liquid. The ability of liquids to withstand tension (which involves their effective tensile strength, denoted  $F_c$ ) is a topic of considerable importance in a number of disciplines in pure, applied science, and industrial applications. It is these applied areas in which cavitation has most bearing on everyday life engineers and marine architects must have an appreciation of the effects of cavitation on hydraulic machinery and ships propellers while the cavitation properties of the liquid coolant can play a large part in the design and safety of fast nuclear reactors.

It is important to understand that there are many different types of cavitation. The term 'cavitation' usually refers to the formation of bubbles in the liquid when it experiences 'negative pressure' (or tension), subsequently these cavitation bubbles collapse resulting in a tremendous "local" force which can cause cavitation damage, sonoluminescence, noise, vibration and loss of performance of hydraulic machines (Hickling, 1994). Two basic forms of cavitation in lubricating films are recognised: *gaseous* and *vapourous*. For gaseous cavitation, gas-filled bubbles expand by diffusion from the liquid when the pressure of a liquid falls below its saturated

pressure. If the pressure in a liquid further falls to its vapour pressure, the liquid may boil at ambient temperature, vapour-filled cavities will be formed and these may later collapse, causing cavitation erosion, this is called vaporous cavitation (Dowson and Taylor, 1979).

*Travelling cavitation* occurs when cavities or bubbles form in the liquid, and travel with the liquid as they expand and subsequently collapse. *Fixed cavitation* occurs when a cavity or pocket attached to the rigid boundary of an immersed body or a flow passage forms, and remains fixed in position in an unsteady state. *Vortex cavitation* occurs in the cores of vortices which form in regions of high shear, and often occurs on the blade tips of ship's propellers (hence the additional name "*tip*" cavitation). For *acoustic cavitation*, in a non-flowing system, the ambient pressure can be varied by sending sound waves through the liquid. If the amplitude of the pressure variation is great enough to bring the pressure locally down to, or below, the vapour pressure in the negative parts of the sound cycle traversing the liquid, any minute cavities or bubbles (or their growth from preexisting nuclei) will grow.

In '*stable cavitation*' the bubble's growth rate during the acoustic rarefaction phase is equivalent to its contraction rate during the compression phase. Such bubbles may oscillate around a mean radius for many acoustic cycles whereas the phenomenon of '*transient cavitation*' exists for only a few cavity cycles, during which time they grow several times larger than their initial size. Their eventual collapse may produce extreme intra-cavity temperatures and pressures. Transient cavitation provides the relatively violent activity usually required in processes such as industrial ultrasonic cleaning, the dispersion of solid particles in liquids, cell disruption and the destruction of microbes. In *optic cavitation* and *particle cavitation* is produced by high intensity (laser) light and any other type of elementary particles (e.g. a proton) rupturing in a liquid. These types of cavitation are achieved by deposition of energy into a limited volume.

## 1.2 Historical Developments in the Field

In 1846, Donny showed that it was possible for a liquid at rest (distinct from a liquid in motion) to sustain tension by using a U-tube apparatus. Berthelot (1850) also

showed that liquids can withstand tension in a sealed tube of the order of tens of atmosphere before it cavitates (Trevena, 1980). A J-tube centrifugal method of applying tension to a liquid was used by Osborne Reynolds who proceeded to describe the first cavitation phenomena in water flowing through a tube with a local constriction. In accordance with Bernoulli's Law, a region of lower pressure is formed in the narrow part of the tube. If the rate of flow is sufficiently great, the pressure falls to a vapour pressure which causes the boiling of the water in a narrow cross section of the tube (Reynolds, 1895). A year later, the word cavitation was first suggested by R.E. Froude, a naval architect, after extensive tests carried out on a navy destroyer revealed that the propellers were not developing enough thrust at high speeds due to the voids and bubbles they created (cavitation) when the local pressure of the liquids dropped below its vapour pressure at the blades. A serious consequence was that the propellers were thereby damaged, making them inoperative after a few hours use. This phenomenon of 'cavitation damage' has been studied intensively ever since, with a notable contribution from Lord Rayleigh whose seminal analysis of the pressures generated by the collapse of a single bubble has proved a significant foundation for later work (Rayleigh, 1917).

### **1.3 Some Processes Involving Cavitation**

In engineering, it was the occurrence of cavitation in hydraulic machinery (Euler, 1754) that prompted research effort into this subject but cavitation is also recognised as an important aspect of some biological processes. Liquids (as sap) in xylem sustain a significant tension in order to transport water from the roots of a tree to the uppermost leaves (Pockman *et al*, 1995). Dixon and Joly (1895) first suggested the way in which the sap can be drawn up to great height is by the existence of a negative pressure in the sap column. The cohesion-tension (C-T) theory explains water transport from the roots of tall trees to the leaves (Tyree, 1997). The transpiration of water from the surfaces of the leaves draws the sap to the full height of the tree. A vacuum pump cannot pull a column of water beyond a height of 33 feet, corresponding to a pressure of one atmosphere. Since many trees are much taller than 33 feet it is argued that there must be a negative pressure in the column that transports the sap. The C-T theory assumes that water, when confined in small tubes with

wettable walls such as xylem elements, can sustain a tension ranging from 3 to 30 MPa.

In the animal world, negative pressure can be generated by an octopus under its liquid-filled suckers. The values of this pressure can be in the 0 to -3 bar range, causing a substantial pressure difference between the inner and outer side of its victim, thus cavitation, the failure of water in tension, may limit the attachment force of suckers (Smith, 1991).

In biomedicine, the cracking of joints is a well known phenomenon, especially in the knee and the knuckle. By suddenly pulling on a 'biological bearing', the lubricant (synovial fluid) within it may be suddenly stretched and subsequently relax by cavitation. The consequent emission of an audible 'crack' has been related to the synovial fluid being no longer able to sustain tension during the joint separation. The resulting vapour bubble collapse being deemed responsible for the accompanying sound (Unsworth *et al*, 1971).

In modern medicine the application of ultrasound scanning has grown apace, fuelled by improved image definition from more powerful sensors and increasingly sophisticated sensory information processing. Recent advances in these areas have led to the development of 3-D scanners such as ultrasonography whose introduction can be expected to stimulate further application of the technique. In addition, low frequencies high-power ultrasound is a recent addition to the list of methods for dissolution of intracoronary plaques and thrombi. When sufficient power is applied, ultrasound pressure waves in liquids cause the formation of cavities, which then implode, sending jets of liquid and shockwave against nearly solid surfaces (Rosenschein and Rassin, 1998). On the other hand, focused acoustic shock waves can break up large kidney stones into smaller pieces that can pass safely through the body and high-intensity focused ultrasound has been used to destroy tissue deep inside the body, opening for non-invasive and bloodless surgery (Cleveland and Crum, 1997). Despite its evident diagnostic and therapeutic benefits, reservations remain concerning ultrasound's ability to trigger health-damaging mechanisms, among which is cavitation of body fluids. Certain low reported values of  $F_c$  are



therefore disquieting due to the fact that some biomedical application of ultrasound can involve transient tension *in vivo* of *ca* 40 bar (Marston and Unger, 1986).

Elsewhere, as in engineering processes such as printing and coating, the tensile strength of a liquid is relevant to printing processes which involve the ‘tack’ of an ink – the maximum tensile stress developed in the splitting of ink films at a printing nip exit, where ink is subjected to an extensional flow in the direction normal to the roller surfaces (Zang, 1991). In lubrication, cavitation also occurs in dynamic journal bearings when the negative pressures in the lubricants drop below its saturated pressure or vapour pressure at the divergent section of wedge-shaped oil films in bearings, giving rise to gaseous or vaporous cavitation. Cavitation has been associated with bearing damage in internal combustion engines, but cavitation does not necessarily have a deleterious effect upon the load-carrying capacity of fluid-film bearings. If the film does not rupture, then the load capacity is zero since the convergent and divergent regions of the film make equal and opposite contributions. Gas releases ensures that the pressure in the divergent section close to the saturation pressure, with a net force normal to the surfaces. In this case the load-carrying capacity results from film rupture (see figure 1.1) (Dowson and Taylor, 1979). It follows that the effective tensile strength of an oil is an important consideration in the assessment of flow boundary conditions, loading bearing capacity and cavitation damage potential.

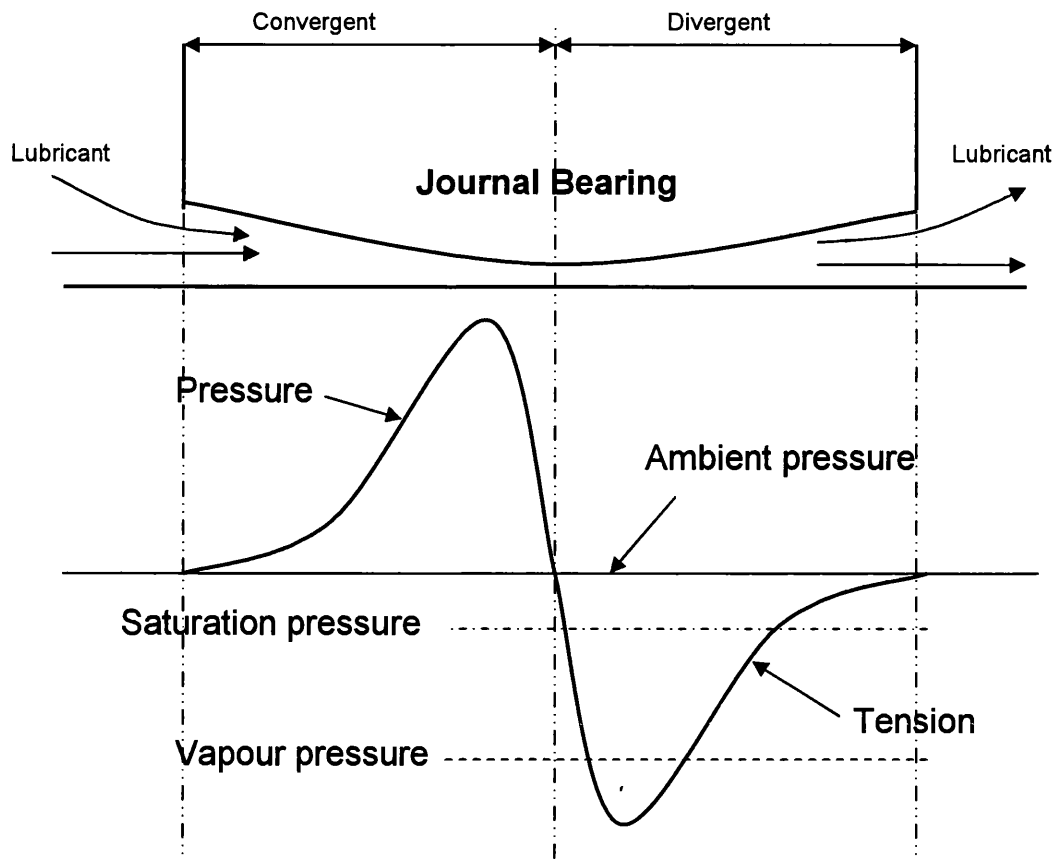


Figure 1.1 Pressure distribution in convergent-divergent lubricating film

#### 1.4 Basic Theoretical Aspects of the Liquid State

Figure 1.2 shows a representation of the phase diagram of pressure,  $P$  and specific volume,  $V$ . The transition from liquid state to the vapour state (and vice-versa) takes place along a horizontal isotherm (solid line, figure 1.2) not along a theoretical isotherm (dashed line, figure 1.2) due to the splitting up of the original homogenous substance in two different coexisting phases (Frenkel, 1955). The critical point is that point at which the maxima and minima in the theoretical isotherm vanish and the discontinuity disappears.

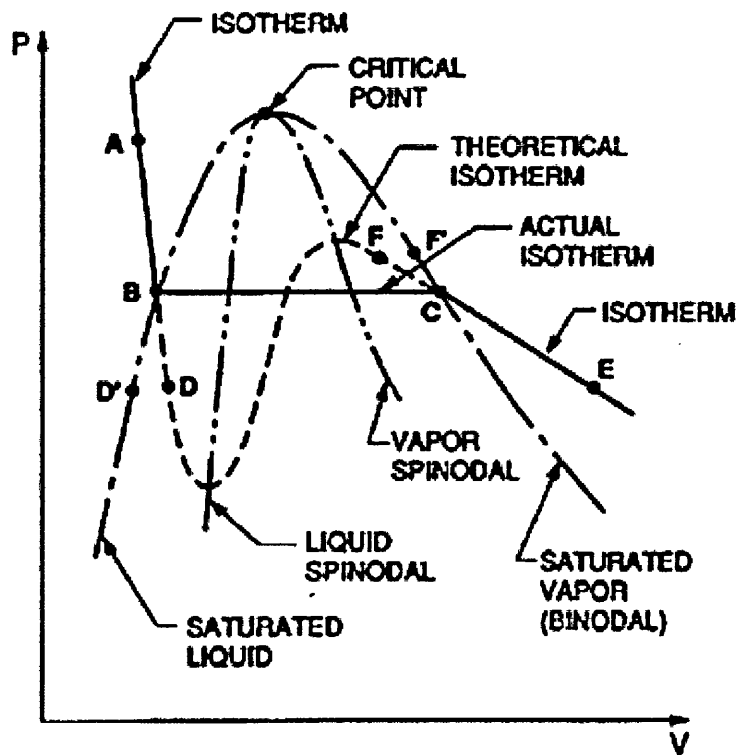


Figure 1.2 Diagram of pressure against specific volume (Brennen, 1995)

The line joining the maxima in the theoretical isotherms is called the vapour spinodal line; the line joining the minima is called the liquid spinodal line. Clearly both spinodals end at the critical point. The two regions between the spinodal lines and the saturated (or binodal) lines are of particular interest because the conditions represented by the theoretical isotherm within these regions can be realized in practice under certain special conditions, where the boundary between metastable and unstable states, the limit of metastability of the system.

Following Brennen (1995) we note that if, for example, a pure liquid at the state A (Figure 1.2) is depressurized at constant temperature, then several things may happen when the pressure is reduced below that of point B (the saturated vapour pressure). If sufficient numbers of nucleation sites of sufficient size are present, the liquid will become vapour as the state moves horizontally from B to C, and at pressure below the vapour pressure the state will come to equilibrium in the gaseous region at a point such as E. However, if no nucleation sites are present, the depressurization may lead to continuation of the state down the theoretical isotherm to a point such as D, called a

“metastable state” since imperfections may lead to instability and transition to the point E. A liquid at a point such as D is said to be in tension, the pressure difference between B and D being the magnitude of the tension. Of course one could also reach a point like D by proceeding along an isobar from a point such as D' by increasing the temperature. Then an equivalent description of the state at D is to call it superheated and to refer to the difference between the temperatures at D and D' as the superheat. In an analogous way one can visualize cooling or pressurizing a vapour that is initially at a state such as F and proceeding to a metastable state such as F' where the temperature difference between F and F' is the degree of subcooling of the vapour (Brennen, 1995).

#### **1.4.1 Theoretical Estimates of Liquid Tensile Strength: Homogeneous Nucleation**

When a liquid is depressed below its saturated vapour pressure, it is expected to transform into its vapour. However, if care is taken to use a very pure liquid in a very clean condition, cavitation may occur only far beyond the line of thermodynamical equilibrium, hence the liquid is subjected to a mechanical tension (Herbert and Caupin, 2005). In other words, a homogeneous liquid can withstand a substantial tensile stress before it cavitates and this ability of a liquid to withstand tensile stress represents the effective tensile strength,  $F_c$ , of the liquid at that temperature. Theory predicts that vapour bubbles will only form in pure liquids as a result of very large tensions, some 1.3-1.4 kbar in the case of water (Fisher, 1948) and even higher negative pressure of  $\sim 1.9$  kbar was found from an interpretation of the thermodynamic properties of stretched water known as the stability limit conjecture (Speedy, 1982).

Zheng *et al* (1991) has reported studies based on a version of the Berthelot method based on a synthetic water inclusion in quartz. A quartz crystal with a microscopic crack is autoclaved in the presence of liquid water. Water fills the crack which then heals at high temperature, thus providing low density water in a small Berthelot tube involving small quantities of pure water ( $20 \mu\text{m}^3$ ). The bubble remaining in the inclusion disappears upon heating, then the sample is cooled down, liquid water

follows a nearly isochoric path, until cavitation occurs. The tensions induced in this water are reportedly close to the homogeneous nucleation limit of 1.4 kbar at 43 °C; in good agreement with Fisher's 1948 vapour nucleation theory. Further improved work on inclusion deals with the use of Brillouin scattering to measure the sound velocity in stretched liquid water reported by Alvarenga *et al* (1993) produced negative pressures as high as 1000 bar at 20 °C before a vapour bubble nucleated.

Theoretical values of  $F_c$  were obtained by Temperley (1947) who assumed that the liquid obeys the van der Waals equation of state (essentially a 'gas-like' approach to liquids, ignoring the non-linearity of the molecule, and complexities of dipole-dipole forces and hydrogen bonds). Temperley (1947) argued that almost any law of intermolecular force between molecules leads to a van der Waals type expression as a first approximation where

$$\left(p + \frac{a}{V^2}\right)(V - b) = RT \quad (1.1)$$

(For one mole of substance) This equation predicts a discontinuous change of state for any region for which  $\left(\frac{\partial P}{\partial V}\right)_T$  is positive (such as portion BC of figure 1.3). The phase change from liquid to vapour or vice-versa normally occurs along the dotted line AD and not the curve ABCD according to the 'rule of equal areas'. But a liquid under tension is in a metastable state, and under certain circumstances the pressure may be reduced below the value at A and still maintain the liquid state. Temperley showed that this was possible, provided the temperature  $T < T_m$  where  $T_m = 27T_c/32$  where  $T_c$  is the critical temperature i.e. where  $\left(\frac{\partial P}{\partial V}\right)_T$  is still negative as in portion AB of Figure 1.3. Clearly then the point B represents the ultimate tensile strength of the liquid at that temperature. At this point,  $\left(\frac{\partial P}{\partial V}\right)_T = 0$  and, differentiating equation with respect to  $V$  and substituting  $\frac{dP}{dV} = 0$  gives the value of the ultimate tensile strength (suitable value of  $a$  and  $b$  being used and  $T$  chosen as room temperature). Thus Temperley (1947) derived a value of ca. 500-1000 bar for the theoretical tensile strength of water at room temperature.

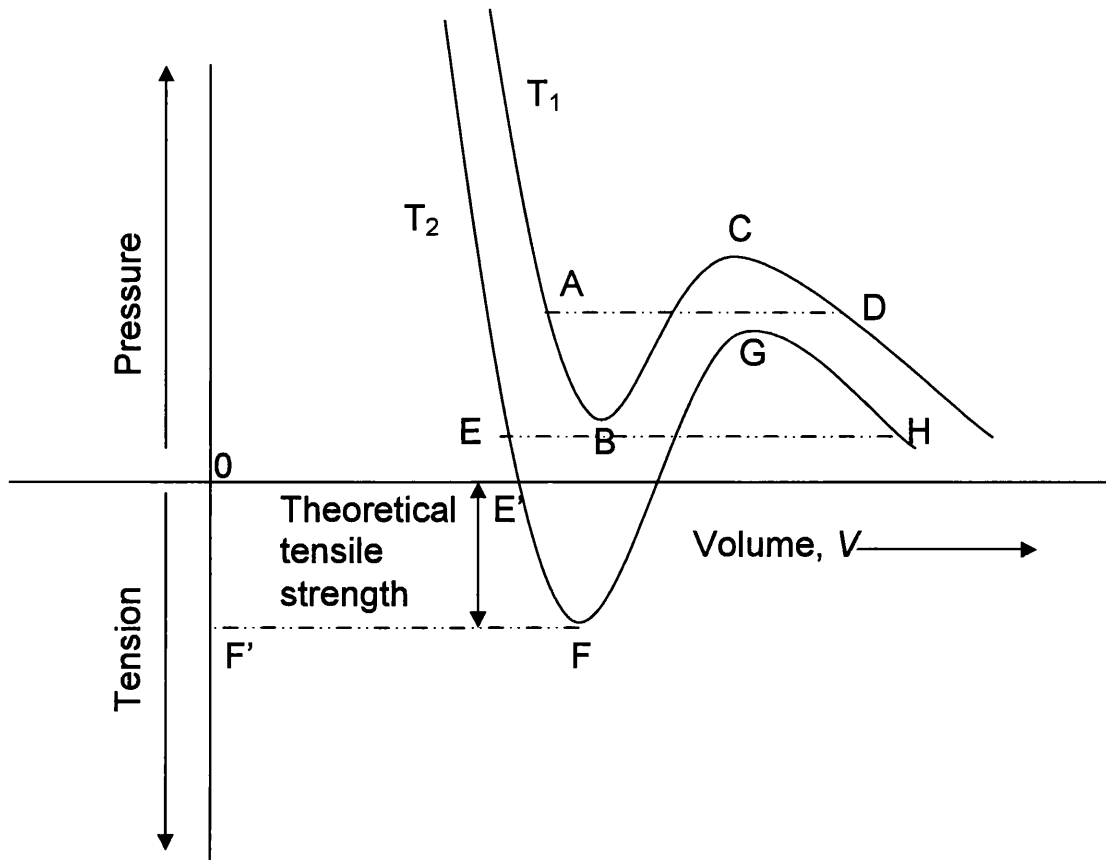


Figure 1.3 The van der Waals equation (Trevena, 1987)

#### 1.4.2 Experimental Measurements of Tensile Strength: Heterogeneous Nucleation

In practical measurements of the tensile strength of liquids, the purity of the liquid, the properties of the solid surfaces of the container, and the presence of small particles suspended in the liquids are very important factors. When heterogeneous nucleation occurs at such a tiny microscopic size contaminant particles such as motes of dirt or dust in the liquids, it is very difficult to distinguish from homogeneous nucleation. Nuclei represent 'holes' in the liquid that grow into macroscopic bubbles (Frenkel, 1955). Thus, in practice, liquids contain nuclei or impurities that greatly lower the breaking tension thus making estimations of the breaking tension very difficult to obtain a consistent, repeatable tensile strength of liquids. Results obtained experimentally for the breaking tensions of liquids in Berthelot tube exhibit a large

scatter in the breaking tensions of any given sample due to the role of surface nucleation sites which provides a possible mechanism to explain this larger scatter (Overton and Trevena, 1980). Therefore, nuclei in the liquid can considerably lower the tensile strength of a liquid help to explain the large differences that exist between theoretically predicted values for the breaking tensions and those obtained experimentally. Indeed, values predicted by theoretical means are usually at least one order of magnitude large than corresponding experimental results. On theoretical grounds, the value of tensile strength of water is enormous since this would imply a minimum tension needed to rupture is equal to the cohesion or intrinsic pressure,  $\frac{a}{V^2}$  in the van der Waals equation (refer to equation 1.1), which is of the order of 10,000 bar (Temperley and Chamber, 1946). However, cavitation experiments using water as the test liquid usually result in breaking tensions in the range of 10 – 270 bar.

It is important to recall that cavitation is initiated in a liquid at a suitable nucleus when the pressure is reduced to a sufficiently low value. It is thought that there are three types of such nuclei. In the first type a liquid may contain a large number of minute spherical gas (air) bubbles which are stabilised against gaseous diffusion by an immiscible skin of organic impurity such as fatty acid and/or protein; this would gradually thicken as the bubble decreased in size until eventually it become sufficiently rigid to inhibit any further shrinkage of the bubble, then the bubble said to be ‘stabilised’. At a later stage, the liquid is subjected to tension, the skin will be torn apart, gas will diffuse into the bubble and cavitation is initiated (Fox and Herzfeld, 1954; Hayward, 1970). The second type is envisaged in the so-called crevice theory, in which there may be solid particles (motes) in the water with gas trapped or stabilised in crevices in these particles (Harvey, 1944). In the third type, gas can be trapped in the tiny crevices in the wall of the vessel containing the liquid (Overton and Trevena, 1980).

Briggs’ centrifugal work, which produced an estimate of the tensile strength of water of 270 bar, emphasised the need for scrupulous cleanliness. In quasi-static Berthelot tube experiments, Overton and Trevena (1980) discuss the attributed failure of the liquid to gas trapped crevices in the walls of the tube which led to the wide scatter obtained in the tensile strength of water. The role of these ‘surface’ nuclei was evident

in the work of Jones *et al* (1981) in which a new modified Berthelot tube was able to evacuated first before introduction of the liquid. This procedure removed much of the gas from wall crevices with the result that far higher tension could be developed in the liquid before fracture. It is generally assumed that cavitation bubbles originate at microscopic bubbles nuclei, although the causes for premature nucleation have been isolated: indications are that cleanliness of the water and of any solid surface (wall of the container) in contact with it are primary importances. Later, by using the same design of modified Berthelot, Overton *et al* (1982) describe experiments in which water was degassed before introducing it into an evacuated tube. By this way, they achieved an 'all-time high' tensile strength for water in steel tube due to the gas nuclei in the water would be removed completely. Iyengar and Richardson (1958) used a focused beam of ultrasound at 442 kHz to cavitate a sample of water. Their results showed that by reducing the air content of water, the breaking tension increased. In addition, Greenspan and Tschiegg (1967) obtained breaking tensions up to 210 bar using filtered, triply distilled water, after thorough cleaning of the apparatus. The discrepancy between theoretical and experimental values of  $F_c$  may be understood by considering that, in experiments, what is actually being measured is the strength of the 'weakest link' in the system.

### 1.4.3 Cavitation Bubble Dynamics

Under the influence of tension, cavities grow from a suitable nucleus to its maximum radius but thereafter (usually as the bubble moves to region of higher pressure) it begins to collapse. It is the collapse phase which results in instances of cavitation damages but the precise details of the mechanism(s) by which this occurs are not yet completely understood.

The first attempt to develop a theory to explain cavitation damage was by Rayleigh (1917). Rayleigh's model treats the problem of a spherical, vapour-filled cavity collapsing under the influence of a steady pressure in the liquid at infinity. He showed that as the collapse nears completion, the inward velocity of the cavity wall and the pressure inside the liquid become indefinitely large. Neglecting surface tension and viscosity, he showed that the bubble boundary  $R(t)$  obeyed the relation



$$R\ddot{R} + \frac{3}{2}(\dot{R})^2 = \frac{p(R) - p_\infty}{\rho} \quad (1.2)$$

where  $\rho$  is the liquid density,  $P_\infty$  is the pressure in the liquid at a large distance from the bubble, and  $P(R)$  is the pressure in the liquid at the bubble boundary.

$$u(r,t) = \frac{R^2}{r^2} \dot{R} \quad (1.3)$$

From the general Bernoulli equation, the pressure in the liquid us found to be

$$p(r,t) = p_\infty + \frac{R}{r}[p(R) - p_\infty] + \frac{1}{2}\rho \frac{R}{r} \dot{R}^2 \left[1 - \left(\frac{R}{r}\right)^3\right] \quad (1.4)$$

where the pressure  $P_\infty$  is constant

Equation (1.2) may be extended to include the effects of surface tension,  $\sigma$  and viscosity,  $\mu$ . For a spherical bubble, viscosity effects only the boundary condition so that it becomes

$$p(R) = p_i - \frac{2\sigma}{R} - \frac{4\mu}{R} \dot{R} \quad (1.5)$$

where  $p_i$  is the pressure in the bubble. Plesset (1949) extended equation (1.2) by allowing  $P_\infty$  to be a function of time. Thus, the generalised Rayleigh equation may be written as

$$R\ddot{R} + \frac{3}{2}(\dot{R})^2 = \frac{1}{\rho} \left( p_i - p_\infty - \frac{2\sigma}{R} - \frac{4\mu}{R} \dot{R} \right) \quad (1.6)$$

This modified equation (1.6) includes the effects of surface tension,  $\sigma$  and shear viscosity,  $\mu$  and the pressure in the gas at the bubble wall  $p_i$  (and  $P_\infty$ ) may be a function of time (Plesset and Prosperetti, 1977). From figure 1.4 shows the results of an integration of equation (1.6) (using a fourth-order adaptive Runge-Kutta method) and this equation is describing the motion of a single cavity and showed how the cavity radius varies with time.

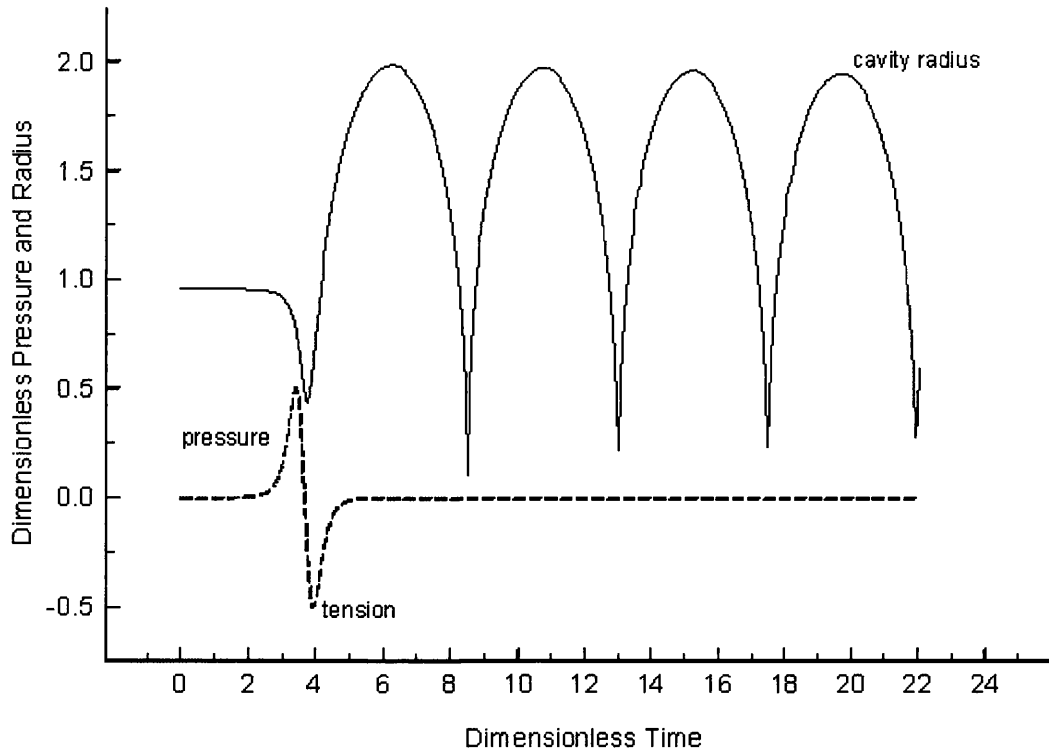


**Figure 1.4** Results of a numerical integration of equation (1.5) illustrating the response of a cavity nucleus (initially at rest) to a pressure-tension cycle generated in the experiments. The resulting change in cavity radius involves several oscillatory cycles, of gradually diminishing amplitude and period (Williams and Williams, 2002).

The change in cavity radius,  $R(t)$ , in response to the pressure-tension cycle involves a series of oscillatory cycles of bubble growth followed by rapid collapse and rebound, in which time is made dimensionless by the appropriate value of the ‘Rayleigh’ collapse time,  $\tau$  where

$$\tau = 0.915R_m \left( \frac{\rho}{p_0 - p_v} \right)^{0.5} \quad (1.7)$$

And the cavity radius is represented by  $\frac{R}{R_m}$  where  $R_m$  is the maximum radius of the cavity (note that the pressure  $p_0$  is atmospheric pressure).

The pressure-tension cycles induced by oscillation of the cavitation bubbles in the liquids have been studied and recorded by numerous workers including Chestermann (1952), Green and Mesler (1970), Overton and Trevena (1982) and Hentschel and Lauterborn (1982); and these have been explained in terms of the growth phase of oscillating cavities (assumed a spherical vapour-filled cavities) by Overton and

Trevena (1981), Williams and William (1996, 1997). High speed photographic studies have been employed to study the formation, growth and rebound of transient cavities. These cavitation experiments such as in dynamic stressing work, Fujikawa and Akamatsu (1978) and Chestermann (1952), quasi-static stressing work, Rogers (2003) and laser work, Lauterborn (1972); Lauterborn and Bolle (1975). In chapter six, high-speed photographic images will be first employed to study the cavitation bubble dynamics accompanying the tensile failure (or “cavitation”) in degassed heavy water (Deuterium oxide 99.9% atom %D) contained in the improved Berthelot tube.

#### 1.4.4 Cavitation Damage

The phenomenon of cavitation damage has been examined by scientists and engineers for a century or more. Components that have proved susceptible to cavitation erosion damage include pump impellers, valves, marine propellers, pipes, cylinder liner and other hydraulic machines. The study of bubble dynamics is essential to clarify the mechanism of the cavitation damage. The collapse phase of the bubbles can be extremely violent resulting in very high, localised pressure shock wave radiated and also due to asymmetrical pressure distribution across bubble causes high velocity liquid jet to form during collapse phase. Thus pressure shock waves and liquid jets associated with the collapse of the bubbles are thought to be responsible for the damage that occurs during cavitation with the impulsive pressure being generated mainly by a shock wave, by a liquid jet or by combination of the shock waves and liquid jets (Tomita *et al*, 1984; Tomita and Shima, 1986). Rayleigh (1917) theoretically pointed out the local high pressure in the final stage of bubble collapse is extremely high pressures (*ca.* 10, 000 bar) and radial velocities may be developed during bubble collapse, necessitating that the compressibility of the liquid be taken into accounts (Hickling, 1994). It is generally understood that cavitation damage is predominantly caused by impulsive pressure produced from collapsing bubbles (Knapps, 1955), later work, Hickling and Plesset (1964) using numerical solutions to modelling a flow in the vicinity of a collapsing spherical bubble in water and concluded that the shock wave does not form during the collapse phase but rebound phase of the cavitation bubble. However, Kornfled and Suvorov (1944) first pointed out that the liquid jet or water hammer, which produced from asymmetric collapse of an initial spherical vapour cavity, is a dominant factor in cavitation damage. Jet

behaviour has been studied by numerous investigators (Naude and Ellis (1961); Benjamin and Ellis (1966); Plesset and Chapman (1971); Lauterborn and Bolle (1975); Gibson and Blake (1982)). Naude and Ellis (1961) concluded that the liquid-jet impact is a major cause of damage on the basis of observations that a stress fringe is caused by jet impingement and that damage pits are much smaller than the minimum bubble base diameter. Shima *et al* (1983) experimentally studied the collapse of a spark-generated bubble near a solid wall and clarified that there are three regions where the impulsive pressure is generated mainly by a shock wave, by a liquid jet, and by cooperation of both a shock wave and a liquid jet. Furthermore, Tomita and Shima (1986) experimentally have shown that cavitation damage caused by the bubble shock-wave interaction essentially results from the impact pressure from a liquid microjet.

## **1.5 Experimental Techniques for Measurement of Liquid Tensile Strength, $F_c$**

At the outset it is important to note that estimates of the effective tensile strength of a liquid vary widely according to the type of techniques employed. The methods used to generate tension in measurements of  $F_c$ , fall (broadly) into two main categories, depending on the rate of stress development. In static (or, more properly, quasi-static) stressing experiments, tension develops gradually (over seconds, or more) whereas in dynamic stressing involves timescales (typically over microseconds to milliseconds range) and develops at enormous rates of  $1 \text{ bar}\mu\text{s}^{-1}$ , or more (Williams and Williams, 2000).

### **1.5.1 Static Stressing Technique**

There are several methods which have been used to stretch a liquid under ‘static’ conditions such as Berthelot tube, the centrifugal method and the tension manometer (that is, ‘negative barometer’) method.

#### **1.5.1.1 The Berthelot Tube Method**

The first studies of liquids under tension were conducted by Marcelin Berthelot (1850). His experiments were conducted under static stressing conditions in the

'Berthelot tube' which is a sealed cylindrical tube which, at room temperature  $T_0$ , is almost completely filled with a liquid while the remaining volume is occupied by air and liquid vapour (condition A, refer to figure 1.5 and 1.6). When the tube and its contents are heated the liquids expands at a greater rate than the Berthelot tube, the air is forced into solution and liquid fills the tube completely at a certain temperature  $T_f$  (condition B, refer to figure 1.5 and 1.6). If the tube is then cooled it is found that the liquid adheres to the whole of the inside wall of the tube and continues to fill it at temperatures below  $T_f$ . It follows that as the temperature falls below  $T_f$  a gradual increasing uniform tension is built up in the liquid (condition C, refer to figure 1.5 and 1.6), until it eventually ruptures at a lower temperature,  $T_b$  (breaking tension at point  $C_{max}$ , refer to figure 1.5 and 1.6). This instant of rupture is invariably accompanied by an audible metallic 'click' and also a sudden increase  $\Delta V$  in the external volume of the Berthelot tube due to the release of tension (Condition D, refer to figure 1.5 and 1.6).

There is considerable evidence that what is actually measured in the Berthelot-tube experiment is not actually the tensile failure of the liquid within itself, but a loss of adhesion between liquid and the wall of the tube (Temperley and Chambers, 1946). An important modification of the Berthelot tube experiment was made by Chapman *et al* (1975) who used an unbonded strain gauge pressure transducer, the diaphragm of which formed one of the sealed ends of the tube. They were thus able to measure pressure variations within the tube directly. Using this technique, Richards and Trevena (1976) were able to plot a family of (tension, pressure) curves for water (figure 1.6). A more comprehensive theory was derived by Williams and Trevena (1977) which made it possible to calculate the values of both the pressure and tension at *any* stage during a Berthelot tube experiment and not merely that of the breaking tension and their calculated values accord closely with the experimental values obtained by Richards and Trevena (1976). Other variants of the Berthelot tube technique have been described by Evans (1979), Meyer (1911) and Henderson and Speedy (1980).

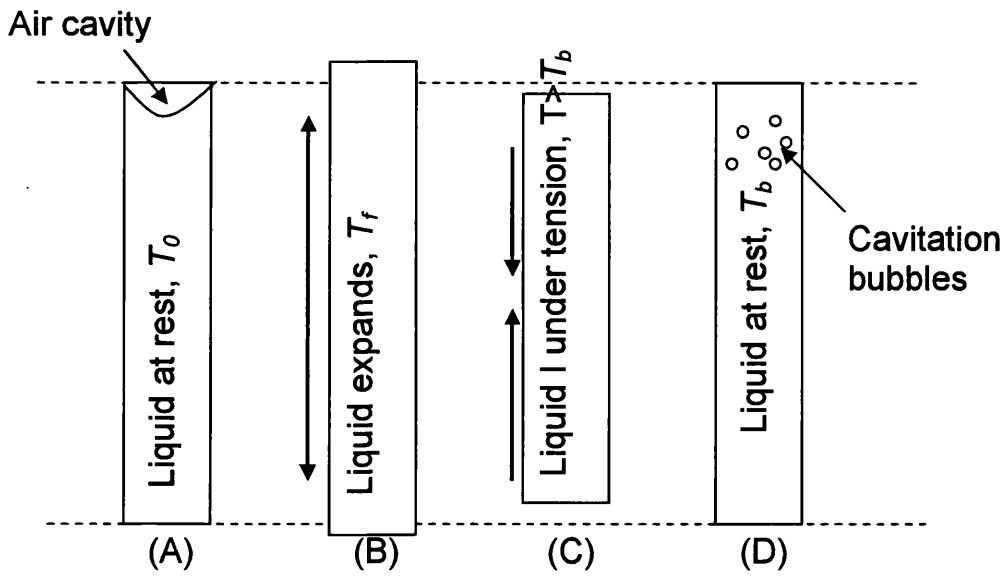


Figure 1.5 Berthelot tube experiment

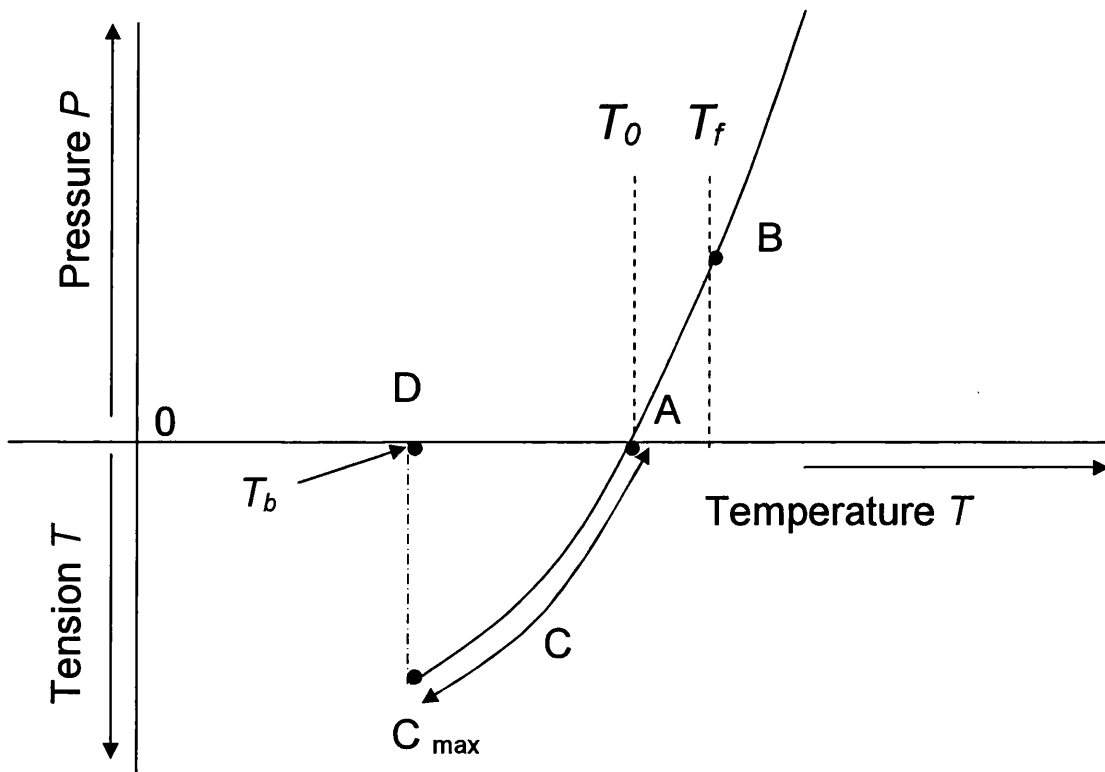


Figure 1.6 General Shape of (pressure, temperature) curve for water in a steel Berthelot tube (Chapman *et al*, 1975)

### 1.5.1.2 Quasi-Static Stressing: The Centrifugal Method

Throughout the past 100 years or so, several workers have used centrifugal methods to subjected liquids to tension (e.g. Reynolds, Worthington). Briggs (1950) reported a 'centrifugal' method in which the liquid was held in a Z-shaped Pyrex capillary, of internal diameter 0.6 mm and open at both ends. This Z-tube was mounted horizontally and spun in its plane about a vertical axis through its centre. With this arrangement the liquid column at this central point was visible even at high angular speeds. In the centrifugal field, one half of the liquid column was pulling against the other and the maximum stress, which was at the centre, was given by

$$F = \frac{1}{2} \rho \omega^2 L^2$$

where  $2L$  was the measured distance between the menisci in the bent legs the tube. As in Reynolds's work, the breaking tension could be calculated from the value of  $\omega_c$  which caused the liquid column to break at its centre. Briggs emphasised the scrupulous cleanliness is necessary in order to produce reliable estimates for the tensile strength of a liquid, and with his apparatus was able to obtain breaking tensions as high as 277 bar for distilled water. This figure 1.7 shows that the breaking tension  $F_c$  has a maximum value of 277 bar around 10 °C and that is decreased to 217 bar as the temperature rose to 50 °C. This gradual decrease in the breaking tension is understandable since Temperley (1947) has shown that the tensile strength of an ideal van der Waals liquid fall, as the temperature rises, to reach a value of zero at  $27T_c/32$ , where  $T_c$  is the absolute value of the critical temperature. So although the van der Waals equation does not represent the behaviour of water quantitatively it nevertheless gives a fair indication that a decrease in  $F_c$  with increasing temperature is to be expected. The figure also shows a rapid fall in the value of  $F_c$  as the temperature fell from 5 to 0 °C. It is widely known that the structure of water begins to change at temperatures below about 4 °C, which may help to explain this anomaly (this will be discussed in chapter six more detail later).

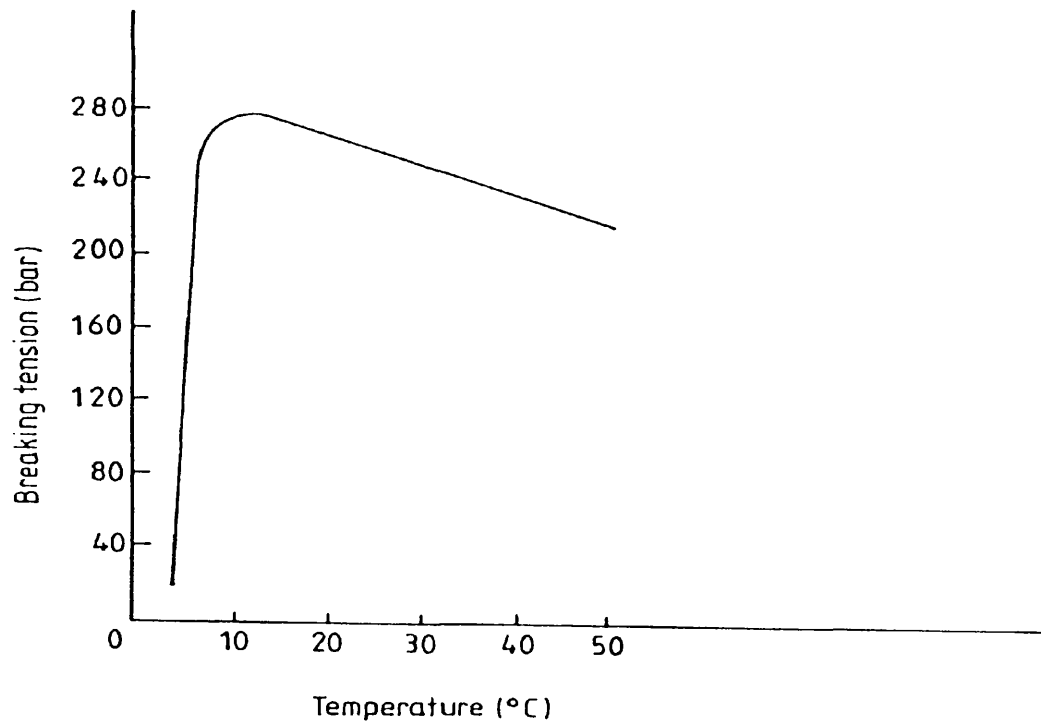


**Figure 1.7** Breaking tension as a function of temperature for water (Briggs, 1950)

## 1.5.2 Dynamic Stressing Technique

There are essentially two ways in which a liquid can be subjected to tension under dynamic stressing. In the first method a tension pulse is generated *ab initio* in the liquid. The second method involves producing a pressure wave in the liquid which is later converted to tension by reflection at a suitable boundary (Trevena, 1987).

### 1.5.2.1 The Tube-Arrest Method

This technique is a development of one used by Chesterman (1952), Overton and Trevena (1981), and Williams *et al* (1996, 1997, 1998, 1999). It involved a vertically mounted cylindrical tube, typically half-filled with liquid (shown in figure 1.8). The tube is pulled downwards against tensioned supports and released, rising through a



distance of several centimetres before being arrested suddenly by a buffer. As the free surface continues to move upwards following the tube's arrest, pressure transducers mounted in the walls of the tube record the development of a tension pulse, *ab initio*, which travels downwards through the liquid column resulting in cavitation of the liquid (Williams *et al*, 1998). By varying the 'impact' velocity  $V$  of the tube the tension pulse amplitude  $F_i$  is varied. When  $F_i$  is gradually increased, the  $(F_i, V)$  graph follows a linear rise up to  $V = V_c$ , rising more gradually thereafter. For  $V < V_c$  no cavitation occurs. For  $V > V_c$  cavitation is induced and associated pressure record has been reported in the form shown in Figure 1.9, in which the *ab initio* pulse is followed, after several milliseconds, by a pressure pulse (Overton *et al*, 1984). This pulse is immediately followed by a secondary tension pulse. Thereafter the record consists of pressure-tension cycles of progressively decreasing amplitude and period. The pressure-tension cycles produced by Tube-Arrest experiment works are similar to the B-P experiment works where as accompanying the cavitation of liquids subjected by dynamic stressing can be explained in terms of the growth phase of oscillating cavities (Williams and Williams, 1996).

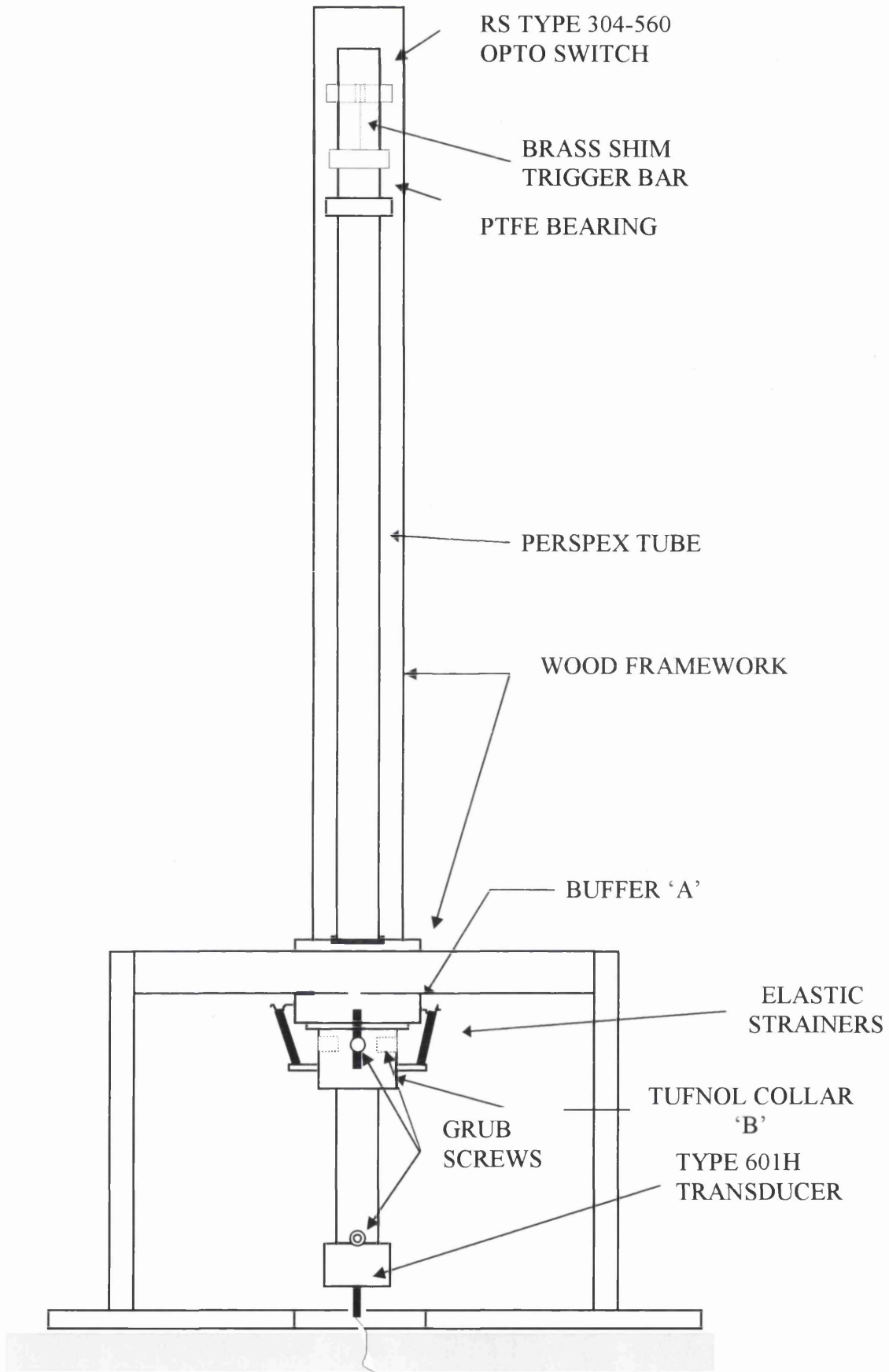


Figure 1.8 Improved Tube-Arrest tube Apparatus (Williams *et al*, 1996)

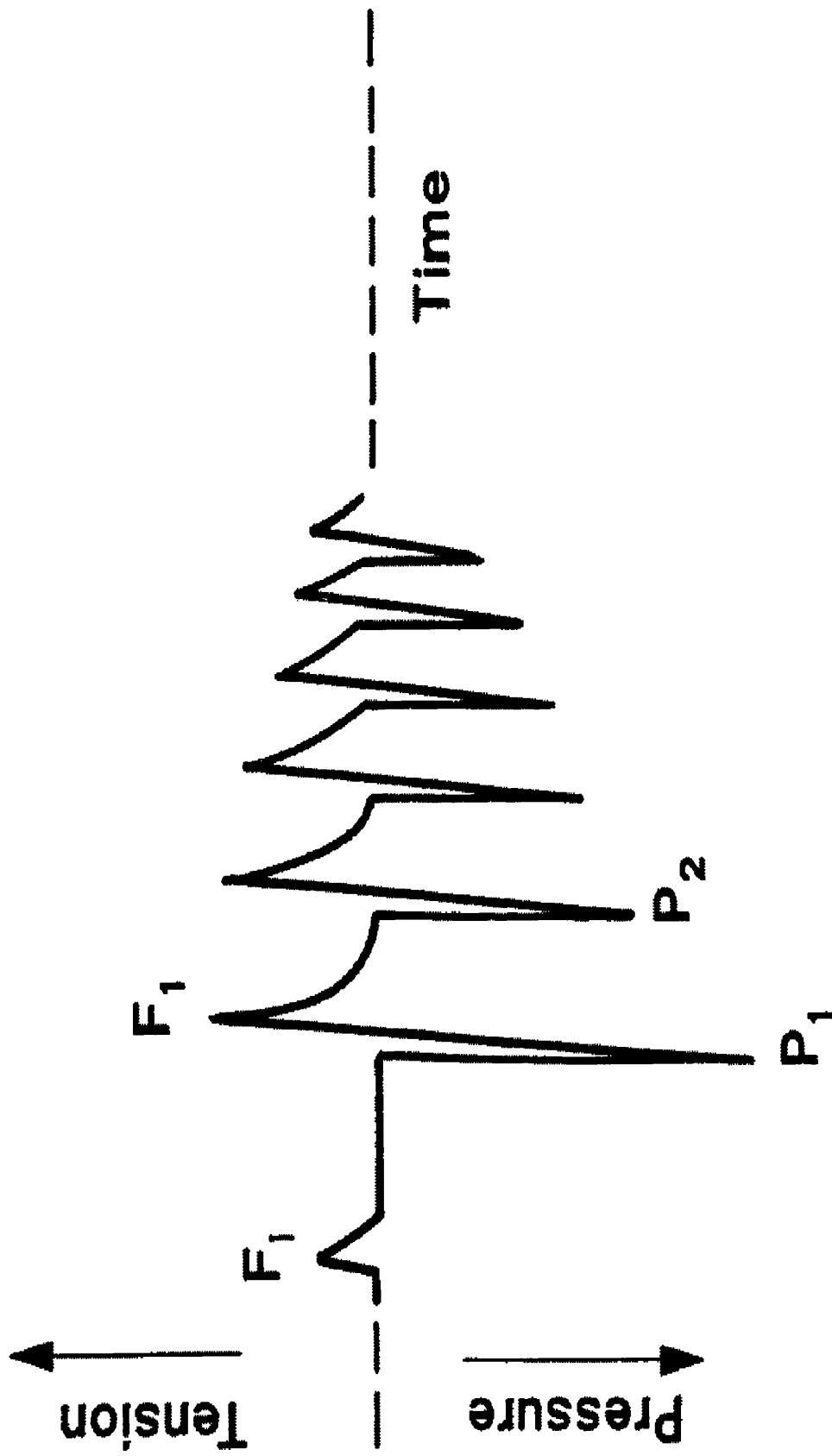
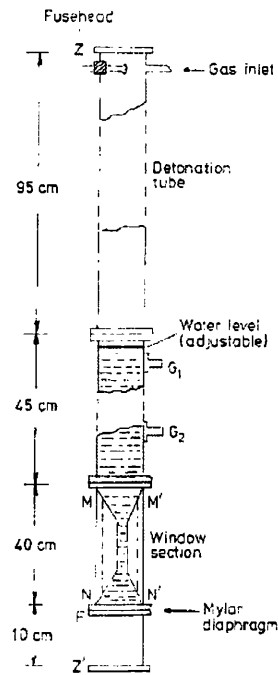


Figure 1.9 Explanatory sketch of cyclic pressure record (after Overton and Trevena, 1981).

### 1.5.2.3 Shock Tube Method

In water shock tube methods, a tension wave is produced in a liquid either directly or by converting a compressional pulse by a suitable reflection method. The shock tube used by Fujikawa and Akamatsu (1978) consisted of a sealed vertical tube approximately 4 m in length with two chambers separated by a diaphragm. The upper chamber contained air at low pressure while the lower chamber was partially filled with the test liquid (degassed tap water). The remaining space above the liquid in the lower chamber contained a helium-air mixture under high pressure. Electrodes built into the bottom of the tube produced hydrogen and oxygen bubbles and the diaphragm was subsequently ruptured producing a tension pulse that travelled down the tube before reflecting off the bottom surface. The reflection tension pulse was subsequently reflected (as a positive pressure pulse) off the liquid-gas interface. Transducers mounted in the tube allowed the dynamic pressure and tension to be monitored while a transparent window section facilitated the use of high-speed photography and in-line Fraunhofer holography to study the dynamical behaviour of vapour bubbles in the tensile field. It should be emphasised that the bubbles studied were not true cavitation bubbles, as they were produced by electrolysis rather than the tension pulse, however, the most important result reported here is the light shed on how cavitation damage on a surface occurs either by the liquid jet or shock wave produced by cavitation bubbles (Trevena, 1984).

Another shock tube method, but based on the reflection method for generating tension, has been described by Richards *et al* (1980). This modified water shock tube is used to produce tension by igniting a combustible gas mixture in the top half of a sealed tube causing a compressional pulse propagated down through the liquid contained in the lower half of the tube (see figure 1.10). This pulse was later reflected by a Mylar diaphragm (noted that the acoustic impedance of the Mylar diaphragm is not much greater than that of water, the Mylar-water interface behaved almost as a free surface and so produced what was virtually a complete phase reversal of the incident compression), 0.05 mm thick firmly clamped by the flanges, which supported the water column.



**Figure 1.10** Sketch showing main features of water shock tube (Richards *et al*, 1980)

Two pressure transducers ( $G_1$  and  $G_2$ ) were used to measure the pressure and reflected tension pulses in the tube while a twin-mirror schlieren system was used to photograph the bubbles produced by reflection tension. The author reported that the peak amplitude of pressure pulse generated by the detonation was about 60 bar while the peak amplitude of reflected tension in the tube never exceed 12 bar although the photographic records proved that the liquid was actually fracturing.

### 1.5.2.2 The Bullet-Piston Method

The Bullet-Piston (B-P) method involves a liquid in a vertical steel cylindrical tube fitted with a piston at its lower end. A pressure pulse is generated in the liquid by a bullet striking the piston, travels up the liquid column to be reflected at the free surface as a pulse of tension. By varying the peak pressure,  $P$ , in the incident pulse, the values of  $P$  and the peak tension,  $F$ , of the reflected pulse are recorded. The ( $F$ ,  $P$ ) curve shows a limiting value which provides an estimate of  $F_c$  (Trevena, 1987). The value of  $F_c$  originally reported for water in a stainless-steel B-P apparatus was 15 bar

(Sedgewick and Trevena, 1974), whereas for water in a stainless-steel Berthelot tube, Jones *et al* (1980) obtained 46 bar. These results are unexpected, given that an important factor determining  $F_c$  is the rate of stressing experienced by a liquid: usually, the higher the rate of stressing, the higher the value of  $F_c$  obtained. The free surface of water is not a perfect reflector for a pressure pulse incident upon it, an observation that has been used in attempts to explain the anomalously low values of tensile strength,  $F_c$  recorded for this liquid in the bullet piston B-P experiment (Temperley and Trevena 1977, 1979, 1987). Williams and Williams (2000, 2002) showed that, in the cavitation experiments of Couzen and Trevena (1969, 1974), a combination of slow response pressure transducer and low data-sampling rates had resulted in considerable underestimates of the amplitude of cavitation-induced tension.

The work reported by Williams and Williams (2000) established the B-P technique as a reliable tool in cavitation research. In particular, it allows the cavitation properties of liquids to be investigated over a wide range of temperatures. This is an important feature in respect of the properties of liquids such as engine lubricants. For this reason the B-P technique was selected as the principal research tool in the work reported in this Thesis. The work reported in Chapter 2 describes the technique in more detail and gives an account of the development of an improved form of the B-P apparatus reported by Williams and Williams (2000).

# Chapter 2

## ***The Development of B-P Experiment***

- 2.1 *Introduction*
- 2.2 *The Bullet-Piston Apparatus: Previous Related Work*
- 2.3 *Inadequate Transduction and a Neglect of the Effects  
of Wave Reflection in the Pulse-Reflection Work*
- 2.4 *Improved Bullet-Piston Apparatus*

## 2.1 Introduction

The free surface of water is not a perfect reflector for a pressure pulse incident upon it, an observation which has been used in attempts to explain the anomalously low values of tensile strength,  $F_c$ , recorded for this liquid in the Bullet-Piston (B-P) experiment (Temperley and Trevena, 1977 & 1979). It is found that the values of  $F_c$  recorded in this experiment, in which a pressure pulse is reflected (as tension) at the free surface of a column of water, are considerably lower than those obtained under static stressing conditions, such as in the Berthelot-tube experiment. The value of  $F_c$  reported for deionised water by the B-P technique is 10 bar (Sedgewick and Trevena, 1976) whereas for water in a stainless steel Berthelot-tube, Jones *et al.* (1981) obtained 46 bar.

These results are unexpected, given that an important factor determining  $F_c$  is the *rate* of stressing experienced by the liquid: usually, the higher the rate of stressing, the higher the value of  $F_c$  obtained (Trevena, 1982). In the Berthelot-tube, tension usually develops over a period of several minutes, whereas in the B-P experiment the time of stress development is typically a few hundred microseconds.

Temperley and Trevena (1979, 1987) proposed an explanation for the anomalously low values of  $F_c$  recorded in B-P experiments which invoked the concept of a metastable transition layer, between liquid and vapour. The transition layer makes the free surface an imperfect reflector, and accounts for the distortion of reflected pulses found in B-P work. This implies *inter alia* that the amplitude of such a reflected pulse is not a reliable indication of the tensile strength of the bulk liquid.

Temperley and Trevena (1987) considered that this explanation accounted for the anomalously low values of  $F_c$  but some points remain unresolved. First, the ratio of (peak tension)/(peak pressure) reported in B-P experiments vary from 0.36 for deionised water, to 0.5 for boiled deionised water. Given that the peak amplitude of the incident pressure pulse could vary between 100 bar and 300 bar (Couzens and Trevena, 1974; Trevena 1987), it follows that tensions of between 40 bar and 100 bar would be expected to ensue. Furthermore, in order to account for the anomalously low values of  $F_c$ , Temperley and



Trevena's theory involving the transition layer between liquid and vapour requires a very large difference between the speed of sound in liquid water,  $c$ , and that in water-vapour,  $c_v$ : this is necessary in order that the wavelength of the pulses undergoing reflection becomes commensurate with the thickness of the transition layer, which is of the order of only a few intermolecular distances (Als-Nielsen, 1985). However, the ratio  $c_v/c$  is around one-third (Bolz and Tuve, 1973), which is far too large to provide a satisfactory explanation. These anomalies in previous B-P work were resolved by Williams and Williams (2000) who showed that a combination of slow pressure transducer response and low sampling rates could account for the discrepancies between various estimates of tensile strength in B-P work.

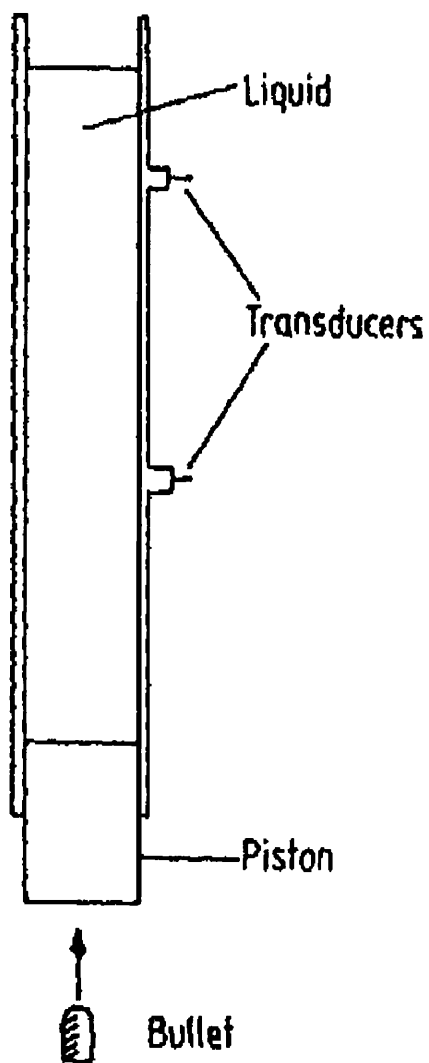
The present chapter reports work involving a new B-P apparatus which improves upon previous B-P and water shock-tube work in employing a new method of estimating  $F_c$ . The new B-P apparatus also involves a new method permitting the rate of tensile stress development to be varied with the liquid sample maintained *in situ*.

### 2.2 The Bullet-Piston Apparatus: Previous Related Work

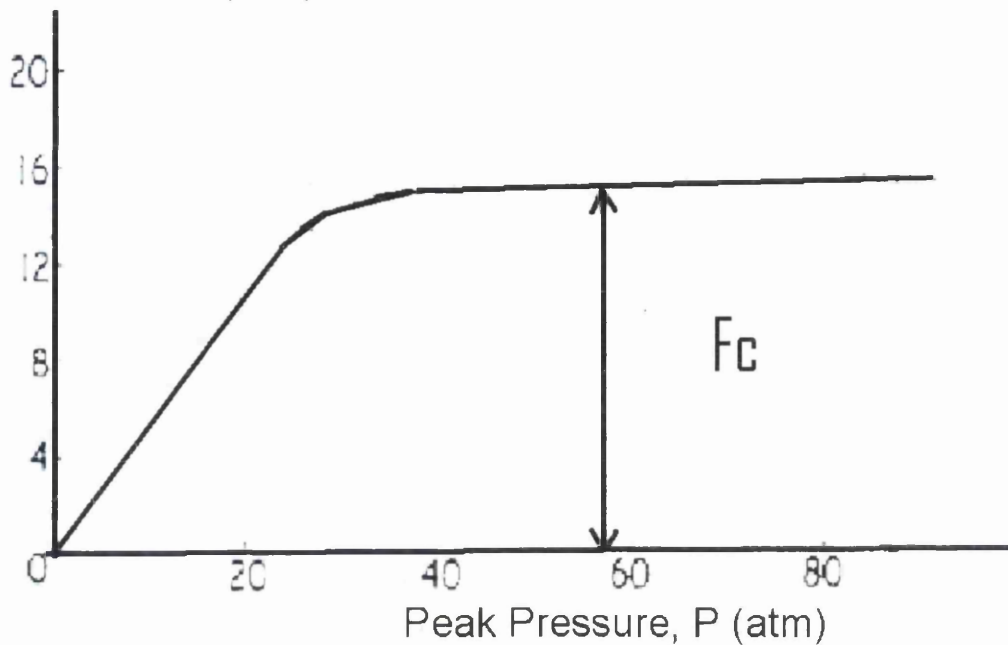
Most previous B-P experiments have involved a vertical tube fitted with a piston at its lower end (see figure 2.1). A pressure pulse generated by a bullet striking the piston travels up a liquid column within the tube, to be reflected at the free surface as tension. By varying the peak pressure,  $P$ , in the incident pulse, the values of  $P$  and the peak tension,  $F$ , of the reflected are recorded by two pressure transducers which could be inserted into port holes at various depths in the wall of the tube (see figure 2.1). The graph (see figure 2.2) shows that the value of  $F$  does not increase linearly value  $P$ . The limiting or 'plateau' value is the maximum tension which the liquid can stand and the breaking tension needed to produce cavitation (Trevena, 1987).

Early B-P work suggested that degassed, distilled water was incapable of sustaining a tension greater than 10 bar (Davies, 1956). In subsequent B-P work, Couzens and Trevena (1969) found a value of 15 bar for degassed, deionised water. Such anomalously

low values have been shown to be a result of inadequacies in the pressure recording equipment previously employed. A critical aspect of this – and one which is overcome in the work reported in this thesis – involves the data sampling rate employed to record rapid variations in pressure occurring within the tube. This aspect of the B-P experiment is now explained in detail below.



**Figure 2.1** Schematic diagram of the early form of bullet-piston apparatus (Trevena, 1987)

Peak Tension,  $F$  (atm)

**Figure 2.2** ( $F$ ,  $P$ ) graph used to estimate the maximum tensile strength,  $F_c$ , of a liquid by Couzen and Trevena (1974)

### 2.3 Inadequate Transduction and a Neglect of the Effects of Wave Reflection in the Pulse-Reflection Work

Williams and Williams (2000) claimed that the anomalously low values of liquid tensile strength obtained in previous B-P work cannot be explained in terms of the effect of the free-surface transition layer in pulse reflection (as Temperley and Trevena's explanation) may be attributed to deficiencies in the techniques previously used to recorded dynamic tensions. Their work in 'tube-arrest' experiment is stimulated by the findings of Williams *et al* (1997, 1999), who showed that, in the cavitation experiments of Overton and Trevena (1981), a combination of slow responding pressure transducers, and low data-sampling rates, had resulted in considerable underestimates of the amplitude of cavitation-induced pressures, and speculated that similar considerations would pertain to the results of B-P experiments, and to those of the water shock tube work of Richards *et al* (1980).

In addition, the previous B-P workers neglected the reflection of downward travelling tension pulse at the face of piston cause of large underestimates of peak tension in previous dynamic stressing B-P reflection work (Williams and Williams, 2002). These combination factors have led to the anomalously low values of liquid tensile strength recorded in previous dynamic stressing experiments involving the reflection of a pressure pulse (as tension) at free surface of a column of water, or at a flexible membrane. The factors that lead to the anomalously low values of tensile strength of water obtained in previous B-P work are being discussed individually.

### 2.3.1 Slow Respond Pressure Transducers

In previous B-P work, a pressure pulse is generated by the impact of the striking bullet to the bottom of the piston travels up a vertical column of liquid, when such a pulse reaches the upper free surface of the liquid it is reflected downwards as a pulse of tension, pressure changes in the water column were monitored by means of two piezoelectric transducers (type 701A, as supplied by Kistler Instruments Ltd) used by Couzen and Trevena (1974) and Sedgewick and Trevena (1976) mounted at different liquid depth in the wall of the tube.

Pressure information in the form of a voltage output from the transducer was fed through an electronic filter to a cathode ray storage oscilloscope and photographic records of the accompanying oscilloscope traces were made. The purpose of the electronic filter was to remove any unwanted frequencies (or mechanical vibration of the system produced by the impact of the bullet to the piston).

The use of the Kistler-type 701A transducer represented a considerable improvement over the strain gauge used by Davies *et al* (1956) and the microphone used by Bull (1956). They found that the maximum amplitude of tension pulses arising from the reflection of compressional waves at a free surface has yielded less than 20 bar. Even lower values of  $F_c$  have also been reported in dynamic stressing experiments on water involving the 'tube-arrest' techniques. The tensile strength of water reported in this experiment is approximately 1 bar (Williams *et al*, 1982; Overton *et al*, 1984).

This results were unexpected due to the static stressing techniques which obtained far more higher tensile strength of water, up to 270 bar using centrifugal method by Briggs (1950) and is at variance with expectation given that an important factor determining  $F_c$  is the rate of stressing: usually, higher the rate of stressing, the higher the value of  $F_c$  obtained (Overton and Trevena, 1982).

The dynamic stressing work involving shock-wave reflection from a Mylar membrane instead of the free surface, Marston and Unger (1986) inferred a maximum tensile strength of water of *ca.* 100 bar, although in the work of Richards *et al* (1980), which involved a similar membrane, the tensile strength of water was similar from that obtained by free surface reflection (*ca.* 10 bar). The main reason of anomalously low value of tensile strength of water obtained by Richards probably caused by the slow respond Kistler-type 701 pressure transducer. The Kistler 603 B pressure transducer was used by Marston and Unger which has a shorter risetime ( $\sim 1 \mu\text{s}$ ) than the Kistler 701A transducers ( $\sim 6 \mu\text{s}$ ). It is emphasised that the Kistler-type 701 pressure transducer used by Richards *et al* (1980), is the same model as used in previous B-P work by Couzen and Trevena (1974), Sedgewick and Trevena (1976) and in the 'tube-arrest' experiments of Overton and Trevena (1981), Overton *et al* (1984) and Williams *et al* (1982).

Therefore, previous dynamic stressing experiments on measurement of  $F_c$  with resort to direct pressure transducer, leads to lower tensile strength of liquid, due to the slow respond Kistler-type 701 pressure transducer which could not fast enough to record these rapid dynamic tension pulses. In addition, previous results relied upon accurate measurements of substantial dynamic negative pressure, using transducers which are designed for use in the range of positive pressures.

In addition, the recorded tension depends markedly on the location of a transducer due to the effect of interference waves in the liquid column of B-P apparatus, this may lead to underestimate the true tensile strength of a liquid (Williams and Williams, 2002). Instead using direct measurement of transducer, alternative way is to measure the velocity of the tension pulses from which  $F_c$  is obtained, such as Carlson (1973, 1975) used the reflection principle to convert a pressure pulse into a tension pulse, was monitored by

means of a velocity interferometer using light from a He-Ne laser. From a series of experiments Carlson and Henry found the tensile strength of glycerol and mercury to be 600 and 19 kbar respectively.

In another type of dynamic stressing 'tube-arrest' experiment carried out by Williams *et al* (1999) on samples of deionised water suggest that this liquid can sustain a transient tension of up to *ca.* 700 bar under dynamic stressing by pulses. The measurements on tensile strength of water are relied on the propagation of velocity of the reflected tension pulse, which later induce cavitation, by using two Kistler 603B pressure transducers. The advantage of this method is the direct measurement of tension by pressure transducer is eschewed. They also found important evidence as the reflected tensions propagate not at the speed of sound in liquid water (*ca.* 1450 ms<sup>-1</sup>) but at that associated with water vapour (495 ms<sup>-1</sup>).

In static stressing work, Alvarenga *et al* (1993) who employed a Brillouin scattering technique to measure the speed of sound in water liquid-vapour inclusions in specimens of quartz, the negative pressures generated in water can be reached as high as 1000 bar but this required long extrapolations into the negative pressure regime using equations of state which had been determined in the range of large positive pressures.

### 2.3.2 Data Sampling Considerations in B-P Work

In practice, the selection of sampling rates for a particular signal depends on how rapidly the signal is changing with time. Since the periodic sampling of pressure-tension record obtained in B-P experiments is roughly about a few microseconds, at least the sampling rates must be up to 1 MHz in order to recover the complete signal waveform by interpolation. However, the ancillary recording equipment (a Tektronix 5113/5B10N cathode ray oscilloscope (CRO) and Z80-based digital transient recorder respectively) used by previous workers, Davies *et al* (1956) estimated to have resulted in low sampling rate of <10 kHz. Further, to simulate the effect of the phosphorescent CRO screen storage mechanism, the artificially slowed pressure record was subjected to a five-point moving-average procedure which effectively reproduces the characteristic 'smearing' effect, it

caused a loss of signal information due to low sampling rates, hence lead to underestimate of the amplitude of the tension pulse is generated in the liquid, therefore a lower  $F_c$  of a liquid is obtained in previous B-P work (Williams *et al*, 1997).

As a result of low sampling rate, in previous B-P work, the first pressure-tension cycle has been reported as single pressure pulse which is immediately followed by a single pulse of tension where  $F_1$  and  $F_2$  are no longer distinct and separate, appearing instead as a broad, single tension pulse of reduced amplitude (sampling rate <10 kHz, see Figure 2.3). However, if the sampling rates >1 MHz shows that two tension pulses ( $F_1$  and  $F_2$ , see Figure 2.3) are actually recorded. The amplitude of the tensions recorded at a sampling rate of 1 MHz was found to be larger than those evident at 10 kHz or less. It can be confirmed that the lower sampling rate results in a significant underestimates of tension (Williams and Williams, 2000 & 2002).

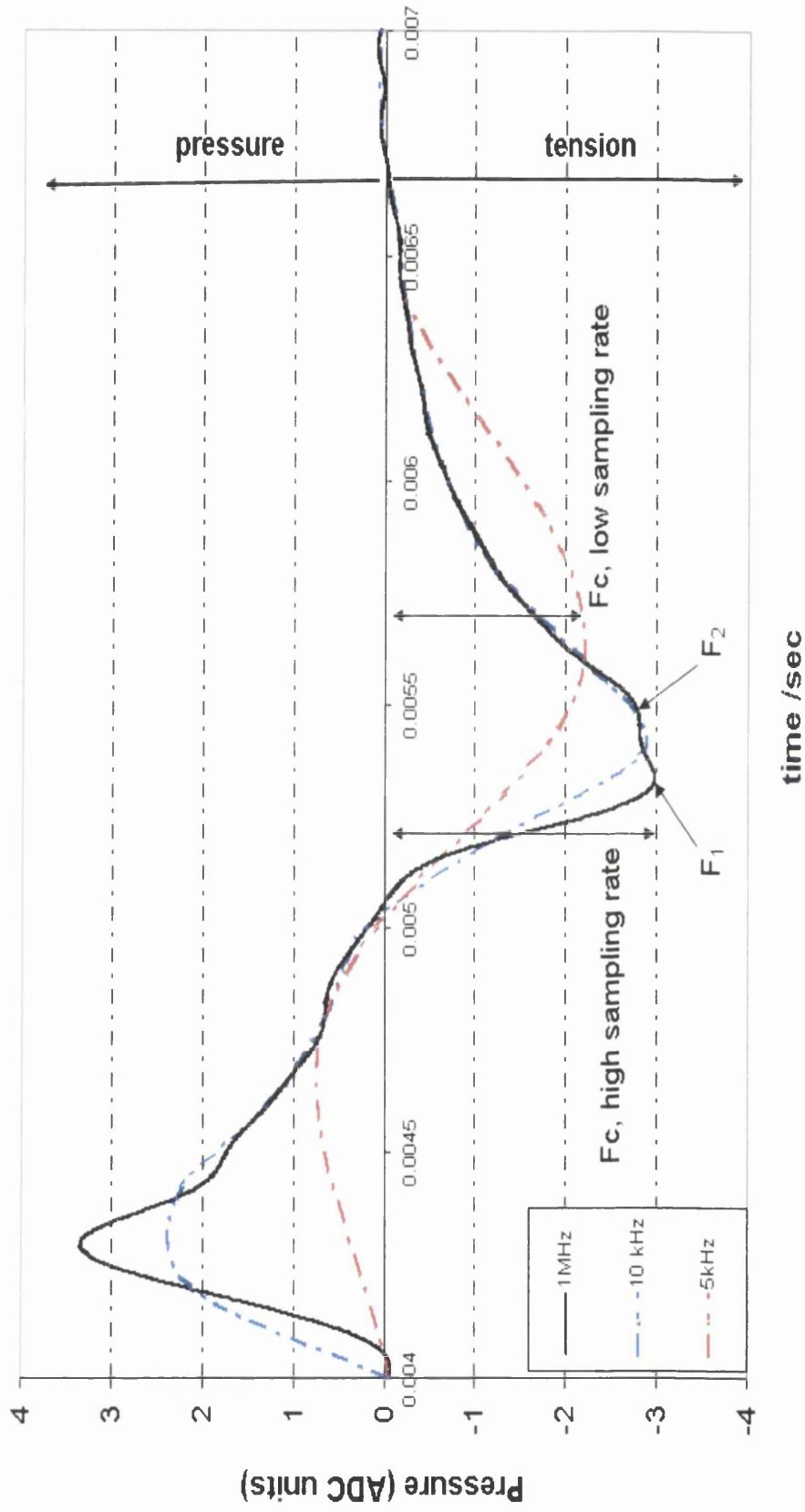


**Figure 2.3** Results of experiments on degassed, deionised water. The pressure-tension cycles were recorded using the Kistler-type 603B at different sampling rates of 1 MHz, 10 kHz and 5 kHz.



### 2.3.3 Wave Interference of Pulse Reflection in B-P Work

Reflection of wave pulses has long been recognised as a factor which may influence the results obtained in B-P experiments (Couzen and Trevena, 1969). Previous B-P work has only involved consideration of the overlap of the incident pressure pulse, and reflected tension pulses at the free surface of the liquid. The resultant pressure variation below the free surface is then determined by the superposition of the pressure pulses and reflected tension pulses whose overlap may be avoided by positioning transducers at a sufficiently large distance from the surface (see figure 2.4(a)). However, the advanced explanation is given by Williams and Williams (2002) for the anomalously low values of  $F_c$  recorded in previous B-P work involves the overlap of tension pulses at the base of the liquid column (See figure 2.4(b)). When cavitation of the liquid accompanies this pulse overlap, the velocity of the pulse may differ significantly, with the result that tension recorded within the liquid appears too low (by an order-of-magnitude).

In the current B-P work reported in this Thesis, pressure changes within the liquid were monitored using three pressure transducers (Kistler type 603B, Kistler, UK) mounted in mechanically isolated ports in the different locations along in the column of water ( $L = 0.95$  m) at 25 °C which are 5, 27 and 66 cm apart from the face of the piston at the bottom of the tube. Care was taken to avoid interference between wave propagation upward and downward, by using non-resonant heights of a liquid column.

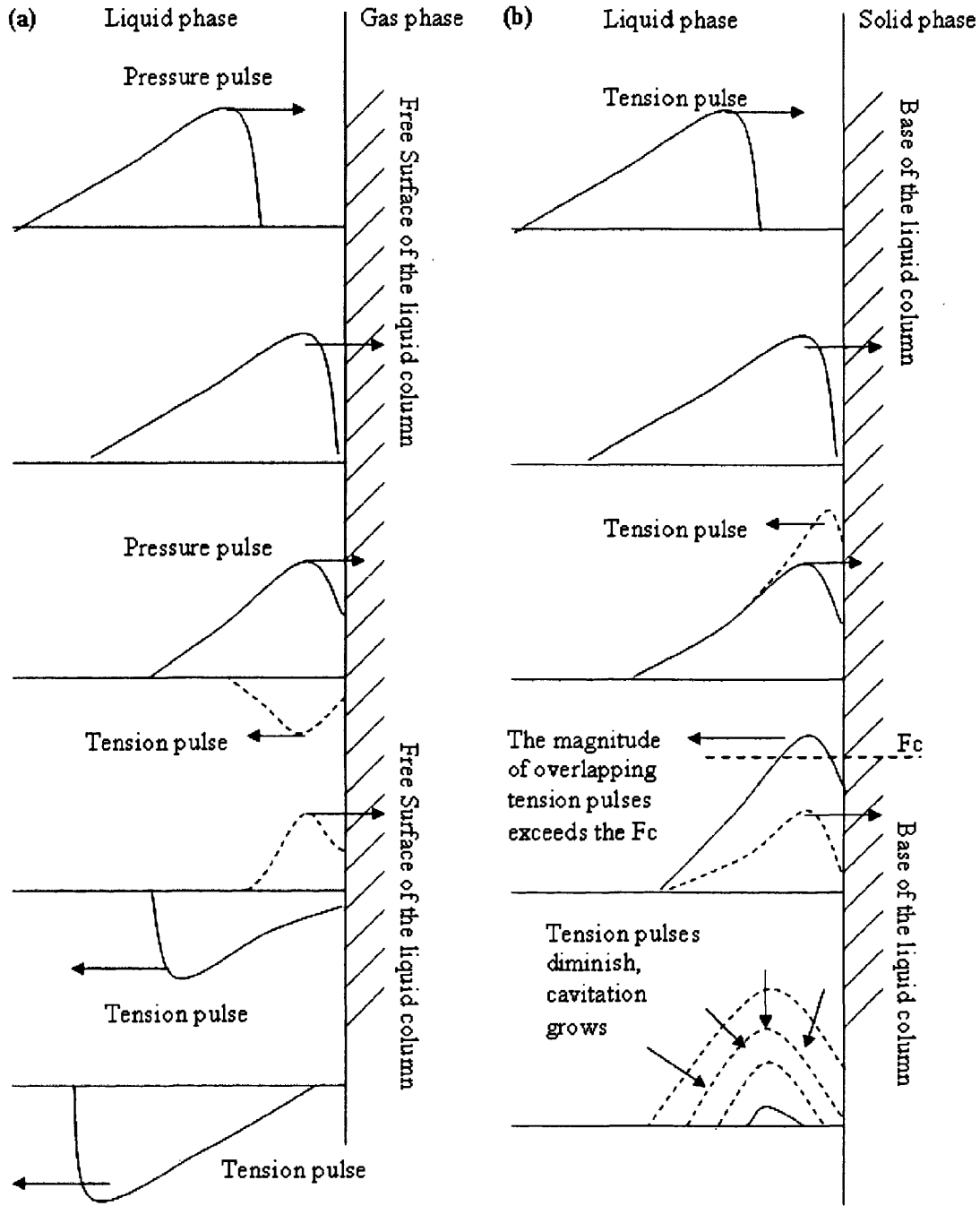


**Figure 2.4** (a) Reflection of pressure pulse at the free surface of liquid column (as a fixed wall) (at the left)  
 (b) Reflection of tension pulse at the base of liquid column (as a free end) (at the right)

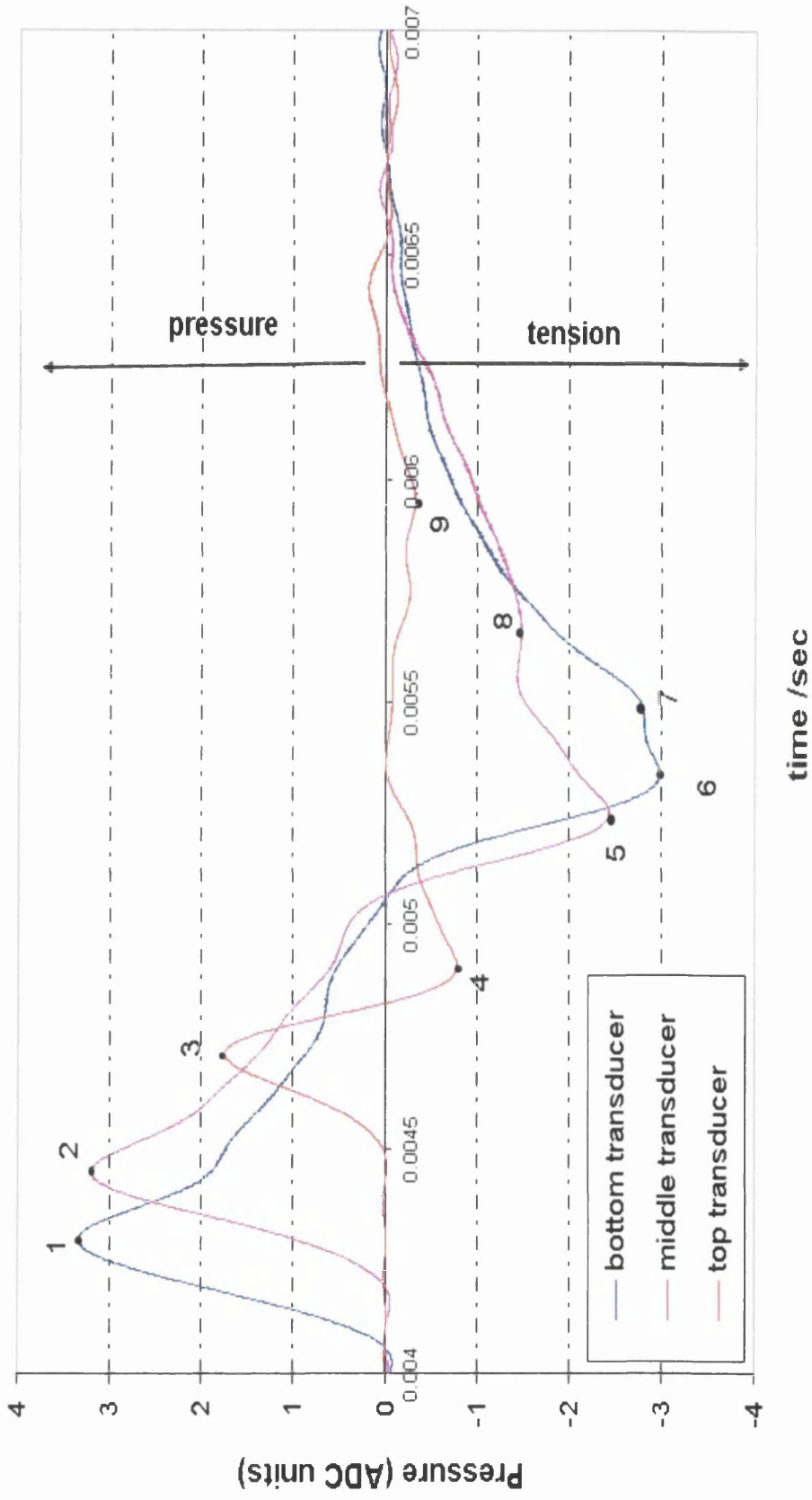


Figure 2.5 Details of first pressure-tension cycle recorded in experiments on water by three dynamic pressure transducers in different locations along the B-P apparatus.

Figure 2.5 shows different amplitudes of the pressure and tension pulses measured at different locations of liquid column. The recorded tension depends markedly on the location of a transducer due to the effect of wave interference. At time = 0.004 s the initial pressure pulse, 1, is recorded by the bottom transducer, followed by pulse 2 is recorded by middle transducer, and then pulse 3 is recorded by the top transducer. This confirms the assumption made by previous workers that the initial pulse travels upwards through the liquid. Pulse 1 and pulse 3 occur at 4.31 ms and 4.73 ms, respectively, in the record; and the distance travelled is 61 cm, corresponding to a velocity of  $1452 \text{ ms}^{-1}$ , this velocity is close to the propagation of sound in liquid water,  $c$  (some  $1435 \text{ ms}^{-1}$ ).

The next feature in the record is the reflected pulse at the free surface as a tension pulse 4 which is first recorded by the top transducer: this is followed by the middle transducer, and then by the bottom transducer. Hence it can be concluded that these pulses move downwards through the liquid column. Their velocity, calculated from the time delay (0.44 ms) between pulses 4 and 6 and the distance travelled (61 cm), correspond to a velocity of  $1386 \text{ ms}^{-1}$ . The total time taken for a pulse travelled along the liquid column between peak pressure pulse 1 and peak tension pulse 6 is 1.20 ms and the total distance is 180 cm (corresponding velocity of  $1500 \text{ ms}^{-1}$ ).

It is instructive to focus on a feature which is absent from previous descriptions of the pressure records in B-P work, namely pulses 7, 8 and 9 (which propagate upwards through the liquid column). This reflected tension pulse 7 is recorded first by the bottom transducer and pulse 8 is then subsequently recorded by the middle transducer and, finally, pulse 9 is recorded by the top transducer. Their velocity, calculated from the time delay (0.157 ms) between reflected tension pulse 6 and 7 and the distance travelled (10 cm) is  $637 \text{ ms}^{-1}$ , this velocity is close to the propagation of sound in water vapour,  $c_v$  (some  $494 \text{ ms}^{-1}$ ), a result which implies that cavitation occurs in the water in this region (Williams *et al*, 1997). This may be expected due to the overlapping tension pulses at the bottom of the liquid column (refer to figure 2.4 (b)). Such a tremendous velocity difference between pulses 6 and 7 (as  $F_1$  and  $F_2$ , respectively, in figure 2.3) will influence estimates of  $F_c$ , (Williams and Williams, 2002).

It is interesting to note that similar observations pertain to the shock-tube method used by Richards *et al* (1980), who in order to increase the magnitude of the reflected tension, placed a converging-diverging nozzle in the test section. When no cavitation occurred, the velocity of both downward-moving compression wave and the upward-moving tension pulse corresponded to the velocity of sound in water (some  $1550 \text{ ms}^{-1}$ ). When cavitation was observed, an accompanying acoustic field radiated by the collapse of bubbles was found to be associated with two velocity components whose values were  $1550 \text{ ms}^{-1}$  and  $550 \text{ ms}^{-1}$ , respectively. The former downward traveling pressure pulse corresponding closely to the speed of sound in water liquid  $c$ , whereas the latter reflected traveling tension pulse corresponding closely to the speed of sound in water vapour,  $c_v$ .

### 2.4 Improved Bullet-Piston Apparatus

In order to overcome the various issues reported above, the current work involved a new B-P apparatus incorporating faster responding pressure measurements, the outputs of which were sampled at higher rates (1 MHz to 20 MHz) by 12-bit analog to digital conversion (Gage Inc., Canada). In addition, previous B-P work used electronic filters and moving average methods to obtain pressure records but these techniques can introduce unwanted artefacts into the records (Williams and Williams, 2000). In the present work the pressure records were transferred to a PC-AT microcomputer for further analysis using a commercial signal processing software package (DADISP; DSP Corp., USA). This package enables effective removal of high frequency noise digitally, without reducing the sampling rate. Hence it was possible to recover the recorded wave forms without *aliasing error*.

In addition to improved signal capture techniques and data analysis methods, the present work improved upon previous B-P studies by employing a new method for estimating the amplitude of tension sustained by the test liquid. This is a significant development as the direct recording of substantial negative pressures using transducers calibrated only in the

positive pressure regime is dubious. The method used in the present work is now explained in Chapter 3, along with a new B-P method in which the rate of tensile stress development is varied.

# Chapter 3

## ***Dynamic Stressing Liquids: Improved B-P Apparatus***

- 3.1 *Introduction*
- 3.2 *The Basic Description of B-P Apparatus*
- 3.3 *Cleaning Procedure*
- 3.4 *Signal Processing and its analytic work*
- 3.5 *Determination of Cavitation Threshold,  $F_c$ , of Liquid  
involving the Application of a Regulated Static  
Pressure*

### 3.1 Introduction

The apparatus described in this Chapter is based on the design of Couzen and Trevena (1969, 1974), Sedgewick and Trevena (1976) but incorporates faster respond pressure transducer and higher data-acquisition rates to overcome the previous significantly underestimation of the value of tensile strength,  $F_c$  of liquids and also an advanced signal-processing software package is utilised for further analytical works deemed necessary after preliminary work described in Chapter 2. In addition, the B-P technique used in previous work has the disadvantage that the means by which P is varied (using different combinations of piston mass, piston length and bullet momentum) necessitates frequently dismantling of the apparatus and removal of the liquid. This (potentially) alters the liquid's nucleation state and is inconvenient for work at high and low temperatures and relies upon accurate measurements of substantial dynamic negative pressures, using transducers which are designed for use in the range of positive pressures. Therefore, the improved B-P apparatus was used in this work to overcome the difficulties of previous works by a method which allows  $F_c$  to be estimated with the same sample remaining *in situ* throughout.

### 3.2 Basic Description of 'Bullet-Piston' Apparatus (see Section 1 in figure 3.1)

The present apparatus consists of a cylindrical, stainless steel tube (length 1.4 m and internal diameter 0.0243 m) closed at its lower end by a piston (figure 3.2). The tube is locked to restraining lugs and is supported by a steel arm (#5 in figure 3.2) on a counter-weighted aluminum stand. The piston's lower surface is impacted by the bolt of a cartridge driven stun-gun (Magnum model 7000, Shelby and Vokes, UK) (#1 in figure 3.2 or refer to figure 3.3) which generates a pressure pulse in a column of liquid within the tube. The impact area between the bolt and bottom piston region is safely guarded by a thick steel gun shield (#8 in figure 3.2). The duration of the pressure pulse is typically 300  $\mu$ s with a rise time to peak amplitude of 50-100  $\mu$ s.



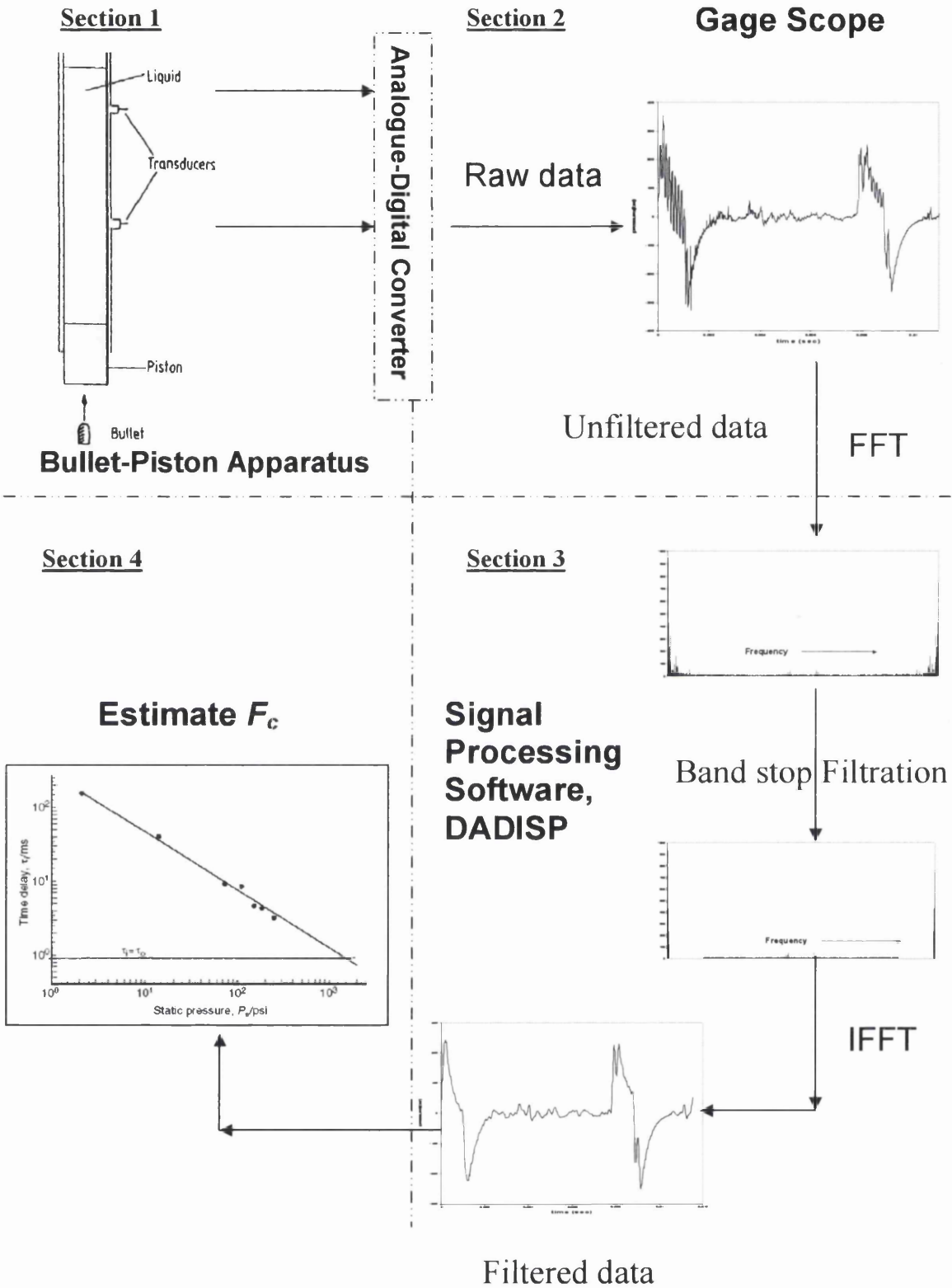


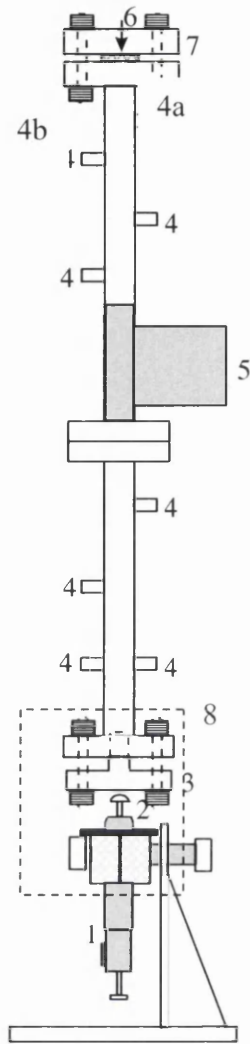
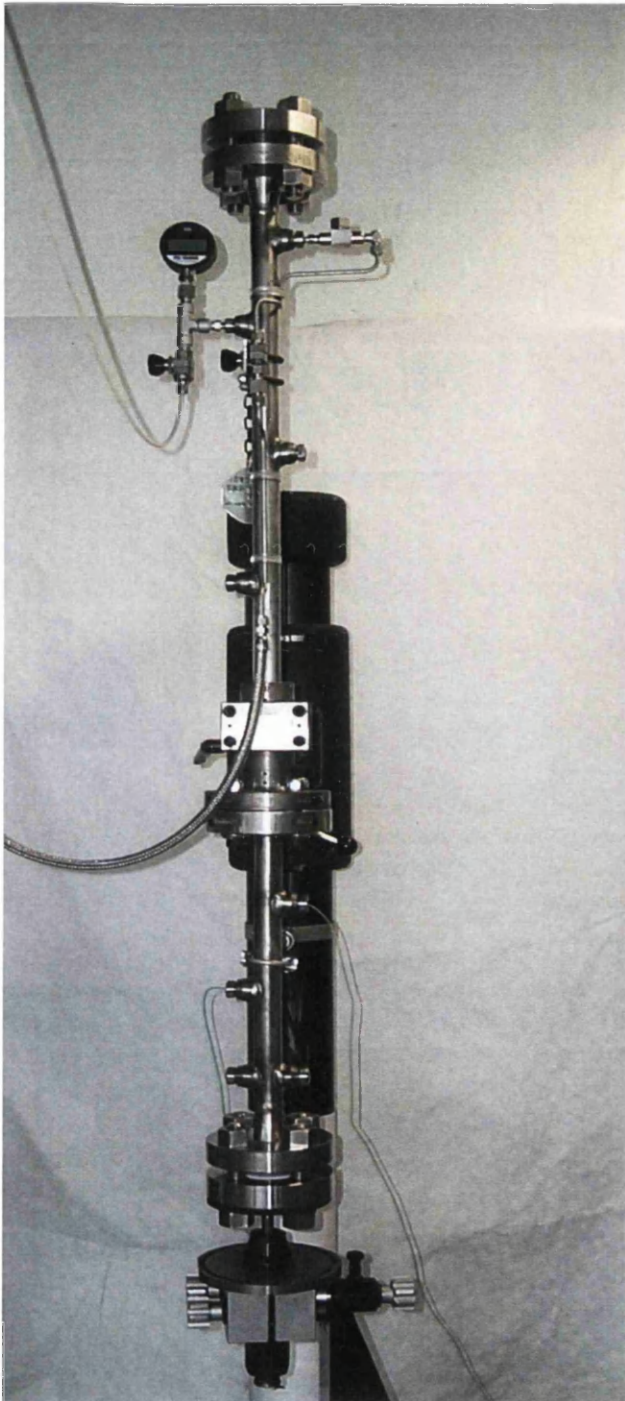
Figure 3.1 Overall descriptions of B-P experiment

Pressure changes within the liquid column were monitored using three dynamic pressure transducers (Kistler 603B, Kistler UK) ( #4 in figure 3.2) mounted in mechanically insulated ports in the tube wall at different depth in the column of liquid, the positions of the transducers above the face of the piston being 5, 27 and 66 cm respectively. In each experiment, the free surface was 0.95 m above the face of the piston at the base of the liquid column. The output voltages of the pressure transducers were recorded by a high speed acquisition system Gage Scope (Gage inc., Canada) specially designed for the capture of rapid transient signals. The transducer output voltage was sampled at 1 MHz by a 12-bit analogue to digital converter with an 8 MB memory buffer. The pressure records were transferred to a PC-AT microcomputer for analysis using signal processing software (DADiSP; DSP Corp., USA).

The upper sections of the apparatus was modified to permit the application of a regulated static pressure above the liquid column, using oxygen-free nitrogen supply and a pressure gauge (PSI-Tronix, USA) was attached, via transducer port (#4a, figure 3.2) in order to record the applied pressure. This system also permits connection of the tube to a vacuum line (-1 bar) (#4b, figure 3.2) and allows the liquid sample inside the column to be thoroughly degassed *in situ* by connecting the upper flange to a vacuum line and the static pressure (or oxygen-free nitrogen gas) also can be removed after the measurement of experiment. Therefore, the static pressure above the liquid column can be controlled. The lower flange houses the piston and provides a connection to a steam condensing system and a liquid drain point.

Temperature control was achieved by combination of a heating tape and a refrigeration unit (see figure 3.4). The refrigeration unit consists of a TAE M10 water chiller (M.T.A.SRL, Italy) connected to a double copper coil (OD 5 mm) system wrapped tightly around the B-P apparatus. The coolant liquid circulated around the apparatus was Go Therm AF200 (Linde, UK), which contains 1, 2 propanediol, and this enables temperature control over the range  $-15\text{ }^{\circ}\text{C} \leq T \leq \text{room temperature}$ . High temperature control is achieved by means of a 3 m heating tape (100 W/m at 230 V), wrapped tightly around the copper cooling coils on the B-P apparatus, and connected to a variac voltage controller (RS, UK). This gives an upper working temperature of  $\approx 135\text{ }^{\circ}\text{C}$ , thus the

heating tape gives the B-P apparatus an operating range of room temperature  $\leq T \leq 135$  °C. Thus the combination of the refrigeration unit and heating tape gives the B-P apparatus an operating range of  $-15 \text{ °C} \leq T \leq 135 \text{ °C}$ . The cooling coil and heating tape are surrounded by Armourflex lagging (IPS Ltd., UK) to provide insulation and improve cooling/heating efficiency. All temperature measurements were made, by the use of thermocouples (Jenway, UK), at the tube's inner surface and minimal temperature variation was observed over the length of the liquid column within the B-P apparatus. All experiments were conducted in a wide range of temperature from  $-15$  to  $135 \text{ °C}$  ( $\pm 1 \text{ °C}$ ), hence ideally suited to the study of liquids in a wide range of temperature.



- 1 Magnum model 7000 cattle stun gun
- 2 Mushroom-headed cosh
- 3 Steel piston
- 4 Transducer ports
- 5 Support arm
- 6 Sealing gasket
- 7 Sealing flange
- 8 Steel gun shield

Figure 3.2 The Bullet-Piston Apparatus (with heating jacket removed)

**Magnum Model 7000 captive-bolt stun gun (Section 1)**  
**(Refer #1 in figure 3.1)**

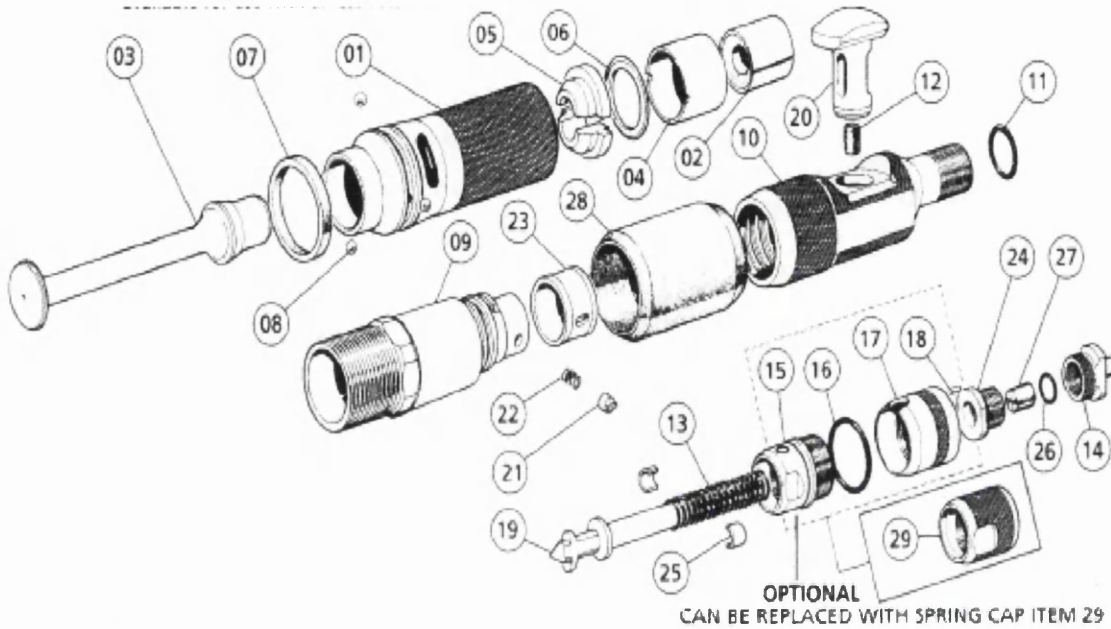


**Figure 3.3** The magnum model 7000 cattle stun gun

1	muzzle	16	safety 'O' ring
2	buffer	17	safety cap outer
3	bolt	18	safety stop pin
4	packing ring	19	firing pin
5	thrust collar (pair)	20	trigger
6	lock washer	21	extractor plunger
7	retaining ring	22	plunger spring
8	ball	23	extractor .25 cal
9	breech	24	pull bush
10	breech cap	25	pull split bush (pair)
11	small 'O' ring	26	pull lock 'O' ring
12	microvon trigger spring	27	pull ring
13	firing pin spring	28	breech locking cover
14	pull	29	spring cap
15	safety cap inner		

**Table 3.1** The table of individual parts of the stun gun

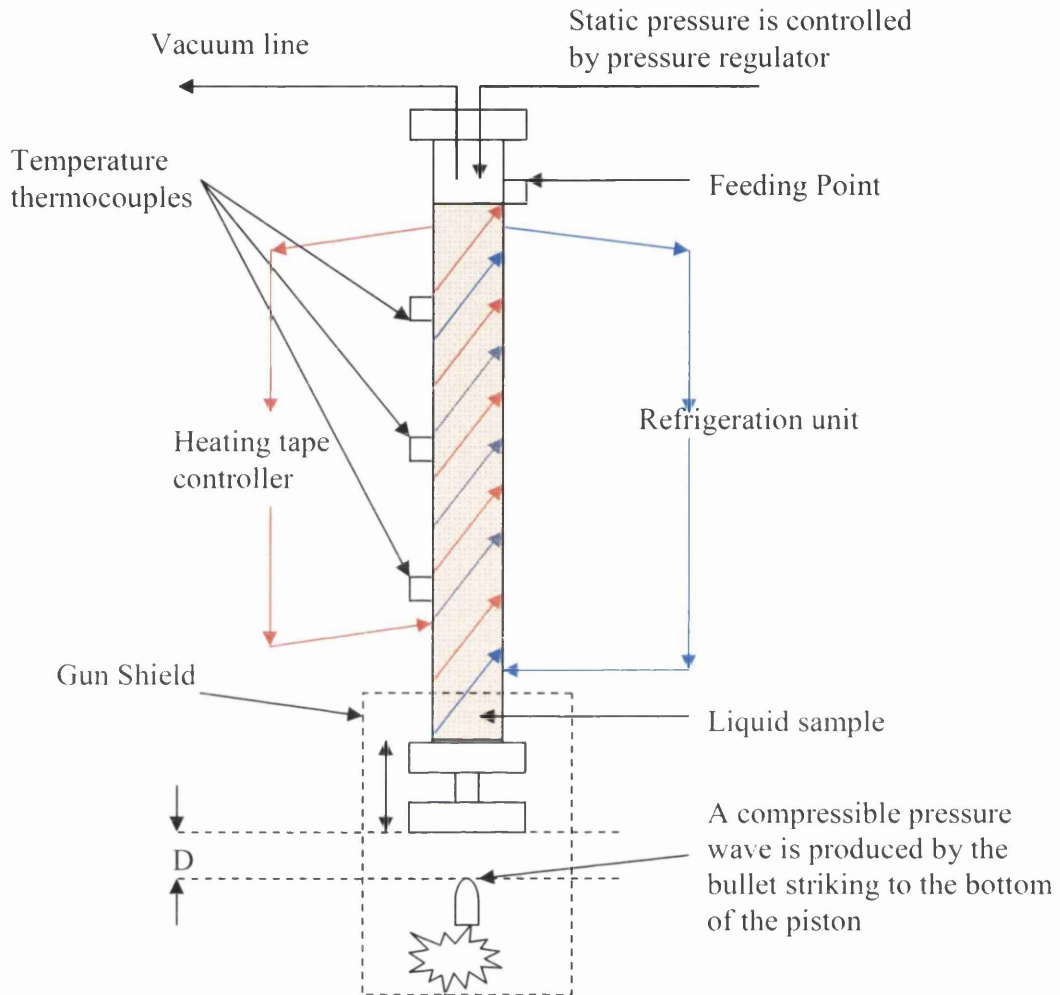


Figure 3.4: Schematic of heating /cooling system

### 3.3 Cleaning Procedure

The improved B-P apparatus was designed in such a way that cleaning procedure can be easily carried out. The top flange is connected to a high steam pressure line and, prior to experiments, superheated (110 °C) steam is blown through the tube and is subsequently drained from the bottom where the lower flange houses the piston which, when removed, provides a connection to a steam condensation system and a liquid drain point. After several hours of steam cleaning, warm water was flushed through the tube several times followed by a rinse with deionised water. If necessary (depending on the degree of contamination) a soap solution was used, and the inner wall of the tube was mechanically brushed from top and bottom. The walls of the open tube were subsequently heated and allowed to dry at 100 °C. Following this procedure the tube was allowed to cool prior to being refilled to the required depth (non-resonant heights of a liquid column) with a fresh sample of liquid which was subsequently heated to the test temperature.

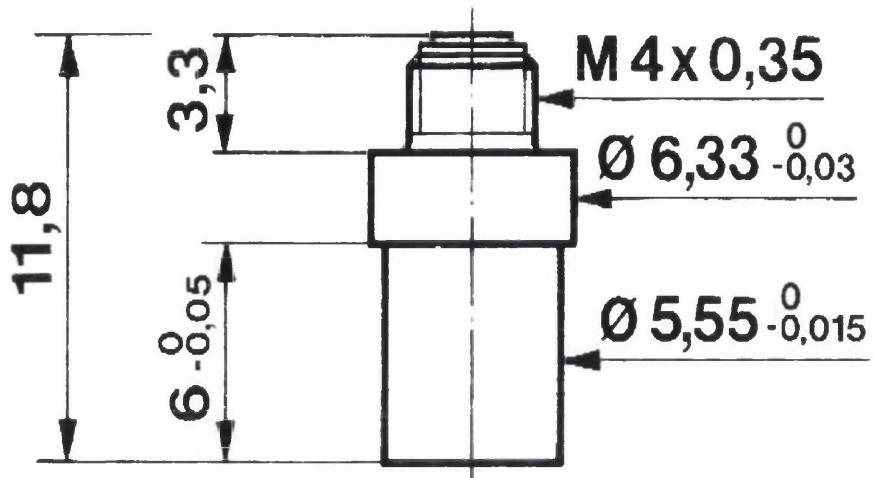
### 3.4 Signal Processing and Analysis

#### 3.4.1 Pressure Transducer (see Section 1 in figure 3.1)

Pressure changes within the liquid were monitored using dynamic pressure transducers (Kistler 603B, see Figure 3.5) mounted in mechanically isolated ports in the wall of the tube where its active surface physically in contact with the liquid in the column. The direction of shock propagation within the test liquid produced by the impact between the bolt and the bottom of piston was normal to the transducer's active surface. The Kistler 603B, which has a short rise-time (1  $\mu$ s), a high natural frequency (>450 kHz) and a 200 bar dynamic range at temperatures up to 200 °C, has been used in other cavitation studies (Tomita and Shima, 1986; Marston and Unger, 1986). It is important to note that the pressure transducer used in previous 'bullet-piston' work by Couzen and Trevena (1974) was a Kistler Type 701A which has a significantly longer rise time than the 603B (some 7  $\mu$ s) in addition to its far lower natural frequency (*ca.* 70 kHz) necessitated the use of extensive electronic filtering circuitry in previous work to avoid mechanically-induced vibrations associated with the 'ringing' of the apparatus.

The basic action of the 603B is based on piezoresistive technology which converts mechanical pressure waves into an electrical signal by deforming through a diaphragm on a quartz crystal, a single silicon crystal as a measuring element which does not undergo any plastic deformation. A Wheatstone bridge arrangement of semiconducting resistor is diffused into the surface of the transducer's diaphragm detects changes in pressure and the bridge circuit is unbalanced proportionally by the applied pressure, which is then amplified and analysed following sampling rate at 1MHz by 12-bit analog to digital convertors (ADCs) (Gage Inc., Canada).





All Dimensions mm



Active surface

Figure 3.5: The Kistler 603B pressure transducer

### 3.4.2 Data Acquisition (see Section 2 in figure 3.1)

The GageScope, manufactured by Gage Applied Sciences Inc, Canada, is a modular data acquisition system designed for the capture of transient voltage signals (see figure 3.6). The GageScope system used in the present work contained the following system control settings, including

- Sampling rate (how many sample points per second should be acquired by the CompuScope Card)
- Capture modes (continuous & one shot mode)
- Trigger level (If the voltages of an input signal crosses the trigger level, a trigger event invokes and subsequent data acquisition)
- Time-out (the amount of time GageScope for Windows wait for a trigger event to occurs)
- Post-trigger depth (signals acquired after the trigger event occurs)
- Pre-trigger depth (signals acquired before the trigger event occurs)
- Trigger depth (total amounts of samples or points can be stored, in current on-board memory of the CompuScope is 1,000,000 points)
- Multiple channels recording

The GageScope control software (Gage Inc., Canada) was used to control the time-base triggering and sampling rates, and also to transfer data to the host PC for analysis. This software controls two channels independently and the recording of data only takes place when the time-base is triggered and the GageScope is armed using 'One shot' software commands. Each channel contains options for changing the settings of individual channels, such as position, vertical scale, input range, and coupling.

In the present work the output voltages of the dynamic pressure transducers (Kistler 603 B) were sampled at sampling rates as high as 100 MHz and were fed into different channels via BNC connectors and RF coaxial cables to a GageScope C1610, 12 bit analogue to digital converter with a 2 MB memory buffer. Input voltage trigger level

could be incrementally selected (independently for each input) from as low as  $\pm 50$  mV to as high as  $\pm 5$  V. The system control can be set to record most of the samples before or after being triggered (using the pre-trigger or post-trigger function), level of trigger, and trigger depth, high sampling rate was utilized to ensure that the high speed process of the entire cavitation event were captured. The data (i.e. voltages corresponding to positive and negative pressures) were saved to computer in 'integer' format with an Gage header file which gave details of the sample rate, date and time of acquisition and channel address, later it converted to ASCII (American standard code of information interchange) file. Finally, the ASCII file which contains waveforms were imported and further analysed using a commercial digital signal processing software package called DADiSP ver. 4.0, (DSP Development Corporation, MA.).

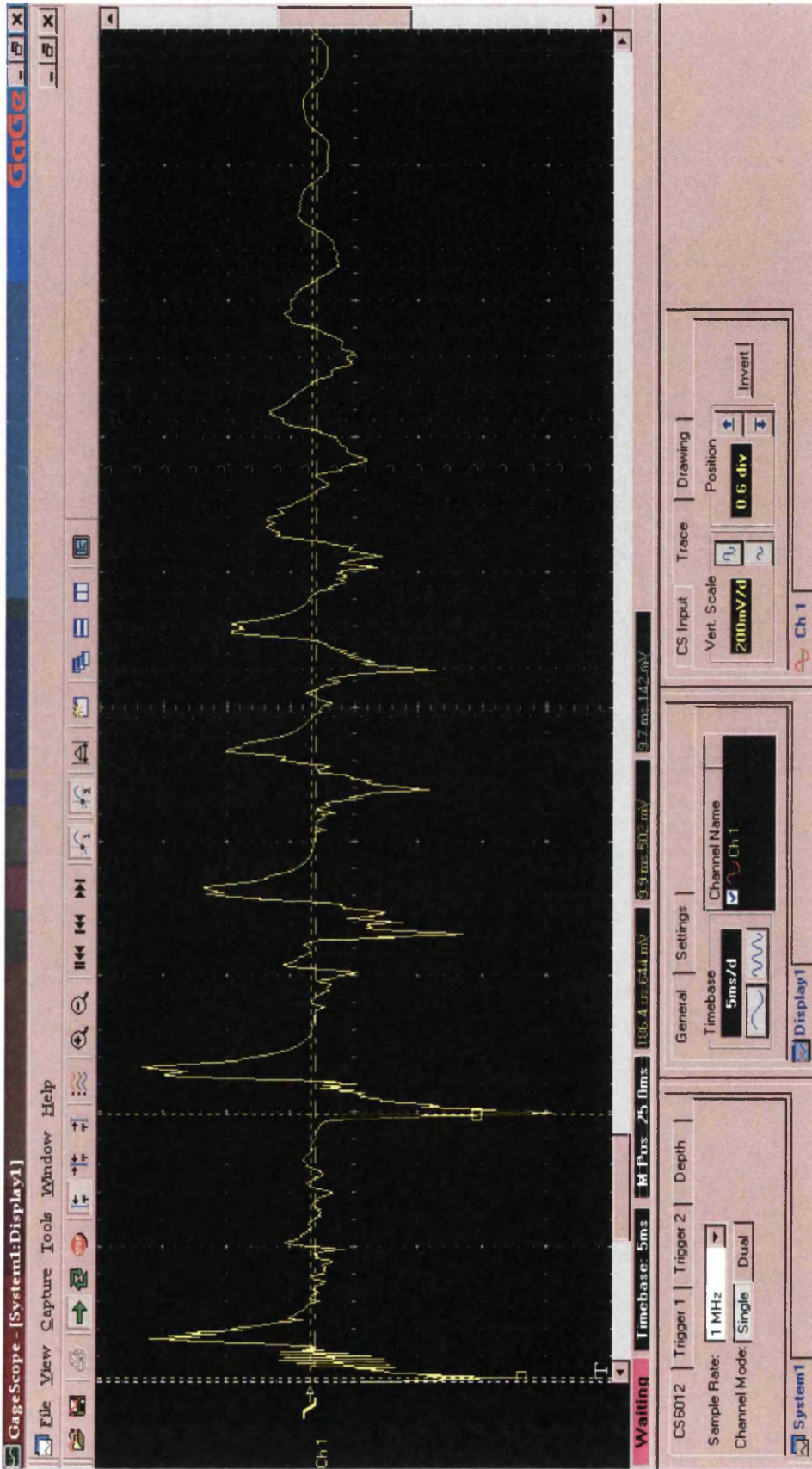


**Figure 3.6** GageScope data acquisition system: A typical pressure record obtained from a 603B transducer in an experiment on degassed, deionised water. The output voltages of the pressure transducer (Kistler 603B) were sampled at sampling rate at 1 MHz and 1,000,000 sampling points then fed into the GageScope C1610, 12 bit analogue to digital converter with 2 MB memory buffer.

### **3.4.3 Digital Signal Processing (DADiSP software) (Section 3 in figure 3.1)**

The DADiSP software package was used in the present work to eliminate the unwanted high frequency signals due to the ‘vibrational noise’ of the system, this noise originating principally due to impact between the bolt and the bottom of the piston. Digital filters were constructed based on the fast Fourier transform (FFT) which transformed the time-series data into a frequency spectrum, thereby allowing the spectrum to be manipulated (i.e. removal of the vibrational noise by band-stop filters) before converting the modified frequency spectrum back into a time-domain signal.

The GageScope file captured from the pressure transducer was converted to ASCII file format prior to importing into DADiSP ver. 4.0, (DSP Development Corporation, MA) (see figure 3.7). The total sampling points were 1,000,000 and sampling rate was 1 MHz (this is the highest speed for Kistler 603B transducer responded) (see figure 3.8). A Bandstop filter was created (see figure 3.9) to remove vibrational noise picked up during the experiments (see figure 3.10). For example, the frequencies of main pressure-tension cycle in figure 3.8, generated by the impact between the bolt and the bottom piston, are between 250-400 Hz. The unwanted vibrational noise generated in the system can be easily calculated in figure 3.8 where their frequencies range as high as 7-10 kHz or higher. Figure 3.9 also shows the main pressure-tension cycles which are associated with cavitation activity.



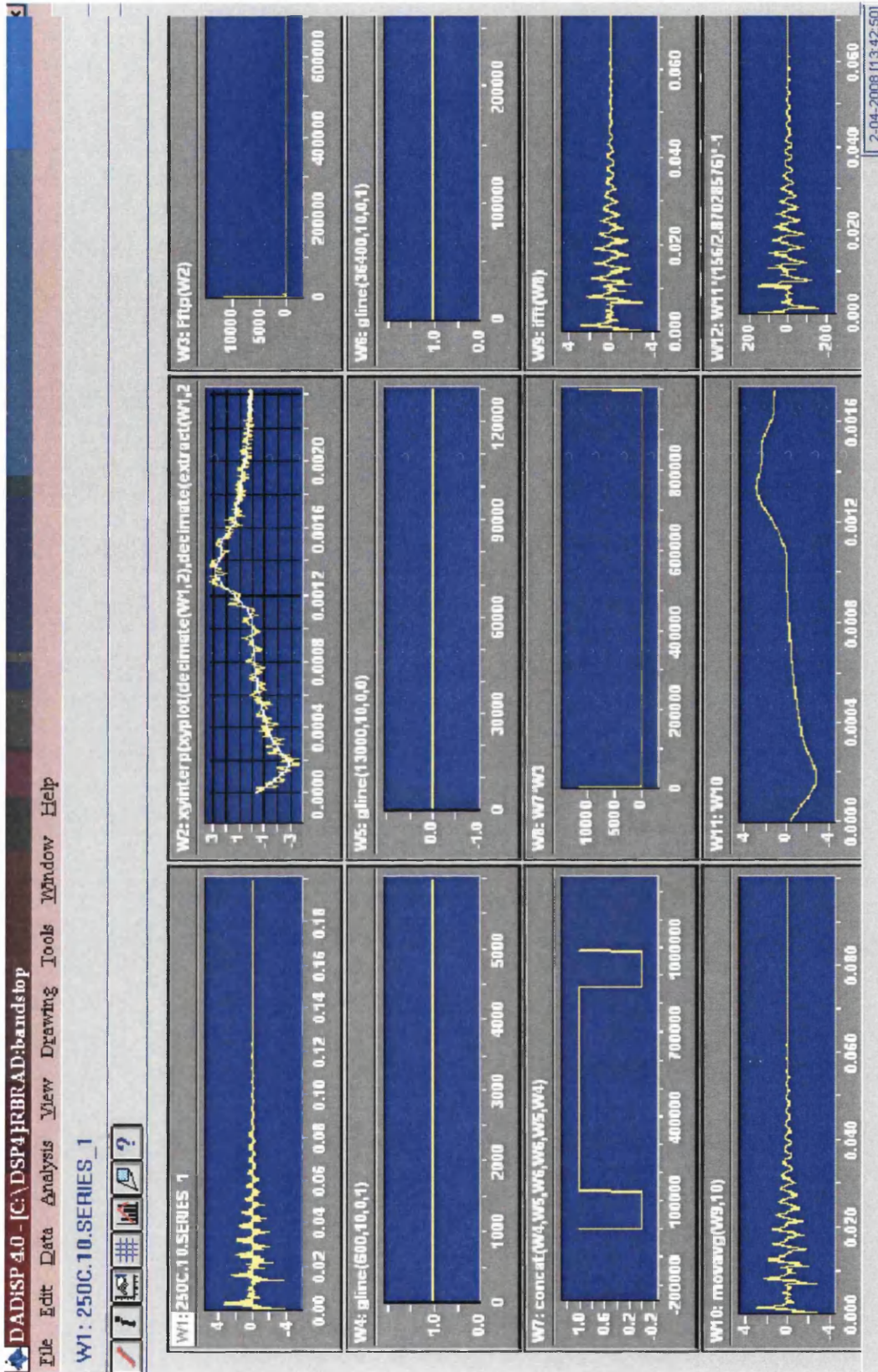
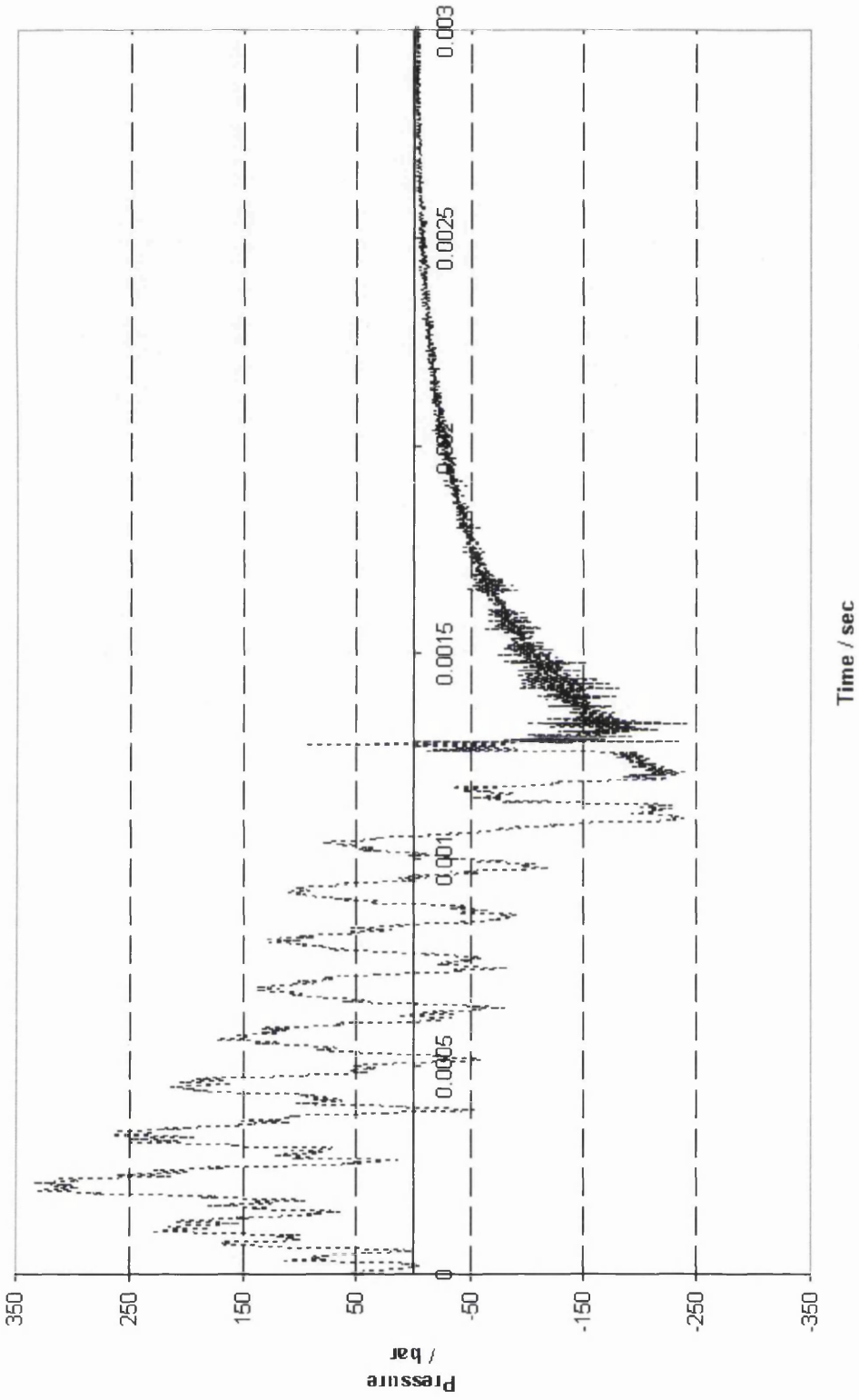


Figure 3.7 The signal processing software, Dadisp 4.0



**Figure 3.8** Results of experiments on degassed, deionised water. The expanded, raw pressure-tension cycle was recorded using the Kistler 603B at a sampling rate of 1MHz with 1,000,000 sample points.

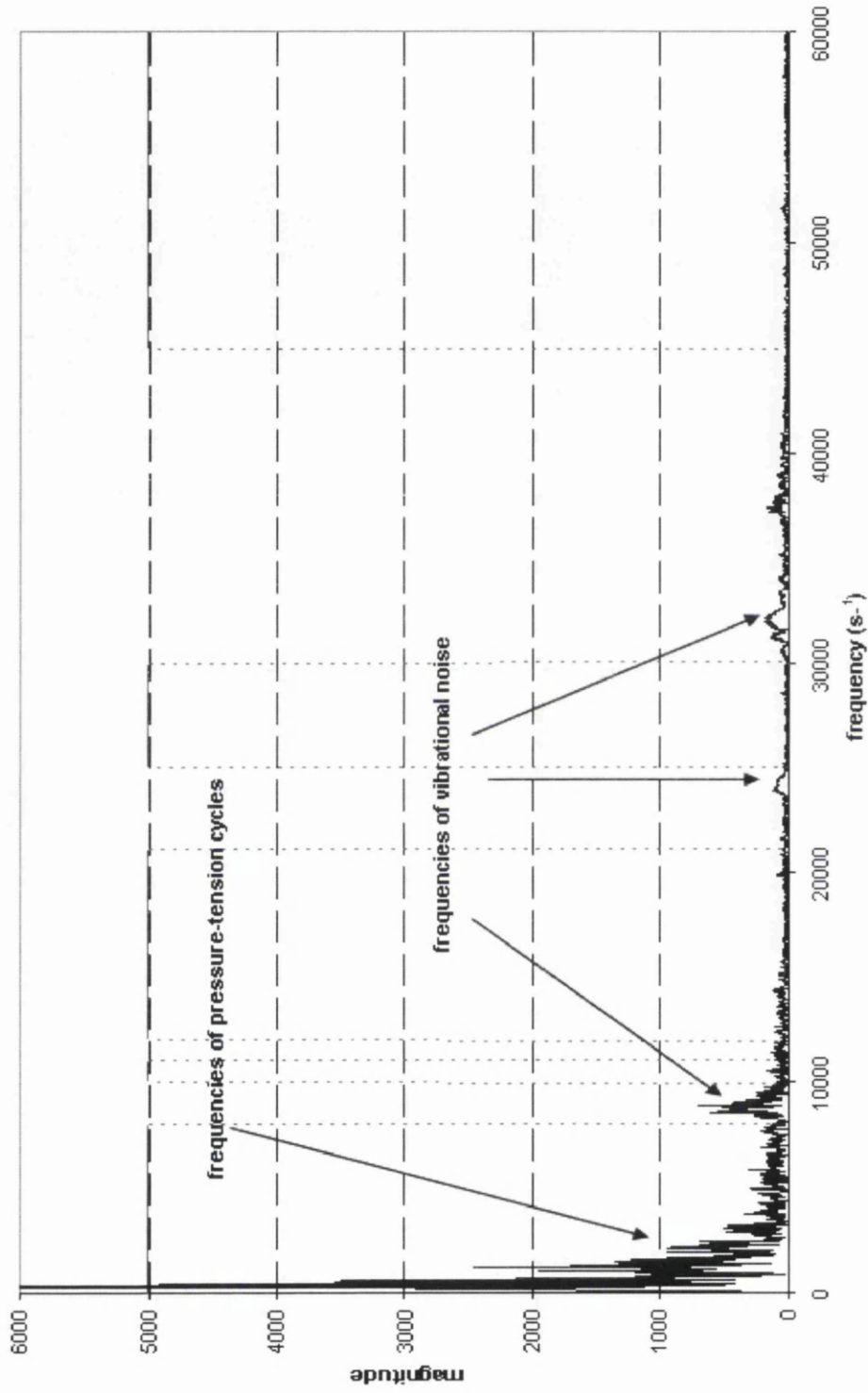


Figure 3.9 Before removal of frequency spectrum



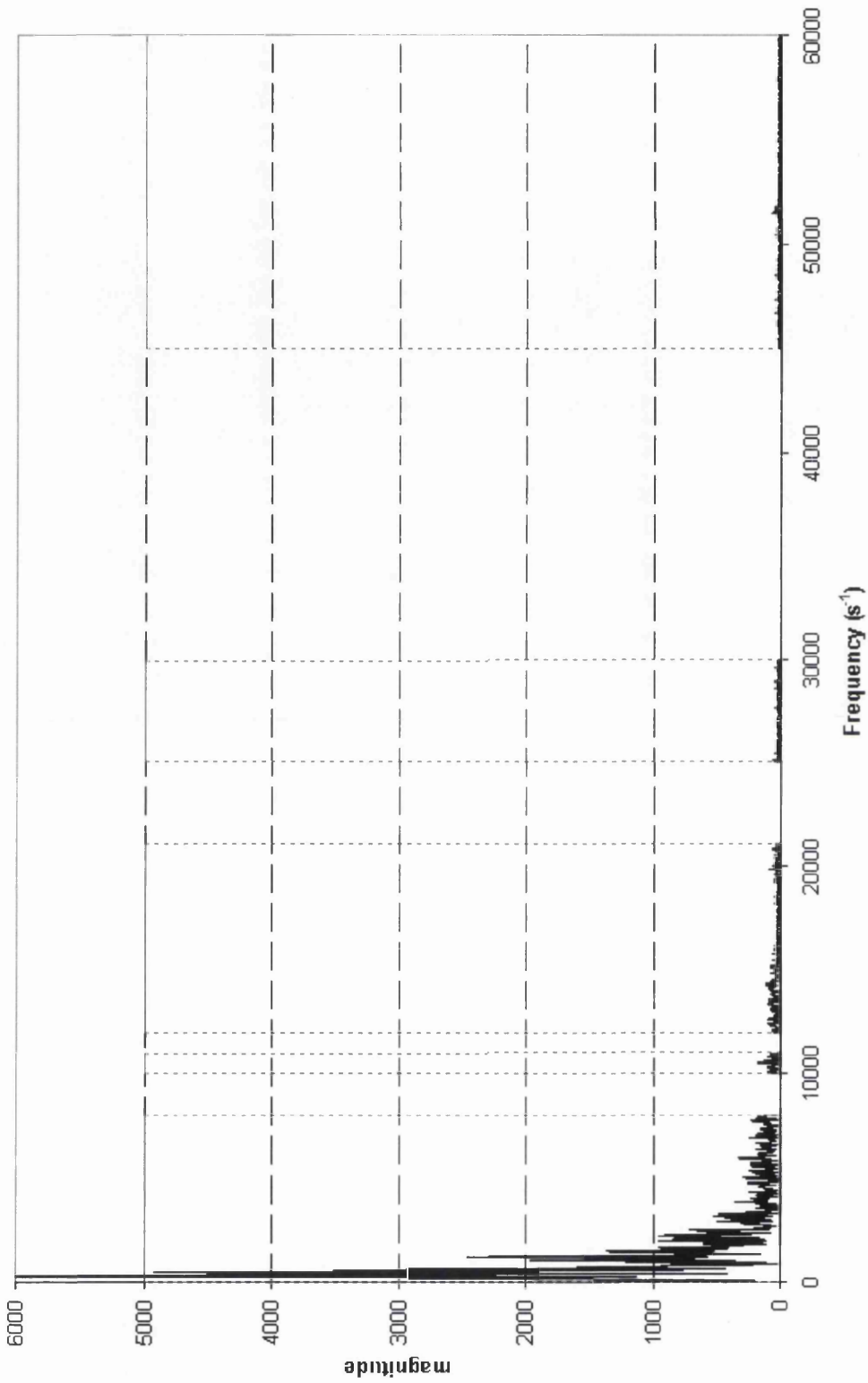
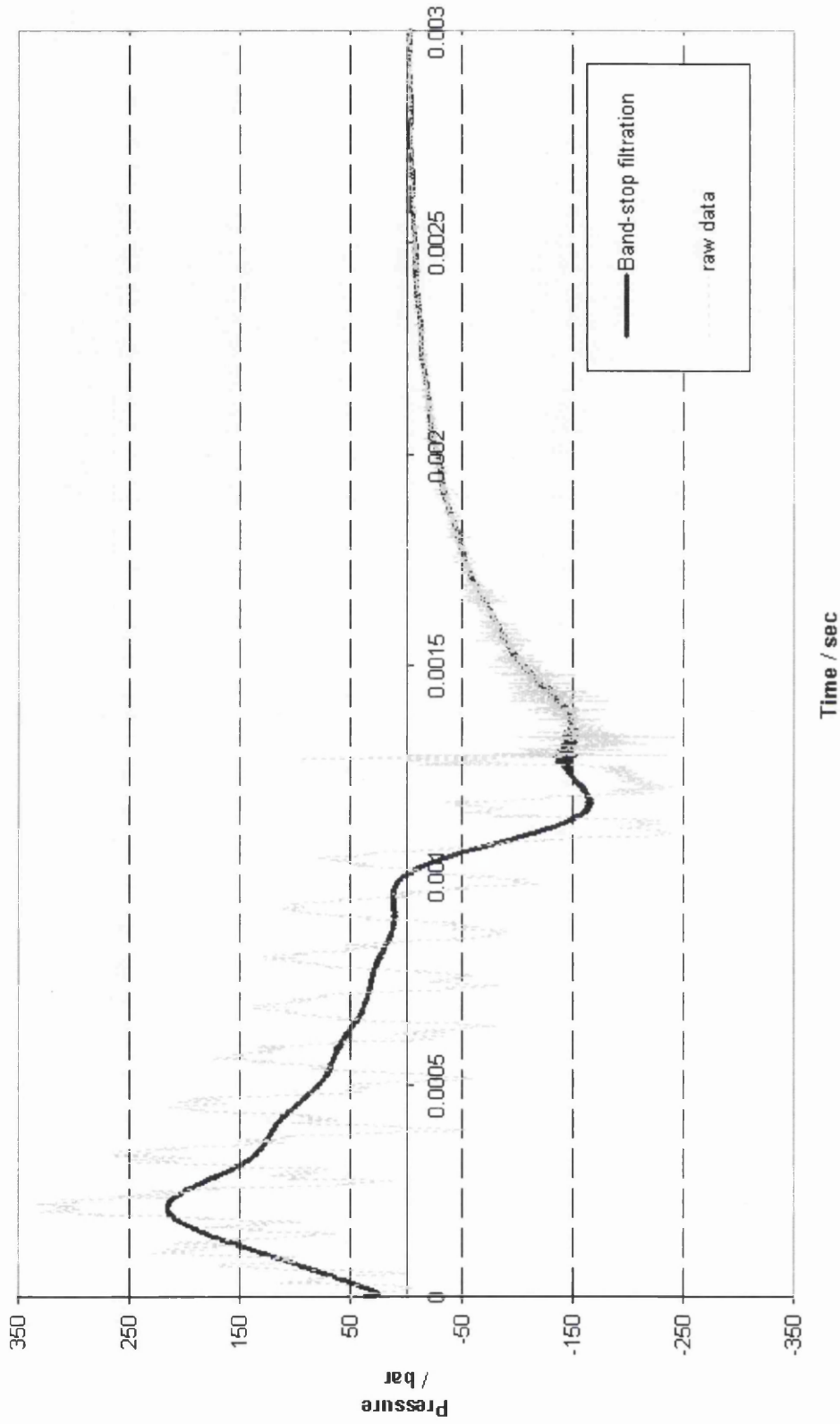


Figure 3.10 After removal of frequency Spectrum



**Figure 3.11** Results of experiments on degassed, deionised water. The filtered pressure-tension cycle

### 3.5 Determination of Cavitation Threshold, $F_c$ of Liquid Involving the Application of a Regulated Static Pressure (see Section 4 in figure 3.1)

The upward-travelling pressure wave generated by the piston is recorded as the pressure pulse denoted #1 in figure 3.12. This pulse is subsequently reflected (as tension) at the free surface of the liquid and is recorded as the downward-travelling pulse denoted #2. This pulse is eventually reflected from the face of the piston and, as the tension increases, cavitation bubbles grow from preexisting nuclei within the liquid. Eventually, these bubbles collapse, thereby compressing their contents (a mixture of non-condensable gas and vapour). Ultimately, the inward motion of the bubble walls is arrested by this compression and the bubble surface rebounds, emitting a pressure wave into the liquid as it does so. This is the origin of the feature labeled #3 in figure 3.12. The subsequent tension pulse (denoted #4) corresponds to the reflection of #3 from the free surface of the liquid (Williams *et al*, 1997).

The improved B-P method involves regulating a static pressure,  $P_s$ , in the space above the liquid column,  $P_s$  being increased gradually in a series of dynamic stressing experiments. From the dynamic pressure records obtained in these experiments a record is made of the time delay,  $\tau_i$ , between the peak incident pressure (corresponding to #1 in figure 3.12) and the first pressure pulse arising from the cavitation bubble collapse (corresponding to #3 in figure 3.12). From the work described in section 2.4.3, it is clear that the B-P experiment involves the transmission of a pulse of tension by the liquid to the face of the piston: and that cavitation may result from the effect of overlapping tension pulses. It follows that in the case of experiments in which cavitational activity is detected, the magnitude of the tension transmitted by the liquid is sufficient to result in the development of a transient net negative pressure in the presence of a background static pressure ( $P_s$ ). It is useful to recall here that, under tension, cavitation bubbles grow from pre-existing nuclei within the liquid and eventually collapse and rebound, emitting a pressure wave into the liquid as they do so. Hence the interval  $\tau_i$ , which encompasses the attainment of maximum cavity radius and its subsequent decrease to a minimum value, is reduced by increasing  $P_s$  ( $\tau_i$  therefore provides a convenient measure of cavitational

activity). Thus, an estimate of the magnitude of tension a liquid experienced before it breaks can be obtained from a knowledge of  $P_s$ , hence the direct measurement of tension by pressure transducers is eschewed.

The results of such experiments on degassed, deionised water are shown in figure 3.13, in which  $\tau_i$  is plotted as a function of  $P_s$  (absolute, in p.s.i.) and from which  $F_c$  is estimated in the following way. The time delay,  $\tau_0$ , between pulses corresponding to '1' and '2' in figure 3.12 represents the time required for the upward-travelling pressure wave to return, as tension, to the bottom transducer's location: it also represents the smallest time interval for which a cavity growth-collapse cycle could occur given that a bubble would have to grow and collapse infinitely quickly in order that  $\tau_i = \tau_0$ . Thus,  $F_c$  is estimated by extrapolation of the data in figure 3.13 to that pressure  $P_s$  at which  $\tau_i = \tau_0$ , this condition representing the complete suppression of cavitation activity. By this procedure, Williams and Williams (1999) found a value of tensile strength of 90 bar for deionised, degassed water which is an order-of-magnitude higher than the previous B-P obtained.

The signal analysis procedures and methodology detailed above were subsequently employed in the improved B-P apparatus to study the cavitation behaviour of water over a range of tensile stress development rates. That work, the first of its kind to be undertaken in dynamic stressing work involving single pulses of tension, is now described in Chapter 4 of this Thesis.

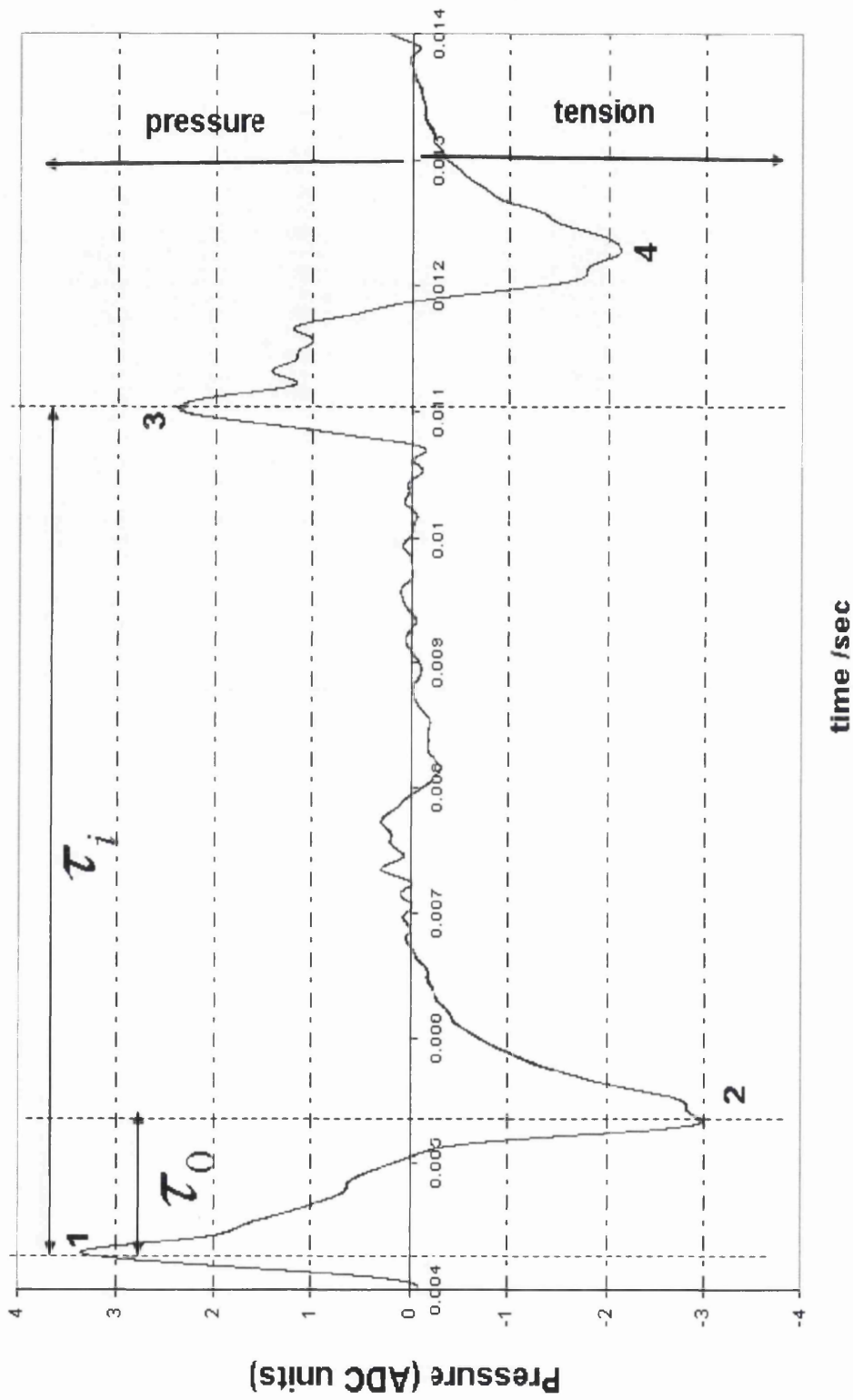
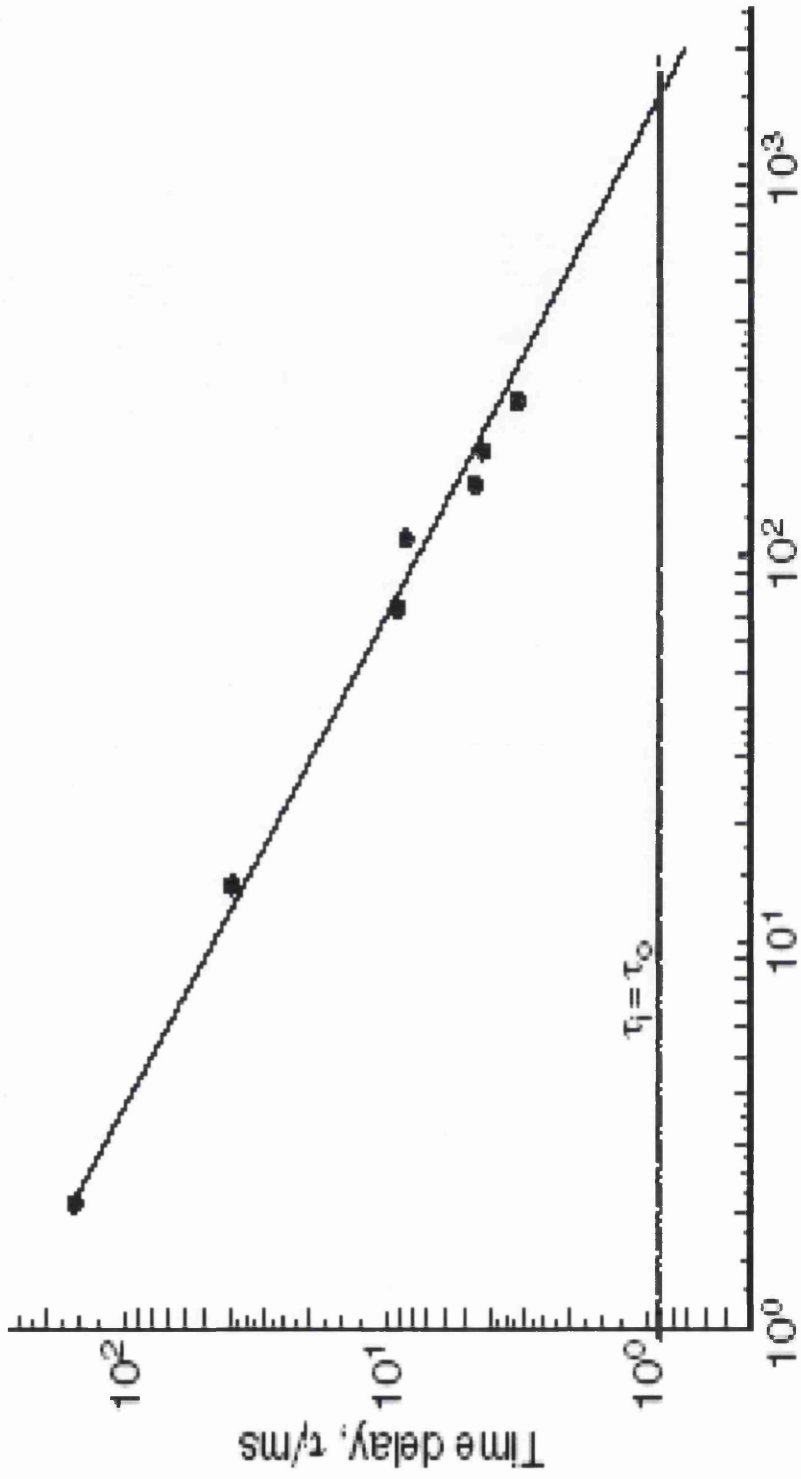
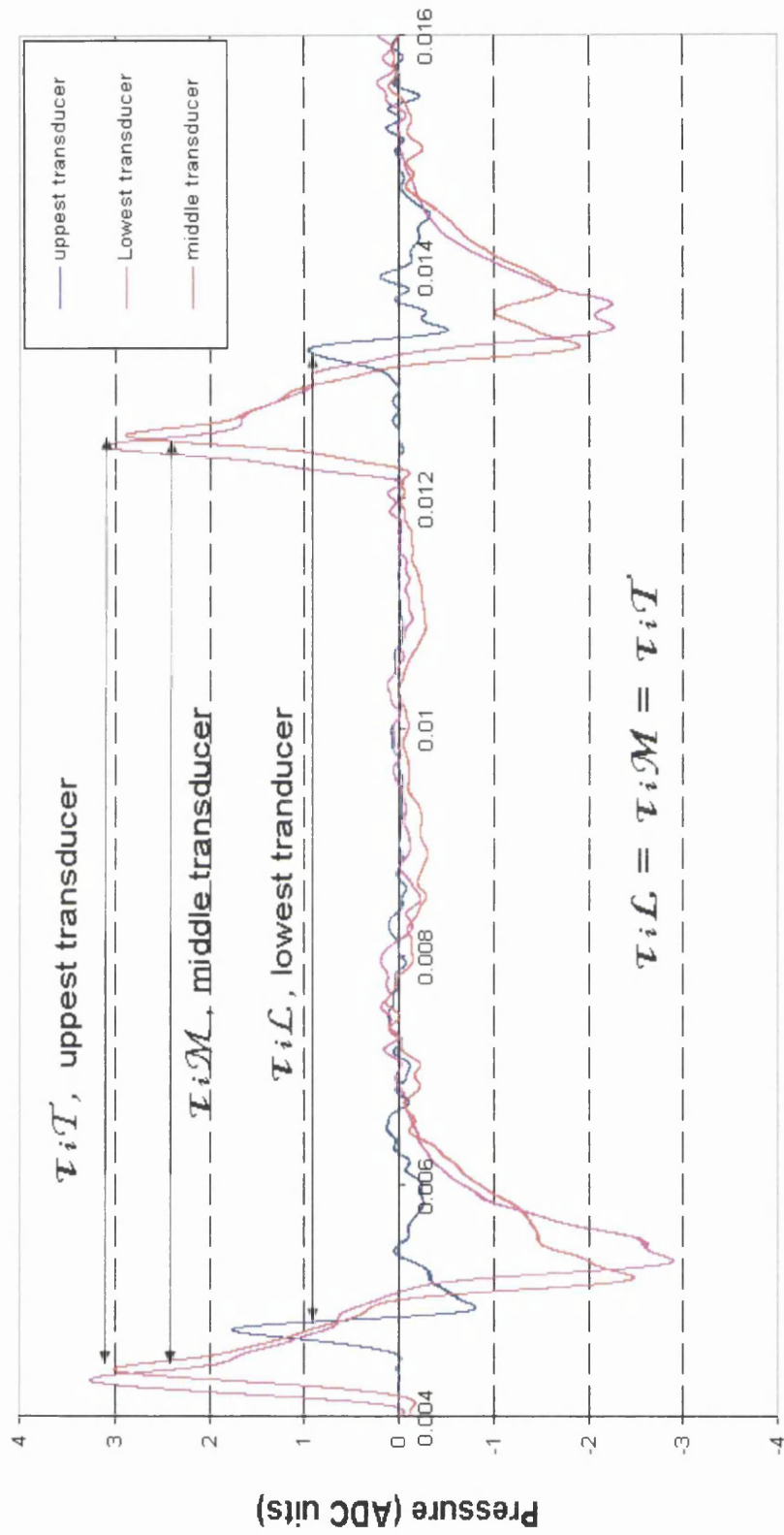


Figure 3.12 Expanded pressure record obtained from a 603B transducer showing the time intervals  $\tau_1$  and  $\tau_0$ .



**Figure 3.13** The time interval,  $\tau_i$  as a function of applied static pressure,  $P$ , (in p.s.i.) for degassed, deionised water at 20 °C. Also shown is the value of the time interval,  $\tau_0$  used to estimate  $F_c$ . (Williams and Williams, 2002)



**Figure 3.14** Details of first pressure-tension cycle produced by the bullet striking to the bottom piston and the first pressure-tension pulse arising from the cavitation bubble collapse recorded in experiments on water by three dynamic transducers in different locations along the B-P apparatus.

# Chapter 4

## *The Effects of the Effective Dynamic Stressing Rates on the Measurements of the Tensile Strength of Deionised Water*

- 4.1 *Abstract*
- 4.2 *Introduction*
- 4.3 *Experimental and Results*
- 4.4 *Discussion*
- 4.5 *Conclusion*



## 4.1 Abstract

This chapter reports the results of experiments in which samples of degassed, deionised water were subjected to dynamic stressing by pulses of tension in the B-P apparatus. The particular pulse reflection technique employed and referred to herein allows the rate of development of tension in the liquid (hereafter denoted  $\dot{\Omega}_r$ ) to be varied in a systematic manner, in order to investigate its influence on the resulting measurement of the liquid's effective tensile strength (or 'cavitation threshold'),  $F_c$ . Results are reported for experiments which involve a range of stressing rates,  $0.43 \text{ bar}\mu\text{s}^{-1} \leq \dot{\Omega}_r \leq 1.79 \text{ bar}\mu\text{s}^{-1}$ , for samples of degassed, deionised water at a constant temperature (25 °C). These experiments, which are the first of their kind to be reported, show an approximately four-fold increase of  $F_c$  at the highest stressing rate in water, this value being 224 bar (for  $\dot{\Omega}_r = 1.79 \text{ bar}\mu\text{s}^{-1}$ ) compared to a value of 60 bar at a lower stress development rate ( $\dot{\Omega}_r = 0.432 \text{ bar}\mu\text{s}^{-1}$ ). These results provide additional insight into the reasons underlying the mechanisms instead of wide ranges of values of  $F_c$  which have been reported in the literature and provide evidence to substantiate the claim, made by previous workers (Overton and Trevena, 1982) that the rate of dynamic stressing is an important consideration in understanding the cavitation properties of liquids.

## 4.2 Introduction

A review (Herbert and Caupin, 2006) of the experimental work on cavitation in water, focusing on the determination of maximum tensile strength,  $F_c$  of water is divided into two broad groups of results. The first group consists of 'quartz inclusion' studies which present values of  $F_c$  in the range  $800 \text{ bar} < F_c < 1400 \text{ bar}$ . Such studies are thought to involve homogeneous nucleation conditions, giving rise to values of  $F_c$  close to theoretical limit, where there is little dependence of  $F_c$  on stressing rate (Fisher, 1948). A second group of results, which produce values of  $F_c$  in the range  $40 \text{ bar} < F_c < 260 \text{ bar}$ , in which heterogeneous nucleation is responsible for the recorded cavitation events, and here a dependence of  $F_c$  on stressing rate may be expected (Trevena, 1982). The results of second group shown in table 4.1 reflect the findings

reported by several workers that in measurements of the maximum tensile strength of water, with different experimental techniques produce a wide range of results.

No fully satisfactory explanation has been given for the extremely broad range of values represented by the results shown in table 4.1. A principal difficulty in reconciling the results of such studies is clearly the diverse range of experimental techniques employed. Each of these techniques has different characteristic in terms of the corresponding rates of tensile stress development it invokes within a test liquid. It is arguable therefore that what has been lacking is a single technique in which the rate of tensile stress development  $\dot{\Omega}_r$  may be varied in a systematic manner in order to investigate its effect on the determination of  $F_c$ . The work now described in this Chapter set out to address this issue by developing, for the first time, a means of varying the stressing rate in the B-P apparatus while keeping the same liquid sample *in situ* within the tube.

Negative Pressure (bar)	research workers (year)	Type of water	Techniques
100	Marston and Unger (1986)	Degassed, deionised water	Impact technique (pulse reflection)
87	Boteler and Sutherland (2004)	Triply distilled, deionised, deionised water	Impact technique (pulse reflection)
96	Williams <i>et al</i> (2000)	Degassed, deionised water	B-P technique (pulse reflection)
260	Briggs (1950)	Degassed water	Z shape-Centrifugal tube
175	Strube and Lauterborn (1970)	Degassed water	Centrifugal tube
100	Henderson and Speedy (1980)	Distilled water	Pyrex glass Berthelot tube
46	Jones <i>et al</i> (1981)	Degassed water	Steel Berthelot tube
200	Galloway (1954)	Degassed water	Ultrasonic stressing
160	Greenspan and Tschiegg (1967)	Degassed water	Ultrasonic stressing
70	Willard (1953)	Degassed water	Ultrasonic stressing
240	Caupin and Herbert (2006)	Degassed water	Ultrasonic stressing

**Table 4.1** Tensile strength of water obtained by different stressing (quasi-static to dynamic) techniques at room temperature

### 4.3 Experimental and Results

#### **The Effective Tensile Strength of Degassed, Deionised Water, $F_c$ on Measurements Using the B-P Apparatus: Variation of Stressing Rate**

The main feature of a typical pressure record obtained from a 603B transducer in an experiment on deionised water is shown in figure 4.1. In this experiment the length,  $L$ , of the liquid column was 0.95 m. The upward-travelling pressure wave generated by the bullet striking to the bottom piston is recorded as the pressure pulse denoted #1 in figure 4.1. This pulse is subsequently reflected (as tension pulse) at the free surface of the liquid (due to the large difference in acoustic impedance, see figure 2.4, part a) and is recorded as the downward-travelling pulse (as a tension pulse) denoted #2 in figure 4.1. This tension pulse is eventually reflected from the face of the bottom piston and the overlapping of tension pulses increases the amplitude of tension locally (see figure 2.4, part b). If the liquid's tensile strength is exceeded cavitation bubbles subsequently grow from the preexisting nuclei within the liquid. Eventually, these bubbles collapse, thereby compressing their contents (a mixture of non-condensable gas and vapour). Ultimately, the inward motion of the bubble walls is arrested by this compression and the bubble surface rebounds due to the cushioning effect, and emitting pressure wave into the liquid denoted #3 in figure 4.1 (Williams and Williams, 1999). We refer to cycle '1-2' in figure 4.1 as the primary-tension cycle. Thereafter, the record comprises 'secondary' pressure-tension cycles ('3-4' and '5-6', etc) which have been associated with cavitational activity.

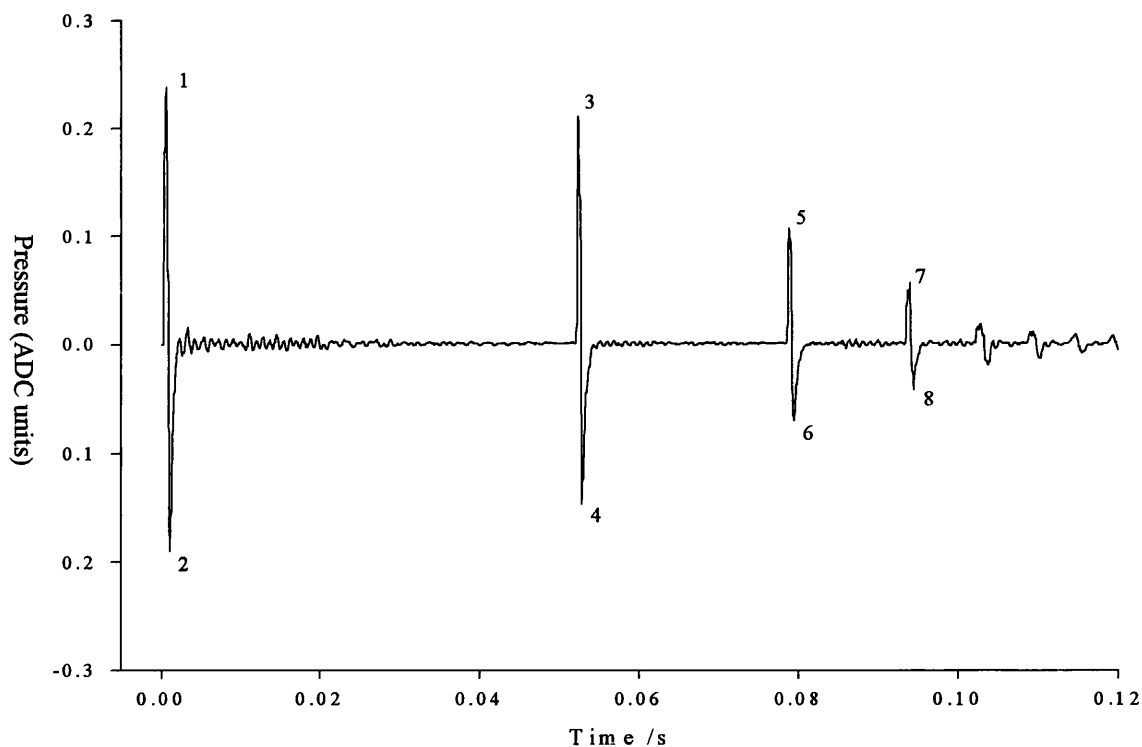


**Figure 4.1** Pressure record showing the initial and reflected pulses produced by the piston (1-2) and the subsequent pressure-tension cycles (3-4), (5-6), (7-8) and etc generated by cavitation activity in experiments on water.

The present improved B-P apparatus described in Chapter 3 was used to produce cavitation in deionised water. The test sample of deionised water used in the experiments was obtained from a two-stage, reverse-osmosis, ion-exchange purification system (Elgastat Spectrum, Elga UK). The latter incorporates a carbon filter for organics, a ‘nuclear grade’ deionisation stage, and a final membrane filter (0.2 $\mu$ m).

Experiments were conducted at room temperature, 25 °C ( $\pm 1$  °C). The cleanliness of the B-P apparatus was ensured (see section 3.3) before the experiments. Fresh deionised water samples were used for each measurement and all the samples were subjected to vacuum (-1 bar) for 30 min before each experiment to ensure a consistent sample state. In the case of experiments performed under an applied static pressure, the sample was pressurized (using oxygen-free nitrogen) for a few seconds before measurement, to minimize any pressure-loading effects. The effective dynamic tension developed in a column of liquid is controlled by variation of applied static pressure in headspace above. For each transducer reading, a record was made of the

time delay,  $\tau_i$ , between the peak pressure (corresponding to #1 in figure 4.1) and the first pressure pulse arising from the cavitation bubble (corresponding to #3 in figure 4.1);  $\tau_i$  was then plotted as a function of  $P_s$  (absolute), as shown in figure 4.2 in a different series of stressing rate conditions of experiments (see section 3.5). In figure 4.2 shown that the higher the dynamic stressing rate water experienced, the longer time delays,  $\tau_i$ , were obtained in each static pressure, hence led to the higher tensile strength,  $F_c$  of water.

It is important to note that although the pressure transducers employed do not record accurate absolute amplitudes of the dynamic tensions, they are capable of accurately recording their temporal development. It follows that by determination of  $F_c$  for various gaps,  $D$ , between the cosh and the piston (hence different stress development rates), a plot may be constructed of the pressure transducer responses to the primary pressure-tension cycle (peak '1-2' in figure 4.1) relative to  $F_c$ , since the maximum tension (or minimum pressure) recorded by the transducers where cavitation occurs is  $F_c$ . This is shown in figure 4.3, in which it is evident that each record has a distinctly different characteristic rise-time.

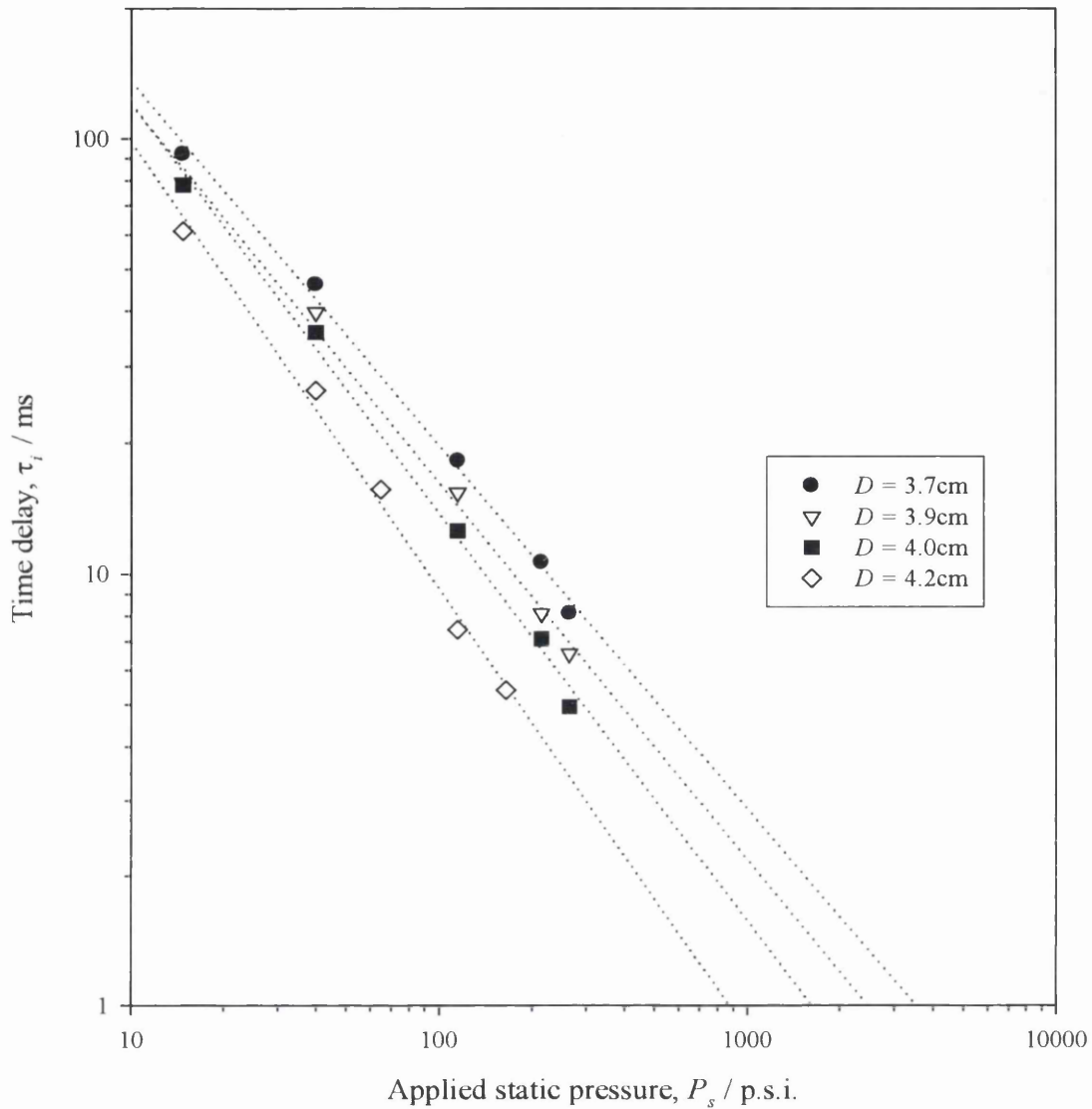


**Figure 4.2:** The time interval,  $\tau_i$ , as a function of applied static pressure (in p.s.i) with four different stressing rates subjected to deionised water at 25 °C.

In these experiments, the stressing rate was varied by varying the gap  $D$  ( $3.7 \text{ cm} \leq D \leq 4.2 \text{ cm}$ ), between the piston face and the cosh, with smallest gap producing the highest stressing rate associated with the corresponding pulse transmitted into the liquid. For each value of the gap  $D$ ,  $F_c$  was determined in the manner described before (see section 3.5, the method involving the application of a regulated static pressure,  $P_s$ ).

In the region where tension develops, the maximum rate of stress development occurs at the maximum gradient of  $P(t)$  for  $P < 0$ . This was calculated from the mean maximum gradient from gradients taken over the values of  $P$ , and corresponding times  $t$ , for  $P = 10\%P_{cav}$ ,  $25\%P_{cav}$ ,  $75\%P_{cav}$  and  $90\%P_{cav}$ , i.e., the mean gradient from the gradient of 10%-90%, 25%-75%, 10%-75% and 25%-90% (see figure 4.4).

This procedure allows the mean maximum stressing rate to be defined as,

$$\dot{\Omega}_F = \left( \frac{d\bar{F}}{dt} \right)_{\max} = - \left( \frac{dP}{dt} \right)_{\max} = \left| \frac{dP}{dt} \right|_{\max, P < 0}$$

The results for experiments at 25 °C on degassed, deionised water at four different values of  $D$  are shown in Figure 4.3. These measurements on degassed, deionised water at 25 °C for different rates of stressing ( $0.432 \text{ bar}\mu\text{s}^{-1} \leq \dot{\Omega}_r \leq 1.790 \text{ bar}\mu\text{s}^{-1}$ ) reveal a marked dependence of  $F_c$  on  $\dot{\Omega}_r$ , with  $F_c$  being significantly larger at the higher stressing rates, some 224 bar ( $\dot{\Omega}_r = 1.79 \text{ bar}\mu\text{s}^{-1}$ ) compared to 60 bar at the lowest stressing rate ( $\dot{\Omega}_r = 0.432 \text{ bar}\mu\text{s}^{-1}$ ). A linear relationship is apparent over the stressing rates considered.



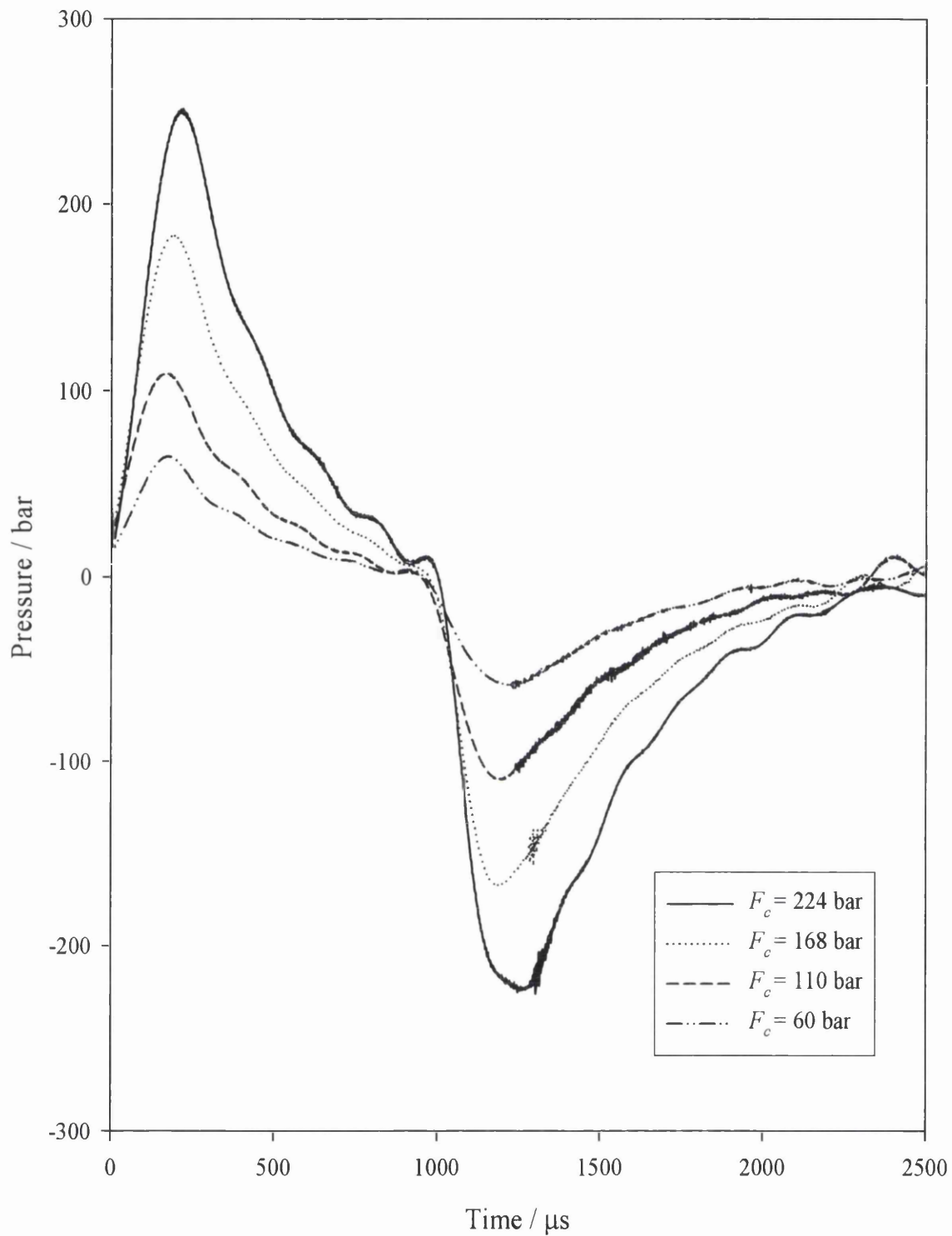


**Figure 4.3** 'Primary' pressure-tension cycles for degassed, deionised water at 25 °C for four different gap widths  $D$  ( $F_c = 224$  bar,  $D = 3.7$  cm;  $F_c = 168$  bar,  $D = 3.9$  cm;  $F_c = 110$  bar,  $D = 4.0$  cm;  $F_c = 60$  bar,  $D = 4.2$  cm).

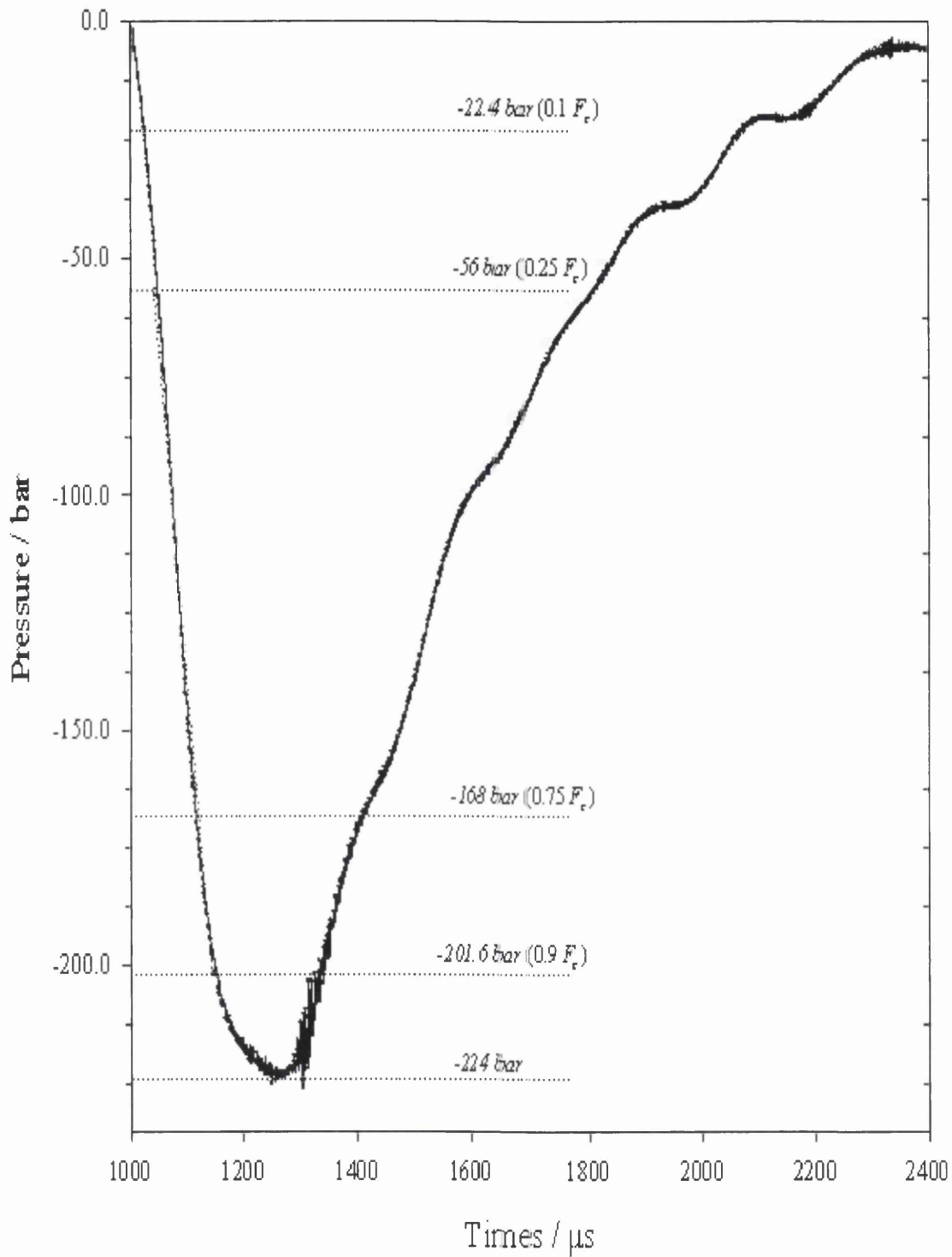


**Figure 4.4** Determination of  $\dot{\Omega}_p$  using a mean gradient approach from 'primary' tension pulse (#2 in figure 4.1) for  $D=3.7$  cm.

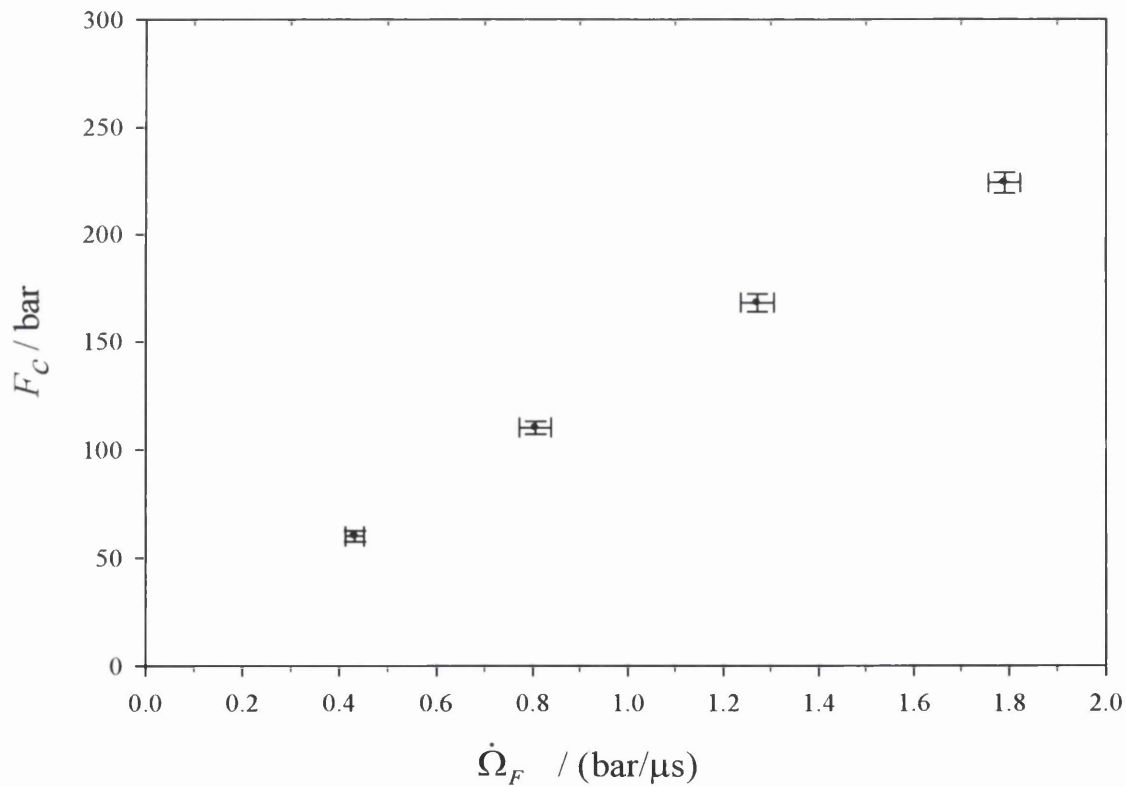
#### 4.4 Discussion

Table 4.2 is the overall summary results of the  $F_c$  as a function of stressing rate for degassed, deionised water at room temperature. These experiments, which are the first reported of their kind on degassed, deionised water, show that  $F_c$  is approximately four times larger at the higher stressing rates (a values of 224 bar at higher stressing rate of  $1.790 \text{ bar}\mu\text{s}^{-1}$ , and a value of 60 bar at lower stressing rate of  $0.432 \text{ bar}\mu\text{s}^{-1}$ ). The different rates of stressing were achieved by varying the gap between the piston and the projecting face of the cattle stun gun, and determined from the knowledge of  $F_c$  which was obtained from a series of experiments involving the application of static pressures, and the gradient of the tension peak (see figure 4.4). From figure 4.3, it is clear that the higher the rate of dynamic stressing,  $\dot{\Omega}_r$ , (i.e. the rate at which tension, or negative pressure, develops within the fluid), the higher the value of  $F_c$  is obtained (Overton and Trevena, 1982). The data in table 4.2 shows that the speed of the travelling pulse inside the liquid column remained approximately the same and close to the propagation of sound in liquid water,  $c$  (some  $1435 \text{ ms}^{-1}$ ) at all the different rates of dynamic stressing.

We recall that in previous cavitation works, involving both static and dynamic stressing, no single apparatus has been capable of producing consistent data at different rates of stressing rate. In the present work the different rates of stressing were achieved by varying the gap between the piston and the projecting face of the stun gun, and were calculated from a knowledge of  $F_c$  and the gradient of the tension pulse.

Different gap distance (cm)	total mean stressing rate, $\dot{\Omega}_F$ (bar $\mu$ s $^{-1}$ )	total standard error stressing rate (bar $\mu$ s $^{-1}$ )	Instant time, $\tau_0$ (ms)	$F_c$ (bar)	Velocity (ms $^{-1}$ ) (distance = 143 cm)
3.7	1.790	0.033	0.98	224	1421.2( $\pm$ 11.2)
3.9	1.271	0.035	0.98	168	1420.1( $\pm$ 6.6)
4.0	0.806	0.033	0.99	110	1429.3( $\pm$ 9.5)
4.2	0.432	0.019	1.00	60	1427.0( $\pm$ 9.4)

**Table 4.2**  $F_c$  as a function of stressing rate for deionised water at 25 °C



**Figure 4.5**  $F_c$  as a function of stressing rate on the water at 25 °C

The results shown in figure 4.5 indicate that the values of  $F_c$  increase linearly with increased rate of stressing. This result reinforces a previous indication in dynamic stressing work (Overton and Trevena, 1982) which is that the breaking tension (i.e. effective tensile strength) of a liquid depends on the rate of stressing: a higher stressing rate leads to a higher breaking tension and vice versa. In addition, the present data can be used to estimate which the result would be obtained under quasi-static conditions (such as in the Berthelot tube). The present data suggests that a value of approximately 12 bar would be obtained under such a low rate stressing conditions and it is noteworthy that this is in good agreement with the results of previously reported Berthelot tube work involving steel tubes (Trevena, 1987).

The data shown in figure 4.3 reveals that the maximum amplitude of the pressure pulse generated in the liquid water was approximately 250 bar, this pulse being subsequently converted to tension by reflection at the free surface, and the highest tension recorded was 224 bar (at  $1.790 \text{ bar}\mu\text{s}^{-1}$ ). It is believed that this is the highest experimental value of tensile strength of water ever reported in the B-P dynamic stressing method. If the stressing rate were to be increased further, it is likely that  $F_c$  would eventually reach a limiting or 'plateau' value which represents the maximum tension the deionised water can withstand under these experimental conditions (Couzen and Trevena, 1969 & 1974).

## 4.5 Conclusion

When measure the value of the experimental breaking tension of a liquid,  $F_c$ , it is most important to realize that they pertain to the prevailing experimental conditions in the particular experiment. In cavitation work involving dynamic stressing it would seem that one of the most important factors is the stressing rate a liquid experiences: a higher stressing rate leads to a higher breaking tension and vice versa (Overton and Trevena, 1982). It is also suggested by Heyes (2008) that the faster the stretching process or the rate of stressing, the higher the negative stress that a liquid can be sustained before cavitation sets in, as liquid-vapour phases separation will ‘intervene’ at higher values along the isotherm (having less time to undergo this process). The present results reveal that under a range of rates of tensile stress development, samples of degassed, deionised water present markedly different values of effective tensile strength which range from ca. 60 bar to ca. 250 bar. These values span the range reported by different experimental results described in table 4.1, which involve various stressing techniques (quasi-static to dynamic), each of which may be assumed to produce a different characteristic rate of tensile stress development.

It is a significant feature of the present work that the results have been produced from a single technique, consisting of experiments conducted within the same apparatus in which the rate of stressing is deliberately varied. The results of such a study have not previously been reported. They clearly establish the importance of stressing rate in considerations of the effective tensile strength of liquids under conditions where heterogeneous nucleation prevails and emphasize that any attempt to reconcile the results of previous cavitation studies should take this factor into account.

It is interesting to note that differences in the tensile strength of glycerol measured in various dynamic stressing experiments have also been explained in terms of stressing rate (Trevena, 1982 & 1984). Carlson and Henry (1973) used the reflection principle to convert a pressure pulse into a tension pulse by a flexible Mylar membrane. From these series of experiments, they found the breaking tension of glycerol to be 600 bar whereas Bull (1956) using a B-P experiment, found a value of about 60 bar for the breaking tension of glycerol. In both experiments cavitation of the liquid is known to occur in the body of the liquid but the rate of stressing is some  $10^4$  times lower in the

B-P experiment than in Carlson and Henry's apparatus. In addition, differences in stressing rate appear to explain the apparent discrepancy between the results of static and (pulse) dynamic stressing experiments on liquid mercury. Briggs (1953) applied a static method (centrifugal tube) and was unable to generate static tensions greater than 425 bar, whereas, in subjecting this liquid to a tension pulse formed by reflection of a pressure pulse at a stretched Mylar film, Carlson (1975) found the tensile failure occurred at a tension of 19,000 bar, at a stressing of ca.  $10^6 \text{ bar}\mu\text{s}^{-1}$ : with a lower stressing rate at  $1 \text{ bar}\mu\text{s}^{-1}$ , Williams *et al* (1998) found a limit for  $F_c$  of ca 3,000 bar by using tube-arrest apparatus.

It is also noteworthy that the characteristic times of the pulses used herein correspond to those involved in some biomedical application of low frequency ultrasound in between a range from 20 kHz to 45 kHz (Rosenschein and Rassin, 1998); and the tensile strength of water reported here considerably exceeds the values of tension thought to be generated *in vivo* by some ultrasound devices. Thus our findings may have significance in the context of assessing the safety of ultrasound application in relation to its potential to induce cavitation (Williams *et al*, 1998).

The outcomes of the study reported in this Chapter also suggest that the new B-P technique might prove a useful research tool for engineering liquids such as motor lubricants which experience ranges of tensile stress development in the action of components such as dynamically loaded journal bearings. The operation of an engine involves different stressing rates so this is a potentially very important development. In order to assess the utility of the new B-P technique in such an application, further work was conducted in which the tensile strength of various engine oils was tested over a range of rates of tensile stress development. This is the first such study ever to be undertaken on these liquids. That work is now described in Chapter 5.

# Chapter 5

## *The Cavitation Properties of Monograde and Multigrade Oils under Dynamic Stressing by Tension Pulses over a Wide Range of Temperature*

- 5.1 *Abstract*
- 5.2 *Introduction*
- 5.3 *Experimental Techniques*
- 5.4 *The Dependence of  $F_c$  on Temperature*
- 5.5 *The Dependence of  $F_c$  on Shear Viscosity,  $\mu$*
- 5.6 *The Dependence of  $F_c$  on Stressing Rate,  $\dot{\Omega}_F$*
- 5.7 *The Influence of the Polymer Concentration on the  $F_c$*
- 5.8 *Conclusion*



## 5.1 Abstract

This chapter reports the effects of temperature, shear viscosity and the rate of stressing,  $\dot{\Omega}_r$  on measured values of the ‘effective’ tensile strength (or ‘cavitation threshold’),  $F_c$ , of commercial monograde and multigrade oils under dynamic stressing by tension pulses, this being a feature of the conditions experienced by a motor lubricant within a ‘divergent section’ of dynamically loaded journal bearing and the method used to estimate  $F_c$  avoids reliance on direct measurements of substantial dynamic tensions using conventional pressure transducers.

Two monograde oils (designated grade API CC), 10W and 40 Diesel, and two multigrade oils (designated grade API CF), 10W40 and 15W40 were tested in this work. Results are reported for B-P experiments involving a range of stressing rates, from  $0.6 \text{ bar}\mu\text{s}^{-1}$  to  $1.4 \text{ bar}\mu\text{s}^{-1}$  for these commercial oils over the temperature range  $25 \text{ }^\circ\text{C} \leq T \leq 110 \text{ }^\circ\text{C}$  which are representative of those encountered under their normal operating conditions. These experiments, which are the first of their kind to be reported, indicate that at any given temperature,  $F_c$  increases with increasing stressing rate ( $157 \text{ bar} < F_c < 220 \text{ bar}$  at  $25 \text{ }^\circ\text{C}$  and,  $130 \text{ bar} < F_c < 157 \text{ bar}$  at  $110 \text{ }^\circ\text{C}$  for the 10W oil;  $172 \text{ bar} < F_c < 223 \text{ bar}$  at  $25 \text{ }^\circ\text{C}$  and,  $146 \text{ bar} < F_c < 172 \text{ bar}$  at  $110 \text{ }^\circ\text{C}$  for 40 Diesel oil;  $175 \text{ bar} < F_c < 200 \text{ bar}$  at  $25 \text{ }^\circ\text{C}$  and  $152 \text{ bar} < F_c < 171 \text{ bar}$  at  $110 \text{ }^\circ\text{C}$  for 10W-40 Diesel oil;  $172 \text{ bar} < F_c < 212 \text{ bar}$  at  $25 \text{ }^\circ\text{C}$  and,  $156 \text{ bar} < F_c < 174 \text{ bar}$  at  $110 \text{ }^\circ\text{C}$  for the 15W-40 Diesel oil).

These results provide evidence to substantiate the claim (made by previous workers – Trevena, 1987) that the rate of dynamic stressing is an important consideration in understanding the cavitation properties of liquids. The experiments also indicate that in addition to shear viscosity and temperature, the stressing rate,  $\dot{\Omega}_r$  may be an important consideration when evaluating a lubricant’s cavitation performance. This chapter also reports complementary experiments to determine the effect of polyacrylamide, PAA additives on the effective tensile strength,  $F_c$  of deionised water.

## 5.2 Introduction

### Cavitation in Bearings

In 1886 Osborne Reynolds published his classic paper on the mechanism of hydrodynamic pressure generation in lubricating films. In this paper, he pointed out the possible influence of cavitation on bearing behaviour. The formation of cavities and their disposition affects the pressure generated in a continuous thin film and hence quantities such as the load capacity of bearings.

The behaviour of lubricating films in bearings has been studied extensively and a comprehensive account has been given by Taylor (1974) and Dowson and Taylor (1975, 1979). They review various boundary conditions that are applicable to the cavitation region. Under conditions of slow viscous flow a wedge-shaped lubricant film with a slight convergence in the direction of motion is found essential if load-supporting pressures are to be generated in the lubricant. This concept - the 'physical wedge' - is the essence of hydrodynamic lubrication theory. Many machine elements, however, present to the lubricating film not only a converging form but also a divergent section (as depicted in figure 5.1). Such machine elements include journal bearings, gears, rolling-element bearings, and some thrust bearings. In the divergent clearance space, the lubricant subjects to negative pressure due to the separation of the bearing surfaces changes with time and eventually give rise to the forms of cavitation.

The principal forms of cavitation in lubricating films are gaseous and vaporous cavitation. Gaseous cavitation may arise as the pressure of the lubricant falls below the saturated pressure of the dissolved gases, at which stages these gases emerge from solution. This type of cavitation is not generally associated with any erosion or damage effect but is an essential contribution to load bearing capacity. Vaporous cavitation occurs if the pressure in the lubricant further falls to its vapour pressure, resulting in (predominantly) vapour-filled cavities which may grow, collapse and rebound violently. It is the dynamics of these bubbles which are associated with the production of shock waves and high speed jets – factors implicated in cavitation erosion or 'pitting' (refer to

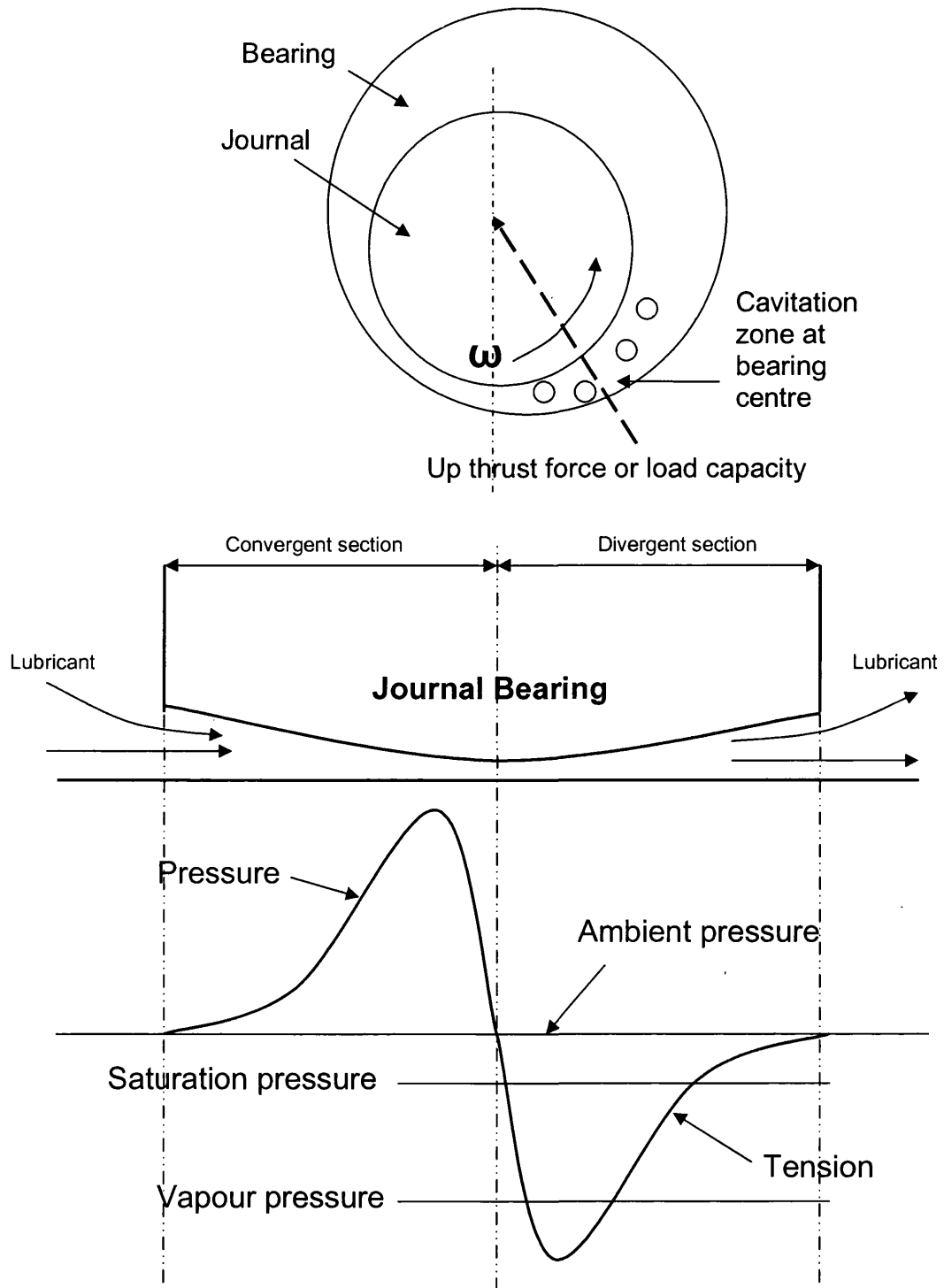


**Figure 5.1** Positive and negative pressure experienced by continuous, incompressible lubricating fluid flow through a journal bearing (from Dowson and Taylor, 1979).

section 1.4.4). Vapourous cavitation is the principal subject of the present Chapter of this Thesis.

Cavitation in fluid-film bearings does not necessarily have a deleterious effect upon bearing loading-carrying capacity. If the lubricant film does not rupture then the force component normal to the surface motion, or load capacity will be zero since the convergent and divergent portions of the film will make equal and opposite contributions. However, when negative pressure in the lubricant exceeds its cavitation threshold,  $F_c$ , the lubricant ruptures (or ‘cavitates’) at the divergent section (see figure 5.1), and there will be a net force component normal to the surfaces due to the anti-symmetrical pressure distribution in the lubricant. Hence it may be seen that the load-carrying capacity results from the occurrence of film rupture (Dowson and Taylor, 1979). Cavitation effects in lubrication are also crucial to the stability characteristics of submerged journal bearings and the absence of cavitation can lead to bearing failure (Li *et al*, 2000 and Sawicki *et al*, 2004). Therefore, the effective tensile strength,  $F_c$  of engine oil is an important consideration in the assessment of flow boundary conditions within fluid film bearing, their loading bearing capacity, and the cavitation damage potential of liquids.

During the flow of an oil within a dynamically loaded journal bearing, the lubricants are exposed to a wide range of temperature, pressure and dynamic stressing conditions. Of particular importance in an automobile context is the ability to perform satisfactorily at the low temperature pumpability at ‘cold-starting’ (by reducing the time it takes to pump oil to critical parts of the engine at such a condition hence able to significantly reduce wear), as well as the relatively high temperature encountered in normal ‘hot-running’. The viscosity of a lubricant decreases significantly with increasing temperature and the ideal lubricant must therefore have a sufficiently low viscosity at low temperature to assist cold starting; and high enough viscosity at normal operating temperatures to support the relevant loads. An essential requirement is therefore a relatively ‘flat’ viscosity-temperature relationship. One way of producing such a lubricant is to add to a mineral oil a small percentage of ‘viscosity-index’ (VI) improver, in the form of oil-soluble long-chain polymers. These ‘multigrade’ oils satisfy the viscosity requirements of

one Society of Automotive Engineers (SAE) grade at low temperatures, and another SAE grade at high temperature (Williamson *et al*, 1997).

Cavitation in lubrication has a huge potential to cause damage to solid surfaces due to the production of shock wave and liquid jets from the asymmetrical cavitation bubbles (Dugdale and Wall, 1965; Shima *et al*, 1983; Tomita and Shima, 1986; Trevena, 1987). One of the large-unsolved questions in fluids engineering concerns the effects of viscoelasticity on cavitation performance involving the additional polymer package, in order to improve energy efficiency and have also been associated with some mitigating effects of viscoelasticity on cavitation (Shima *et al*, 1985; Berker *et al*, 1995). The role of fluid elasticity in modifying the collapse of cavities may reduce their cavitation damage potential by reducing the amplitude of the shock waves associated with the rebound of cavities and the interaction of shocks with cavities can produce the local high pressure. Since the high-speed liquid jet is formed due to the asymmetry of collapse as a result of a pressure gradient across the cavity, so special polymer additives in the lubricant may reduce the non-sphericity of cavities in shear shields, thereby reducing the tendency for the liquid jet formation – the pressure developed in this case can be an order of magnitude lower than for non-spherical bubbles (Chahine and Bovis, 1981; Kezios and Schowalter, 1986). In addition, Williams *et al* (1998) using an improved T-A experiment (see section 1.5.2.1) demonstrated that the suppression of the liquid jet is due to an increased resistance to elongational flow conferred upon the liquid by the polymer additive hence reduce cavitation damage. Therefore, the non-Newtonian rheological properties conferred upon lubricants by polymer additives might have a mitigating effect on a potentially damaging cavitation-related mechanism (Barrow *et al*, 2004).

Although the precise mechanisms underlying any such effects remain unresolved, they may involve the influence of polymer additives on the maximum tension which the liquid can withstand before rupture (its cavitation threshold, or effective tensile strength  $F_c$ ) (Williams and Williams, 2002). Under conditions of dynamics stressing by tension (such as occurs in dynamically-loaded journal bearings) there is evidence that the presence of polymer can lower the cavitation threshold. Such a result was reported by Sedgewick and Trevena (1978) for experiments involving the stressing of water containing

polyacrylamide additives by the ‘bullet-piston’ reflection method. That work demonstrated that the presence of the polymer additives leads to a reduction in the tensile strength; the greater the concentration of the polymer the greater is this reduction in the tensile strength. They claimed that due to the long polymer molecules ‘crowd together’ at a point to form a nucleus on which cavitation could set in and such a possibility is more likely to occur in the more polymer added solution. However, the same solutions investigated using T-A dynamics stressing technique, the tensile strength increased by the same polymer addition (Overton *et al*, 1984), and when subjected to quasi-static stressing in the Berthelot tube, the presence of polymer additives in the water makes no discernible difference to the effective tensile strength of the liquid obtained (Sedgewick and Trevena, 1978).

In this chapter, results are reported for B-P experiments involving a range of stressing rates ( $0.40 \text{ bar}\mu\text{s}^{-1} \leq \dot{\Omega} \leq 1.60 \text{ bar}\mu\text{s}^{-1}$ ) for two different commercial multigrade oils (10w-40 oils; API CF, and 15W-40 oil; API CF) and two commercial monograde oils (API CC), 10W and 40, over the temperature range  $25 \text{ }^\circ\text{C} \leq T \leq 110 \text{ }^\circ\text{C}$ . For the first time, the rate of stress development and the temperature of the oil are considered in relation to their influence on  $F_c$ . An important motivation in the present work is the fact that no single technique has previously been established as a reliable means of measuring tensile strength of various commercial motor lubricants under conditions of engineering relevance.

### 5.3 Experimental Techniques

The B-P apparatus used in the present work is essentially that described in chapter three. Measurements were conducted by the dynamic stressing technique described in chapter four, using a pulse of tension (‘negative pressure’) created by the reflection of a pressure pulse at a boundary, but the present experiments involved a wide range of temperatures,  $T$ ,  $25 \text{ }^\circ\text{C} \leq T \leq 110 \text{ }^\circ\text{C}$ , which there is a paucity of data concerning the temperature dependence of  $F_c$  under appropriate conditions of dynamic stressing especially in the case of engineering fluid such as motor lubricants.

The duration of the pressure (or tension) pulses is typically 200-500  $\mu\text{s}$ , with a rise time to peak amplitude of 50-100  $\mu\text{s}$ . The characteristic time of the pulse is an important feature of the B-P techniques in terms of its relevance to lubrication phenomena. Within a dynamically loaded journal bearing, for example, at typical engine speeds between 2000 and 6000 rpm, the characteristic times of rate of tensile stress development in oils within the engine bearings are commensurate with the times scale of stressing associated with the action of the present B-P apparatus.

In the present work, dynamic stressing experiments were conducted on commercial samples of two monograde oils (API CC), 10W and 40 Diesel, and two multigrade oils (API CF), 10W40 Diesel and 15W40 Diesel. In each experiment, the free surface was 0.95 m above the face of the piston at the base of the liquid column. All the samples were subjected to vacuum (-1 bar) for 40 min before each experiment to ensure a consistent sample state. In the case of experiments performed under an applied static pressure, the sample was pressurized (using oxygen-free nitrogen) for a few seconds before measurement, to minimize any pressure-loading effects. The effective dynamic tension developed in a column of liquid was controlled by variation of applied static pressure in headspace above.

In these experiments, the stressing rate was varied by varying the gap  $D$  ( $3.7 \text{ cm} \leq D \leq 4.2 \text{ cm}$ ), between the piston face and the cosh, with smallest gap producing the highest stressing rate associated with the corresponding pulse transmitted into the liquid. For each value of  $D$ ,  $F_c$  was determined in the manner described before (see section 3.5). The shear viscosity of the liquids was measured using an ARES controlled-strain rheometer (Rheometric Sci., USA) fitted with a cone-and-plate geometry.

#### 5.4 The Dependence of $F_c$ on Temperature

In the present B-P apparatus, the measurements of  $F_c$  of various engine oils were made over the range from  $25\text{ }^\circ\text{C} \leq T \leq 110\text{ }^\circ\text{C}$ . It is useful to recall here that, under tension, cavitation bubbles grow from preexisting nuclei within the liquid and eventually collapse and rebound, emitting a pressure wave into the liquid as they do so. Hence the time delay,  $\tau_i$  which encompasses the attainment of maximum cavity radius and subsequent decreases to a minimum value, is reduced by increasing  $P_s$ ,  $\tau_i$  therefore provides a convenient measure of cavitation activity.

The 'prime' pressure-tension cycles for 10W-40 Diesel oil obtained in experiments at two temperatures of  $25\text{ }^\circ\text{C}$  and  $110\text{ }^\circ\text{C}$  are shown in figure 5.2. The time delay  $\tau_0$  represents the time required for the upward travelling pressure wave to return, as tension, to the lower transducer's location, which its speed of the pulse decreases with increasing the temperature ( $\tau_{0,110^\circ\text{C}} \gg \tau_{0,25^\circ\text{C}}$ ). The overall results of measured variation of tensile strength and its viscosity with temperature for the test oils is reported in table 5.1 to 5.4 and shown graphically in figure 5.3. The estimated uncertainty in the determination of the effective tensile strength of the samples is  $\pm 5\%$  in each case.

The monograde and multigrade oils are all capable of sustaining a substantial transient tension, in excess of 150 bar, over the range of temperatures employed. The commercial samples of two monograde and multigrade engine oils were studied experimentally to assess the effect of polymer additives. It is interesting to note that the tensile strengths of the 10W-40 Diesel multigrade oils were found to be comparable to the 10W oil  $F_c$  at  $25\text{ }^\circ\text{C}$  and tending towards the 40 Diesel oil  $F_c$  value at  $110\text{ }^\circ\text{C}$ , indicating that their formulation encompasses 10W oil behaviour at low temperature whilst tending 40 Diesel oil behaviour at high temperatures. In another words, the multigrade oils consisting of two SAE grades at low and high temperatures due to the polymeric effect. In addition, the  $F_c$  of the 15W-40 Diesel multigrade oils were found slightly higher than  $F_c$  of 10W-40 multigrade oils at  $25\text{ }^\circ\text{C}$  and almost similar value of  $F_c$  at  $110\text{ }^\circ\text{C}$ .



In these experiments, the constant gap between the piston and the projecting face of the cattle stun gun was 3.9 cm. It should be noted that these values are higher than those previously reported (Williams and Williams, 2003 & 2005) due to the higher rate of stressing employed in the current work. It is expected that higher the rate of dynamic stressing,  $\dot{\Omega}$ , the higher the value of  $F_c$  obtained (refer to chapter four).

T / °C	$F_c$ (10W; API CC) (bar)	Viscosity (Pa s)
25	185.2	0.054
50	166.0	0.008
70	156.0	0.003
90	152.0	0.002
100	152.4	0.001
110	150.0	0.001

**Table 5.1:** Tensile strength and viscosity data for 10W monograde oil at various temperature under dynamic stressing with width gap D = 3.9 cm

T / °C	$F_c$ (40D; API CC) (bar)	Viscosity (Pa s)
25	210.0	0.203
50	195.0	0.049
70	185.0	0.015
90	170.0	0.010
100	168.0	0.007
110	165.0	0.006

**Table 5.2:** Tensile strength and viscosity data for 40 Diesel monograde oil at various temperature under dynamic stressing with width gap D = 3.9 cm

T / °C	$F_c$ (10W-40D; API CF) (bar)	Viscosity (Pa s)
25	191.0	0.092
50	185.3	0.027
70	179.0	0.013
90	170.0	0.007
100	171.0	0.005
110	170.0	0.004

**Table 5.3:** Tensile strength and viscosity data for 10W-40 Diesel multigrade oil at various temperature under dynamic stressing with width gap  $D = 3.9$  cm

T / °C	$F_c$ (15W-40D; API CF) (bar)	Viscosity (Pa s)
25	201.6	0.136
50	184.3	0.026
70	181.6	0.012
90	173.5	0.006
100	172.5	0.005
110	171.5	0.004

**Table 5.4:** Tensile strength and viscosity data for 15W-40 Diesel multigrade oil at various temperature under dynamic stressing with width gap  $D = 3.9$  cm

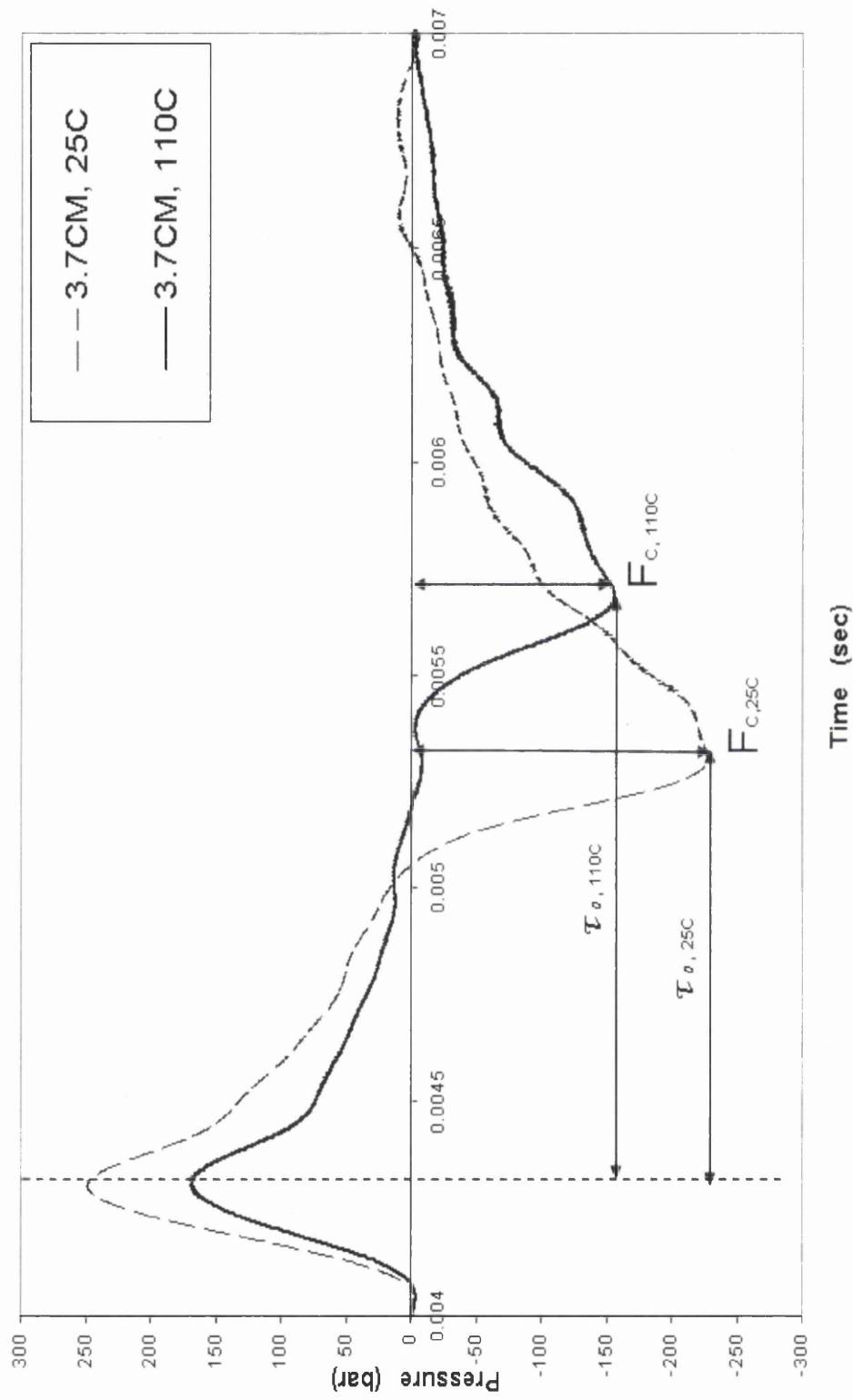


Figure 5.2 Primary pressure-tension cycles for SAE 10W-40 Diesel oil at two temperatures, 25 °C and 110 °C.

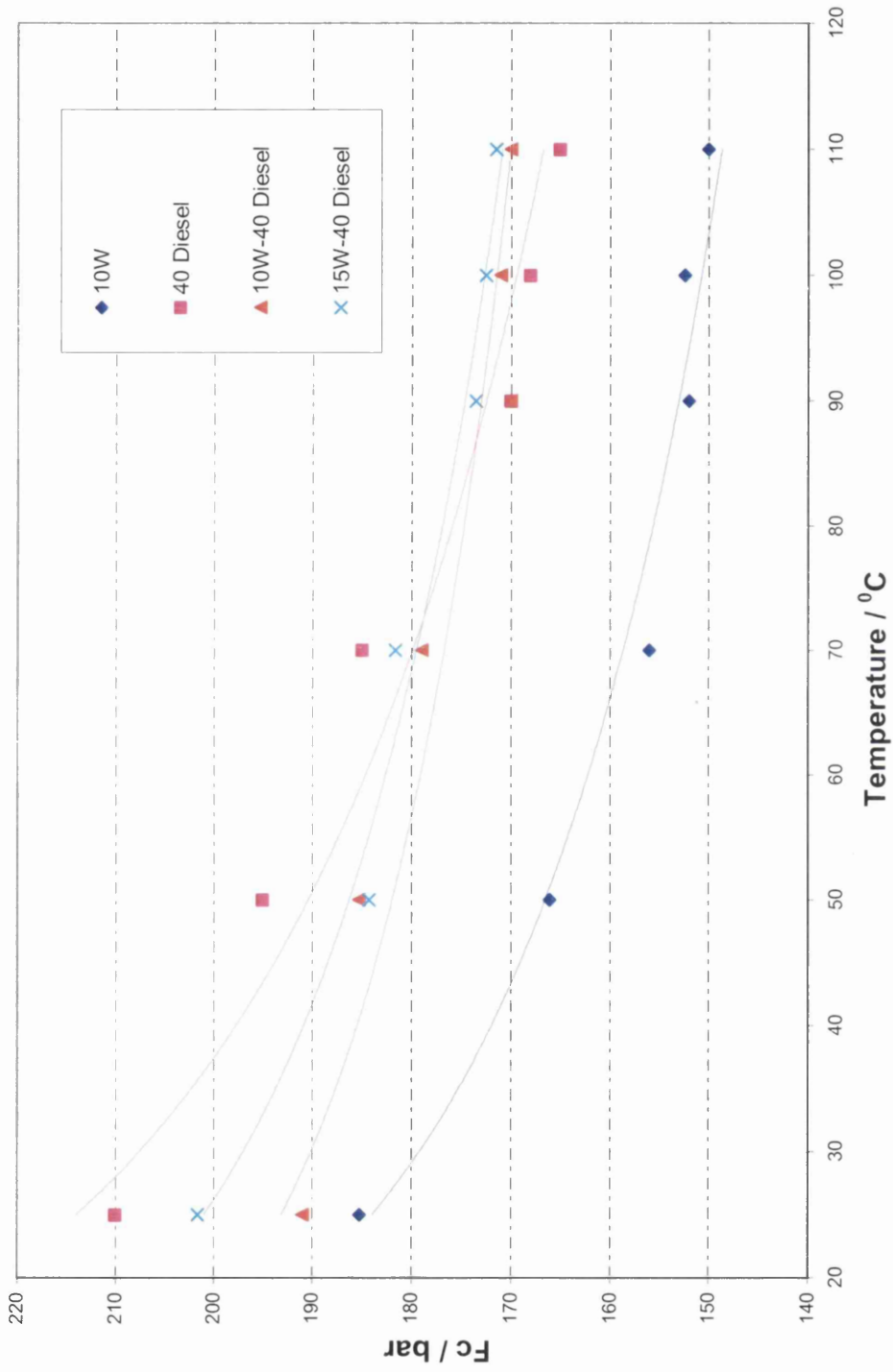


Figure 5.3  $F_c$  as a function of temperature for monograde (10W, 40 Diesel) and multigrade (10W-40 Diesel, 15W-40 Diesel)

### 5.5 The Dependence of $F_c$ on Shear Viscosity, $\mu$

Very few studies of the dependence of  $F_c$  on shear viscosity,  $\mu$  have been conducted but, among the work reported, pulse reflection methods have figured prominently, the B-P experiment being the most widely employed. Bull (1956), Couzen and Trevena (1974) reported that their results be represented by an expression of the form  $F_c \propto \mu^n$ , the value of  $n$  being 0.2 in the former study, whereas the latter workers reported a value of 0.056.

The relationship form  $F_c \propto \mu^n$  obtained by Bull (1956) in the pulse reflection work on samples of water, olive oil, glycerol and syrup has been attributed as due more to a coincidental distribution of nuclei in these different liquids than to other, more basic features of cavitation. Williams and Williams (2002) used a version of the present improved B-P method on a range of Newtonian silicone oils (Dow Corning 200 series, BDH Chemicals, UK) of different shear viscosities (1, 50, 100 and 350 cS). Their results may be represented by an expression of the form  $F_c \propto \mu^n$ , where  $n = 0.09 (\pm 0.005)$  a finding corresponding more closely to that ( $n = 0.056$ ) reported by Couzen and Trevena (1974) for silicone oils, in similar viscosity range. It is noteworthy that both involved a series of silicone oils with a range of viscosities, rather than a range of different fluids, with different viscosities, as in the work of Bull (1956).

Carlson and Levine (1975) reported a power-law relationship for samples of glycerol whose viscosity was varied by changing the test temperature, the value of  $n$  found in their work being 0.3. In the present B-P experiments, where both similar measurements of  $F_c$  are based the reflection principle was used to convert a pressure pulse into a tension pulse and in which the liquid's viscosity was varied by changing its temperature (as in the case of the present work involving different types of engine oils), the measured variation of tensile strength,  $F_c$  with temperature for the test oils is reported in table 5.1 to 5.4 and figure 5.3, and the viscosity measurements at each temperature ( $25\text{ }^\circ\text{C} \leq T \leq 110\text{ }^\circ\text{C}$ ) were made using the Rheometrics Scientific (USA) ARES rheometer with a cone and plate geometry are shown in figure 5.4.

In figure 5.4 shows the shear viscosity as a function of temperature for monograde (10W, 40 Diesel) and multigrade (10W-40 Diesel, 15W-40 Diesel) oils. The relationship of temperature / viscosity improvement is vital physical parameter to a lubricant where at low temperature is thin enough to flow, at high temperature is thick enough to protect the engine bearings.  $F_c$  as a function of viscosity for four engine oils for constant gap, 3.9 cm widths D, the results may be represented by an expression of the form  $F_c \propto \mu^n$ , where  $n = 0.054$  and  $n = 0.07$  for monograde oils of 10W and 40 Diesel respectively;  $n = 0.048$  and  $n = 0.045$  for multigrade oils for 10W-40 Diesel and 15W-40 Diesel respectively (refer to figure 5.5). Surprisingly, the value of  $n$  found in the multigrade oils were slightly lower than monograde oils, it indicates that the  $F_c (\mu)$  of multigrade oils are less dependent on temperature due to the effects of polymer additives. The difference in  $n$  value for the engine oils studied may reflect differences in formulation in terms of the type of polymer additives and their relative concentrations in oil treatments.

All  $n$  found in present work are closed to  $n$  obtained by Couzen and Trevena (1974) and Williams and Williams (2002) which involved the same dynamic stressing. However, the values of  $n$  obtained by Carlson and Levine (1975) is much greater than the present work, it may be due to the rate of tensile stress development used before is approximately  $10^4$  times higher than the present work. In figure 5.6 and figure 5.7 indicate that  $n$  is dependent on the stressing rate,  $\dot{\Omega}$ , where the higher the rate of stressing the liquid experienced, the higher the  $n$  is obtained. Figure 5.8 is a semi-logarithmic plot of the tensile strength,  $F_c$ , of four engine oils (10W, 40 Diesel, 10W-40 Diesel and 15W-40 Diesel) against shear viscosity,  $\mu$ , where its viscosities decrease with increasing the temperature ( $25\text{ }^\circ\text{C} \leq T \leq 110\text{ }^\circ\text{C}$ ). Figure 5.9 shows that the velocity of the travelling pulse within the test sample generated by the piston, decreases as temperature increasing. Therefore, the expanded series of 'prime' pressure-tension records obtained from different temperatures of experiments ( $25\text{ }^\circ\text{C} \leq T \leq 110\text{ }^\circ\text{C}$ ) with the constant gap, D = 3.9 cm in figure 5.10 shows that as the temperature increases, the speed of the pulses decreases (time delay,  $\tau_0$  increases) due to the decrease in its viscosity,  $\mu$ .

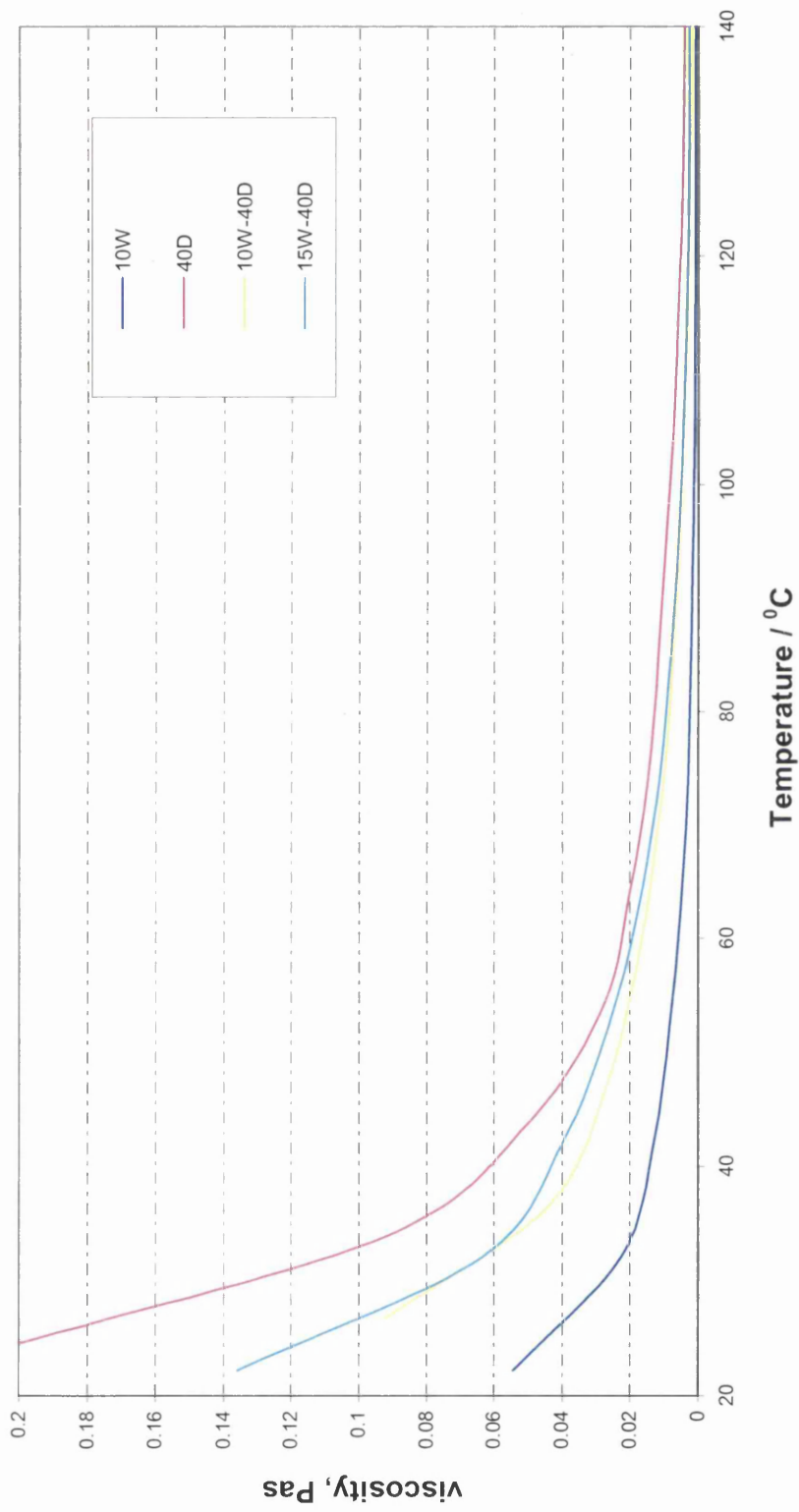


**Figure 5.4** Shear viscosity as a function of temperature for monograde (10W, 40 Diesel) and multigrade (10W-40 Diesel, 15W-40 Diesel) oils. These shear viscosities of the four types of engine oils were measured by ARES controlled-strain Rheometer (Rheometric Sci., USA)

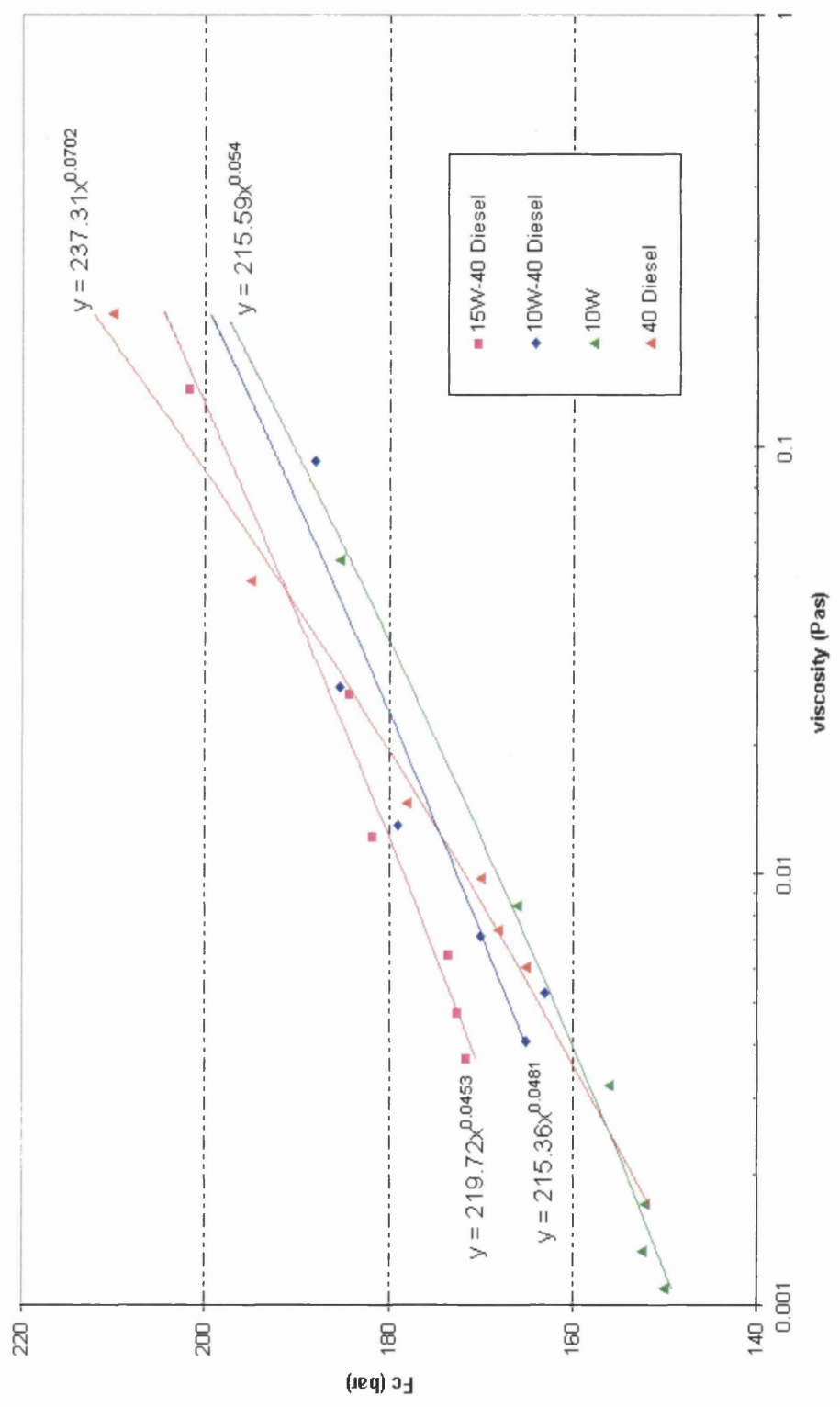


Figure 5.5  $F_c$  as a function of viscosity for various engine oils for constant gap, 3.9 cm widths D



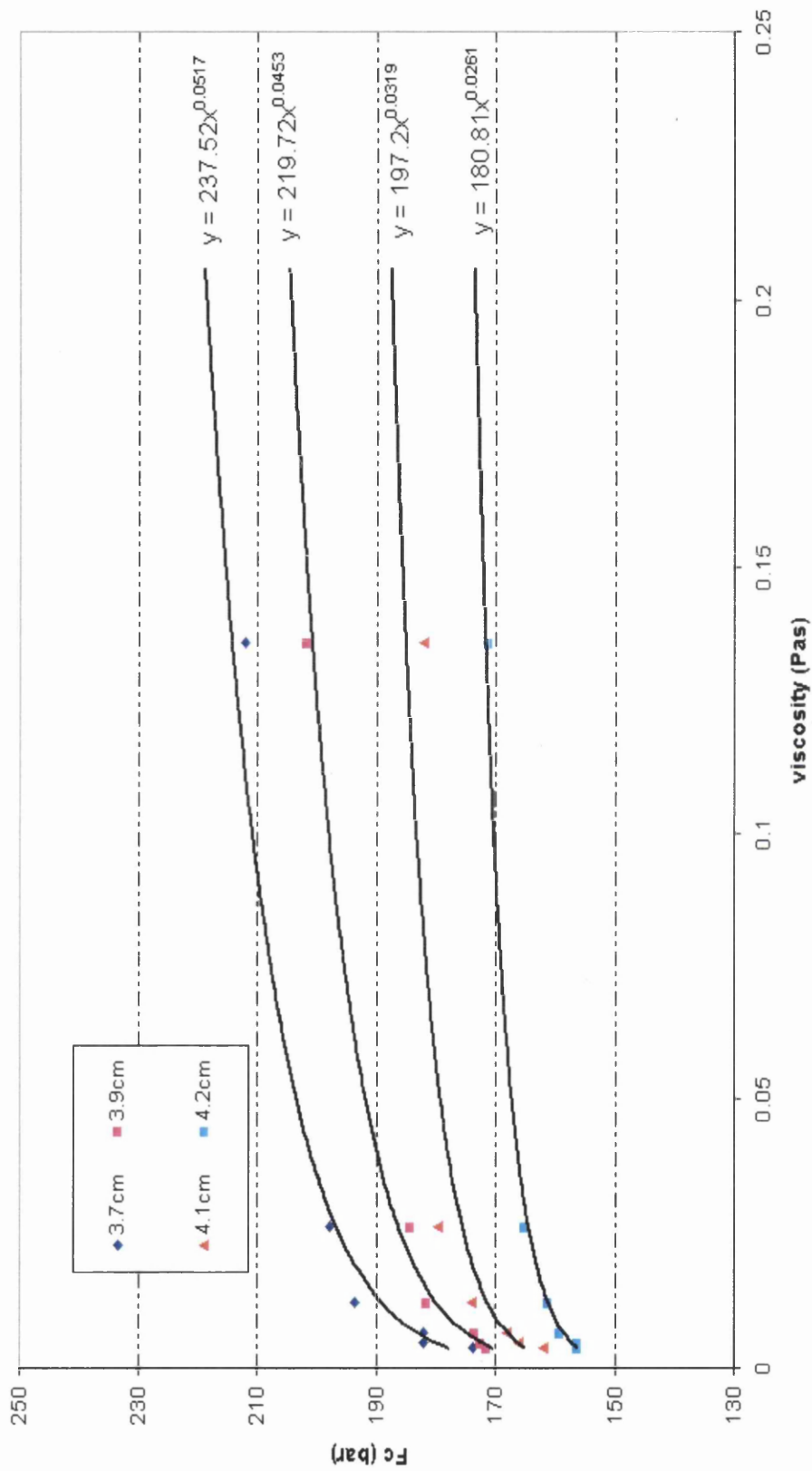


Figure 5.6  $F_c$  as a function of viscosity for 15W-40 Diesel multigrade oil for four gap widths D

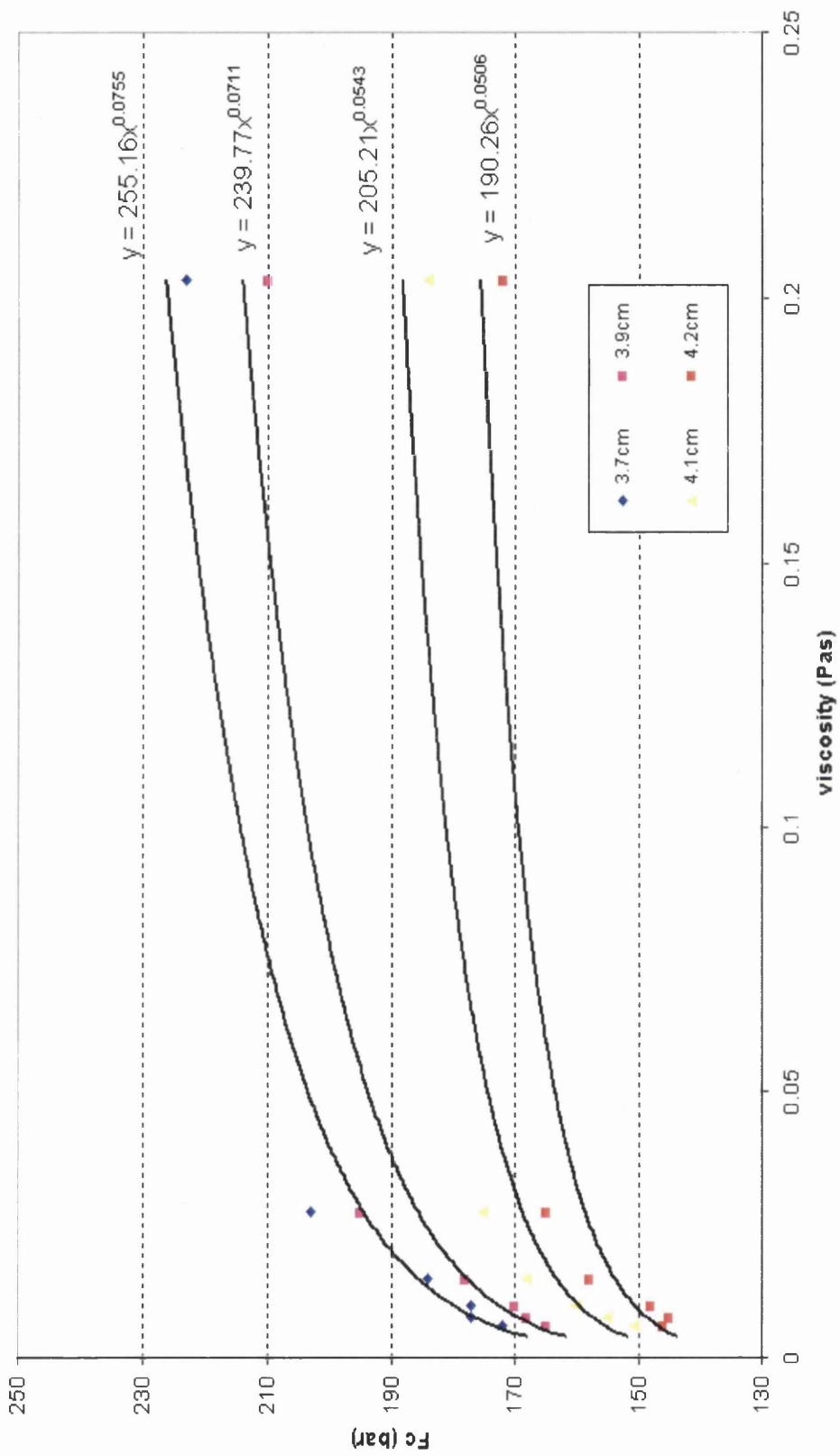
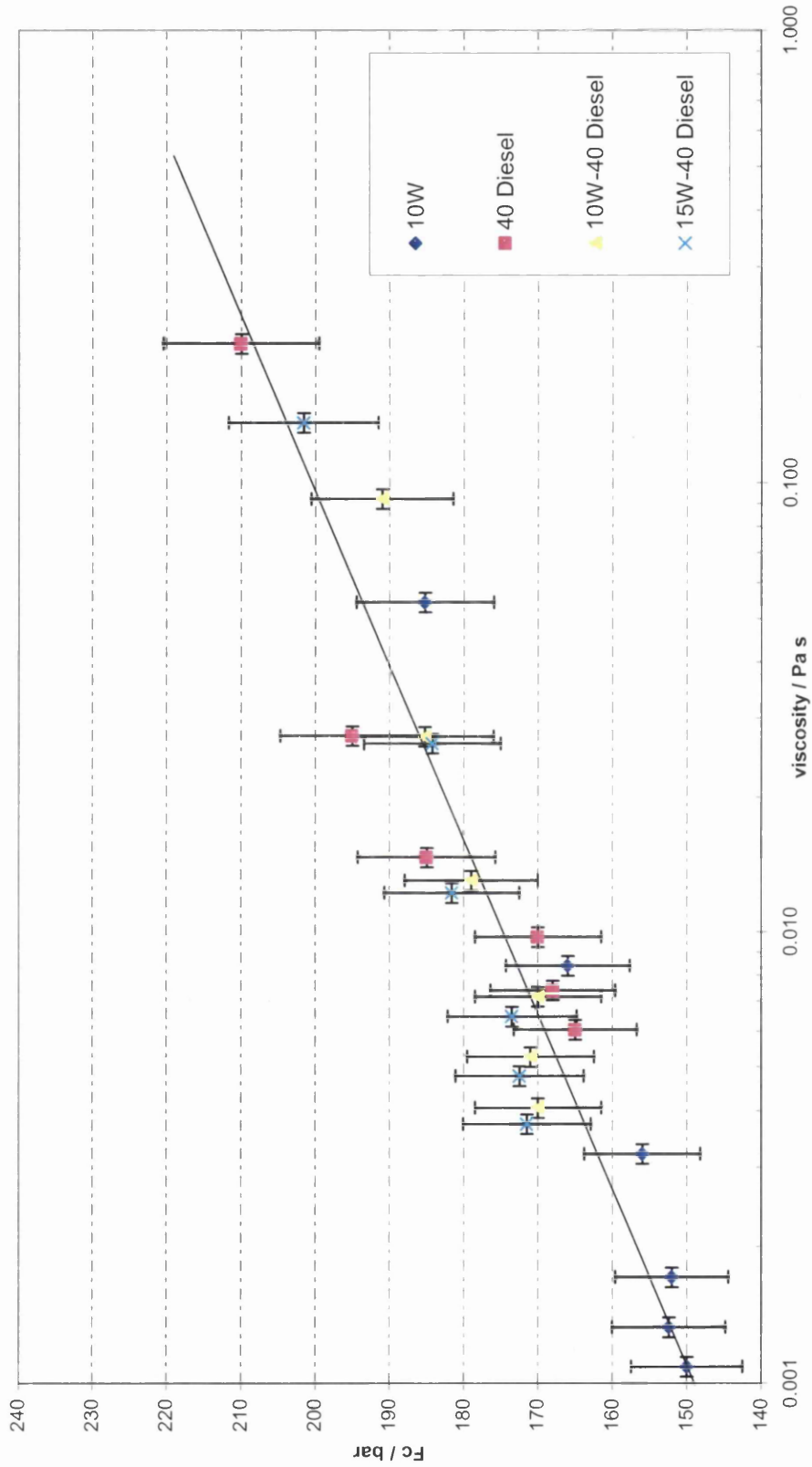
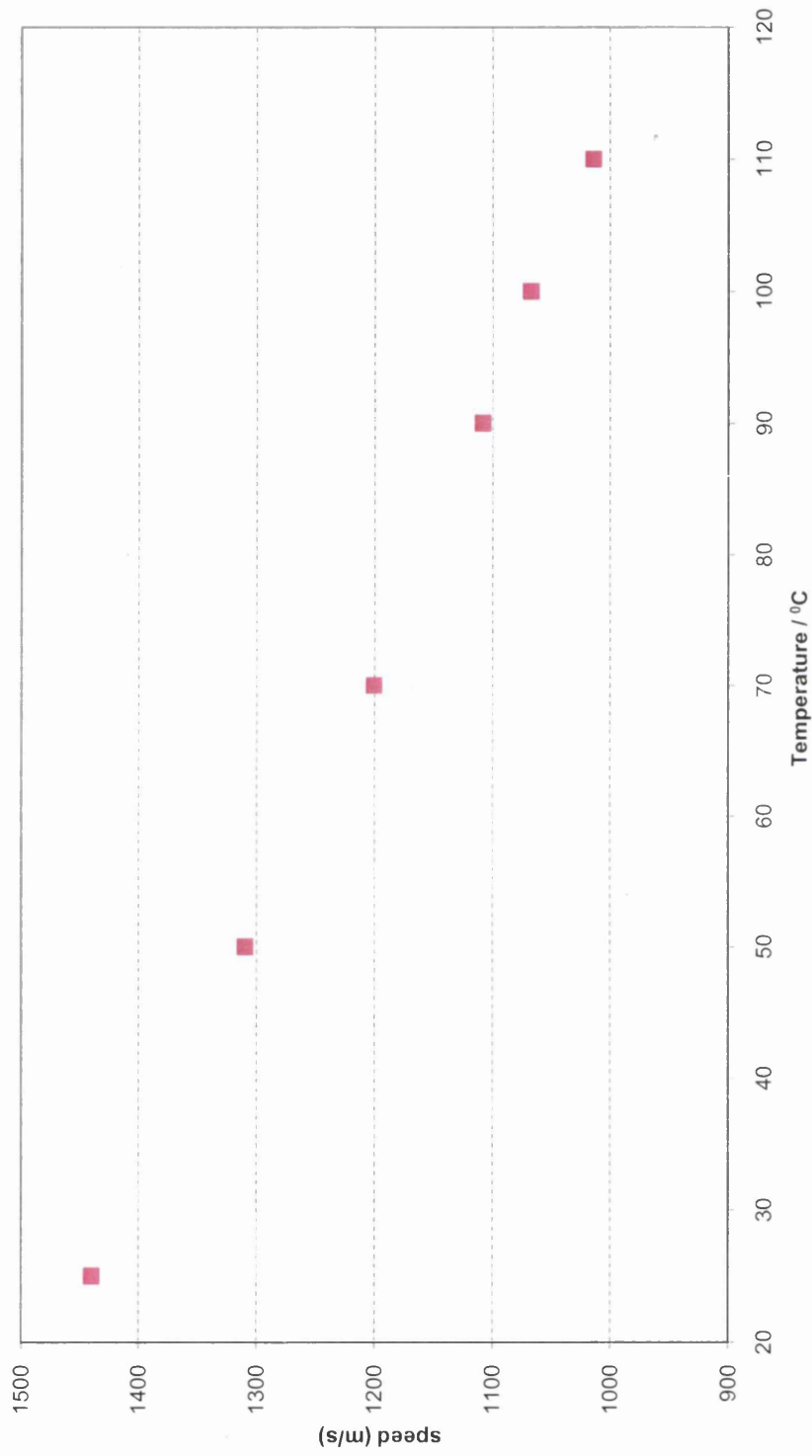


Figure 5.7  $F_c$  as a function of viscosity for 40 Diesel monograde oil for four gap widths D



**Figure 5.8**  $F_c$  as a function of shear viscosity,  $\mu$  for four engine oils (10W, 40 Diesel, 10W-40 Diesel and 15W-40 Diesel) over the temperatures ( $25^\circ\text{C} \leq T \leq 110^\circ\text{C}$ ) for constant gap, 3.9 cm widths D



**Figure 5.9** The average speed of pulse produced by a bullet striking to the piston travels up the liquid column within the tube then return to the lower transducer's location over a wide range of temperature.

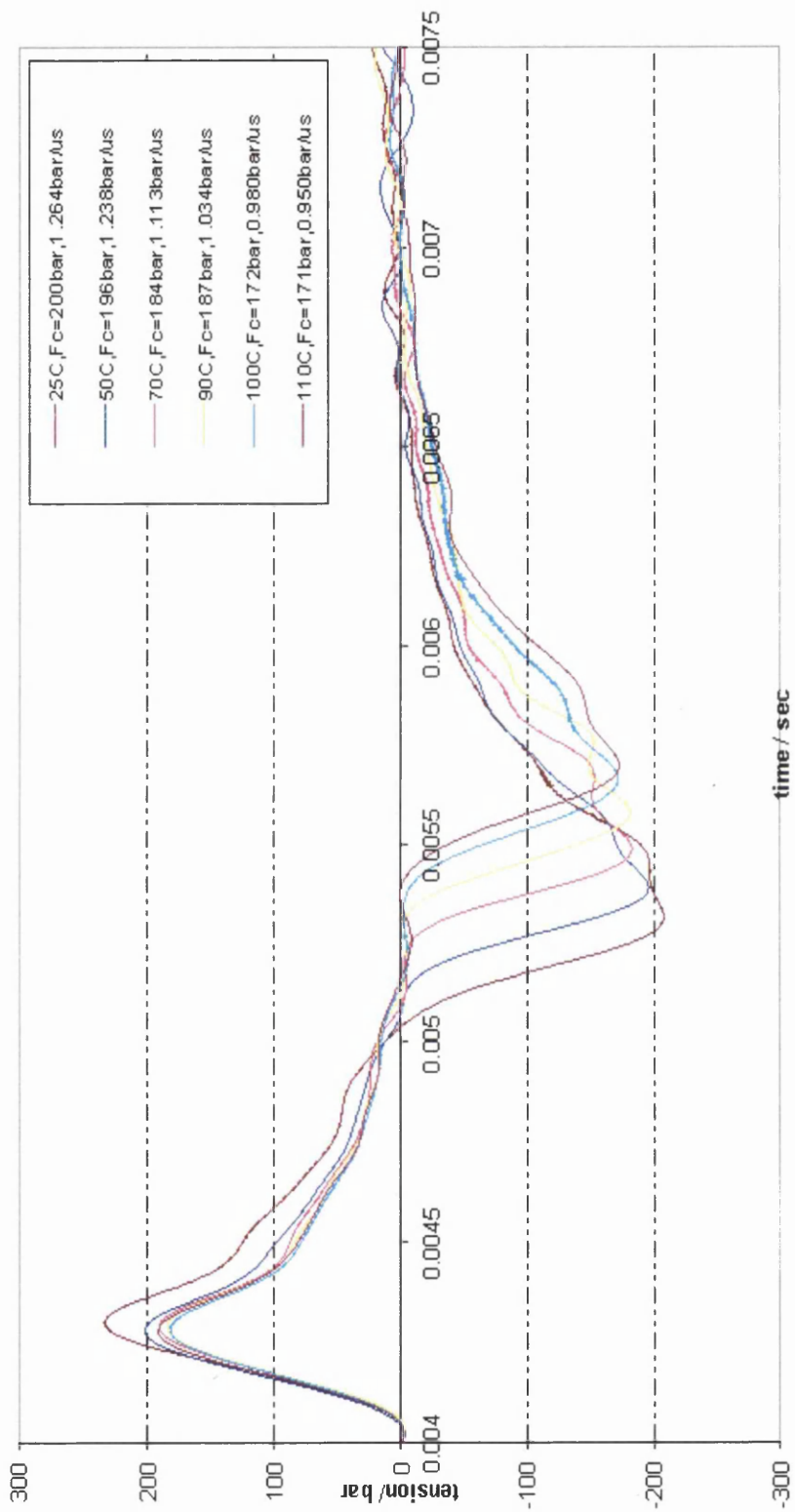


**Figure 5.10** Expanded series of 'prime' pressure-tension records obtained from different temperatures of experiments ( $25^{\circ}\text{C} \leq T \leq 110^{\circ}\text{C}$ ) with the constant gap,  $D = 3.9$  cm.

## 5.6 The Dependence of $F_c$ on Stressing Rate, $\dot{\Omega}_f$

In dynamically loaded journal bearings, one of the most important factors that affects  $F_c$  of lubricant is rate of stressing,  $\dot{\Omega}_f$ . In the combination effects of temperature change and the rate of dynamic stressing [rotating a shaft in an eccentric journal bearing at velocities change from 209 to 628  $\text{rads}^{-1}$  (2000 to 6000 rpm)] are important consideration in understanding the cavitation properties and performance of engine oils (Braun and Hendricks, 1982). Therefore, this experimental method was employed to study  $F_c(\dot{\Omega}_f)$ , over the temperature ranges  $25\text{ }^\circ\text{C} \leq T \leq 110\text{ }^\circ\text{C}$ .

In figure 5.11 and 5.13 have shown that the expanded series of ‘prime’ pressure-tension cycle at  $25\text{ }^\circ\text{C}$  and  $110\text{ }^\circ\text{C}$  individually records for 10W-40 Diesel oil with four gap widths  $D$ , it indicate that at a given temperature,  $F_c$  increases with increasing stressing rate. In the region where tension develops, the maximum rate of stress development occurs at the maximum gradient of  $P(t)$  for  $P < 0$ . This was calculated from the *mean maximum gradient* from gradients taken over a range of values of  $P$ , and corresponding time  $t$ , it was the same procedures of calculations the rates of stressing,  $\dot{\Omega}_f$ , on water experienced in chapter four. In figure 5.12 and 5.14 have shown that the time delay,  $\tau_i$  as a function of applied static pressure  $P_s$  (in p.s.i) for SAE 10W-40 Diesel oil at  $25\text{ }^\circ\text{C}$  and  $110\text{ }^\circ\text{C}$  individually with two different gap widths  $D = 3.7\text{ cm}$  and  $4.2\text{ cm}$ . The results are shown in figure 5.15 to 5.18. These measurements indicate that, at any given temperature,  $F_c$  increases with increasing  $\dot{\Omega}_f$  (10W:  $157\text{ bar} \leq F_c \leq 220\text{ bar}$  for stressing rates  $0.870\text{ bar}\mu\text{s}^{-1} \leq \dot{\Omega}_f \leq 1.370\text{ bar}\mu\text{s}^{-1}$  at  $25\text{ }^\circ\text{C}$  and,  $130\text{ bar} \leq F_c \leq 157\text{ bar}$  for stressing rates  $0.665\text{ bar}\mu\text{s}^{-1} \leq \dot{\Omega}_f \leq 0.860\text{ bar}\mu\text{s}^{-1}$  at  $110\text{ }^\circ\text{C}$ ; 40 Diesel :  $172\text{ bar} \leq F_c \leq 223\text{ bar}$  for stressing rates  $0.918\text{ bar}\mu\text{s}^{-1} \leq \dot{\Omega}_f \leq 1.356\text{ bar}\mu\text{s}^{-1}$  at  $25\text{ }^\circ\text{C}$  and,  $146\text{ bar} \leq F_c \leq 172\text{ bar}$  for stressing rates  $0.706\text{ bar}\mu\text{s}^{-1} \leq \dot{\Omega}_f \leq 0.917\text{ bar}\mu\text{s}^{-1}$  at  $110\text{ }^\circ\text{C}$ ); 10W-40 Diesel :  $175\text{ bar} \leq F_c \leq 200\text{ bar}$  for stressing rates  $1.03\text{ bar}\mu\text{s}^{-1} \leq \dot{\Omega}_f \leq 1.264\text{ bar}\mu\text{s}^{-1}$  at  $25\text{ }^\circ\text{C}$ ,  $152\text{ bar} \leq F_c \leq 171\text{ bar}$  for stressing rates  $0.787\text{ bar}\mu\text{s}^{-1} \leq \dot{\Omega}_f \leq 0.950\text{ bar}\mu\text{s}^{-1}$  at  $110\text{ }^\circ\text{C}$ ); 15W-40 Diesel :  $172\text{ bar} \leq F_c \leq 212\text{ bar}$  for stressing rates  $0.965\text{ bar}\mu\text{s}^{-1} \leq \dot{\Omega}_f \leq 1.356$

$\text{bar}\mu\text{s}^{-1}$  at 25 °C,  $156 \text{ bar} \leq F_c \leq 174 \text{ bar}$  for stressing rates  $0.840 \text{ bar}\mu\text{s}^{-1} \leq \dot{\Omega}_r \leq 0.970 \text{ bar}\mu\text{s}^{-1}$  at 110 °C).

The overall results for 10W and 40 Diesel monograde oils and 10W-40 Diesel and 15W-40 Diesel multigrade oils is shown in figure 5.19 indicates that  $F_c$  depends on stressing rate,  $\dot{\Omega}_r$  for over the temperature range  $25 \text{ °C} \leq T \leq 110 \text{ °C}$ . These results indicate that stressing rate has marked effect on  $F_c$  at any given temperature.

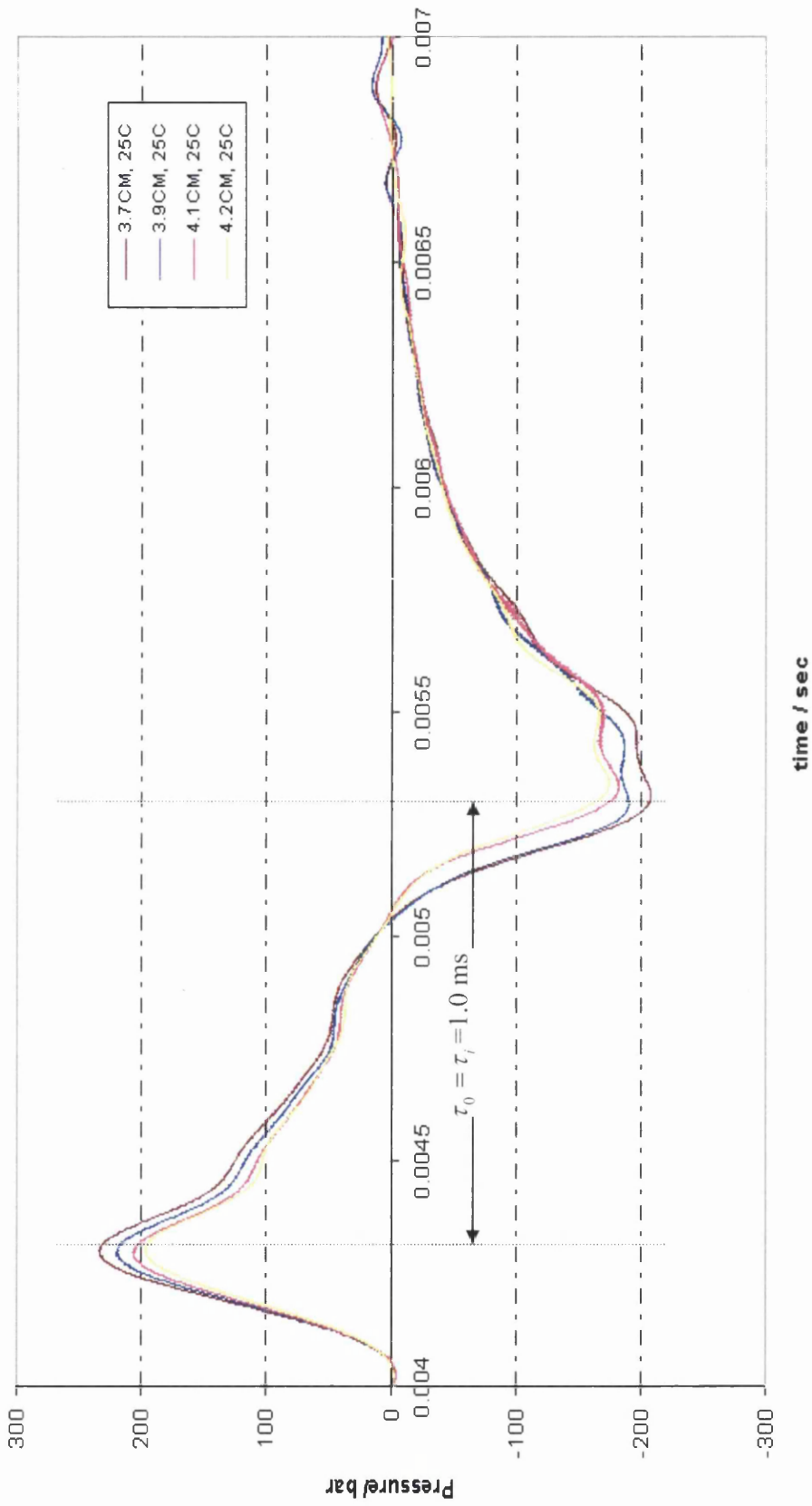


**Figure 5.11** Expanded series of 'prime' pressure-tension cycle at 25 °C records for 10W-40 Diesel oil for four gap widths  $D$  ( $F_c = 203$  bar,  $D = 3.7$  cm;  $F_c = 188$  bar,  $D = 3.9$  cm;  $F_c = 183$  bar,  $D = 4.1$  cm;  $F_c = 175$  bar,  $D = 4.2$  cm).



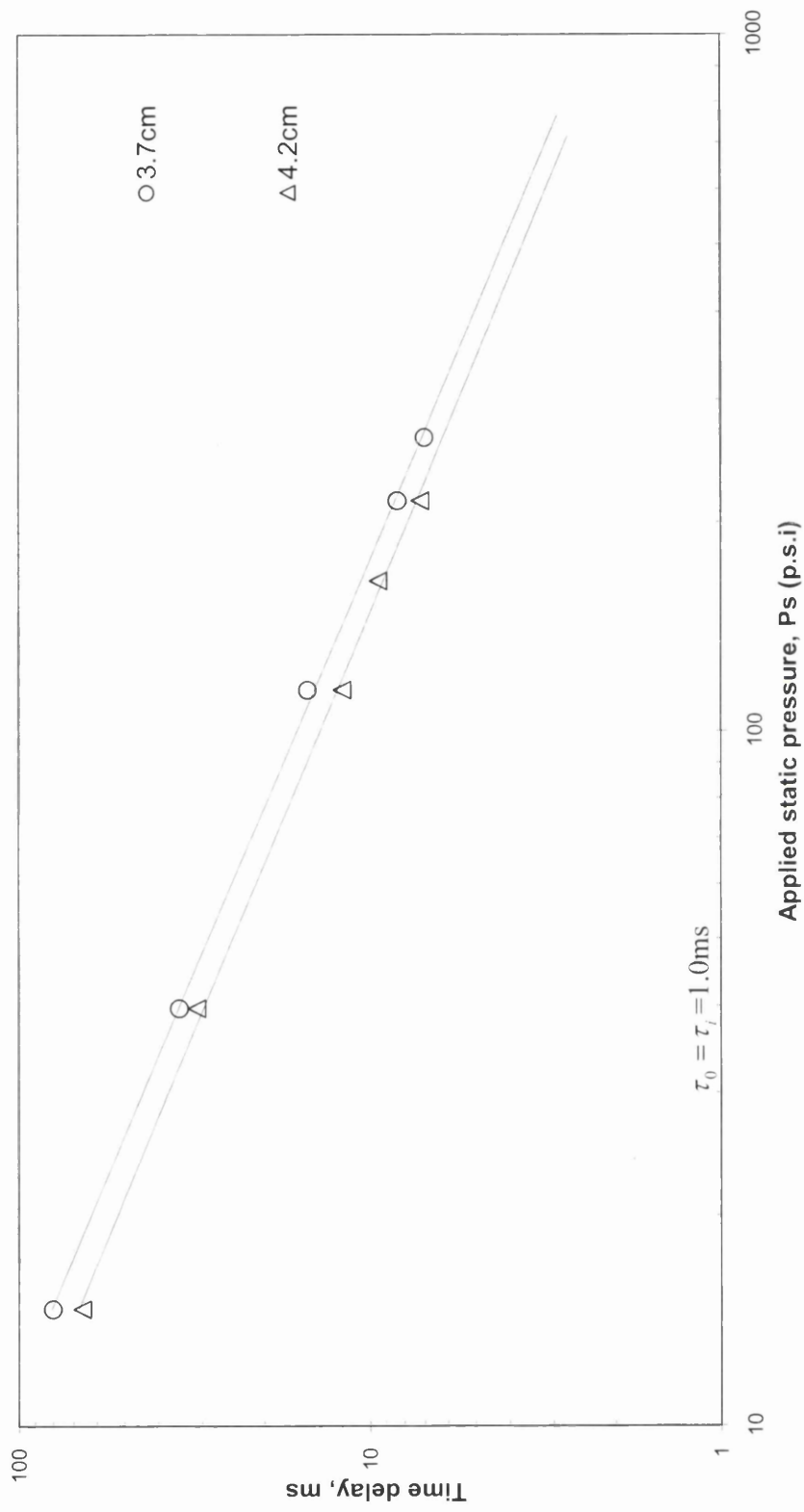


**Figure 5.12** The time delay,  $\tau_f$  as a function of applied static pressure  $P_s$  (in p.s.i.) for SAE 10W-40 Diesel oil at 25 °C with two different gap widths D ( $F_c = 203 \text{ bar}$ , D = 3.7 cm;  $F_c = 175 \text{ bar}$ , D = 4.2 cm)

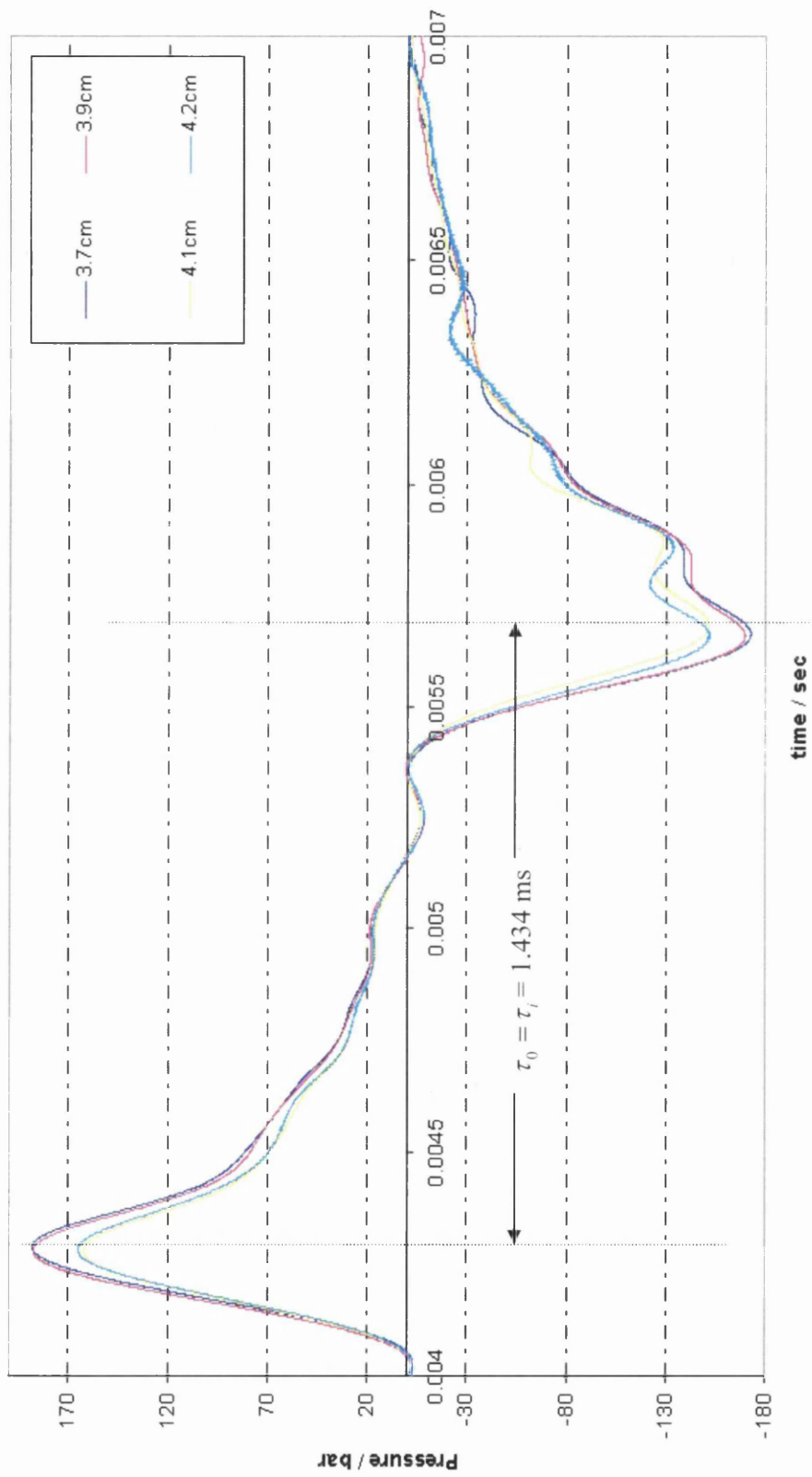


**Figure 5.13** Expanded series of 'prime' pressure-tension cycle at 110 °C records for 10W-40 Diesel oil for four gap widths  $D$  ( $F_c = 171$  bar,  $D = 3.7$  cm;  $F_c = 165$  bar,  $D = 3.9$  cm;  $F_c = 153$  bar,  $D = 4.1$  cm;  $F_c = 152$  bar,  $D = 4.2$  cm).

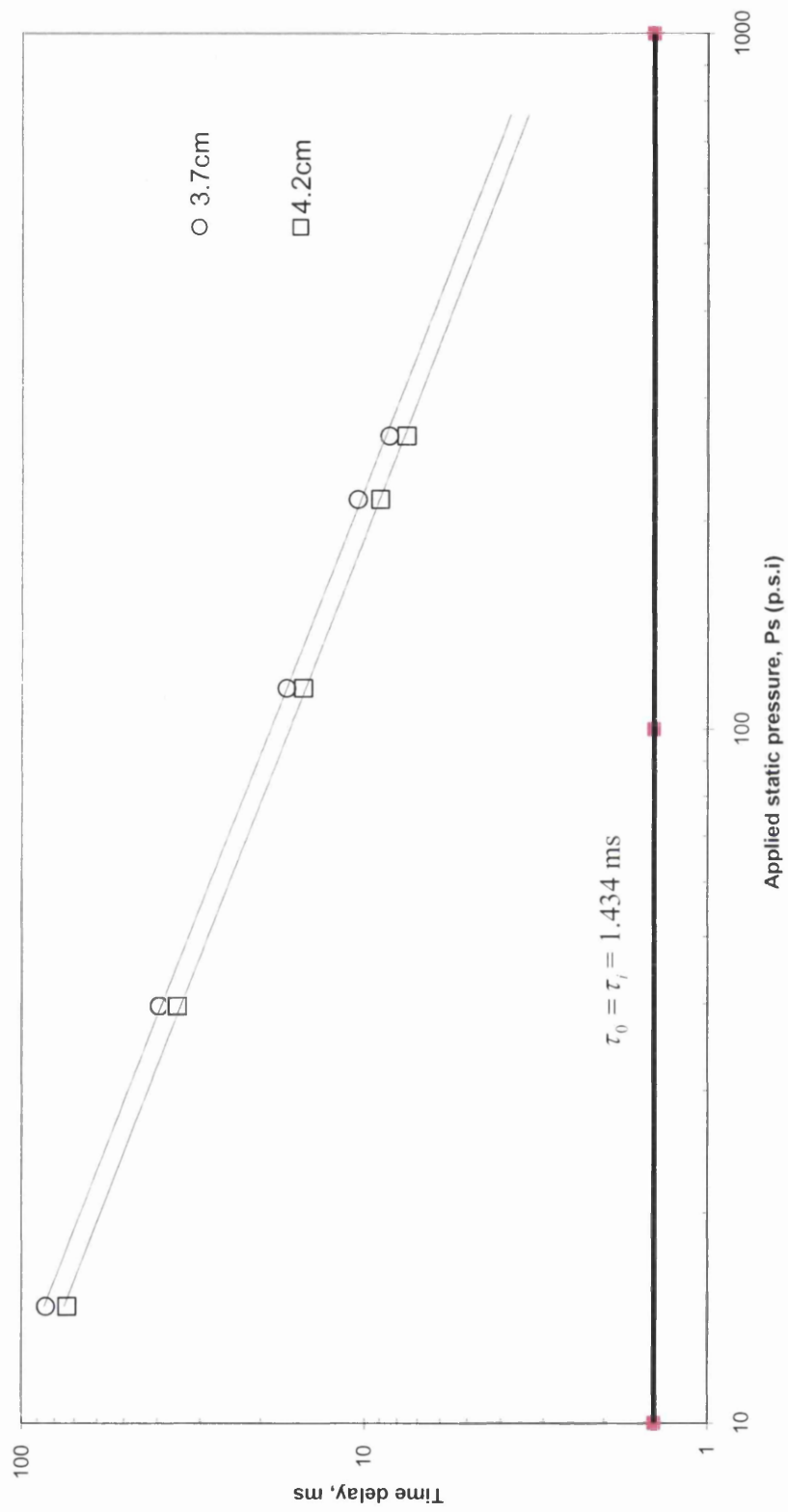


**Figure 5.14** The time delay,  $\tau_f$  as a function of applied static pressure  $P_s$  (in p.s.i) for SAE 10W-40 Diesel oil at 110 °C with two different gap widths D ( $F_c = 171 \text{ bar}$ , D = 3.7 cm;  $F_c = 152 \text{ bar}$ , D = 4.2 cm)

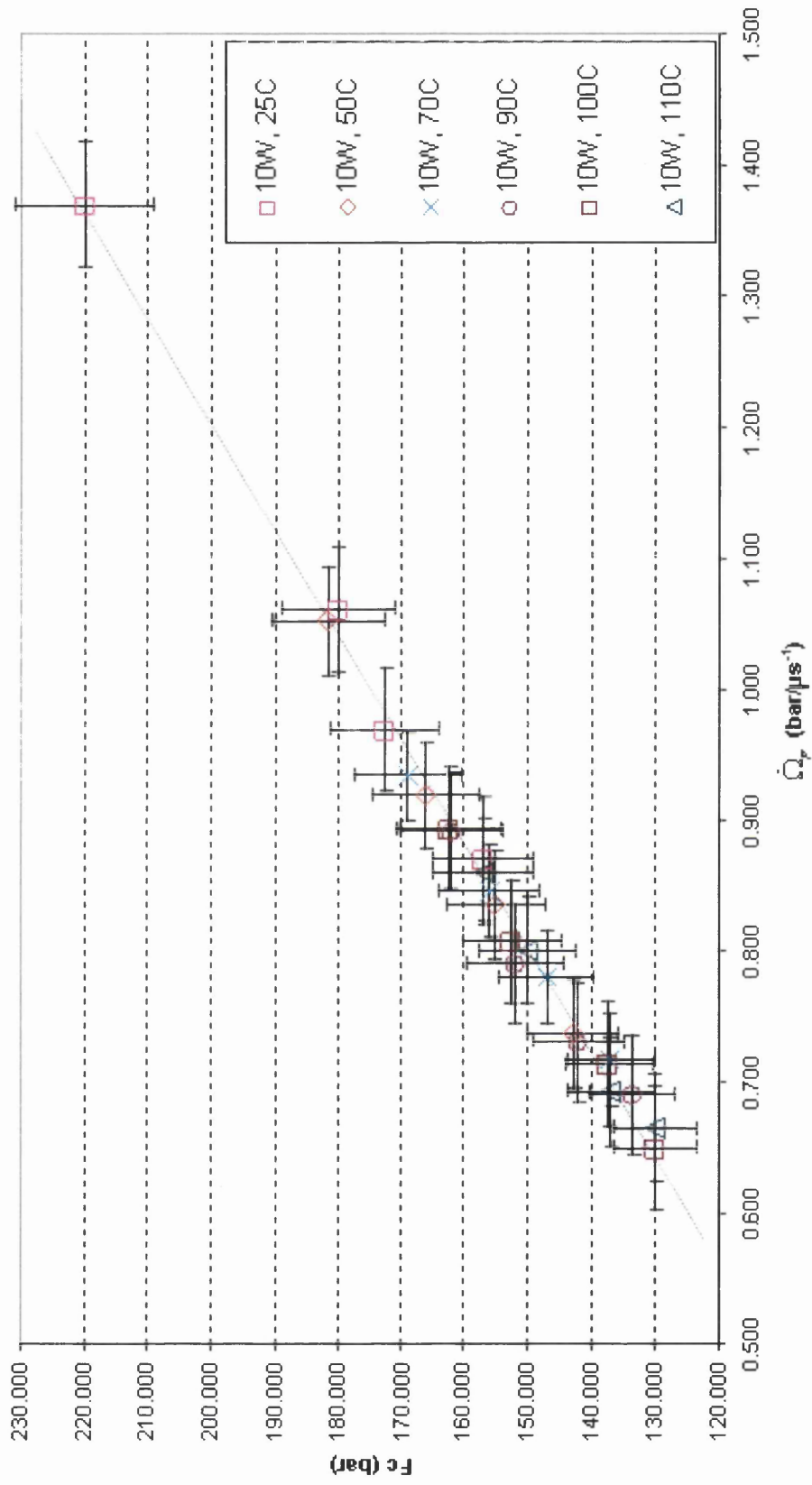


Figure 5.15  $F_c$  as a function of  $\dot{\Omega}_c$  for 10W oils over the temperature range  $25^\circ\text{C} \leq T \leq 110^\circ\text{C}$

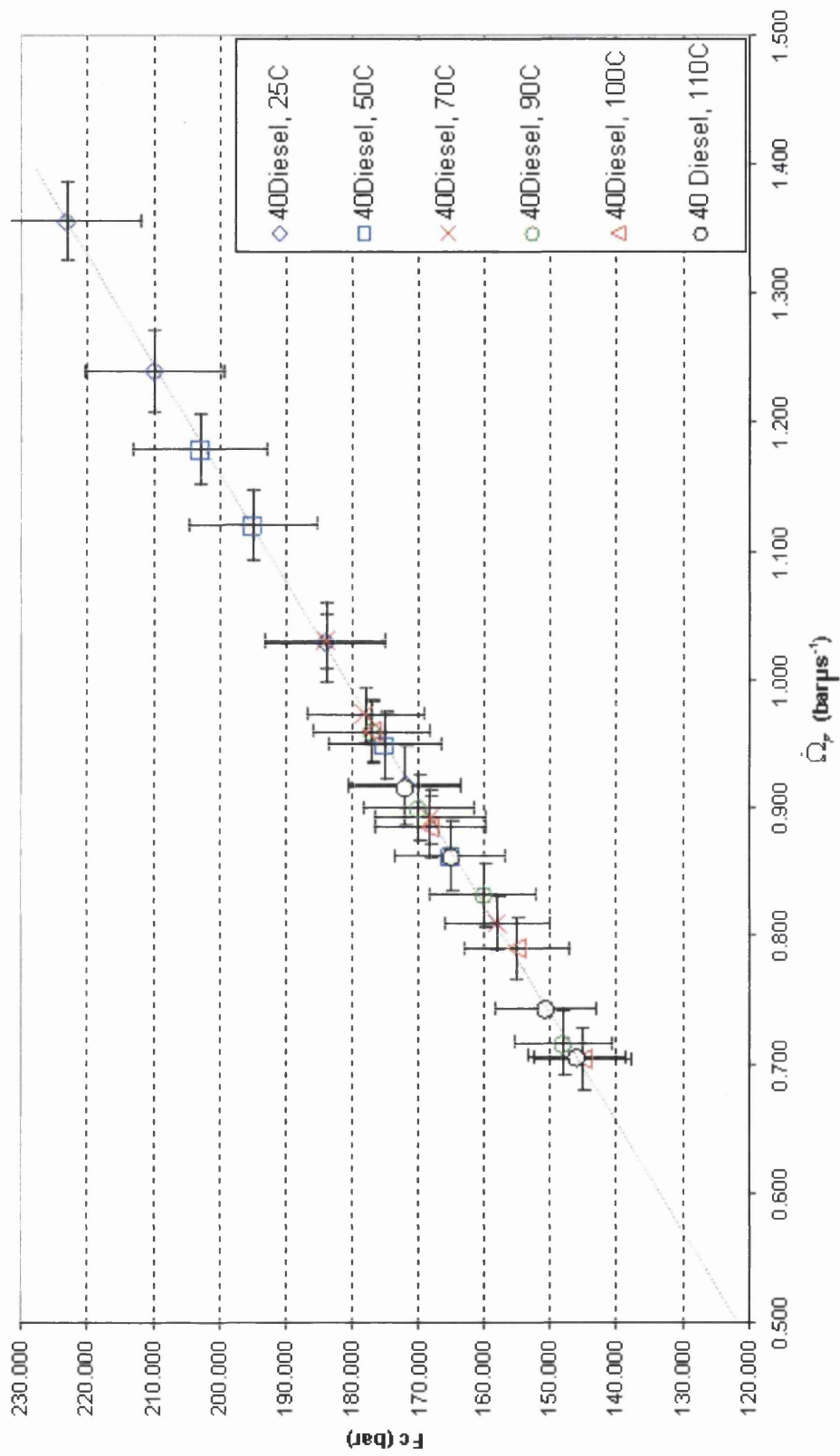


Figure 5.16  $F_c$  as a function of  $\dot{\Omega}_r$  for 40 Diesel oils over the temperature range  $25^\circ\text{C} \leq T \leq 110^\circ\text{C}$

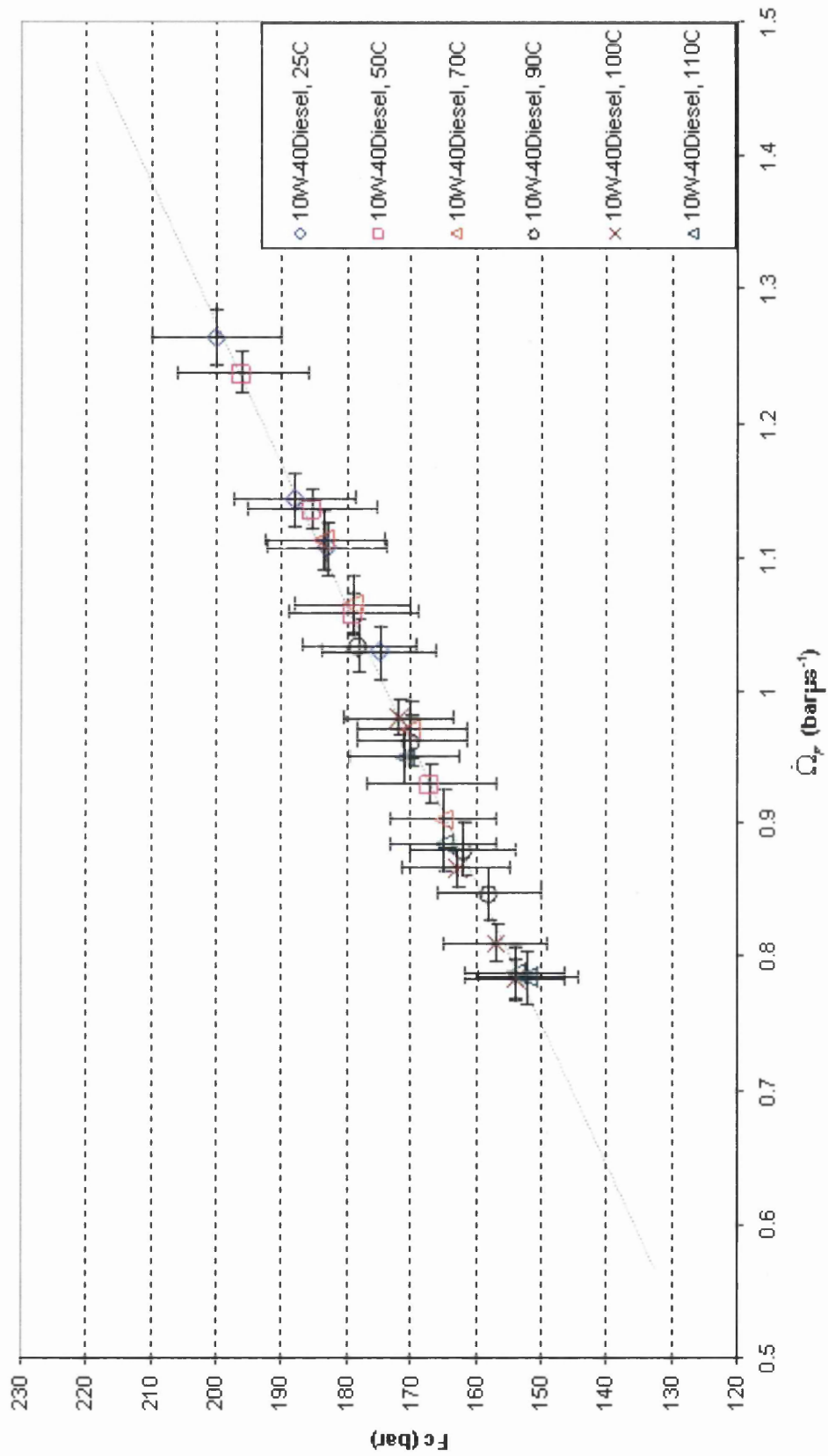


Figure 5.17  $F_c$  as a function of  $\Omega_{cr}$  for 10W-40 Diesel oils over the temperature range  $25^\circ\text{C} \leq T \leq 110^\circ\text{C}$

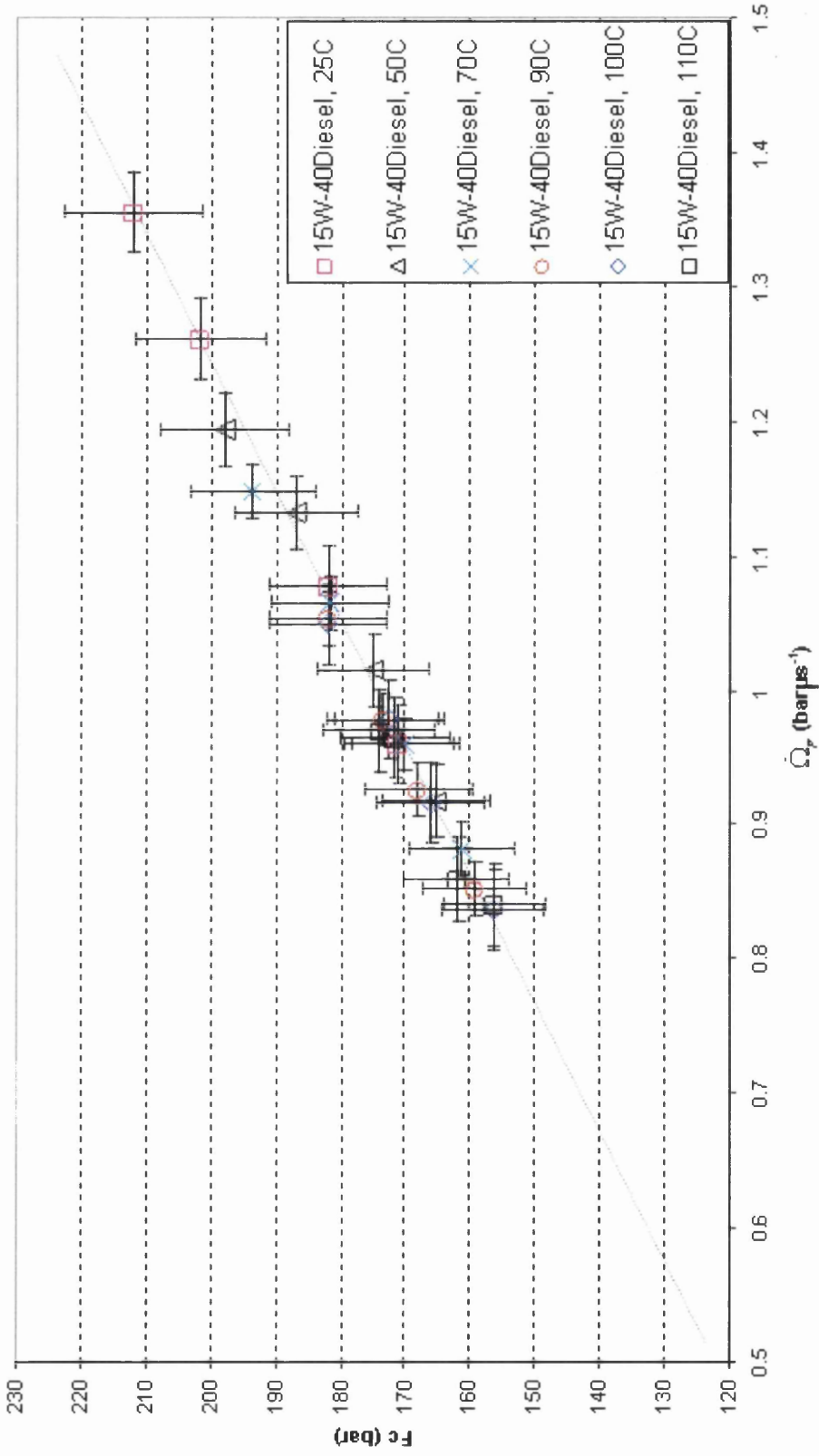
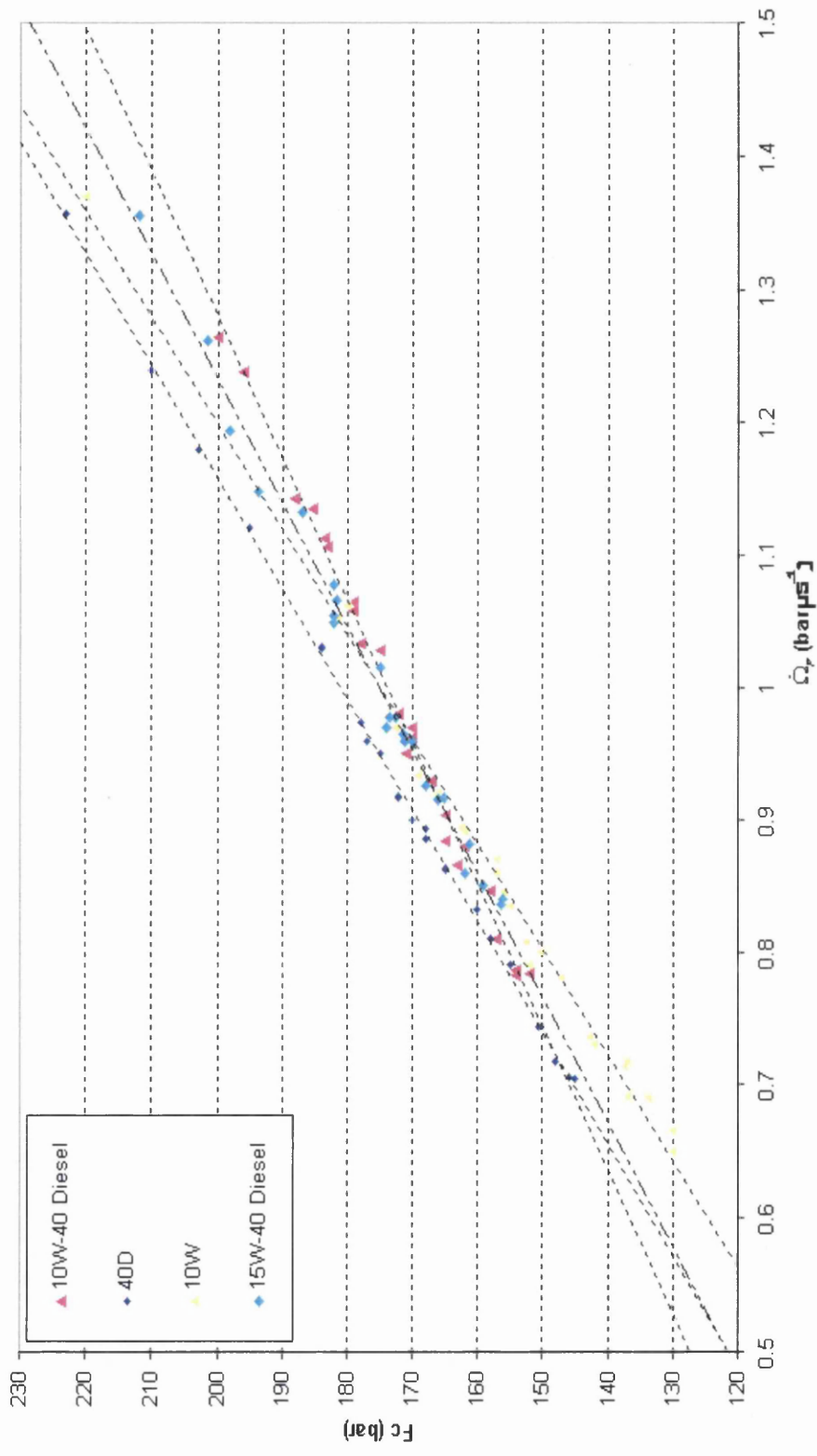


Figure 5.18  $F_c$  as a function of  $\dot{\Omega}_c$  for 15W-40 Diesel oils over the temperature range  $25^\circ\text{C} \leq T \leq 110^\circ\text{C}$



**Figure 5.19**  $F_c$  as a function of  $\Omega_T$ , for 10W and 40 Diesel monograde oils and 10W-40 Diesel and 15W-40 Diesel multigrade oils over the temperature range  $25^\circ\text{C} \leq T \leq 110^\circ\text{C}$



### 5.7 The Influence of the Polymer Concentration on the $F_c$

The study of cavitation in water has been carried out more than 200 years and vast amount of literature on the subject exists but very little information is available to show how the addition of water soluble polymers to water influence the onset of cavitation and its tensile strength,  $F_c$ . The multigrade oils are made viscoelastic by polymer additives (monograde oil or so called base stock plus small percentage amounts of polymer from 0.05 to 2.0 wt%) to improve their performance over the wide range of operating conditions which are encountered within automotive engines (Williamson *et al*, 1997). Therefore, the viscoelastic effect of polymer additives on lubricant performance in dynamic journal bearings has been a topic of considerable interest.

A recent study of the effects of polymer additives on flow in dynamically loaded journal bearings has included that their role in reducing wear does not arise from enhanced oil film thickness but may be associated with some ‘mitigating effects’ of viscoelasticity on cavitation (Berker A *et al*, 1995). Latter, an improved ‘tube-arrest’ experiment used to study liquid jet production by bubble collapse under cavitation-generated shock waves and the influence of polymer additives on their development, the commercial multigrade oils are found to exhibit significantly larger resistance to extensional flow than their Newtonian counterparts, which the results provide evidence in support of a mitigating effect of viscoelasticity on cavitation (Williams *et al*, 1997; Brown and Williams, 2000; Barrow *et al*, 2004).

The two monograde oils (essentially Newtonian) and the multigrade engine oils (non-Newtonian) were studied experimentally to assess the effect of polymer additives. A further series of experiments was conducted to study the effect, if any, of polymer concentration, polyacrylamide, PAA (Magnafloc LT20) alone on the tensile strength,  $F_c$ , in deionised water under dynamics stressing by tension at room temperature. In these experiments the B-P apparatus was set to operate with a constant gap,  $D = 4.1$  cm which in between the piston and the projecting face of the cattle stun gun.

Figure 5.20 shows the results for  $F_c$  for deionised water (at different stressing rates,  $0.43 \text{ bar}\mu\text{s}^{-1} \leq \dot{\Omega}_F \leq 1.79 \text{ bar}\mu\text{s}^{-1}$ , refer to chapter 4) and aqueous polyacrylamide, PAA, solutions (non-Newtonian), using the improved B-P apparatus. The results clearly indicate that the effective tensile strength of the polymer solution increases with increasing concentration of the polymer ( $0.10 \text{ wt}\% \leq C \leq 0.80 \text{ wt}\%$ ).

The tensile strength of 0.80 wt% polymer solution was 230 bar under same dynamic stressing condition with constant gap,  $D = 4.1 \text{ cm}$  where it is closed to the tensile strength of degassed, deionised water with constant gap,  $D = 3.7 \text{ cm}$ . These results shown the presence of the polymer additives leads to the increments in the tensile strength; the more polymer present in the deionised water the greater the increments in the tensile strength, however, these results were found in contrast to the experimental results obtained by Sedgewick and Trevena (1978).

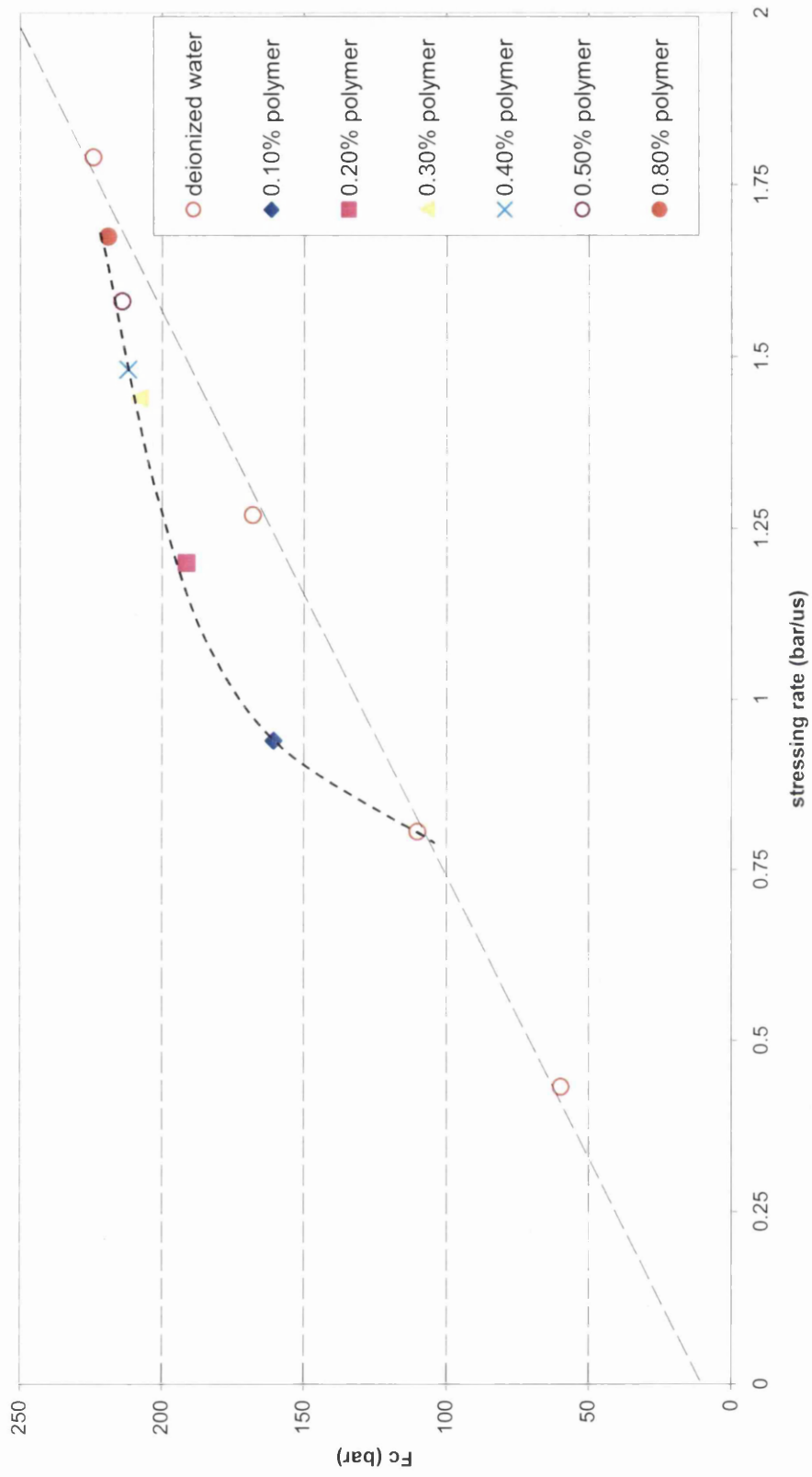


**Figure 5.20** The effect of polymer concentration, PAA on tensile strength of water under dynamic stressing with a constant gap,  $D = 4.1$  cm at  $25^\circ\text{C}$

## 5.8 Conclusion

This chapter describes a technique in which motor lubricants (or perhaps other common engineering liquids) may be subjected to a range of rates of dynamic stressing by pulses of tension, at temperatures representative of those encountered in their normal operating environment. It is important to note that the present work does not represent an attempt to recreate the complicated flow field experienced by a lubricant within a bearing, this being a mixture of shear and extensional flow (Gupta and Chan, 1990); rather, it is concerned solely with isolating, for separated detailed study, the effects (nonetheless important) of subjecting a liquid to a pressure-tension cycle (which is also a feature experienced by a lubricant during its passage through a bearing) (Williams and Williams, 2005).

These results indicate that the effects of temperature, shear viscosity and the rate of dynamic stressing are important considerations in understanding the cavitation properties. It is therefore possible that, in the absence of nuclei, that the lubricants studied herein may be substantially resistant to (vapourous) cavitation at high stressing rates, even at high temperatures, this may have serious consequences in terms of the load-carrying capacity of fluid-film bearings, given the stabilizing influence of cavitation on journals (Li *et al*, 2000 ; Brindley *et al*, 1983).

Also reported are values of  $F_c$  for degassed samples of several commercial monograde and multigrade oils which are the first of their kind to be reported for these lubricants at elevated temperature and also different rates of dynamic stressing. The results for 10W, 40 Diesel, 10W-40 Diesel and 15W-40 Diesel oils indicate that temperature, shear viscosity and stressing rate have a marked effect on  $F_c$ . It is significant that in the present work, results have been produced from a single technique, consisting of experiments conducted within the same apparatus in which the rate of stressing is deliberately varied. The results of such a study have not previously been reported. They clearly establish the importance of stressing rate in considerations of the effective tensile strength of liquids under conditions where heterogeneous nucleation prevails, and in assessing the cavitation performance of lubricants.

This chapter also shown that the effect of polymer additives on the effective tensile strength of deionised water, which increase the polymer in the deionised water, lead to increase the effective tensile strength of the solution. The results obtained suggested that further experiments should now be conducted using this technique in order to study the effect of the presence of dissolved (permanent) gases in the cavitation of motor lubricants under dynamic stressing by pulses of tension.

Temp , gap	$F_c$ / bar	stressing rate / bar $\mu$ s <sup>-1</sup>	standard error / bar $\mu$ s <sup>-1</sup>	instant time /ms	Velocity /ms <sup>-1</sup>
25 °C, 3.7 cm	220.0	1.373	0.010	0.979	1389.0 (±11.9)
25 °C, 3.9 cm	185.2	1.062	0.026	1.000	1391.5 (±10.0)
25 °C, 4.1 cm	172.6	0.970	0.023	0.980	1396.2 (±39.2)
25 °C, 4.2 cm	156.7	0.876	0.020	0.985	1419.0 (±12.0)
50 °C, 3.7 cm	181.5	1.053	0.018	1.089	1318.5 (±19.2)
50 °C, 3.9 cm	166.0	0.919	0.017	1.090	1309.4 (±24.6)
50 °C, 4.1 cm	155.0	0.835	0.029	1.080	1317.7 (±28.6)
50 °C, 4.2 cm	142.8	0.736	0.016	1.083	1306.6 (±34.6)
70 °C, 3.7 cm	169.0	0.934	0.023	1.180	1217.8 (±14.3)
70 °C, 3.9 cm	156.0	0.844	0.032	1.166	1229.0 (±21.0)
70 °C, 4.1 cm	147.0	0.780	0.023	1.170	1210.0 (±9.40)
70 °C, 4.2 cm	137.0	0.717	0.016	1.130	1235.7 (±33.0)
90 °C, 3.7 cm	163.0	0.891	0.019	1.303	1100.0 (±12.0)
90 °C, 3.9 cm	152.0	0.807	0.012	1.300	1109.7 (±17.6)
90 °C, 4.1 cm	142.1	0.730	0.020	1.297	1103.4 (±5.80)
90 °C, 4.2 cm	133.6	0.693	0.033	1.292	1098.2 (±25.3)
100 °C, 3.7 cm	162.4	0.894	0.014	1.345	1053.4 (±19.3)
100 °C, 3.9 cm	152.4	0.790	0.015	1.364	1072.7 (±25.2)
100 °C, 4.1 cm	137.3	0.713	0.009	1.345	1060.8 (±23.8)
100 °C, 4.2 cm	130.0	0.649	0.019	1.330	1082.0 (±19.0)
110 °C, 3.7 cm	156.6	0.860	0.024	1.403	1024.2 (±12.5)
110 °C, 3.9 cm	150.0	0.800	0.027	1.405	1019.5 (±2.40)
110 °C, 4.1 cm	137.0	0.692	0.019	1.404	1022.5 (±26.0)
110 °C, 4.2 cm	130.0	0.665	0.001	1.393	1021.0 (±3.20)

**Table 5.5** Tensile strength data for 10W; API CC at various temperature and rate of dynamic stressing.

Temp , gap	$F_c$ / bar	stressing rate / bar $\mu$ s <sup>-1</sup>	standard error / bar $\mu$ s <sup>-1</sup>	instant time /ms	Velocity /ms <sup>-1</sup>
25 °C, 3.7 cm	223.0	1.356	0.026	0.997	1437.0 (±43.0)
25 °C, 3.9 cm	210.0	1.240	0.020	0.995	1440.8 (±53.0)
25 °C, 4.1 cm	184.0	1.030	0.020	0.998	1437.0 (±53.0)
25 °C, 4.2 cm	172.0	0.918	0.031	1.003	1430.0 (±53.0)
50 °C, 3.7 cm	203.0	1.180	0.027	1.077	1330.0 (±28.0)
50 °C, 3.9 cm	195.0	1.122	0.020	1.076	1330.6 (±28.0)
50 °C, 4.1 cm	175.0	0.950	0.027	1.070	1339.0 (±29.0)
50 °C, 4.2 cm	165.0	0.862	0.020	1.091	1313.0 (±38.0)
70 °C, 3.7 cm	184.0	1.031	0.020	1.180	1221.8 (±1.7)
70 °C, 3.9 cm	178.0	0.973	0.021	1.177	1214.9 (±4.0)
70 °C, 4.1 cm	168.0	0.893	0.016	1.185	1207.0 (±11.0)
70 °C, 4.2 cm	158.0	0.810	0.009	1.189	1206.5 (±50.0)
90 °C, 3.7 cm	177.0	0.960	0.019	1.299	1100.6 (±2.0)
90 °C, 3.9 cm	170.0	0.900	0.022	1.306	1096.0 (±19.0)
90 °C, 4.1 cm	160.0	0.832	0.025	1.308	1094.0 (±16.0)
90 °C, 4.2 cm	148.0	0.717	0.017	1.300	1100.0 (±0.0)
100 °C, 3.7 cm	177.0	0.960	0.016	1.350	1061.9 (±37.3)
100 °C, 3.9 cm	168.0	0.885	0.024	1.349	1061.6 (±30.0)
100 °C, 4.1 cm	155.0	0.791	0.021	1.365	1050.5 (±39.0)
100 °C, 4.2 cm	145.0	0.704	0.019	1.355	1059.1 (±46.0)
110 °C, 3.7 cm	172.0	0.917	0.016	1.362	1053.6 (±44.4)
110 °C, 3.9 cm	165.0	0.863	0.016	1.353	1058.4 (±30.4)
110 °C, 4.1 cm	150.6	0.744	0.015	1.391	1030.5 (±37.2)
110 °C, 4.2 cm	146.0	0.706	0.016	1.377	1042.2 (±43.4)

**Table 5.6** Tensile strength data for 40 Diesel; API CC at various temperature and rate of dynamic stressing.

Temp , gap	$F_c$ / bar	stressing rate / bar $\mu$ s <sup>-1</sup>	standard error / bar $\mu$ s <sup>-1</sup>	instant time /ms	Velocity /ms <sup>-1</sup>
25 °C, 3.7 cm	200.0	1.264	0.017	1.055	1470.0 (±21.0)
25 °C, 3.9 cm	188.0	1.143	0.019	1.029	1472.0 (±40.0)
25 °C, 4.1 cm	183.0	1.106	0.015	1.020	1462.0 (±06.3)
25 °C, 4.2 cm	175.0	1.029	0.024	1.066	1454.0 (±62.0)
50 °C, 3.7 cm	196.0	1.238	0.013	1.130	1337.1 (±22.6)
50 °C, 3.9 cm	185.3	1.136	0.015	1.136	1332.5 (±07.4)
50 °C, 4.1 cm	179.0	1.059	0.011	1.143	1300.9 (±80.5)
50 °C, 4.2 cm	167.0	0.930	0.008	1.109	1342.2 (±11.5)
70 °C, 3.7 cm	183.4	1.113	0.014	1.233	1218.1 (±04.8)
70 °C, 3.9 cm	179.0	1.065	0.022	1.244	1215.3 (±06.9)
70 °C, 4.1 cm	170.0	0.970	0.011	1.235	1216.2 (±06.3)
70 °C, 4.2 cm	165.0	0.903	0.007	1.233	1214.5 (±07.8)
90 °C, 3.7 cm	178.0	1.034	0.018	1.324	1101.5 (±06.1)
90 °C, 3.9 cm	170.0	0.963	0.010	1.346	1076.7 (±51.7)
90 °C, 4.1 cm	162.0	0.880	0.009	1.311	1099.0 (±2.06)
90 °C, 4.2 cm	158.0	0.847	0.007	1.332	1110.5 (±28.4)
100 °C, 3.7 cm	172.0	0.980	0.009	1.402	1007.4 (±02.0)
100 °C, 3.9 cm	163.0	0.866	0.014	1.420	1015.1 (±12.5)
100 °C, 4.1 cm	157.0	0.810	0.010	1.404	1020.9 (±34.3)
100 °C, 4.2 cm	154.0	0.783	0.011	1.422	1008.3 (±03.4)
110 °C, 3.7 cm	171.0	0.950	0.017	1.433	1008.3 (±04.6)
110 °C, 3.9 cm	165.0	0.884	0.010	1.440	1013.9 (±05.1)
110 °C, 4.1 cm	153.0	0.784	0.008	1.431	1012.2 (±05.0)
110 °C, 4.2 cm	152.0	0.787	0.008	1.435	1007.3 (±04.3)

**Table 5.7** Tensile strength data for 10W-40 Diesel; API CF at various temperature and rate of dynamic stressing.



Temp , gap	$F_c$ / bar	stressing rate / $\text{bar}\mu\text{s}^{-1}$	standard error / $\text{bar}\mu\text{s}^{-1}$	instant time /ms	Velocity / $\text{ms}^{-1}$
25 °C, 3.7 cm	212.0	1.356	0.018	1.035	1382.0 ( $\pm 10.5$ )
25 °C, 3.9 cm	201.6	1.262	0.017	1.029	1472.0 ( $\pm 18.0$ )
25 °C, 4.1 cm	182.0	1.079	0.024	1.020	1462.0 ( $\pm 43.3$ )
25 °C, 4.2 cm	171.5	0.965	0.033	1.066	1454.0 ( $\pm 48.3$ )
50 °C, 3.7 cm	198.0	1.194	0.021	1.122	1274.5 ( $\pm 34.2$ )
50 °C, 3.9 cm	187.0	1.133	0.014	1.136	1332.5 ( $\pm 31.7$ )
50 °C, 4.1 cm	175.0	1.016	0.027	1.143	1300.9 ( $\pm 28.6$ )
50 °C, 4.2 cm	165.2	0.917	0.026	1.109	1342.2 ( $\pm 12.5$ )
70 °C, 3.7 cm	193.6	1.148	0.017	1.191	1200.7 ( $\pm 14.5$ )
70 °C, 3.9 cm	181.6	1.066	0.017	1.244	1215.3 ( $\pm 18.6$ )
70 °C, 4.1 cm	170.0	0.960	0.012	1.235	1216.2 ( $\pm 08.0$ )
70 °C, 4.2 cm	161.2	0.882	0.019	1.233	1214.5 ( $\pm 07.8$ )
90 °C, 3.7 cm	182.0	1.055	0.018	1.324	1080.0 ( $\pm 21.1$ )
90 °C, 3.9 cm	173.5	0.979	0.018	1.346	1076.7 ( $\pm 14.6$ )
90 °C, 4.1 cm	168.0	0.926	0.010	1.311	1099.0 ( $\pm 14.9$ )
90 °C, 4.2 cm	159.2	0.851	0.019	1.332	1110.5 ( $\pm 03.1$ )
100 °C, 3.7 cm	182.0	1.050	0.011	1.399	1022.2 ( $\pm 31.3$ )
100 °C, 3.9 cm	172.5	0.979	0.019	1.420	1015.1 ( $\pm 02.5$ )
100 °C, 4.1 cm	166.0	0.916	0.018	1.404	1020.9 ( $\pm 23.9$ )
100 °C, 4.2 cm	156.3	0.836	0.027	1.422	1008.3 ( $\pm 04.6$ )
110 °C, 3.7 cm	174.0	0.970	0.017	1.462	9781.1 ( $\pm 26.6$ )
110 °C, 3.9 cm	171.5	0.917	0.031	1.440	1013.9 ( $\pm 16.1$ )
110 °C, 4.1 cm	162.0	0.859	0.028	1.431	1012.2 ( $\pm 28.7$ )
110 °C, 4.2 cm	156.2	0.840	0.005	1.435	1007.3 ( $\pm 06.8$ )

**Table 5.8** Tensile strength data for 15W-40 Diesel; API CF at various temperature and rate of dynamic stressing.

# Chapter 6

## *Studies of Doubly Metastable (d-m) Liquids under Quasi-Static Isotropic Tension in Berthelot Tube*

- 6.1 *Introduction*
- 6.2 *Previous Related Work*
- 6.3 *The Modified Berthelot Tubes*
- 6.4 *Determination of the Sealing Temperature,  $T_0$ , in order  
to bring  $D_2O$  (heavy water) Liquid samples into the  
Double Metastable Region in the Modified Berthelot  
Tube*
- 6.5 *The Records obtained from high-Speed Imaging  
System*
- 6.6 *Conclusion*

### 6.1 Introduction

The work reported in previous Chapters of this Thesis demonstrates the ability of water to sustain considerable negative pressure under conditions of dynamic stressing by pulses of tension. Water (and many other liquids) are also able to sustain considerable levels of tension under *quasi*-static stressing for considerable periods of time (often minutes, or hours, if suitably prepared). Whereas studies involving the subjection of liquids to dynamic stressing by pulses of tension are widely reported and have direct relevance to engineering applications (e.g. in ultrasound scanning), the behaviour of liquids under quasi-static tension over sustained periods is less well studied. However, the ability to induce, manipulate and sustain tension in a liquid over a sustained period is a potentially valuable tool in extending studies of fundamental aspects of the liquid state (Trevena, 1987). The work described in this Chapter has this as its focus and involves the development and refinement of a technique in which water was subjected to progressively greater tensions over a very wide range of temperatures which extended into the supercooled regime.

It is useful to recall that a liquid under tension is called a stretched liquid or superheated liquid (i.e. it is metastable with respect to liquid plus vapour). Figure 6.1 shows the phase diagram for water. This behaviour encompasses the possibility of superheating liquids well above their boiling point (for example, in figure 6.1 '0-Y' line shows water can be heated to 280 °C without explosion at atmospheric pressure (Apfel, 1972)), and the multitude of effects associated with "cavitation", as shown in figure 6.1 ('0-Z' line). A related phenomenon involves the metastability associated with the freezing transition (for example, in figure 6.1 '0-V' line shows water at atmospheric pressure can exist as a liquid state down to -40 °C (Taborek, 1985)), a fact which is of great importance in meteorology): this supercooled liquid is also in metastable condition (Temperley and Trevena, 1993). In practical terms (i.e. in experiments) a condition is eventually reached in which boiling, or cavitation or freezing can no longer be prevented, and a new phase appears suddenly as the system is driven towards a condition of greater stability (Debenedetti, 1996).

Liquid water under tension can be cooled below its melting point without immediately experiencing cavitation. The generation of negative pressures (to  $-60$  bar) in supercooled water (at  $-18$  °C) was reported by Henderson and Speedy (1980). No ice was detected, nor was cavitation evident; and they concluded that lower temperatures were not reached due only to the limitation of their cooling apparatus. The results of this rare excursion into the doubly metastable regime differ from those of Hayward (1971), in whose work water was held at  $-0.2$  bar and  $-5$  °C: on further cooling the water froze and the intervening water boiled at the same instant, but in deaerated water ice appeared without disrupting the negative pressure. This latter observation is significant. It suggests that ice crystals may both form and grow under sustained negative pressure – a very different environment from that in which nucleation is accompanied by the relief of tension, and ice subsequently develops under ‘normal’ supercooled conditions (i.e. at atmospheric pressure) to form natural hexagonal ice (*I<sub>h</sub>*). Ice phases with different crystalline structures exist at lower temperatures and positive pressures ( $> 2$  kbar) but the phase diagram is sparsely populated with data at negative pressures. In the ‘full’ locus of the Ice I–liquid phase transition line for water, the negative pressure portion is largely a matter of conjecture, but estimates of the locus of stability for water extend to  $-2$  kbar (Speedy, 1982).

The condition of simultaneously supercooled and superheated (or doubly metastable or d-m) water in a Berthelot tube type experiment is illustrated in the double shaded region of phase diagram for water in figure 6.1 where water remains as a liquid phase in the doubly metastable region. AB is the saturation line (boiling point line), that is, that normally separates the liquid and vapour phases of water; if any water remains liquid in the region below AB it is in the metastable condition of superheated. CD is the melting line, which is the line that normally separates the liquid and solid phases of water. If any water remains liquid in the region to the left of CD it is in the metastable condition of being supercooled, the point E where AB and CD intersect is the triple point. Therefore, the small double shaded area AEC is the doubly metastable region where water, if it remains liquid, must be in a state of superheating and supercooling simultaneously. This region has remained largely unexplored and the work described in this chapter seeks to

investigate the doubly metastable regime using an improved form of the Berthelot-type experiment.

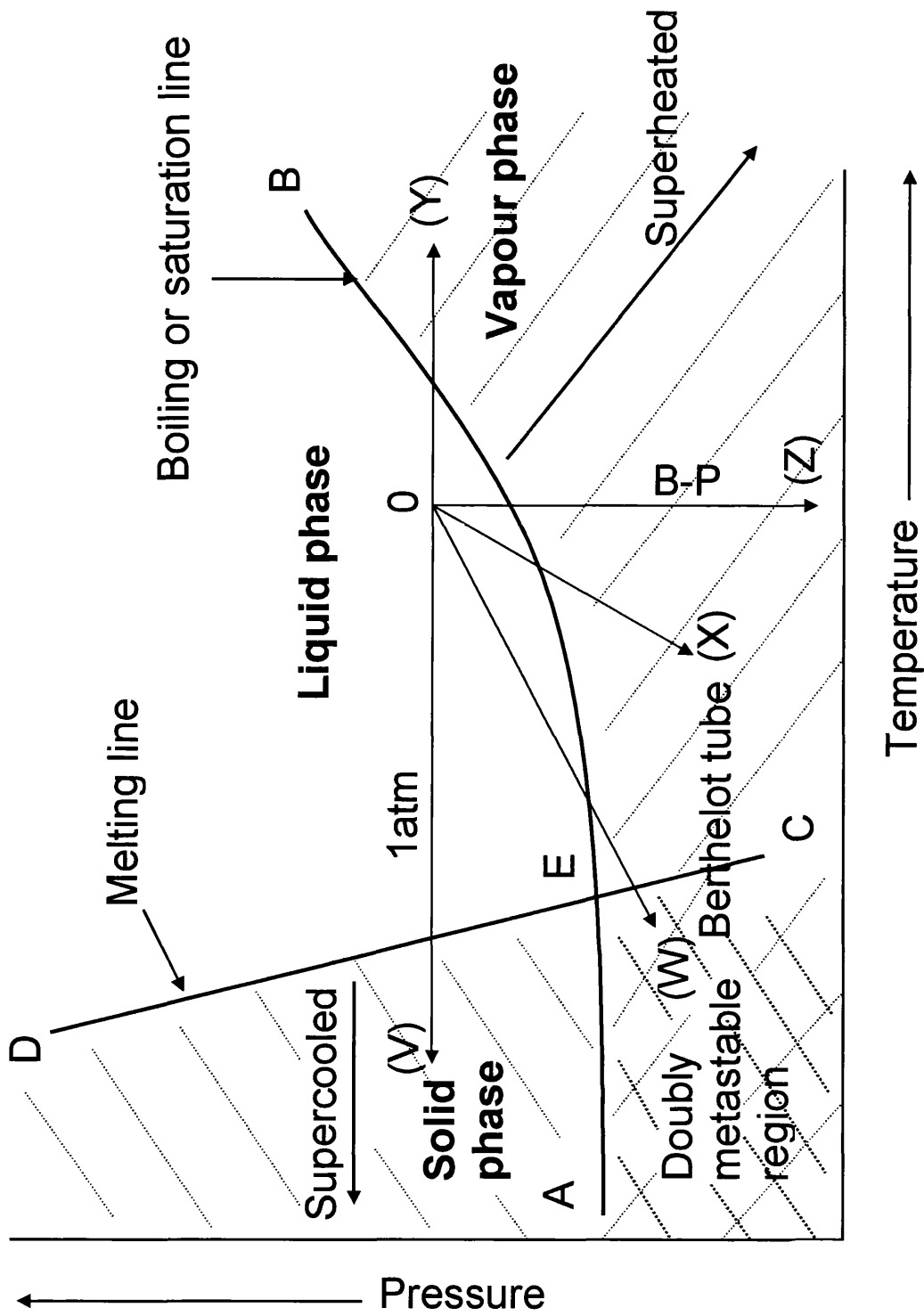
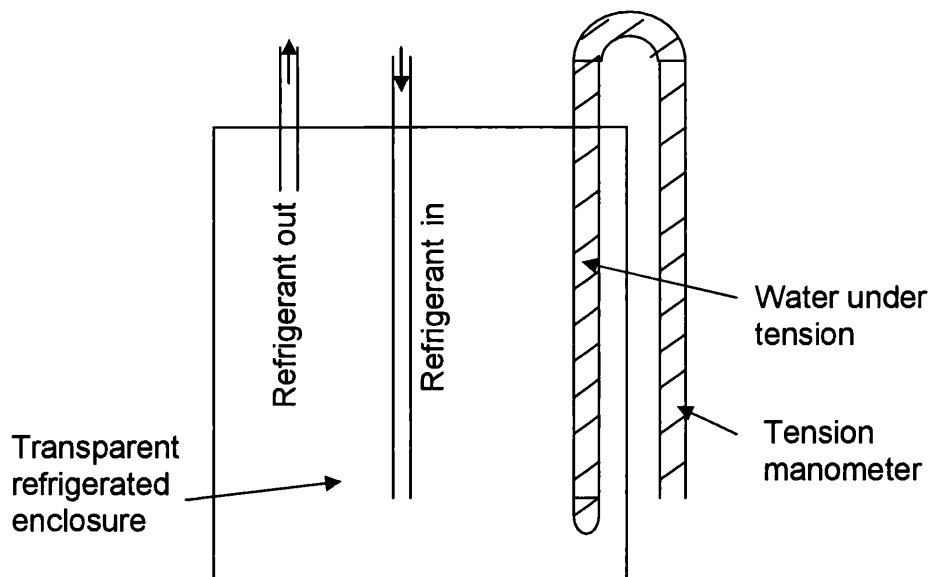


Figure 6.1 Phase diagram for water

## 6.2 Previous Related Work

It should be noted at the outset that relatively little work has been reported in this area. One of the few experimental studies was reported by Hayward (1971) who was the first to report water in the doubly metastable region by using a tension manometer which is shown in figure 6.2. Hayward (1971) reported that water at a tension of 0.2 bar can be cooled to at least  $-5\text{ }^{\circ}\text{C}$  before freezing. Hayward noted that, at a point below  $-5\text{ }^{\circ}\text{C}$ , the water suddenly froze and generally also cavitated at the same instant, thus relieving the negative pressure within the sample. The water thus makes a sudden leap to the triple point, the unique combination of temperature and pressure where solid, liquid and vapour can coexist in equilibrium. Hayward also reported the unusual finding that, on rare occasions, a network of ice crystals filled the test section without disrupting the tension within the sample. This only happened if the water sample was thoroughly de-aerated before the experiment.



**Figure 6.2** Head of tension manometer modified, by bending, to allow supercooled of water under tension (after Hayward (1971)).

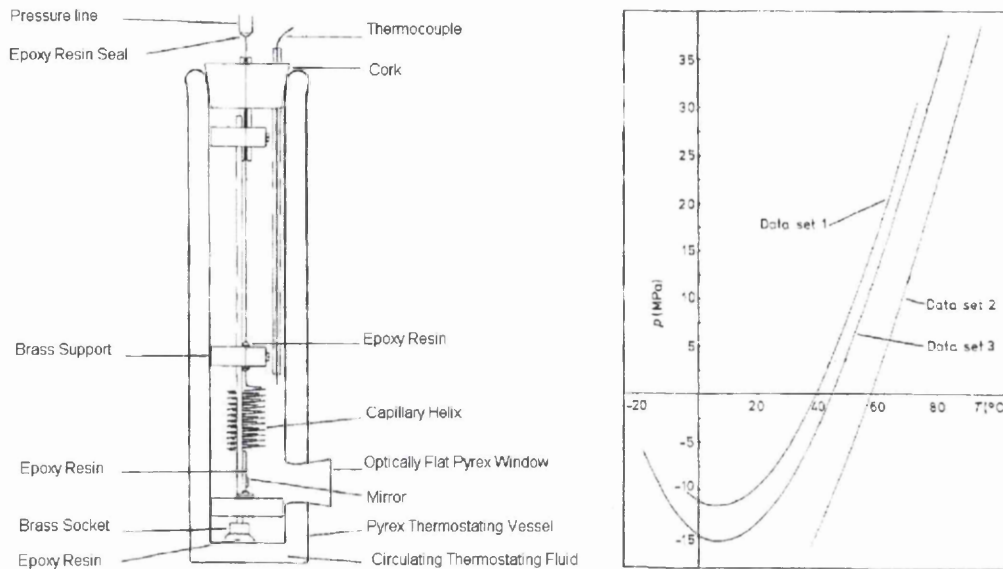


**Figure 6.3** The Berthelot-Bourdon tube and its (P, T) curve for water under tension (from Henderson and Speedy, 1980)

Following Hayward's initial studies, Henderson and Speedy (1980) used a spirally wound glass capillary (exploiting the Bourdon tube principle) within which liquid was stretched (the Berthelot tube principle) to examine the doubly metastable state of water. They managed to cool the 'stretched' water to  $-18\text{ }^{\circ}\text{C}$  and reported that the water neither froze nor cavitates. Their apparatus is shown in Figure 6.3. The total volume of test liquid in the tube was only  $2\text{ to }4\text{ mm}^3$ ; the advantage of such a small liquid specimen being that it would not contain many 'nucleation points' in the bulk liquid. The maximum tension achieved in Henderson and Speedy's apparatus was 156 bar at the temperature of maximum density (corresponding to a temperature of  $6.7\text{ }^{\circ}\text{C}$  at these conditions). Further cooling resulted in a decrease in tension due to the anomaly that water expands when cooled below the temperature corresponding to the point of maximum density. At  $-18\text{ }^{\circ}\text{C}$  (the limit of their cooling equipment) the tension had decreased to a value of 60 bar.

Fascinating questions are raised by these issues. Can superheated ice be formed from d-m water? If such ice forms, what form of ice is it? And can a way be found to manipulate negative pressure in structural studies of the formation process? These are challenging



issues whose resolution promises significant scientific and technological gains. As an example we may consider recent technological responses to environmental change. Attempts to moderate rising electrical power loads due to air-conditioning involve developing 'cold-energy' storage and transport devices. The working fluid for such devices is 'ice slurry', a mixture of fine ice crystals and liquid water whose use is limited by undesired freezing of supercooled water during transport. What is required is a means of controlling the nucleation of solid from supercooled water on demand. But recent theories which describe the role of cavitation in such a process have serious shortcomings. They invoke the collapse of a spherical bubble, in which situation it has been estimated that water near the bubble wall may experience sufficient pressure ( $10^4$  bar) to nucleate 'high pressure' ice (Inada, 2001). As such pressure persists for only a nanosecond; it has been assumed that normal ice subsequently grows on a 'high pressure' ice nucleus. But it is difficult to generate a spherical cavitation bubble, let alone maintain the requisite sphericity during collapse. The existence of such a 'high pressure' ice nucleus has not been verified. Clearly an alternative theoretical explanation is required. Such an explanation was advanced by Rogers (2004) who proposed a theory which involved the growth of a cavitation bubble in the supercooled liquid and the corresponding production of hydrodynamic pressures in a thin 'shell' of liquid close to the bubble wall. Due to the initial outward acceleration of the bubble wall, this liquid experiences a wave of pressure which acts to prevent ice nucleation by reducing the degree of effective supercooling. Subsequently, as the bubble wall decelerates, the shell of water is subjected to a wave of negative pressure which increases the degree of effective supercooling and promotes a high probability of nucleation. As a result the bubble is encapsulated by a 'shell' of ice, whose establishment within a wave of negative pressure in turn provides a fresh nucleating surface for subsequent bubble growth. This nascent bubble in its turn freezes a shell of ice around itself and, in principle; this process may be maintained throughout the available volume of liquid.

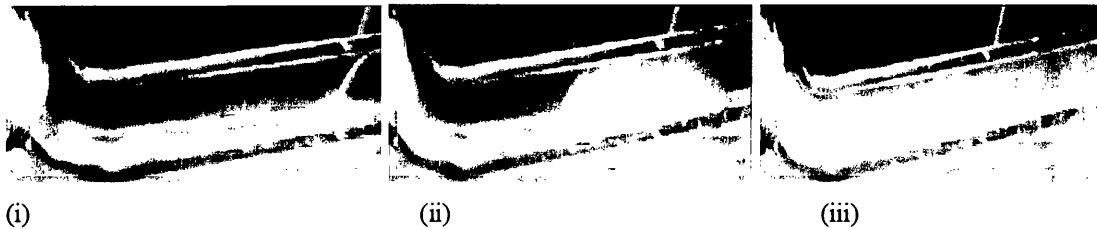


**Figure 6.4** Images from a high speed video sequence showing nucleation and propagation of ice from d-m water in a 10 cm long NMR sample tube adapted to function as a ‘Berthelot tube’ (Rogers, 2004). (i) A cavitation bubble grows from the tube wall (right) following tensile failure of the liquid at *ca.*  $-40$  bar. As a result of the induced hydrodynamic pressure changes around the bubble it becomes encapsulated by a ‘shell’ of ice. (ii) The ice shell, formed in a wave of negative pressure, provides a new nucleating surface for subsequent bubble growth and the ice ‘front’ propagates through the supercooled water ( $-18$  °C) by further bubble growth-freezing cycles. (iii) The process continues, at speeds commensurate with cavitation bubble growth but far more quickly than allowed by the free crystal growth rate. The tube is filled with an ice-air mixture in  $< 1$  second.

A key finding in support of this theory was the observation made by Rogers (2004) that in experiments involving the nucleation and propagation of ice from d-m water, measurements showed that the ice ‘front’ propagates through the supercooled water (presumably by further bubble growth-freezing cycles) at speeds commensurate with cavitation bubble growth but far more quickly than allowed by the free crystal growth rate (see Figure 6.4). For instance Hillig (1958) produced experimental data relating the velocities of an ice front in a glass tube to the degree of supercool (see figure 6.5). It can be seen that, under the conditions encountered in the experiments of Rogers (2004), the ice front would be expected to progress at a velocity in the order of  $0.1$  to  $1$   $\text{cm s}^{-1}$  in a direction parallel to the longitudinal axis of the tube. Surprisingly, the analysis of the images captured during ice formation gave the velocity of the ice front to initially be at least an order of magnitude higher than this, indicating that some other driving force may be involved in the formation of ice under these conditions.

Thus a key objective of the present work was to re-examine the experimental conditions used in the work reported by Rogers (2004) in order to verify that such high speeds of ice formation and ice front propagation account ice production from d-m water. That work

involved the development and testing of new Berthelot tubes and employed high speed video image capture and analysis work which is now described below.

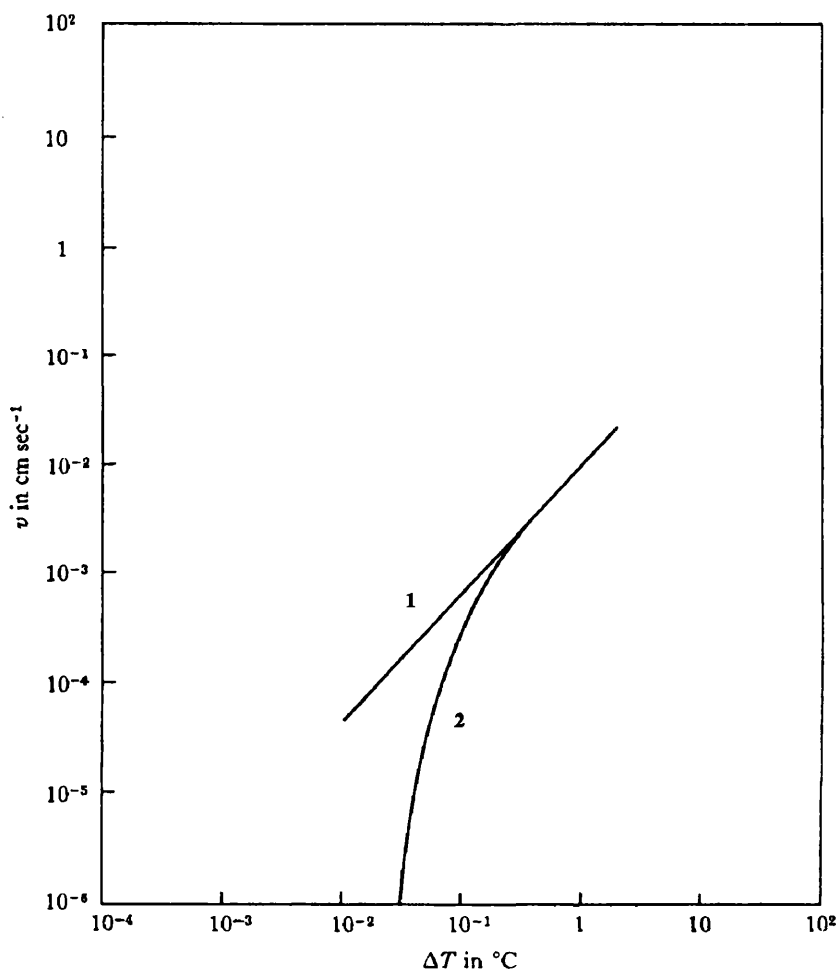


**Figure 6.5** Hillig's experimental results for the ice front velocity,  $v$ , as a function of the degree of supercooling for ice formation in a glass tube (line 1 is for imperfect crystal formation and line 2 is for perfect crystal formation) (from the chemical physics of ice, 1970)

### 6.3 The Modified Berthelot tube

The present Berthelot tube experiment in this chapter is concerned with the behaviour of a liquid which was subjected to tension under 'quasi-static' due to the difference in expansion-contraction of glass and liquid. This is an isochoric cooling method for obtaining tensions on liquids was used to determine the heterogeneous nucleation limit for stretching of water at variety of water density as shown in figure 6.6. The principle mechanism for inducing tension and subsequent lead to cavitation in a Berthelot tube is explained in section 1.5.1.1. The main interest of present chapter is to examine water under doubly metastable conditions.

These modified Berthelot tubes were fabricated from borosilicate (Pyrex) glass with a polytetrafluoroethylene (PTFE) sealing vacuum valve (See figure 6.7 and figure 6.8) allowing it to withstand a very high pressure while permitting direct observation of any cavitation/nucleation event and facilitating the recording of it using a high speed camera. The modified Berthelot tube incorporates a sidearm which allows the tube to be connected to a vacuum pump in order to degass the test sample (See figure 6.7). The whole Berthelot tube assembly was immersed in the temperature control water bath (thermometric 5510, thermostatically controlled) and was subsequently cooled – typically at a rate of 1 °C per minute until ice or cavitation (or both) occurred in the tube. Cavitation was usually accompanied a clearly audible metallic 'click' (as has been noted by previous workers (Trevena, 1987)). Preliminary tests established that if the Berthelot tube was sufficiently clean, samples of deionised water could be set into tension and supercooled, down to -20 °C without cavitating or freezing. In these preliminary experiments the whole Berthelot tube assembly was immersed in the temperature control water bath (Thermometric 5510 Thermostat). This was used to cool the tube at 1 °C per minute until ice or cavitation (or both) were recorded. The Berthelot tube was then removed from the water bath as soon as possible.

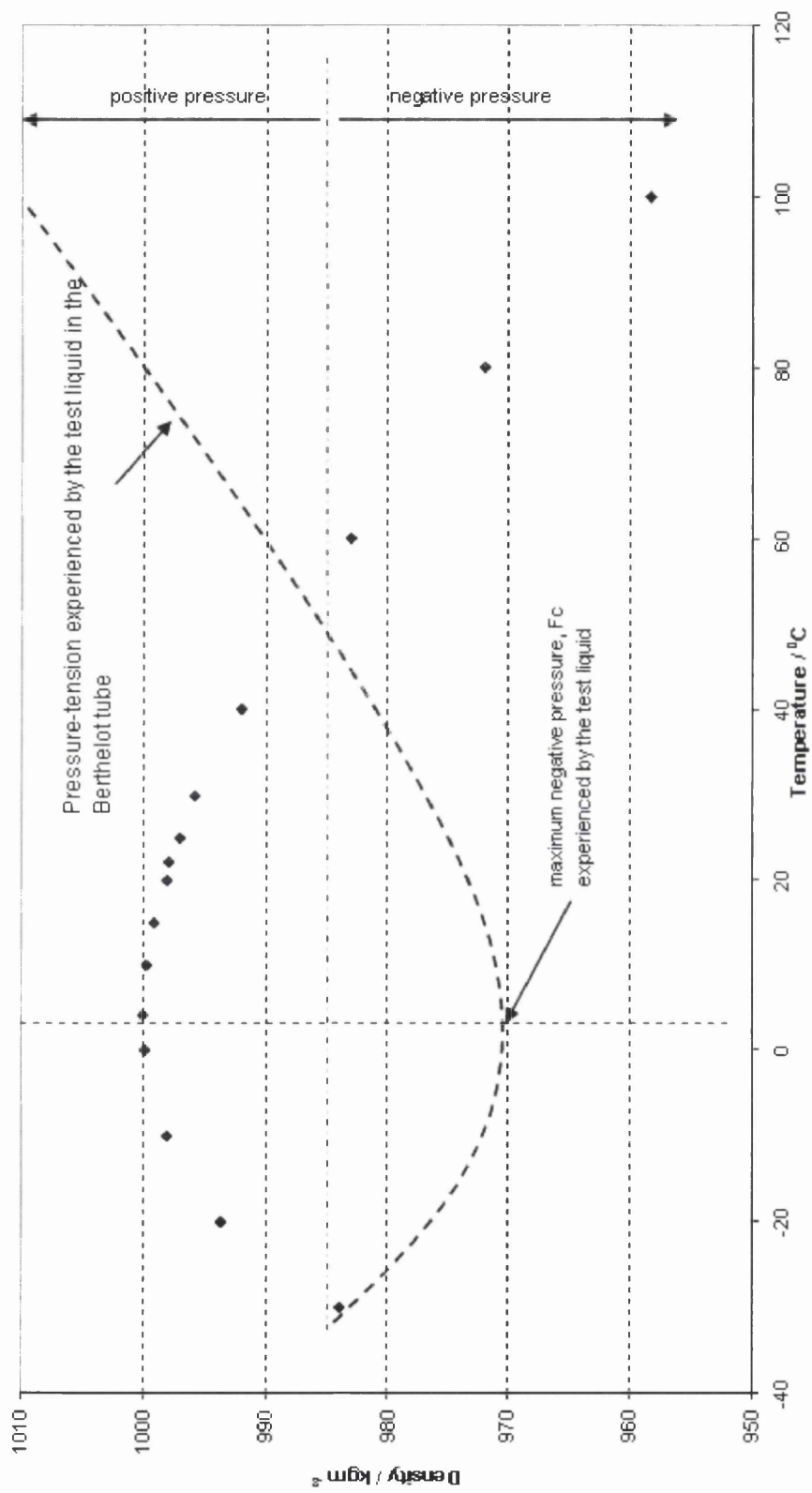


**Figure 6.6** Density against temperature curve for water under pressure and tension in the Berthelot tube experiments



Figure 6.7 Photograph of various lengths of the blue capped modified Berthelot tubes



Figure 6.8 Photograph of yellow capped modified Berthelot tubes

#### **6.4 Determination of the Sealing Temperature, $T_0$ , in Order to Bring D<sub>2</sub>O (Heavy Water) Liquid Samples into the Doubly Metastable Region in the Modified Berthelot Tube**

Before describing this work it is instructive to review the previous Berthelot tube work reported by Jones *et al* (1981) who showed the relationship between the sealing temperature and the maximum tension achievable in water in a Berthelot tube experiment over a wide range of temperature. Figure 6.9 shows the sealing temperature,  $T_0$  which produces tension at temperatures of 14.5, 16.6, 23.5, 30.4 and 34.4 °C. In the case (low sealing temperature,  $T_0 < 17$  °C) of A and B, it was possible to monitor tensions changes in the liquid down below the melting temperature without the onset of any cavitation. Both curves show a minimum at around 4-5 °C (corresponding to the maximum density of the water, see figure 6.6). At these minima the corresponding values of the maximum tension are 13.5 atm (curve A) and 20.5 atm (curve B). Curve B clearly has a higher chance to penetrate the doubly metastable region than curve A on further cooling as the tension generated in curve A might be diminished at supercooling region due to the expansion of the anomalous hydrogen bonds in the water. In case C ( $T_0 = 23.5$  °C) it was not possible to go below 6 °C without the occurrence of cavitation, the corresponding tension achieved being 46 atm which was the highest tension obtained in the experiment.

Clearly, the sealing temperature,  $T_0$  is the crucial factor in using the Berthelot tube experiment to produce doubly metastable water (refer to figure 6.1, line OW). With a high sealing temperature, more tension will be generated when the tube is being cooled, but there is a higher probability that the water cavitates before it reaches its supercooled region. However, with a low sealing temperature, the supercooled region can be entered without the onset of cavitation, but the tension generated in the liquid might be diminished.

In present experiments, heavy water (Deuterium Oxide, D<sub>2</sub>O) was used as a test sample. This Thesis contains the first report of the behaviour of heavy water in the Berthelot tube experiment. Deuterium is an isotope of hydrogen; D<sub>2</sub>O having somewhat different physical properties from ordinary water (see table 6.1). A systematic series of

experiments was necessary in order to establish the value of the highest achievable sealing temperature,  $T_0$  for heavy water which enabled the liquid to enter the supercooled region without cavitation (recalling that the higher the sealing temperature,  $T_0$ , the higher the value of negative pressure which can be generated in the liquid as shown in figure 6.9).



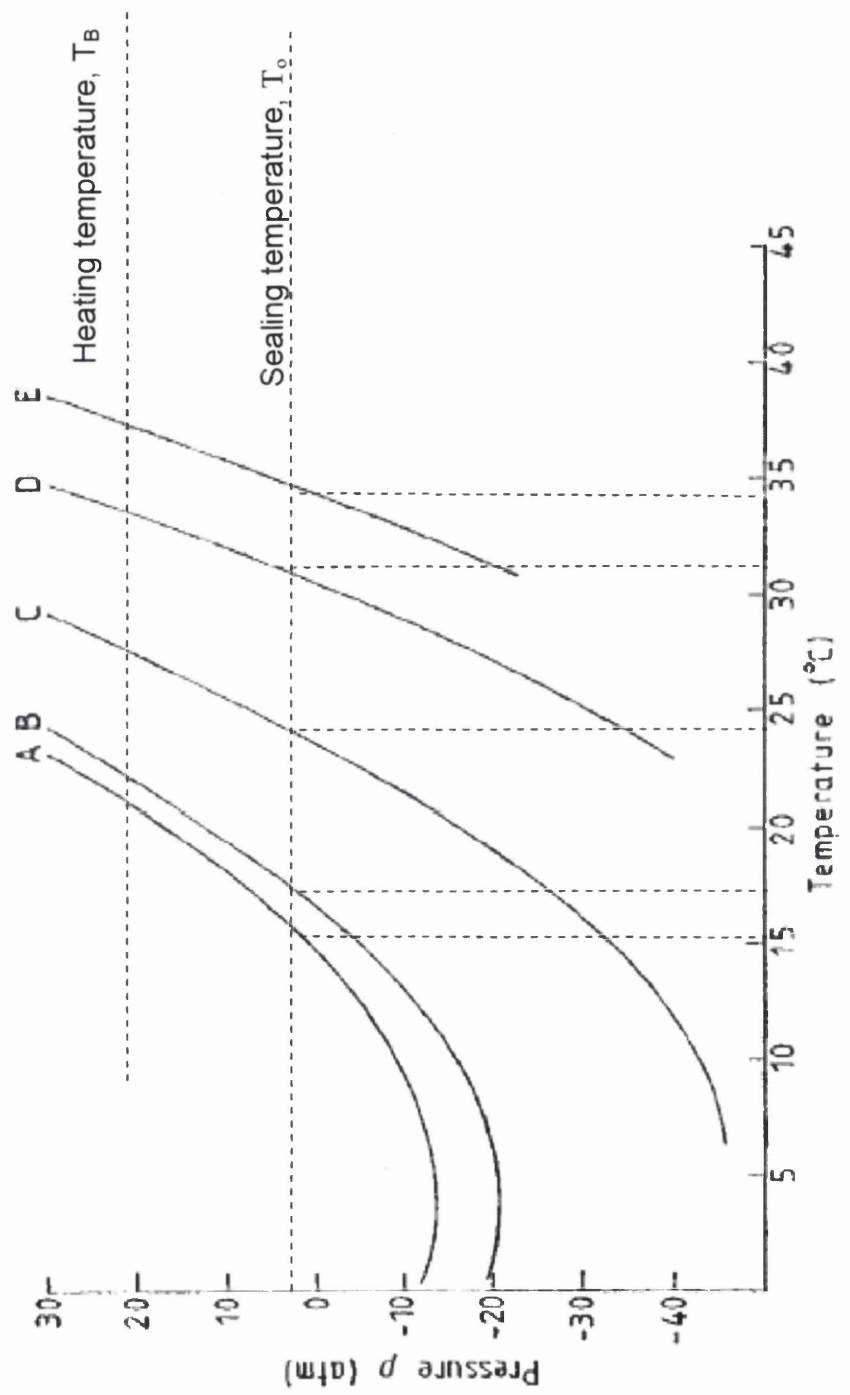


**Figure 6.9** Five (pressure, temperature) curves for water under tension in the Berthelot tube experiments (Jones *et al.*, 1981).

Property	D <sub>2</sub> O (Heavy water)	H <sub>2</sub> O (Ordinary water)
Freezing point (°C)	3.82	0
Boiling point (°C)	101.4	100
Density (20 °C, g/mL)	1.1056	0.9982
Temp. of maximum density (°C)	11.6	4
Viscosity (at 20 °C, mPa·s)	1.25	1.005
Surface Tension (at 25 °C, μJ)	7.193	7.197
pH (at 25 °C)	7.41	7

**Table 6.1** Differences in physical properties between heavy water and ordinary water

A problematic aspect of the Berthelot tube technique is that each individual tube has its own characteristics, and the range of tensions achievable can vary from tube to tube due to differences in the smoothness of the inner wall surface (Lewis, 1961). Five replicate Berthelot tubes were tested in the present experiments.

A range of sealing temperatures,  $T_0$  was employed (from 20 °C to 40 °C), the sample and tube being heated to 10 °C above the sealing temperature in each case after sealing for twenty minutes to make sure that all the liquid filled up the Berthelot tube completely due to the expansion of the test liquid. The Berthelot tube was subsequently cooled at a rate of 1.0 °C per minute using the water bath (containing water + glycerol) while the tube was carefully observed for the first appearance of a bubble. This appearance was usually accompanied by a sharp metallic click. If there was no cavitation during the cooling process, then the cooling was continued into the liquid's supercooled temperature region (see figure 6.1 in which AEC is the doubly metastable region).

Table 6.2 shows the results obtained from the experiments involving a range of sealing temperatures. The results indicated that the 'yellow capped' set of tubes were more

promising in terms of their ability to bring the liquid into its supercooled regime without cavitation. However, the yellow capped tubes were associated with a markedly softer 'click' on cavitation than were the blue capped tubes in which a loud, sharp metallic click was heard on cavitation of the liquid. The experimental results indicate that those tubes with sealing temperature,  $T_0$  of 30 °C generated the most severe cavitation events in the heavy water samples. None of the tubes was found able to cool down heavy water to supercooling temperatures without the occurrence of cavitation if the sealing temperature was greater than 40 °C.

Sealing Temp (°C)	Number of experiments	Average breaking temp (°C)	Average temp difference observed (°C)	Percentage to produce superheated ice (%)
20	10	-10.6	30.6	100
25	20	-11.5	36.5	97
30	10	-9.5	39.5	83
35	10	20.0	15.0	19
40	10	28.1	11.9	0

First yellow capped Berthelot tube

Sealing Temp (°C)	Number of experiments	Average breaking temp (°C)	Average temp difference observed (°C)	Percentage to produce superheated ice (%)
20	10	-10.6	30.6	100
25	20	-12.2	37.2	100
30	10	-10.4	40.4	83
35	10	-10.0	45.0	50
40	10	23.4	16.6	0

Second yellow capped Berthelot tube

Sealing Temp (°C)	Number of experiments	Average breaking temp (°C)	Average temp difference observed (°C)	Percentage to produce superheated ice (%)
20	10	-8.3	28.3	100
25	20	-10.2	35.2	90
30	10	-10.0	40.0	40
35	10	26.0	9.0	0
40	10	31.9	8.1	0

Third blue capped Berthelot tube

Sealing Temp (°C)	Number of experiments	Average breaking temp (°C)	Average temp difference observed (°C)	Percentage to produce superheated ice (%)
20	10	-12.1	32.1	100
25	20	-7.9	32.9	100
30	10	-8.1	38.1	50
35	10	26.8	8.2	0
40	10	30.2	9.8	0

Fourth blue capped Berthelot tube

Sealing Temp (°C)	Number of experiments	Average breaking temp (°C)	Average temp difference observed (°C)	Percentage to produce superheated ice (%)
20	10	-9.5	29.5	100
25	20	-11.0	36.0	95
30	10	-11.2	41.2	55
35	10	23.8	11.2	0
40	10	31.0	9.0	0

Fifth blue capped Berthelot tube

**Table 6.2** Results obtained from experiments involving a range of sealing temperatures.

## 6.5 The Records Obtained From High-Speed Imaging System

High-speed images and high speed video photographic records of cavitation in a Berthelot tube were first reported by Rogers (2004). Although high-speed pictures of cavitation bubbles in various other cavitation apparatus have been published previously, the images obtained from the Berthelot tube are of special interest for two reasons. Firstly, many of the images previously reported are taken of bubbles that have been produced artificially e.g. by introduction from the syringe or by electrolysis) and as such do not capture the initial growth of the bubble as the liquid cavitates. Secondly, many of the images previously reported are obtained from system where cavitation has been produced by an external dynamic stimulus. Conversely the cavitation events within the Berthelot tube are the result of quasi-static stressing of a liquid and as such the growth and collapse of the bubble is due entirely to the liquid cavitating rather than any extraneous external factors. It follows that when ice forms in such an experiment in the d-m regime the ice may actually itself be in a 'superheated' state.

Direct observation remains the most satisfactory method of studying cavitation. In order to observe the cavitation events occurring within the Berthelot tube, a high speed camera (FastCam Ultima APX Imager) was used. Clearly, the ability to directly observe cavitation events is highly desirable but in view of the typical timescales of cavitation activity (milliseconds, or less) this necessitates high-speed photographic techniques. Surprisingly, only few previous studies of liquids in a Berthelot tube have reported the use of high-speed photography although the results of visual observation (by the unaided eye) are well documented (Rogers, 2004). The role of the liquid-solid boundary is a very important factor in the onset of cavitation in the case of Berthelot tube measurements. Rogers (2004) confirmed that the PTFE valve surface in contact with the deionised water test sample is the 'weakest link' in the system, as the cavitation bubbles nearly always occurred on, or in close proximity to, the PTFE valve surface.

### 6.5.1 Initial Test Results

Figure 6.10 to 6.12 show various experiments of consecutively captured frames (frame rate 24,000 fps) illustrating the initial formation, growth and collapse of a single cavitation bubble in degassed heavy water (Deuterium oxide 99.9 atom %D) in the present Berthelot tube (length 60 mm; inner and outer diameter 7 mm and 10 mm respectively). The tube was permanently sealed at one end (see figure 6.7). Cavitation bubble initially appeared near the centre surface of the PTFE valve. This is the loss of adhesion between the liquid and the wall of PTFE valve which is the precursor to the cavitation event.

It can be seen from figure 6.10 that the initial formation of the cavity first appears in frame 2. In this sequence the value of the elapsed time is set such that  $t = 0$  is at the instant of frame 2. The cavitation bubble continues to grow during frames 2, 3, 4, 5 until it reaches a maximum diameter of approximately 3.45 mm in frame 6, corresponding to a total elapsed time of 168  $\mu\text{s}$ . The bubble then begins to collapse (frames 7, 8, 9) until it reaches minimum radius (frame 10). The dynamics of the initial bubble was then investigated and the calculated average diameter of oscillating cavitation bubble as a function of elapsed time is shown in figure 6.14. It was observed, after examination of the high-speed images, that the initial collapse of a cavitation bubble that formed on, or in close proximity to, the PTFE valve often resulted in a liquid 'jet' that effectively split the bubble in two (see figure 6.10 from frame 6 to frame 10). The jet formed by the bubble collapse always started in the main body of the liquid and propagated towards the PTFE surface. As the bubble begins to collapse (frame 7 and 8) the pressure wave causes the surrounding liquid to deform the bubble. The average velocity of the jet was  $11.2 \text{ ms}^{-1}$  travelling toward at the centre wall of PTFE. The formation of liquid jets produced by cavitation bubbles has been extensively studied but never previously based on the Berthelot tube technique. Liquid jets are one of the principle mechanisms of surface erosion or cavitation damage (Trevena, 1987). The other model proposed to explain how surface erosion occurs is that of the 'shock wave' model (Lush *et al*, 1983) which attributes the damages to the very high pressures associated with the collapse and rebound of the cavitation bubbles. The extent to which each of these two mechanisms or

the effect of combination of both mechanisms are responsible for cavitation damage is the subject of much ongoing debate, as the mechanism of surface erosion during cavitation is not yet fully understood.

It can be seen from figure 6.12 that the initial formation of the cavity first appears in frame 2. The cavitation bubble continues to grow until it reaches a maximum in frame 6, corresponding to an elapsed time of 174  $\mu\text{s}$ . It can be seen that the single (approximately spherical) cavity reached its maximum size,  $d = 5.1 \text{ mm}$  prior to collapse and form a liquid jet through frame 7 to 8. The average velocity of the jet was  $16.2 \text{ ms}^{-1}$  travelling toward at the centre wall of PTFE. Frame 11 to 14 show the point at which the bubble begins to rebound before growing in size again, albeit to a smaller diameter than the initial maximum. This growth and collapse cycles continues at an almost constant frequency (although the amplitude is gradually damped over each cycles), until the bubble comes to rest. In frame 10, the huge cavitation bubble collapsed and approached a minimum size and completely disappeared for a short time ( $\sim 42 \mu\text{s}$ ) before re-emerged again. It is believed that this phenomenon occurs only when the magnitude of the pressure-tension wave is relatively high in the water system which able to temporary force all the gas and vapour in the cavity condense in the liquid.

In figure 6.13 shows consecutive frames (frame rate 24,000 fps) are illustrating the initial formation, growth and collapse of a single cavitation bubble in deionised water. Interestingly, the cavitation event is seen to start with an apparently single, approximately spherical cavity, growing not at (or from) the tube walls, but from within the main body of the liquid. Frame 9 and frame 10 show the formation of a liquid jet ( $v = 10.5 \text{ ms}^{-1}$ ) shortly after the cavitation bubble collapses.

The results of these initial experiments are noteworthy as they indicate that the Berthelot tube technique may have wider utility in cavitation research than has previously been thought. The ability to generate and study the behaviour of a single approximately spherical bubble formed in the body of a liquid under tension is potentially valuable in enabling studies of cavitation bubble dynamics – a very substantial area of cavitation research. Previous use of the Berthelot tube has been largely confined to measurements of

the cavitation threshold of liquids. The work reported here shows that its use may be usefully extended to the study of potential cavitation damage mechanisms. In this respect it is interesting to note that the average velocities of the jets produced shortly after the cavitation bubble collapses in the present work on heavy water is typically  $17 \text{ ms}^{-1}$  (or less), this being significantly lower than the values of ca  $170 \text{ ms}^{-1}$  (or more) considered necessary to damage a solid boundary (Plesset and Chapman, 1971).





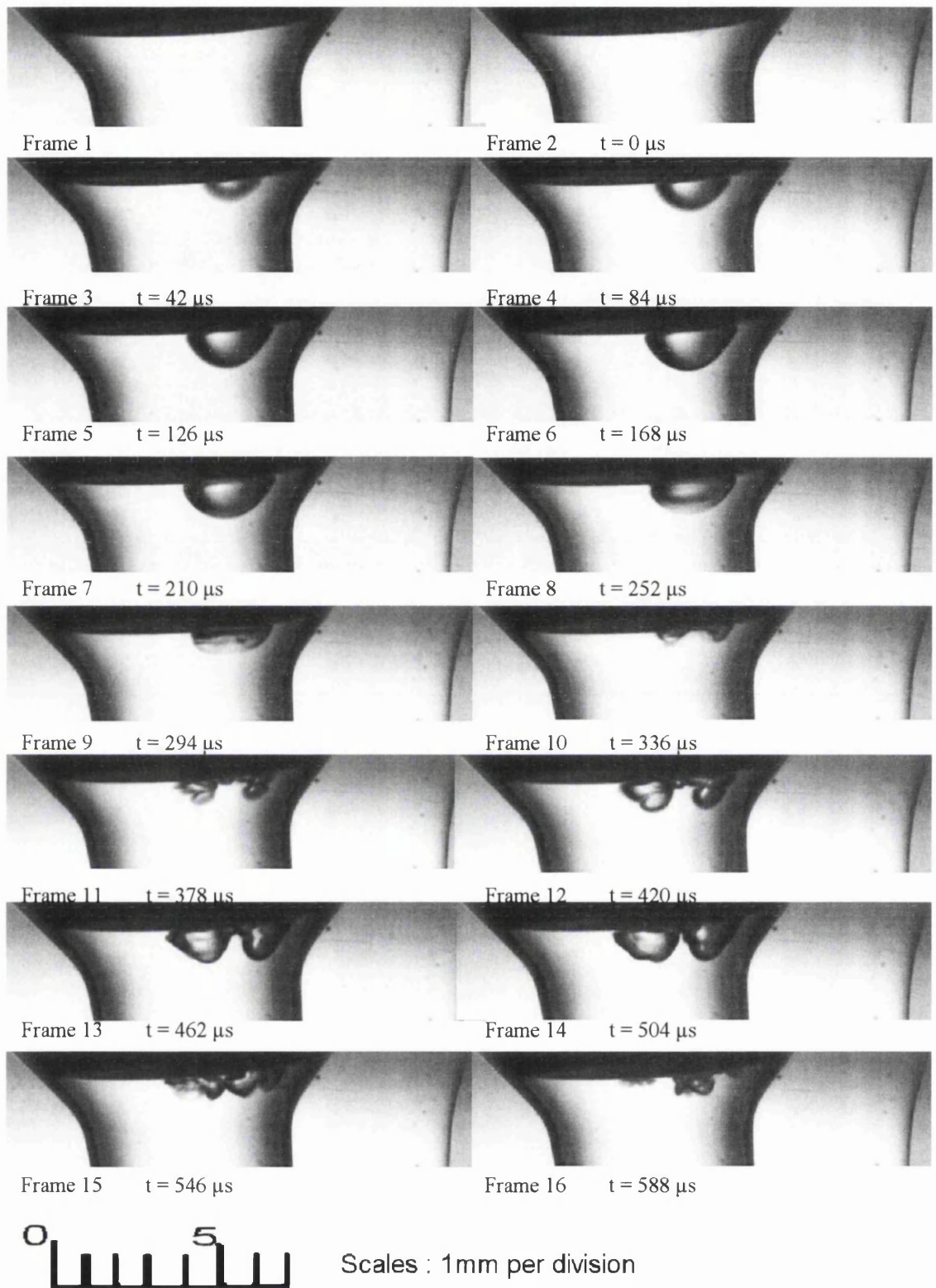


**Figure 6.11** High-speed images (captured at 24,000 fps) of the initial formation, growth and collapse of a single cavitation bubble in degassed heavy water ( $D_2O$ ) in an improved Berthelot tube (inner diameter 7 mm)

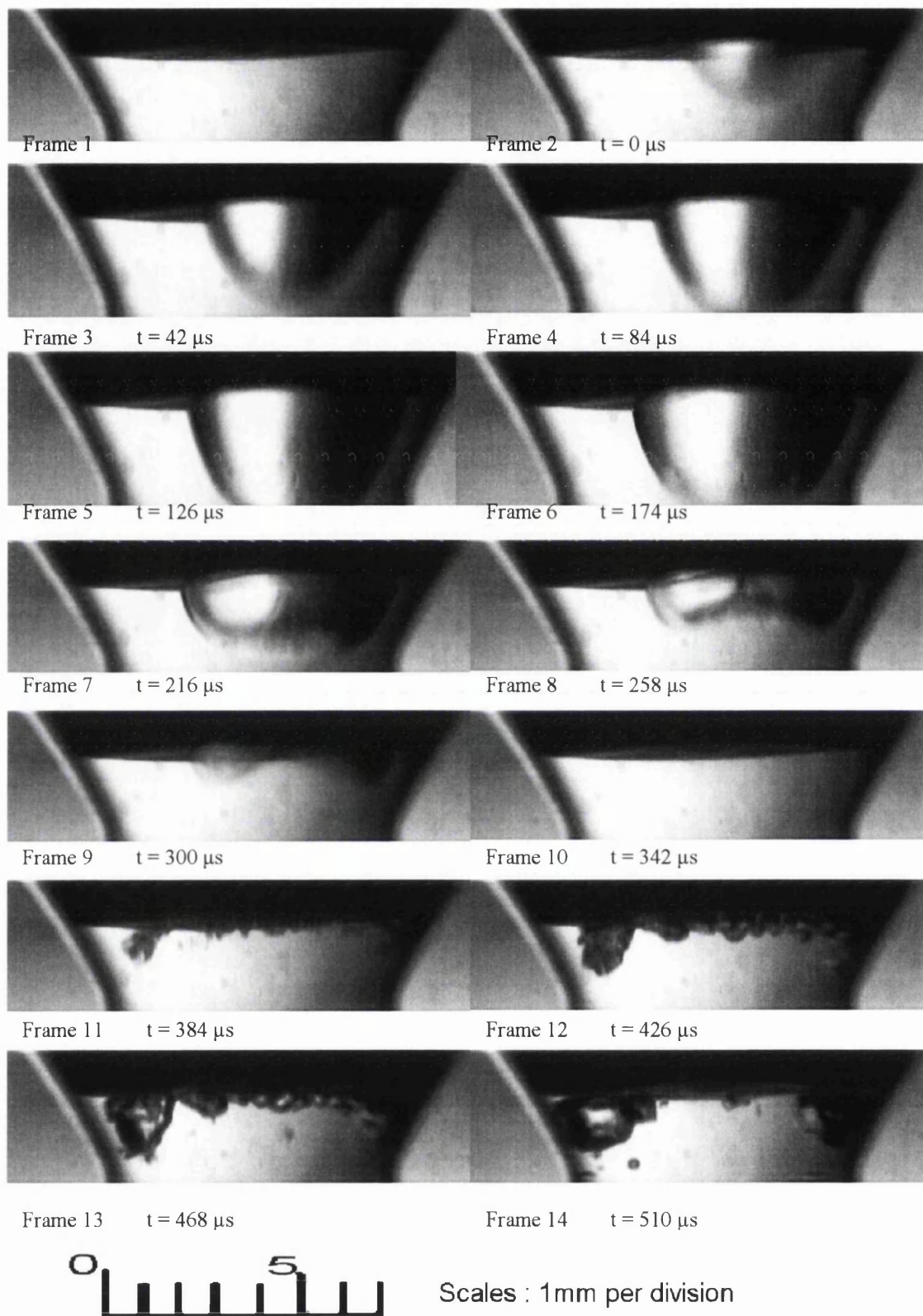


**Figure 6.12** High-speed images (captured at 24,000 fps) of the initial formation, growth and collapse of a single cavitation bubble in undegassed heavy water ( $D_2O$ ) in an improved Berthelot tube (inner diameter 7 mm).



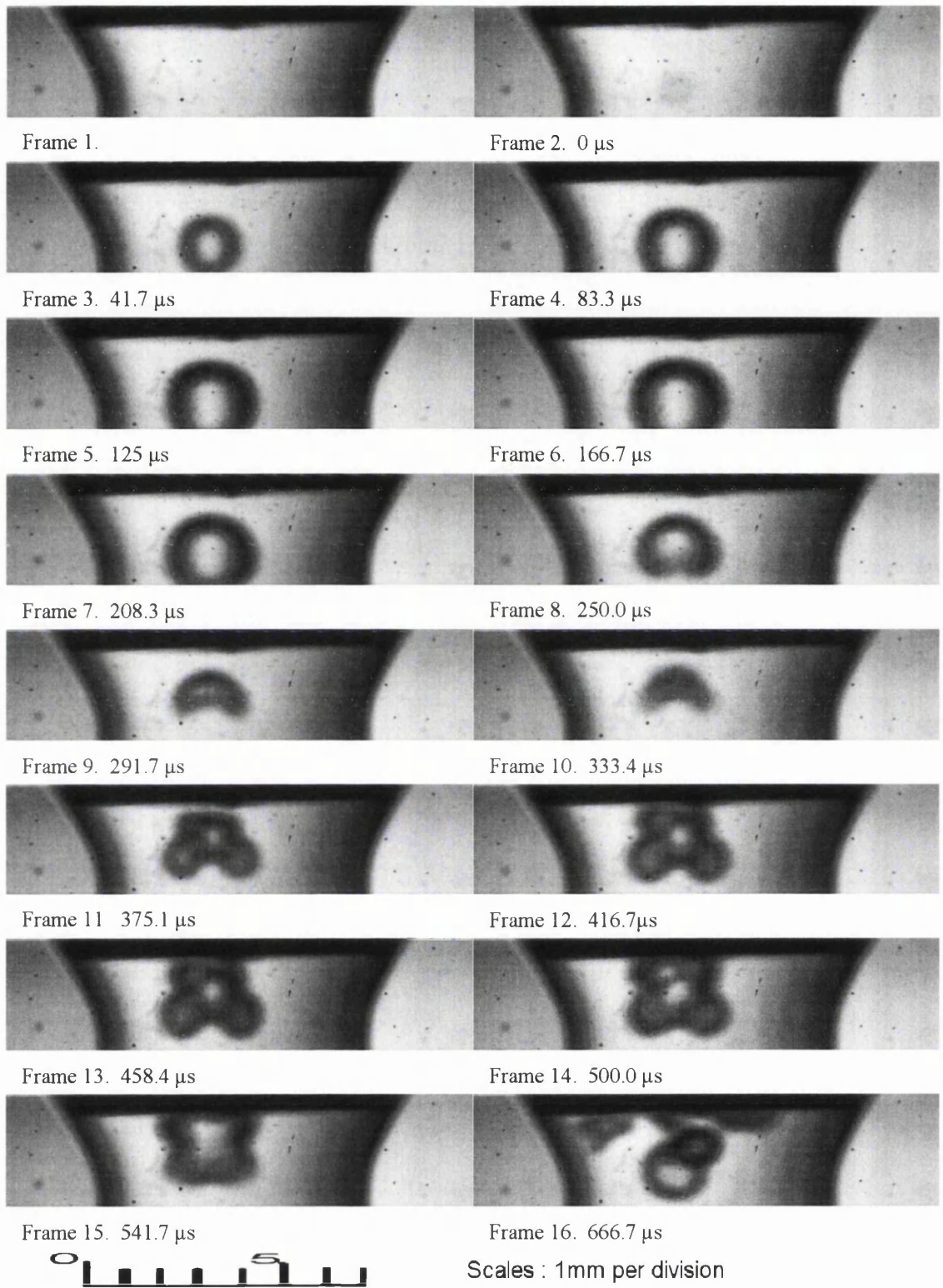


**Figure 6.13** High-speed images were captured at 24,000 f.p.s shown that the initial formation of single, spherical cavity, apparently growing not from the PTFE walls, but in the body of a liquid. After the bubble collapse begins a liquid jet forms, the jet being directed towards the end of the tube.

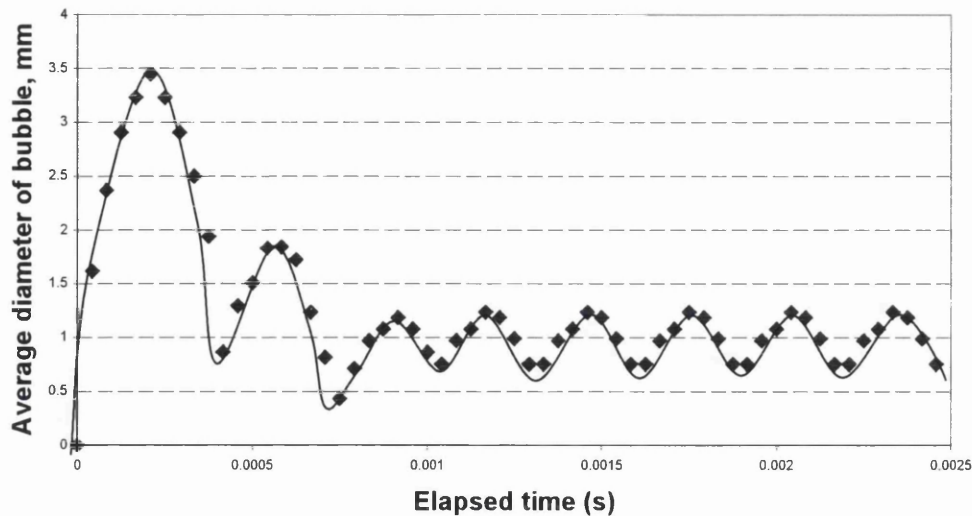


**Figure 6.14** The calculated average diameter of oscillating bubble as a function of elapsed time.

### 6.5.2 Experiments Involving d-m Heavy Water

Figure 6.15 shows a sequence of high speed images (captured at 24,000 frames per second) from an experiment in which degassed heavy water was supercooled down to  $-9.5\text{ }^{\circ}\text{C}$  prior to ice formation. The growth of dendritic ice crystals was recorded (see Chow, 2004), the ice forming initially near the PTFE valve. A network of ice crystals gradually filled the test section without, apparently, disrupting the state of tension within the sample. No cavitation event was recorded. However, in another case (see figure 6.16) it was found to be possible to achieve a supercooled to  $-19.5\text{ }^{\circ}\text{C}$ : cavitation was produced and ice crystals were nucleated in the immediate vicinity of the bubble. It is believed that the water thus makes a sudden leap to the triple point, the unique combination of temperature and pressure where solid, liquid and vapour can coexist in equilibrium; this phenomenon was first observed by Hayward (1971) with unaided eye. However, the work reported in this Thesis is the first in which evidence is presented that the formation and growth of a cavitation bubble results in the nucleation of ice formation.

Twelve frames in figure 6.16 captured ice formation from the doubly metastable water. The sealing temperature,  $T_0$  was  $20\text{ }^{\circ}\text{C}$ . Frame 2 in figure 6.16 shows the first single cavitation bubble event followed after an interval of approximately two milliseconds by ice formation (frame 5 until frame 10). In Frame 8, the water thus

makes a sudden leap to the triple point. The results reported are further evidence to support the hypothesis (Rogers, 2004) that the pressure changes induced by the dynamics of cavitation bubbles are responsible for the ice nucleation process.

The ideas which support this hypothesis may be explained as follow. The ‘Rayleigh-Plesset’ equation has been widely studied in terms of cavity collapse and the consequent pressure generation in the surrounding liquid but herein we focus on the initial cavity growth phase and the corresponding development of hydrodynamic pressures at various distances about the growing cavity. The hydrodynamic pressure  $p$  at a point  $r$  in the liquid in the neighbourhood of the bubble is given by the Bernoulli equation (Trevena, 1987):

$$p = \rho \frac{d\phi}{dt} - \frac{1}{2}(\rho v^2) + p_{\infty}$$

where  $p_{\infty}$  is the pressure in the undisturbed water,  $\rho$  is the density and  $v = -\frac{d\phi}{dr}$  is the

radial velocity at that point, with velocity potential  $\phi = \frac{R^2}{r} \left( \frac{dR}{dt} \right)$ . The pressure variation  $\Delta p$  at  $r$  due to cavity motion is

$$\Delta p = p - p_{\infty}$$

$$\Delta p = \frac{\rho}{r} \frac{d}{dt} \left( R^2 \frac{dR}{dt} \right) - \frac{\rho R^4}{2r^4} \left( \frac{dR}{dt} \right)^2$$

Overton & Trevena (1981) used the Bernoulli equation to account for the pressure-tension cycles recorded in their bubble oscillation experiments and in so doing associated the peak values of tension with the attainment of maximum cavity volume. When the cavity volume  $V$  reaches a maximum,  $d^2V/dt^2$  is negative and this results in the development of tension due to the fact that, for values of  $r$  which are large enough to discount the second term in the above equation,  $d^2V/dt^2 \propto \Delta p$ . Subsequent work (Williams *et al*, 1999) established that the maximum negative values of  $d^2V/dt^2$  (and hence the maximum value of tension) may precede the attainment of maximum cavity

volume. From this it follows that a pulse of negative pressure is generated about a cavity during its growth phase and it follows that this pulse of negative pressure, confined within a thin shell of liquid close to the expanding cavity wall, will act to suddenly increase the effective supercool of the adjacent liquid. These sudden increases in effective supercool then initiate ice formation from the d-m water but at a propagation velocity comparable with the velocity of bubble expansion during the latter stages of expansion. Such velocities are commensurate with those recorded herein for the ice front propagation but are far higher than allowed by the free crystal growth rate.



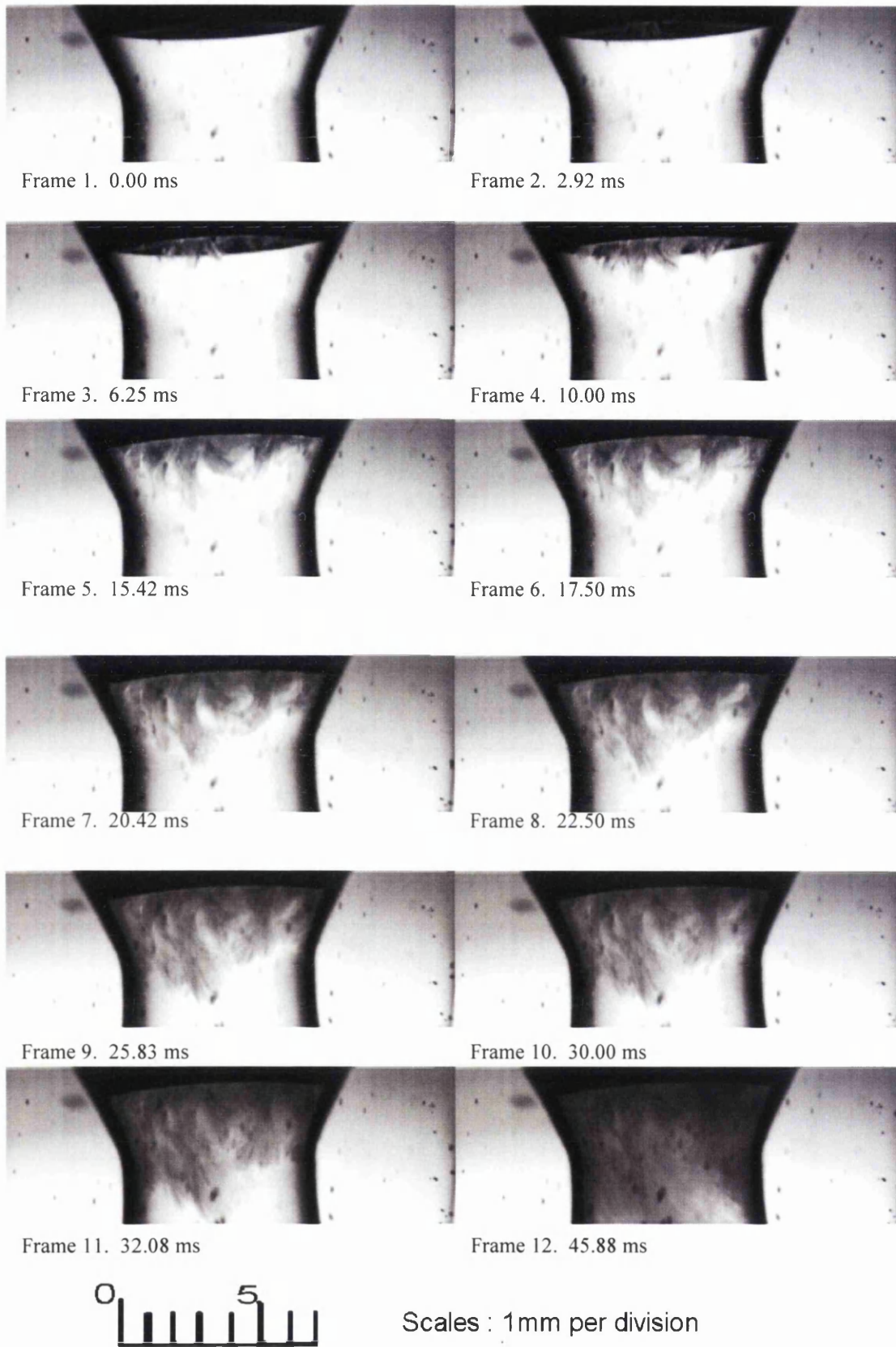


**Figure 6.15** Twelve frames captured during ice formation in degassed heavy water contained in an improved Berthelot tube.



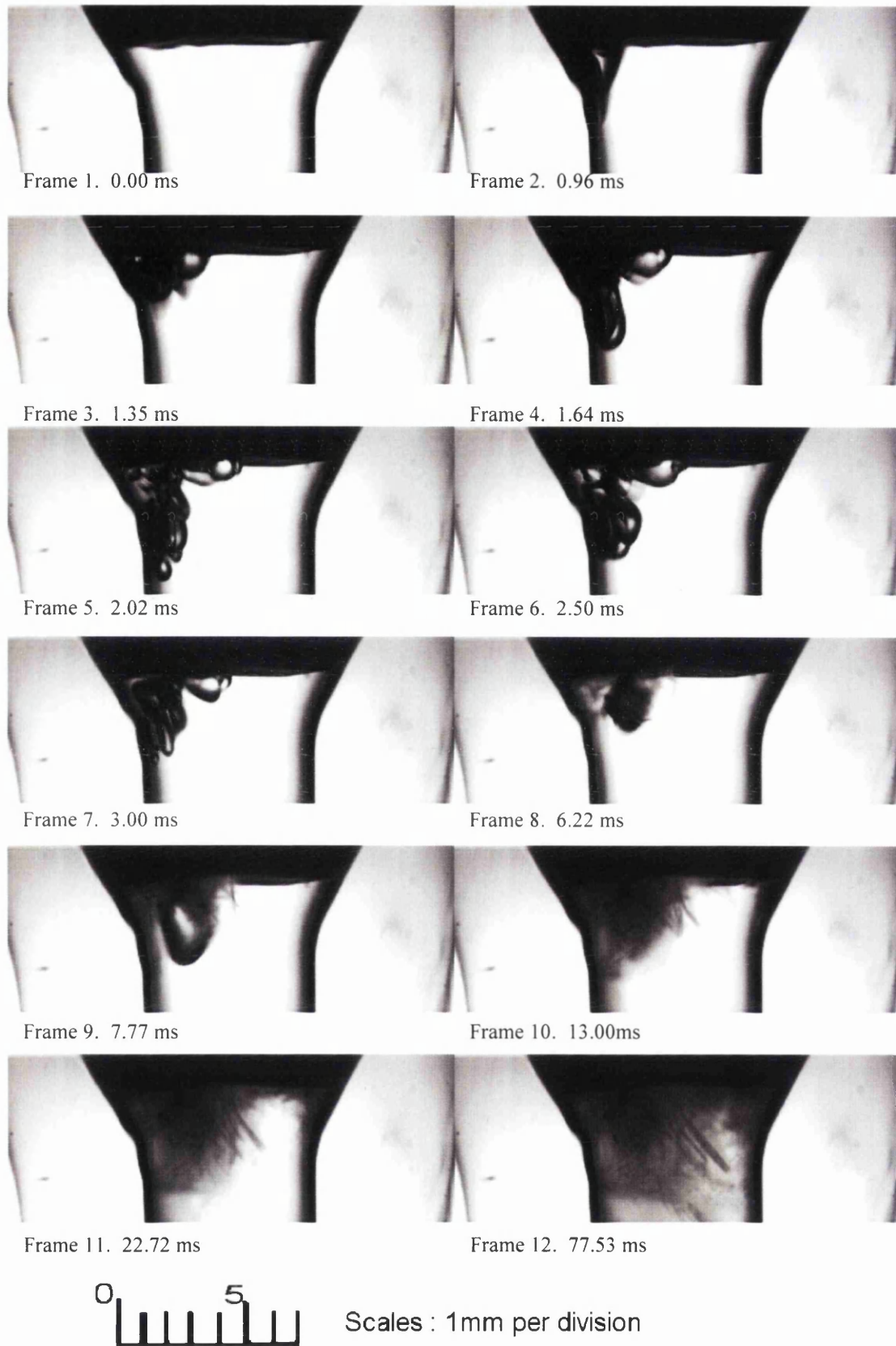


**Figure 6.16** Twelve frames captured during ice formation after cavitation event took place contained in an improved Berthelot tube. In frame 8-9, three phases which are liquid, solid and vapour states coexists together in the deionised, degassed and boiled water at  $-19.5\text{ }^{\circ}\text{C}$  and unknown pressure.

### 6.5.3 Results of Experiments Involving Ice Formation in the d-m Regime.

In this set of experiments the sealing temperature,  $T_0$  was set at 20 °C and the tube (and liquid) was subsequently heated following sealing to 27 °C for 10 minutes prior to cooling into the supercooled regime. The vertical axis of the Berthelot Tube is shown horizontally in figures 6.17 to 6.19 record events which accompanied these experiments during which the high-speed video system was operating at 500 frames per second (f.p.s). These high speed records were used to estimate the ice front's velocity of propagation. The data in figure 6.20 shows estimates of the ice front velocity,  $v$ , as a function of the degree of supercooling. It indicates that the velocity of the ice front depends on the degree of supercooling of the liquid water, the lower the freezing temperature, the higher the velocity of the ice's propagation. This trend is in accord with previous work on supercooled water (Hillig, 1958). However the velocities recorded in the present work (on d-m water) are substantially higher than those previously reported for supercooled water at comparable temperatures – by an order of magnitude, or more (the maximum velocity,  $8 \text{ cms}^{-1}$  was recorded in the present work at a temperature of -14 °C). The present experiments confirm the velocities reported for ice front propagation by Rogers (2004).

In Berthelot tube experiment, suspended impurities at the wall of the tube can trigger the appearance of a new phase (Debenedetti, 1996). The vertical axis of the Berthelot tube is shown horizontally in figure 6.21 and 6.22 proved that superheated ice also can produce from doubly metastable orange squash in the improved Berthelot tube at -12 °C. The high-speed video system was operating at 500 frames per second (f.p.s). The average velocity of the both cases of ice front was approximately  $3.00 \text{ cms}^{-1}$ . The ice nucleation started from the bottom of the tube (or at the wall of the tube) then subsequent filled up the remaining test liquid. It is believed that orange squash contained some small amount of precipitates which had sunk at the bottom of the tube or stuck at the wall of the tube. The suspended impurities provide a nucleation site for the system where the bubble or ice nucleation can easily grows. Whereas in the case of clean water, the cavitation bubble or ice nucleation always start at the 'weakest-link' of the system between the test liquid and PTFE valve.

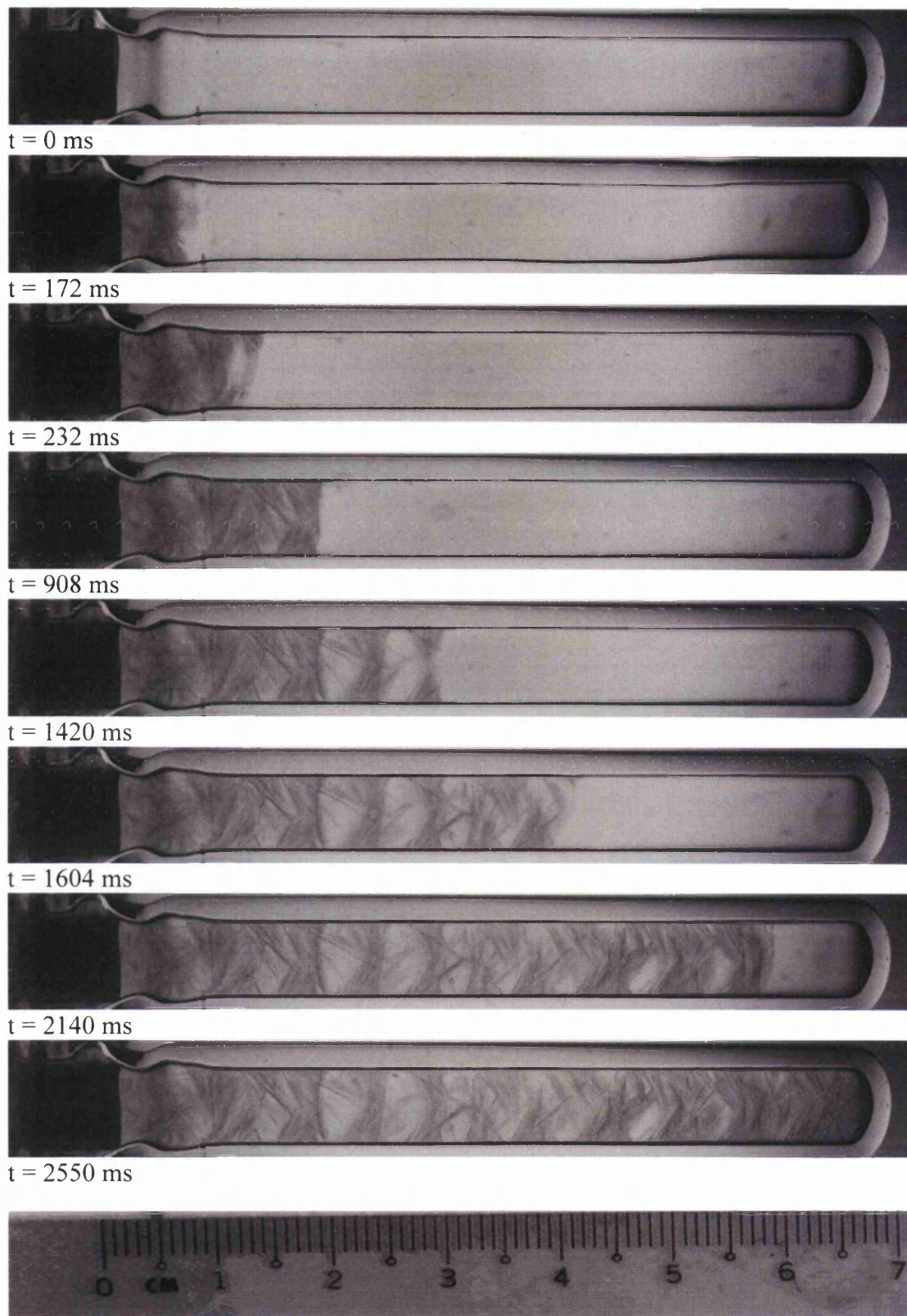


**Figure 6.17** Superheated ice produced from doubly metastable water in the improved Berthelot tube at  $-8.0\text{ }^{\circ}\text{C}$ . The high-speed video system was operating at 500 frames per second (f.p.s). The velocity of the ice front was  $2.78\text{ cm s}^{-1}$ .



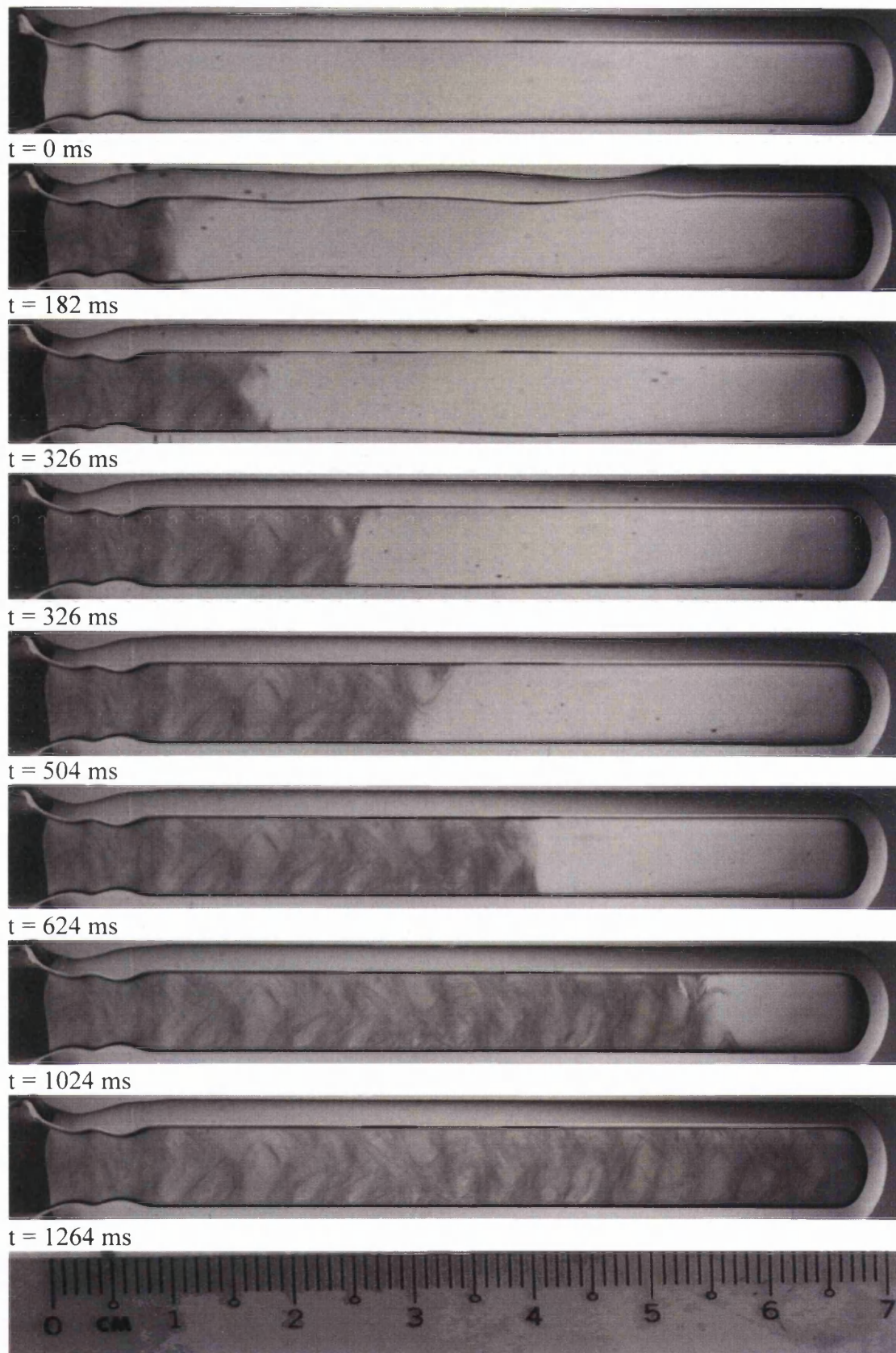


**Figure 6.18** Superheated ice produced from doubly metastable water in the improved Berthelot tube at  $-10\text{ }^{\circ}\text{C}$ . The high-speed video system was operating at 500 frames per second (f.p.s). The velocity of the ice front was  $5.62\text{ cm s}^{-1}$ .

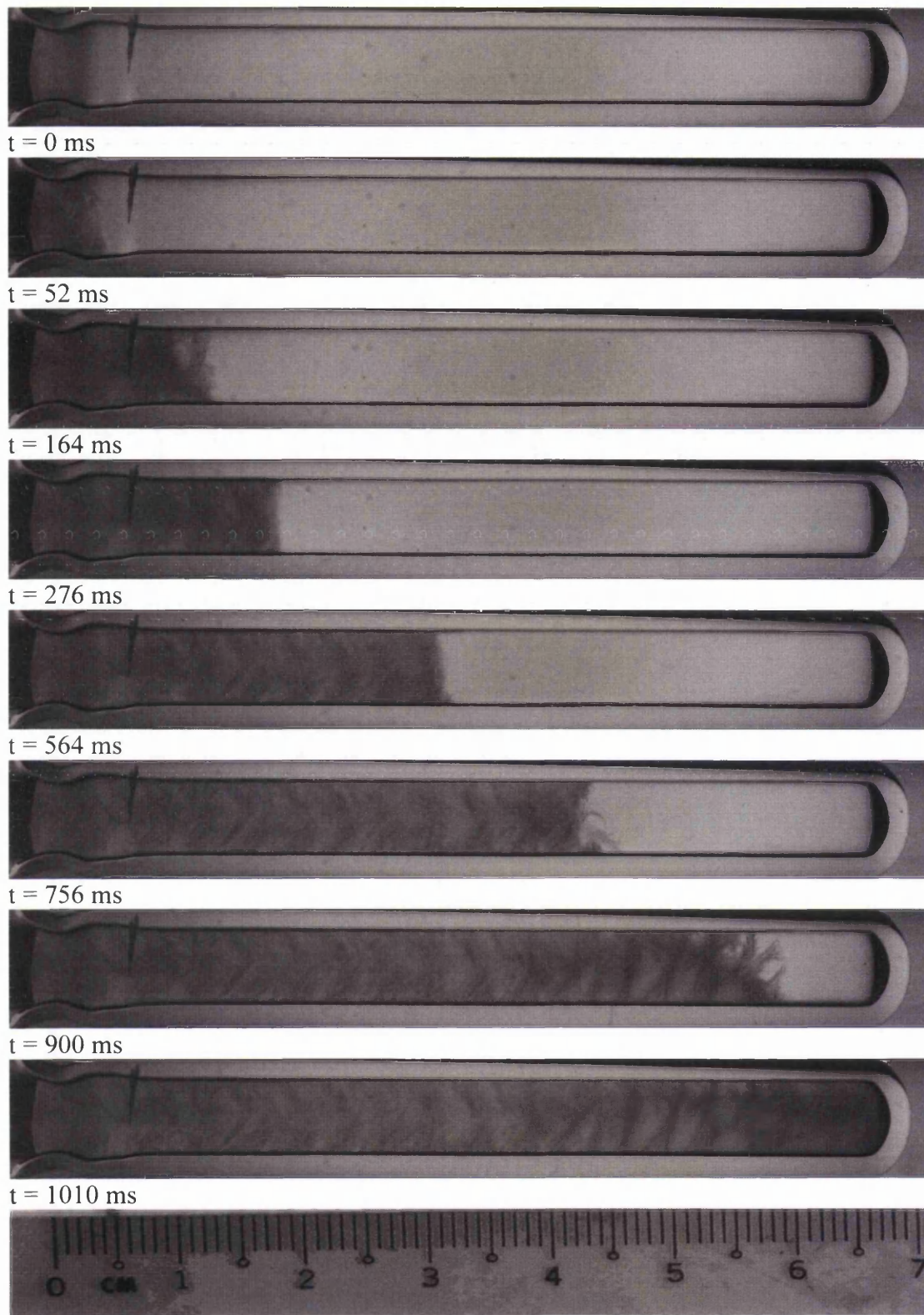


**Figure 6.19** Superheated ice produced from doubly metastable water in the improved Berthelot tube at  $-12$  °C. The high-speed video system was operating at 500 frames per second (f.p.s). The velocity of the ice front was  $7.03 \text{ cms}^{-1}$ .

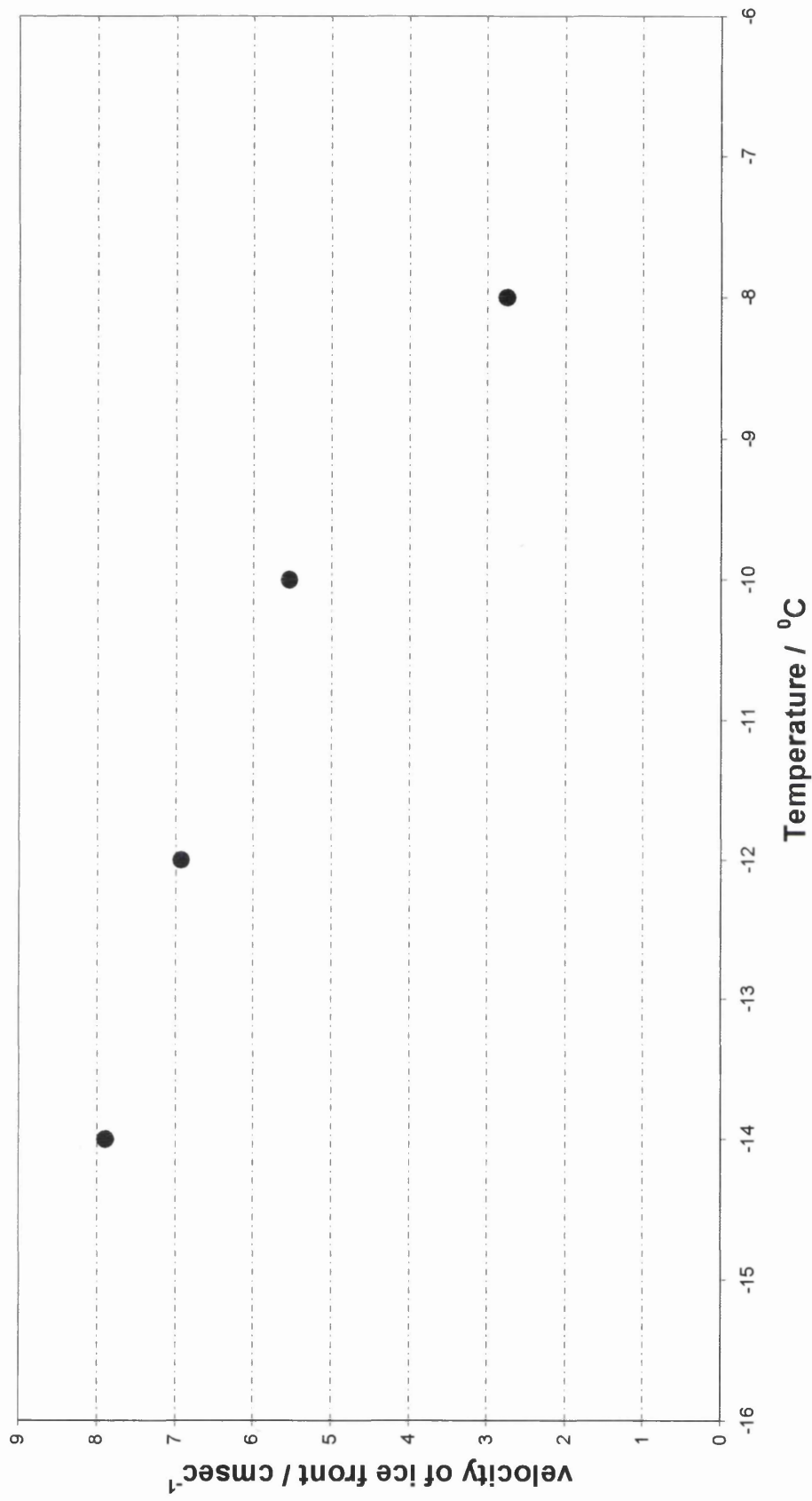
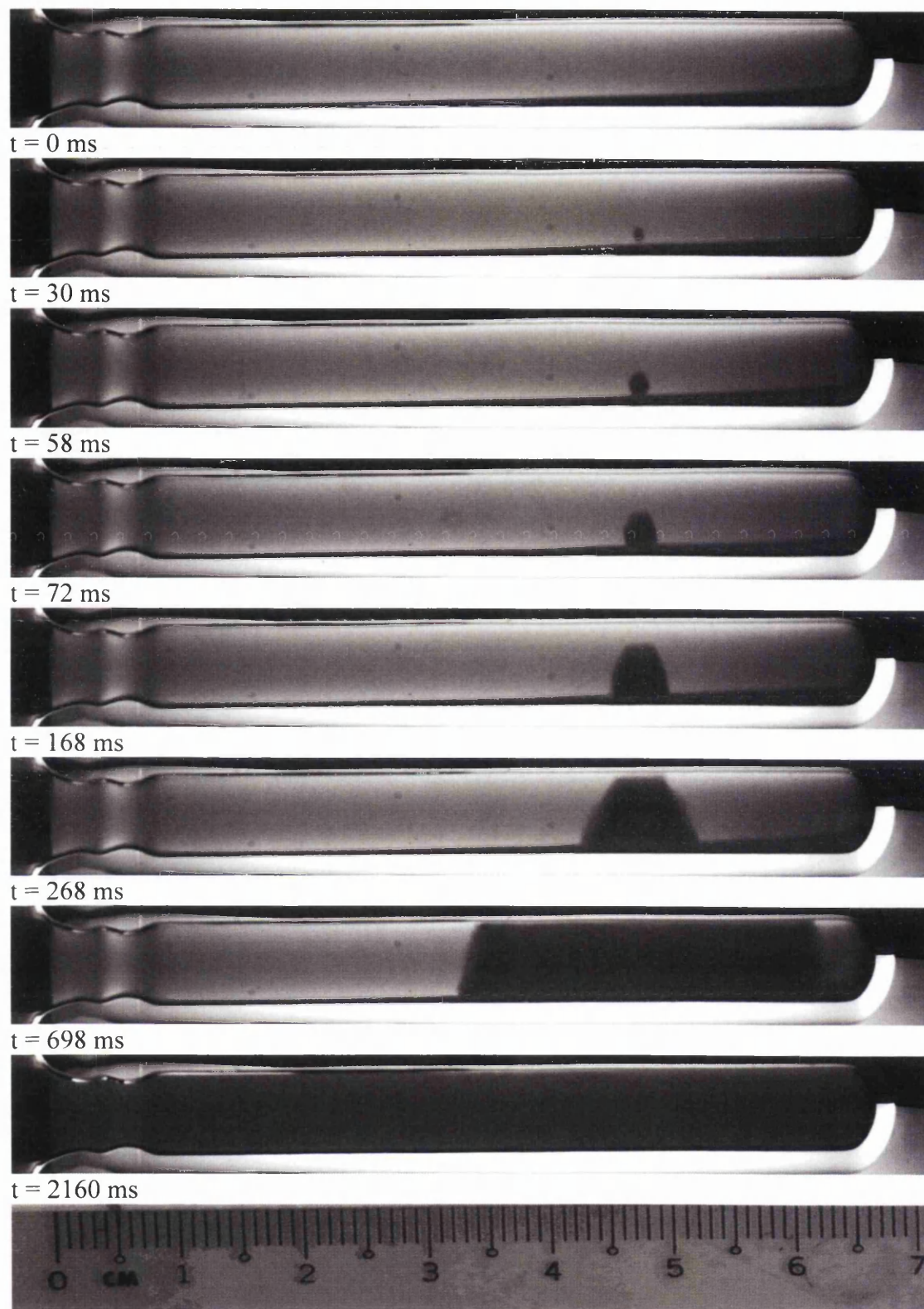


Figure 6.20 Experimental results for the ice front velocity,  $v$ , as a function of the degree of supercooling for the ice formation in the modified Berthelot tube.





**Figure 6.21** Superheated ices produced from doubly metastable orange squash in the improved Berthelot tube at  $-12$  °C. The high-speed video system was operating at 500 frames per second (f.p.s). The velocity of the ice formation is  $2.78 \text{ cm s}^{-1}$ .



**Figure 6.22** Superheated ices produced from doubly metastable orange squash in the improved Berthelot tube at  $-12\text{ }^{\circ}\text{C}$ . The high-speed video system was operating at 500 frames per second (f.p.s). The velocity of the ice formation is  $3.29\text{ cm s}^{-1}$ .



## 6.6 Conclusion

The results of these initial experiments are noteworthy as they indicate that the Berthelot tube technique may have wider utility in cavitation research than has previously been thought. The ability to generate and study the behaviour of a single approximately spherical bubble formed in the body of a liquid under tension is potentially valuable in enabling studies of cavitation bubble dynamics – a very substantial area of cavitation research. Previous use of the Berthelot tube has been largely confined to measurements of the cavitation threshold of liquids. The work reported here shows that its use may be usefully extended to the study of potential cavitation damage mechanisms.

In these (d-m) experiments, samples of degassed, deionised water supercooled down to  $-19.5\text{ }^{\circ}\text{C}$ : cavitation was produced and ice crystals were nucleated in the immediate vicinity of the bubble. It is believed that the water thus makes a sudden leap to the triple point, the unique combination of temperature and pressure where solid, liquid and vapour can coexist in equilibrium; this phenomenon was first observed by Hayward (1971) with unaided eye. However, the work reported in this Thesis is the first in which evidence is presented that the formation and growth of a cavitation bubble results in the nucleation of ice formation.

The results indicate that the velocity of the ice front depends on the degree of supercooling of the liquid water, the lower the freezing temperature, the higher the velocity of the ice's propagation. This trend is in accord with previous work on supercooled water (Hillig, 1958). However the velocities recorded in the present work (on d-m water) are substantially higher than those previously reported for supercooled water at comparable temperatures – by an order of magnitude, or more (the maximum velocity,  $8\text{ cm s}^{-1}$  was recorded in the present work at a temperature of  $-14\text{ }^{\circ}\text{C}$ ). The present experiments confirm the velocities reported for ice front propagation by Rogers (2004).

In conclusion, Berthelot tube experiment is possible to investigate the stretched water (water under tension) under supercooled condition over sufficiently long lifetimes. Photographic evidence shown that cavitation bubbles can be occurred not only in

metastable water but also in doubly metastable (simultaneously supercooled and superheated) water. The outcomes of the study reported in this chapter also suggest that it will be an interesting area to investigate and further explore the molecular structure of liquids under tension and also doubly metastable (simultaneously superheating and supercooled) conditions of quasi-static way in the improved Berthelot tube and provided the explanation of the unique structure of liquid water on molecular scale under such unique conditions, these experiments, by using neutron diffraction technique or synchrotron X ray technique or spectroscopic instrument such as NMR spectroscopic instrument. In addition, there is no structural information exists for ice formed from doubly metastable water, or any other doubly metastable liquids. It will be another interesting area to investigate the changes that occur on a molecular scale by these techniques.

# *Chapter 7*

## *Conclusion and Recommendation for Future Work*

This Thesis contains an account of work in which both quasi-static and dynamic stressing techniques were used to subject samples of liquid to tension (or ‘negative pressure’). For dynamic stressing, an improved form of the ‘Bullet-Piston’ apparatus described by Couzens and Trevena (1969, 1974) was employed, whereas for quasi-static stressing, a version of the Berthelot tube (Berthelot, 1850) combined with high speed video photography was used.

The work reported in Chapter 4 concerns the results of experiments in which samples of degassed, deionised water were subjected to dynamic stressing by pulses of tension in the B-P apparatus. The particular pulse reflection technique employed and referred to herein allows the rate of development of tension in the liquid (hereafter denoted  $\dot{\Omega}_r$ ) to be varied in a systematic manner, in order to investigate its influence on the resulting measurement of the liquid’s effective tensile strength (or ‘cavitation threshold’),  $F_c$ . Results are reported for experiments which involve a range of stressing rates,  $0.43 \text{ bar}\mu\text{s}^{-1} \leq \dot{\Omega}_r \leq 1.79 \text{ bar}\mu\text{s}^{-1}$ , for samples of degassed, deionised water at a constant temperature (25 °C).

These experiments, which are the first of their kind to be reported, show an approximately four-fold increase of  $F_c$  at the highest stressing rate in water, this value being 224 bar (for  $\dot{\Omega}_r = 1.79 \text{ bar}\mu\text{s}^{-1}$ ) compared to a value of 60 bar at a lower stress development rate ( $\dot{\Omega}_r = 0.432 \text{ bar}\mu\text{s}^{-1}$ ). These results provide additional insight into the reasons underlying the mechanism rather wide ranges of values of  $F_c$  which have been reported in the literature and provide evidence to substantiate the claim that the rate of dynamic stressing is an important consideration in understanding the cavitation properties of liquids.

The work reported in Chapter 5 investigates the effects of temperature, shear viscosity and the rate of stressing,  $\dot{\Omega}_r$ , on measured values of the ‘effective’ tensile strength (or ‘cavitation threshold’),  $F_c$ , of commercial monograde and multigrade oils under dynamic stressing by tension pulses (this being a feature of the conditions experienced by a motor lubricant within a ‘divergent section’ of dynamically loaded journal bearing). Two monograde oils (designated grade API CC), 10W and 40 Diesel, and

two multigrade oils (designated grade API CF), 10W40 and 15W40 were tested in this work.

Results are reported for B-P experiments involving a range of stressing rates, from  $0.6 \text{ bar}\mu\text{s}^{-1}$  to  $1.4 \text{ bar}\mu\text{s}^{-1}$  for these commercial oils over the temperature range  $25 \text{ }^\circ\text{C} \leq T \leq 110 \text{ }^\circ\text{C}$  which are representative of those encountered under their normal operating conditions. These experiments, which are the first of their kind to be reported, indicate that at any given temperature,  $F_c$  increases with increasing stressing rate ( $157 \text{ bar} < F_c < 220 \text{ bar}$  at  $25 \text{ }^\circ\text{C}$  and,  $130 \text{ bar} < F_c < 157 \text{ bar}$  at  $110 \text{ }^\circ\text{C}$  for the 10W oil;  $172 \text{ bar} < F_c < 223 \text{ bar}$  at  $25 \text{ }^\circ\text{C}$  and,  $146 \text{ bar} < F_c < 172 \text{ bar}$  at  $110 \text{ }^\circ\text{C}$  for 40 Diesel oil;  $175 \text{ bar} < F_c < 200 \text{ bar}$  at  $25 \text{ }^\circ\text{C}$  and  $152 \text{ bar} < F_c < 171 \text{ bar}$  at  $110 \text{ }^\circ\text{C}$  for 10W-40 Diesel oil;  $172 \text{ bar} < F_c < 212 \text{ bar}$  at  $25 \text{ }^\circ\text{C}$  and,  $156 \text{ bar} < F_c < 174 \text{ bar}$  at  $110 \text{ }^\circ\text{C}$  for the 15W-40 Diesel oil).

These results provide evidence to substantiate the claim (made by previous workers – Trevena, 1987) that the rate of dynamic stressing is an important consideration in understanding the cavitation properties of liquids. The experiments also indicate that in addition to shear viscosity and temperature, the stressing rate,  $\dot{\Omega}$ , may be an important consideration when evaluating a lubricant's cavitation performance.

Chapter 5 also reports complementary experiments to determine the effect of polyacrylamide, PAA additives on the effective tensile strength,  $F_c$  of deionised water. The results clearly indicate that the effective tensile strength of the polymer solution increases with increasing concentration  $C$  of the polymer (in the range  $0.10 \text{ wt}\% \leq C \leq 0.80 \text{ wt}\%$ ). These results show that the presence of the polymer additives leads to an increase in the liquid's tensile strength: the more polymer present in the deionised water the greater the increase in the tensile strength. This result accords with other published work in the field.

A significant aspect of this work is that, contrary to previously reported studies, results have been produced from a single technique, consisting of experiments conducted within the same apparatus in which the rate of stressing is deliberately varied in a systematic manner. The results of such a study have not previously been reported. The results clearly establish the importance of stressing rate in

considerations of the effective tensile strength of liquids under conditions where heterogeneous nucleation prevails, and in particular in assessing the cavitation performance of lubricants. The results obtained suggest that further experiments should now be conducted using this technique in order to study the effect of the presence of dissolved (permanent) gases in the cavitation of lubricants under dynamic stressing by pulses of tension.

The work reported in Chapters 4 and 5 of this Thesis demonstrated the ability of water and other liquids to sustain considerable negative pressure under conditions of dynamic stressing by pulses of tension. Whereas studies involving the subjection of liquids to dynamic stressing by pulses of tension are widely reported, and may have direct relevance to engineering applications (e.g. in ultrasound scanning), the behaviour of liquids under quasi-static tension over sustained periods has been less intensively studied. However, the ability to induce, manipulate and sustain tension in a liquid over a sustained period is a potentially valuable tool in extending studies of fundamental aspects of the liquid state. The work described in Chapter 6 involved the development and refinement of a technique (based on the Berthelot tube) in which water was subjected to progressively greater tensions over a very wide range of temperatures which extended into the supercooled regime.

Berthelot tube experiments involving high speed video photography at up to 24,000 frames per second recorded the initial formation and growth of a single, isolated, and apparently spherical cavitation bubble within a bulk sample of water. The cavitation event was seen to start with a single, approximately spherical cavity, growing not at (or from) the tube walls, but in the body of the liquid. The bubble collapse phase clearly showed the formation of a liquid jet directed at the solid surface adjacent to the bubble. Such a feature of cavitation bubble dynamics has never previously been reported in Berthelot tube work.

The results of these initial experiments are noteworthy as they indicate that the Berthelot tube technique may have wider utility in cavitation research than has previously been thought. The ability to generate and study the behaviour of a single approximately spherical bubble formed in the body of a liquid under tension is potentially valuable in enabling studies of cavitation bubble dynamics – a very

substantial area of cavitation research. Previous use of the Berthelot tube has been largely confined to measurements of the cavitation threshold of liquids. The work reported here shows that its use may be usefully extended to the study of potential cavitation damage mechanisms. The formation of liquid jets produced by cavitation bubbles has been the topic of much research, largely due to their implication in instances of surface erosion (cavitation damage). The extent to which the liquid jet phenomenon is responsible for cavitation damage is the subject of ongoing debate and the work reported herein suggests that further studies of jets formed by cavitation bubble dynamics in Berthelot tube experiments could be a valuable source of information in future work based on this new adaptation of the technique.

Also reported is work in which quasi-static stressing was extended into the supercooled regime for water to produce doubly-metastable (d-m) liquid (i.e. water which is simultaneously superheated by tension and thermally supercooled). The high-speed video system, operating at 500 frames per second, was used to estimate the ice front's velocity of propagation following the initiation of nucleation (both ice formation and cavitation). The data provides estimates of the ice front velocity,  $v$ , as a function of the degree of supercooling and indicates that the velocity of the ice front depends on the degree of supercooling of the liquid water, the lower the freezing temperature, the higher the velocity of the ice's propagation. This trend is in accord with previous work on supercooled water (Hillig, 1958). However the velocities recorded in the present work (on d-m water) are substantially higher than those previously reported for supercooled water at comparable temperatures – by an order of magnitude, or more (the maximum velocity,  $8 \text{ cm s}^{-1}$  was recorded in the present work at a temperature of  $-14 \text{ }^\circ\text{C}$ ). The present experiments confirm the velocities reported for ice front propagation by Rogers (2004). The work reported in this Thesis is the first in which evidence is presented that the formation and growth of a cavitation bubble results in the nucleation of ice formation. Further Berthelot tube work allied to high speed photography is now required to confirm the mechanism of propagation of the ice front by the cavitation bubble growth mechanism explained in Chapter 6. Neutron scattering experiments could be used to investigate the structure of the ice formed by such a mechanism.

# *References*



## References

---

Als-Nielsen, J. (1985). "The liquid vapour interface." Z. Phys. B-Condensed Matter **61**: 411-414.

Alvarenga, A. D., M. Grimsditch and R. J. Bodnar (1993). "Elastic properties of water under negative pressures." J. Chem. Phys **98** (11): 8392-8396.

Apfel, R. E. (1970). "The role of impurities in cavitation threshold in cavitation threshold determination", J. Acoustic Soc. Am., **48**, 1179-1186.

Apfel, R. E. (1971). "A novel technique for measuring the strength of liquids", J. Acoustic Soc. Am., **49**, 145-155.

Apfel, R. E. (1972). "Tensile strength of liquids." Scientific American **227**: 58.

Apfel, R. E. (1972). "Water superheated to 279.5°C at atmospheric pressure." Nature Phys. Sci., **238**, 63-64.

Apfel, R. E. (1981). "Acoustic cavitation Ultrasonics ed P D Edmonds." (New York: Academic) chapter 7.

Barrow, M. S., W. R. Bowen, N. Hilal, A. Al-Hussany, P. R. Williams, R. L. Williams and C. J. Wright (2003). "A study of the tensile properties of liquids in confined spaces using an atomic force microscope." Proc. Royal Society (London) A **459**: 2885-2908.

Barrow, M. S., S. W. J. Brown, S. Cordy, P. R. Williams and R. L. Williams (2004). "Rheology of Dilute Polymer Solutions and Engine Lubricants in High Deformation Rate Extensional Flows Produced by Bubble Collapse." ASME **126**: 162-169.

Barrow, M. S., S. W. J. Brown and P. R. Williams (2004). "Extensional flow of liquid jets formed by bubble collapse in oils under cavitation-generated pressure waves." Experiments in Fluids **36**: 463-472.

Benjamin, T. B. and A. T. Ellis (1966). "The collapse of cavitation bubbles and the pressures thereby produced against solid boundaries." Phil. Trans. R. Soc **260**: 221-240.

Berker, A., M. G. Bouldin, S. J. Kleis and W. E. VanArsdale (1995). "Effect of polymer on flow in journal bearings." Journal of Non-Newtonian fluid mechanics **56**: 333-347.

Berlin, H. M. (1977). Design of active filters with experiments.

Berthelot, M. (1850). Ann. Chim. Phys. (3) **30**: 232-7.

Binding, D. M., M. A. Couch and K. Walters (1999). "The rheology of multigrade oils at elevated pressures." J. Non-Newtonian Fluid Mech. **87**: 155-164.

Blake, J. R., and Gibson, D. C., (1981) "Growth and collapse of a vapour cavity near a free surface", J. Fluid Mech., **111**, 123-140.

## References

---

Bolz R. and Tuve G. (ed) (1973) CRC Handbook of tables of Applied Engineering Science 2<sup>nd</sup> edn (Boca Raton, FL: CRC press)

Boteler, J. M. and G. T. Sutherland (2004). "Tensile failure of water due to shock wave interactions". J. Appl. Phys. **96**: 6919.

Braun, M. J. and R. C. Hendricks (1982). "Experimental investigation of the vapour / gaseous cavity characteristics of an eccentric journal bearing." NASA Technical Memorandum 82996, Joint Lubrication conference corresponded by the American Society of Mechanical Engineers and the American Society of lubrication Engineers.

Brennen, C. E. (1995). "Cavitation and bubble dynamics ". Oxford University Press.

Briggs, L. J. (1950). "Limiting negative pressure of water." J. Appl. Phys. **21**: 721-722.

Briggs, L. J. (1953). "The limiting negative pressure of mercury in Pyrex glass." J. Appl. Phys. **24**: 488-490.

Brindley, J., L. Elliott and J. T. MacKay (1983). "The role of cavitation in whirl instability in a rotor bearing." ASME J. Appl. Mech. **50**: 877-890.

Brown, S. W. J. (1999). Cavitation phenomena in liquids subjected to tension by dynamic stressing. Department of Chemical and Biological Process Engineering. Swansea, University of Wales Swansea.

Brown, S. W. J. and P. R. Williams (2000). "The tensile behaviour of elastic liquids under dynamic stressing." Journal of Non-Newtonian Fluid Mechanics. **90**: 1-11

Bull, T. H. (1956). "The tensile strength of viscous liquids under dynamic loading." British Journal of Applied Physics **7**: 416-418.

Carlson, G. A. (1975). "Dynamic tensile strength of mercury." J. Appl Phys. **46**: 4069-4070.

Carlson, G. A. and K. E. Henry (1973). "Technique for studying dynamic tensile failure in liquids: application to glycerol." J. Appl Phys. **44**: 2201-2206.

Carlson, G. A. and H. S. Levine (1975). "Dynamic tensile strength of glycerol." J. Appl. Phys. **46**: 1594-1600.

Caupin F. and Eric Herbert (2006). "Cavitation in water." C. R. Physique **7**: 1000-1017

Chahine, G. L. and A. G. Bovis (1980). "Oscillations and collapse of a cavitation bubble in the vicinity of a two-fluid interface." Cavitation and inhomogeneities in underwater acoustic, ed. W. Launterborn. Berlin : Springer-Verlag. 319 pp.

## References

---

- Chapman, P. J., B.E. Richards and D.H. Trevena (1975). "Monitoring the growth of tension in a liquid contained in a Berthelot tube." J. Phys. E. **8**: 731.
- Chestermann, W. D. (1952). "The dynamics of small transient cavities." Proc. Phys. Soc **65**: 846-858.
- Chow, R., R. Mettin, B. Lindinger, T. Kurz and W. Lauterborn (2003). "The importance of acoustic cavitation in the sonocrystallisation of ice-high speed observation of a single acoustic bubble." Ultrasonics, 2003 IEEE Symposium on **2**: 1447-1450.
- Chow, R., R. Blindt, R. Chivers and M. Povey (2004). "A study on the primary and secondary nucleation of ice by power ultrasound." Ultrasonics **43**(4): 227-230.
- Chow, R., Renoo Blindt, Arnold Kamp, Peter Grocutt, Robert Chivers (2004). "The microscopic visualisation of the sonocrystallisation of ice using a novel ultrasonic cold stage." Ultrasonics Sonochemistry **11**: 245-250.
- Cleverland, R. and L. Crum (1997). "Bubbles generate unexpected stresses." Physics world.
- Cochard Herve, Tete Barigah, Eric Herbert and Frederic Caupin (2006). "Cavitation in plants at low temperature: is sap transport limited by the tensile strength of water as expected from Briggs' Z-tube experiment?" New Phytologist **173**(3): 571-575
- Couzen, D. C. F. and D. H. Trevena (1969). "Critical tension in a liquid under dynamic conditions of stressing." Nature **222**: 473-474.
- Couzen, D. C. F. and D. H. Trevena (1974). "Tensile failure of liquids under dynamic stressing." J. Phys. D : Appl. Phys. **7**: 2277-2287.
- Crum, L. A. and J. B. Fowlkes (1986). "Acoustic cavitation generated by microsecond pulses of ultrasound." Nature **319**: 52-54.
- Davies, R. M., D. H. Trevena, N. J. M. Rees and G. M. Lewis (1956). "The tensile strength of liquids under dynamic stressing." Proceedings of the National Physical Laboratory Symposium
- Debenedetti, P. G. (1996). Metastable Liquids : Concepts and Principles.
- Dixon, H. H. and J. Joly (1895). Phil. Trans. R. Soc **186**: 563-576.
- Dowson, D., M. Godet and C. M. Taylor (1975). Cavitation and related phenomena in lubrication : proceedings of the firsts - Lyon symposium on tribology.
- Dowson, D. and C. M. Taylor (1979). "Cavitation in bearings." Annual reviews. Fluid mech. **11**: 35-66.

## References

---

Dugdale I. and Wall R. (1965) "Cavitation corrosion and its prevention in diesel engines" Symposium, 10 November 1965, organised by British Rail Chemical Research division and held at Alexandra Palace, London.

Evans, A. and D. N. Walder (1969). "Significance of gas micronuclei in the aetiology of decompression sickness." Nature **222**(5190): 251-2.

Evans, A. (1979) J. Phys. E: Sci. Instrum. **12**: 276-81.

Fisher, J. C. (1948). "The fracture of liquids." J. Appl Phys. **19**: 1062-1067.

Fox, F. E. and K. F. Herzfeld (1954). "Gas Bubbles with organic skin as cavitation nuclei." The journal of the acoustical society of America **26**(6): 984-989.

French, A. P. (1971). Vibrations and waves, Chapman and Hall.

Frenkel, J. (1955). "Kinetic Theory of Liquids." Dover Publication : New York.

Fujikawa, S. and T. Akamatsu (1978). "Experimental investigations of cavitation bubble collapse by a water shock tube." Japanese Soc. Mech, Eng **21**: 223-230.

Fujikawa, S., and Akamatsu T. (1980) "Effects of the non-equilibrium condensation of vapour on the pressure wave produced by the collapse of a bubble in a liquid", J. Fluid Mech., **97**, 481-512.

Galloway, W. J. (1954). "An experimental study of acoustically induced cavitation in liquids." J. Acoustical Society of America **26**: 849-857.

Gibson, D. C. and J. R. Blake (1982). "The growth and collapse of bubbles near deformable surfaces." Applied Scientific Research **38**: 215-224.

G. M. Lewis (1961) "The tensile strength of liquids in the Berthelot tubes" Proc. Phys. Soc. **78** 133-144

Green, N. W. and R. B. Mesler (1970). "An experimental study of transient pressure accompanying vapour bubble collapse in water." ASME, United Engineering Centre, 345 East 47th street, New York, N.Y.100.

Green, N. W. and R. B. Mesler (1970). "An experimental study of transient pressure accompanying vapour bubble collapse in water." Proc. ASME Conf. (Detroit)1970 (New York: ASME), 1-8.

Greenspan, F. R. and C. E. Tschiegg (1967). "Radiation-induced acoustic cavitation apparatus and some results." J. Res. Nat. Bur. Stand. Sect. C71: 299-312.

Gupta, R. K. and R. C. Chan (1990). "Flow of multigrade motor oils in an extensional flow field." J. Rheology **34** (8): 1373-1380.

## References

---

Gwynllyw, D. R., A. R. Davies and T. N. Phillips (1996). "On the effect of a piezoviscous lubricant on the dynamics of a journal bearing." Journal of Rheology **40**: 1239-1266.

Harvey, E. N. (1944). "Bubble formation in animals." Part 1 and 2., J Cellular Comp. Physiol **24**: 23-24.

Hayward, A. T. J. (1967). "Tribonucleation of bubbles." J. Appl. Phys. **18**: 641-644

Hayward, A. T. J. (1970). "The role of stabilised gas nuclei in hydrodynamic cavitation inception." J. Phys. D: Appl Phys. **3**: 574-579.

Hayward, A. T. J. (1971). "Negative pressures in liquids: can it be harnesses to serve man?" American Science **59**: 434-443.

Henderson, S. J. and R. J. Speedy (1980). "A Berthelot-Bourdon tube method for studying water under tension." J. Phys. E: Sci. Instrum. **13** (Printed in Great Britain).

Hentschel, W. and W. Lauterborn (1982). "Acoustic emission of single laser-produced cavitation bubbles and their dynamics." Applied Scientific Research **38**: 225-230.

Herbert, E. and F. Caupin (2005). "The limit of metastability of water under tension: theories and experiments." JOURNAL OF PHYSICS-CONDENSED MATTER **17**: S3597-S3602.

Heyes, D. M (2008). "Liquid at positive and negative pressure." J. Phys., stat. sol. (b) **245**, No 3, 530-538.

Hickling, R. (1965). "Nucleation of freezing by cavities collapse and its relation to cavitation damage." Nature **206**: 915-917.

Hickling, R. (1967). "Nucleation of freezing by cavitation in supercooled liquids." Nature **214**: 379.

Hickling, R. (1994). "Transient, high pressure solidification associated with cavitation in water." Physical review letters **73**.

Hickling, R. and M. S. Plesset (1964). "Collapse and rebound of a spherical bubble in water." Phys. Fluids **7**: 7-14.

Hillig, W. B. (1958). "The kinetics of freezing of ice in the direction perpendicular to the basal plane." Growth and Perfection of Crystals, R. H. Doremus, B. W. Roberts, and D. Turnbull, Eds., John Wiley and Sons, 350-360.

Hunt, J. D. and K. A. Jackson (1966). "Nucleation of the solid phase by cavitation in an undercooled liquid which expands on freezing." Nature **211**: 1080-1081.

## References

---

Inada Takaaki, Xu Zhang, Akira Yabe and Yoshiyuki Kozawa (2001). "Active control of phase change from supercooled water to ice by ultrasonic vibration 1. Control of freezing temperature", International journal heat mass transfer., **44**: 4523-4531.

Iyengar, K. S. and E. G. Richardson (1958). "Measurements on the air-nuclei in natural water which give rise to cavitation." J. Appl. Phys. **9**: 154-158.

Jones, W. M. and D. H. Trevena (1980). "A thermomechanical study of a water-steel Berthelot tube system." J. Phys. D: Appl Phys. **13**: 1871-8.

Jones, W. M., G. D. N. Overton and D. H. Trevena (1981). "Tensile strength experiments with water using a new type of Berthelot tube." J. Phys. D : Appl. Phys. **14**: 1283-91.

Kezios, P. S. and W. R. Schowalter (1986). "Rapid growth and collapse of single bubbles in polymer solutions undergoing shear." J. Phys. Fluids **29**: 3172-3181.

Knapp, R. T., A. Hollander, Pasadena and Calif (1948). "Laboratory investigations of the mechanism of cavitation." ASME.

Kornfeld, M. and L. H. Suvarov (1944). "On the destructive action of cavitation." J. Appl. Phys. **15**: 495-506.

Kuper, C. G. and D. H. Trevena (1951). "The effect of dissolved gases on the tensile strength of liquids." Proc. Royal Society (London) A **65**: 46-54.

Launterborn, W. (1972). "Laser-induced Cavitation." The journal of the acoustical society of America **52**: 151.

Lauterborn, W. and H. Bolle (1975). "Experimental investigations of cavitation-bubble collapse in the neighbourhood of a solid boundary." Journal of Fluid Mechanics **72**: 391-399.

Launterborn, W. and C.-D. Ohi (1997). "Cavitation bubble dynamics." Ultrasonics Sonochemistry **4**: 65-75.

Lewis, G.M. (1961). "The tensile strength of liquids in Berthelot tubes." Proc. Phys. Soc. **78** 133-144

Li, X. K., D. R. Gwynllyw, A. R. Davies and T. N. Phillips (2000). "On the influence of lubricant properties on the dynamics of two-dimensional journal bearings." J. Non-Newtonian Fluid Mech. **93**: 29-59.

Lush P. A. (1983). "Impact of a liquid mass on a perfectly plastic solid." Journal of Fluid Mechanics. **135** 373-387.

Marston, P. L. and B. T. Unger (1986). "Rapid cavitation induced by the reflection of shock waves." Journal of Acoustic Society of America. **72**: Issue 1 pp. S40-S40.

## References

---

Meyer J. (1911). "Negative pressures in liquids (in German)." Abh. D. Bunsen-Ges. 6: 1-53.

Nakagawa, Kyuya *et al* (2006). "Influence of controlled nucleation by ultrasounds on ice morphology of frozen formulations for pharmaceutical proteins freezing-drying." Chemical Engineering and Processing. 45, 783-791

Naude, C. F. and A. T. Ellis (1961). "On the mechanism of cavitation damage by nonhemispherical cavities collapsing in contact with a solid boundary." Trans. ASME, J. Basic. Engng. D83: 648.

Overton, G. D. N. and D. H. Trevena (1980). "Cavitation experiments with water in a steel Berthelot tube." J. Phys. D: Appl. Phys 13: 1309-1314.

Overton, G. D. N. and D. H. Trevena (1981). "Cavitation phenomena and the occurrence of pressure tension cycles under dynamic stressing." J. Phys. D : Appl. Phys. 14: 241-250.

Overton, G. D. N. and D. H. Trevena (1982). "Some factors which influence the observed dynamic breaking tensions of a liquid." J. Phys. D : Appl. Phys. 15: L3-L6.

Overton, G. D. N., M. J. Edwards and D. H. Trevena (1982). "Dissolved gas content and the static breaking tension of water." J. Phys. D : Appl. Phys. 15: L129-131.

Overton, G. D. N., P. R. Williams and D. H. Trevena (1984). "The influence of cavitation history and entrained gas on liquid tensile strength." J. Phys. D : Appl. Phys. 17: 979-987.

Parsons, S. C. (1895). Newcomen Society.

Plesset, M. S. (1949). "The dynamics of cavitation bubbles." J. Fluid Mech. 16: 277-282

Plesset, M. S. and R. B. Chapman (1971). "Collapse of an initially spherical vapour cavity in the neighbourhood of solid boundary." J. Fluid Mech 47: 283-290.

Plesset, M. S. and A. Prosperetti (1977). "Bubble Dynamics and Cavitation." Annual Reviews. Fluid Mech 9: 145-85.

Pockman William T, John S. Sperry & James W. O'Leary (1995) "Sustained and significant negative water pressure in xylem" Nature 378, 715 – 716

Rayleigh, Lord (1917). "Dynamics of revolving fluids." American meteorological society 45(8): 413-414.

Rayleigh, Lord (1917). "On the pressure developed in a liquid during the collapse of a spherical void. Phil. Mag. 34, 94.

Reynolds, O. (1886). "On the theory of lubrication and its application." The Royal Society of London 177: 157-234.

## References

---

Reynolds, O. (1894). "Experiments showing the boiling of water in an open tube at ordinary temperature." *British Assoc. Adv. Sci. Report* 564. (See also *Science Papers* 2, p. 578, 1901.)

Reynolds, O. (1895). "On the dynamical theory of incompressible viscous fluids and the determination of the criterion." *Royal society*.

Richards, B. E., D. H. Trevena and D. H. Edwards (1980). "Cavitation experiments using a water shock tube." *J. Phys. D : Appl. Phys.* 13: 1315-1323.

Richards, B. E. and D. H. Trevena (1976) "The measurement of positive and negative pressures in a liquid contained in a Berthelot tube" *J. Phys. D : Appl. Phys.* 9: L123-126.

Roedder, E. (1967). "Metastable superheated ice in liquid-water inclusions under high negative pressure." *Science* 155: 1413-1417.

Rogers, D. (2004). An examination of bubble dynamics and double metastability within a glass Berthelot tube. Department of chemical and biological process engineering. Swansea, University of Wales Swansea, PhD Thesis

Rogers, D., P. R. Williams, R. L. Williams, P. M. Williams, M. S. Barrow and A. Al-Hussany (2004). "Cavitation and the development of static and dynamic tensions in doubly metastable liquids." *Computational methods in multiphase flow* 2 37: 407-414.

Rosenschein, U. and T. Rassin (1998). "Ultrasound Thrombolysis." *Science and Medicine* 5: 36-43.

Sawicki, J. T. and T.V.V.L.N. Rao (2004). "Cavitation effects on the stability of a submerged journal bearing." *International journal of rotating machinery* 10 (3): 227-232.

Sedgewick, S. A. and D. H. Trevena (1976). "limiting negative pressure of water under dynamic stressing." *J. Phys. D : Appl. Phys.* 9: 1983-1990.

Sedgewick, S. A. and D. H. Trevena (1978). "Breaking tension of dilute polyacrylamide solutions." *J. Phys. D: Appl Phys.* 11: 2517-2526.

Shima, A., K. Takayama, Y. Tomita and N. Ohsawa (1983). "Mechanism of the impact pressure generation from sparked generation-bubble collapse near a wall." *AIAA Journal* 21: 55-59.

Shima, A., T. Tsujino, H. Nanjo and N. Miura (1985). "Cavitation damage in polymer aqueous solutions." *ASME* 107: 134-138.

Smith, A. M. (1991). "Negative pressure generated by octopus suckers: A study of tensile strength of water in nature" *Journal of Experimental Biology* 157: 257-271.

Speedy, R. J. (1982). "Stability-Limit Conjecture. An interpretation of the properties of water." *J. Phys. Chem* 86: 982-991.



## References

---

Strube, H. W. and W. Launterborn (1970). "Investigation by the centrifuge method of cavitation nuclei at the interface between glass and water." Z. Angew. Phys. **29**: 349-357.

Taborek, P. (1985). "Nucleation in emulsified supercooled water." Phys. Rev. B **32(9)**: 5902-5906.

Taylor, C. M. (1974). "Separation cavitation in lightly loaded fluid film bearings with both surfaces in motion." Journal mechanical engineering science **16**: 147-155.

Temperley, H. N. V. (1947). "The behaviour of water under hydrostatic tension 3." Proc. Phys. Soc **59**: 199-208.

Temperley, H. N. V. and Chamber (1946). "The behaviour of water under hydrostatic tension 1." Proc. Phys. Soc. **58**: 420-436.

Temperley, H. N. V. and D. H. Trevena (1977). "The metastability of phase transitions and the tensile strength of liquids." Proc. Royal Society. A **357**: 395-402.

Temperley, H. N. V. and D. H. Trevena (1978). *Liquids and their properties - a molecular and macroscopic treatise with applications*, Ellis Horwood Limited.

Temperley, H. N. V. and D. H. Trevena (1979). "Metastable effects associated with the reflection of a pressure pulse at the free surface of water." J. Phys. D : Appl. Phys. **12**: 1887-1894.

Temperley, H. N. V. and D. H. Trevena (1987). "Why is the tensile strength of water measured dynamically less than that measured statically?" J. Phys. D : Appl. Phys. **20**: 1080-1081.

Temperley, H. N. V. and D. H. Trevena (1993). "Metastability of the liquid-vapour transition and related effects." Journal of Statistical Physics **77**: 501-508.

Thomycroft, S. and S. W. Barnaby (1895). "Torpedo-Boat destroyers." *Proced. Inst. Civil Engrs.*

Tomita, Y. and A. Shima (1984). "Collapse of multiple gas bubbles by a shock wave and induced impulsive pressure." J. Phys. D: Appl. Phys. **56**: 125-131.

Tomita, Y. and A. Shima (1986). "Mechanisms of impulsive pressure generation and damage pit formation by bubble collapse." J. Fluid Mech **169**: 535-564.

Trevena, D. H. (1975). "The Liquid Phase." Wykeham Publications (London) Ltd

Trevena, D. H. (1980). "The pioneer work of Francois Donny on the existence of tension in liquids." Annual of Science **37**: 379-386.

## References

---

- Trevena, D. H. (1982). "Time effects in cavitation experiments." J. Phys. D: Appl. Phys. **15**: L111-114.
- Trevena, D. H. (1984). "Cavitation and the generation of tension in liquids." J. Phys. D: Appl. Phys. **17**: 2139-2164
- Trevena, D. H. (1987). "Cavitation and Tension in liquids" (Bristol: Adam Hilger) West, R.C., and Selby, S.M., (1967) Handbook of Chemistry and Physics (Cleveland, OH: CRC), E-37 48.
- Tyree, Melvin T. (1997). "The Cohesion-Tension theory of sap ascent." Journal of Experimental Botany **48**: 1753-1765.
- Unsworth, A., D. Dowson and Wright. V (1971). "Cracking joints – Bioengineering study of cavitation in metacarpophalangeal joint." Annals of the Rheumatic diseases **30**: 348-358.
- Vincent, R. S. and G. H. Simmonds (1943). "The examination of the Berthelot method of measuring tension in liquids". Proc. Phys. Soc **55** 376-382.
- Willard, G. W. (1953). "Ultrasonically induced Cavitation in water: A step-by-step Process." J. Acoustical Society of America **25**: 669-686.
- William M. Kier and Andrew M. Smith "The structure and adhesion mechanism of octopus suckers" Integr. Comp. Biology **42**: 1146-1153 (2002).
- Williams, P. M. (1999). The formation and activity of bubbles during cavitation produced by dynamic stressing. Department of Chemical and Biological Process Engineering. Swansea, University of Wales Swansea. PhD Thesis
- Williams, P. R., G. D. N. Overton, W. M. Jones and D. H. Trevena (1982). "Prior stressing and cavitation inception." proc. Forum Cavitation and Polyphase Flow (New York) Paper 2.
- Williams, P. R. and P. M. Williams (1996). "Pressure-tension cycles induced by dynamic stressing and cavitation in liquids." J. Phys. D : Appl. Phys. **29**: 1904-1909.
- Williams, P. R., P. M. Williams and S. W. J. Brown (1997). "Pressure waves arising from the oscillation of cavitation bubbles under dynamic stressing." J. Phys. D : Appl. Phys. **30**: 1197-1206.
- Williams, P. R., P. M. Williams and S. W. J. Brown (1998). "Cavitation phenomena in water involving the reflection ultrasound pulses from a free surface, or from flexible membranes." J. Phys. Med. Biol. **43**: 3101-3111.

## References

---

Williams, P. R., P. M. Williams and S. W. J. Brown (1998). "A study of liquid jets formed by bubble collapse under shock waves in elastic and Newtonian liquids." J. Non-Newtonian Fluid Mech. **76**: 307-325.

Williams, P. R., P. M. Williams and S. W. J. Brown (1998). "Tensile properties of liquid mercury under pulsed dynamic stressing." J. Phys. D : Appl. Phys. **31**: 1923-1926.

Williams, P. R., P. M. Williams, S. W. J. Brown and H. N. V. Temperley (1999). "On the tensile strength of water under pulsed dynamic stressing." Proc. R. Soc. Lond. A. **455**: 3311-3323.

Williams, P. R. and R. L. Williams (2000). "On anomalously low values of the tensile strength of water." The Royal Society **456**: 1321-1332.

Williams, P. R. and R. L. Williams (2002). "Cavitation of liquids under dynamics stressing by pulses of tension." J. Phys. D : Appl. Phys. **35**: 2222-2230.

Williams, P. R. and R. L. Williams (2003). "Measurements of the cavitation threshold of multigrade engine oils under dynamic stressing by pulses of negative pressure." International Journal of Engine Research. **4**: 269-282.

Williams, P. R. and R. L. Williams (2004). "Cavitation and the tensile strength of liquids under dynamic stressing." Molecular physics **102**: 2091-2102.

Williams, P. R. and R. L. Williams (2004). "Cavitation of multigrade oils under dynamic stressing at elevated temperatures." Computational methods in multiphase flow **2** **37**: 415-427.

Williams, P. R. and R. L. Williams (2005). "Cavitation properties of oils under dynamic stressing by tension." ASME **127**(282-289).

Williams, P. R., M. Barrow, H. H. Chan, J.C. Dore and M. C. Bellissent-Funel (2009). "Cavitation nucleation in 'doubly metastable' water: a neutron diffraction and time-lapse photographic study", in preparation for submission to Journal of Nature, 2009.

Williams, R. L., P. R. Williams and A. Al-Hussany (2004). "The tensile strength of water as a function of temperature." Proceedings of the ASME fluids engineering division summer conference **2**: 525-530.

Williams, R. L., P. R. Williams and H. H. Chan (2007). The effects of temperature and rate of dynamic stressing on the tensile strength of monograde and multigrade oils. SAE, San Antonio, Texas, Small engine technology Conference and exposition, November 2006.

Williams, R. L., P. R. Williams and H. H. Chan (2008). "The effects of stressing rate on measurements of the cavitation threshold of monograde lubricant by pulses of tension." XVTH International congress on Rheology – the society of Rheology 80TH annual meeting, PTS 1 AND 2 1027: 1180-1182.

## References

---

Williams, R. L., P. R. Williams and H. H. Chan (2009). "The effects of dynamic stressing rate on the tensile strength of water", in preparation for submission to *Journal of fluid engineering*, 2009.

Williams Terrence L. and D. H. Trevena (1977). "Improved and extended theory of the Berthelot tube method of studying liquids under tensile stress". *Nature* **265**: 612 - 613

Williamson, B. P., K. Walters, T. W. Bates, R. C. Coy and A. L. Milton (1997). "The viscoelastic properties of multigrade oils and their effect on journal-bearing characteristics." *J. Non-Newtonian Fluid Mech.* **73**: 115-126.

Wilson, B. P. (1997). Ultrasound, cavitation and cleaning. Department of Chemical and Biological Processing Engineering. Swansea, University of Wales Swansea. Master Philosophia.

Wilson, D. A., J. W. Hoyt and J. W. McKune (1975). "Measurement of tensile strength of liquids by an explosion technique." *Nature* **253**: 723-725.

Zang, Y. H. (1991). "Direct measurement of tensile stress ("tack") in thin ink films." *J. Rheology* **35**: 345-361.

Xiao C. and D. M. Heyes (2002). "Cavitation in stretched liquids." *Proc. R. Soc. Lon. A* **458**: 889-910.

Zhang, X., T. Inada and A. Tezuka (2003). "Ultrasonic-induced nucleation of ice in water containing air bubbles." *Ultrasonics Sonochemistry* **10**: 71-76.

Zheng, Q., D. J. Durben, G. H. Wolf and C. A. Angell (1991). "Liquids at large negative pressures – Water at the homogeneous nucleation limit." *Science* **254(5033)**: 829-832.

Zheng, Liyun and Sun, DaWen (2006). "Innovative application of power ultrasound during food freezing processes – a review". *Trends in food Science and technology* **17**: 16-23.